

# **From Packing Generation to Single Pellet String Reactor Characteristics: A Numerical Approach to Fixed-Bed Reactors**

Johanna Fernengel

Vollständiger Abdruck der von der Fakultät für Chemie der Technischen Universität München zur Erlangung des akademischen Grades einer

Doktorin der Ingenieurwissenschaften (Dr.-Ing.)

genehmigten Dissertation.

Vorsitzender: Prof. Dr. Klaus Köhler

Prüfer der Dissertation: 1. Prof. Dr.-Ing. Kai-Olaf Martin Hinrichsen  
2. Prof. Dr.-Ing. Harald Klein

Die Dissertation wurde am 06.04.2022 bei der Technischen Universität München eingereicht und durch die Fakultät für Chemie am 18.08.2022 angenommen.



# Danksagung

Mein Dank geht zu allererst an meinen Doktorvater Professor Hinrichsen, für all die schönen Jahre an seinem Lehrstuhl - zu Studien- wie zu Promotionszeiten. Ich danke Ihnen herzlich für die Aufnahme in Ihre Arbeitsgruppe, die fortwährende Unterstützung, das mir entgegengebrachte Vertrauen und den damit einhergehenden Freiheiten bei der Bearbeitung meines Themas.

Ich danke Professor Klein für die Übernahme des Zweitgutachtens und Professor Köhler für den Prüfungsvorsitz. Sie haben damit einen wunderbaren Rahmen um meine Zeit an der TUM gespannt.

Ein spezieller Dank geht an Heidi Holweck für ihre Unterstützung bei all den kleinen und großen, nicht nur bürokratischen, Herausforderungen.

Ebenso danken möchte ich Thomas Michel und meinen Kollegen Franz, Franz, Flo, Chris, Moritz, Stefan, Sebastian, Philipp, Jennie, Julia, Thomas, Daniel, My, Tabea und Matthias. Ihr habt unsere gemeinsame Zeit an der TC1 zu etwas Besonderem gemacht, danke!

Bei Omar, Christina, Benedikt, Stephan, Konstantin, Aisyah, Edwin, Maximilian, Christian, René, Chelston, Helen, Moritz, Yong Sook und Dilbeste bedanke ich mich für ihr Interesse an simulativen Fragestellungen. Ich hoffe, dass Ihr im Rahmen Eurer Arbeiten einen spannenden Einblick bekommen konntet.

Special thanks go to Les Bolton for tremendously fruitful discussions and insights from an industrial and academic expert in the field of chemical reaction engineering. Also, I would like to thank the active EUROKIN members for their splendid questions and input. I thoroughly enjoyed my EUROKIN-time and the work on the single pellet string reactor would not have been the same without you!

Danke an Professor Richard Fischer und Normen Szesni, stellvertretend für die Firma Clariant, für die spannende Fragestellung rund um den Einfluss der Pelletschrumpfung auf das Katalysatorbett im Rahmen eines MuniCat-Projektes.

Let me take this opportunity to thank an often forgotten group - the numerous anonymous reviewers - for their challenging and demanding but also encouraging feedback. No doubt, your comments have taught me a lot and added value to the publications.

Zu guter Letzt danke ich meiner Familie, besonders meinen Eltern, die mich seit klein auf in meinem Tun bestärken. Allen voran gilt mein Dank meinem Mann Jürgen. Du hast mir in all den Jahren den Rücken freigehalten und mich geerdet. Danke!





*To my family.*



# Abstract

Catalytic fixed-bed reactors are the working horse of the chemical industry and optimal reactor operation is vital in many aspects, such as product quality and profit as well as resource and environmental management. Besides operator experience, computer aided analysis is becoming an important tool in advanced reactor optimisation, which requires numerical models of various levels of detail. For particle resolved models, the random nature of pellet arrangement within packed beds requires means of obtaining this type of information, either from experiment or numerical simulation, before the reactor operation can be simulated. Furthermore, it would be highly beneficial to be able to predict the performance of industrial catalytic reactors based on experimental data at lab-scale, without the need of costly pilot plant units. This is another aspect of catalytic reactor operation where a deeper insight into reactor performance by numerical simulation proves to be most valuable.

The present thesis can be divided into two major parts. The first part deals with numerical packing generation, considering random packed beds of spheres within cylindrical confining walls with moderate cylinder-to-pellet diameter aspect ratios. In addition, the response of packed beds of tablets to pellet shrinkage, as for example during a reductive catalyst activation step, is investigated. The second part, on the other hand, focuses on the operating behaviour of single pellet string reactors, a very special type of fixed-bed reactor where pellets are packed in tubes of only slightly larger diameter, which is investigated by means of computational fluid dynamics (CFD) simulations. This reactor type shows great potential for catalyst testing at lab-scale but under industrial conditions. Modelling and simulation are performed with open-source software only, namely Blender™ and LIGGGHTS® for packing generation and OpenFOAM® for CFD simulations. To address usability, the simulation routines are automated by means of Bash and Python scripts.

Feasibility of the automated simulation routine covering multiple entire simulation runs with geometry and mesh generation as preprocessing, CFD simulation and post-processing steps including parameter variations in the set-up is demonstrated.

Thorough investigation of the numerical packing generation based on rigid body physics is presented with emphasis on the influence of material properties. It is shown that wide range of pellet arrangements from loose to dense can be obtained and that the coefficient of friction and the coefficient of restitution, the latter limited to rough pellets, are most influential on the resulting bed structure. Detailed analysis of the local pellet arrangement by means of radial voidage profiles is used to propose an expression to determine the position of the local voidage minimum next to the confining wall.

The feasibility of incorporating pellet shrinkage as may be encountered in industrial catalyst activation into the packing generation routine is demonstrated. Analysis of the simulation results reveals the importance of considering local structure rather than solely relying on mean bed properties, which may falsify the results.

A systematic investigation of the flow and conversion behaviour within a series of single pellet string reactors considering laminar flow and an isothermal, irreversible hypothetical first order reaction  $A \longrightarrow B$  that is taking place at the surface of the non-porous catalyst pellets shows close similarities to plug flow at favourable parameter settings. The applicability of existing design criteria for conventional fixed-bed reactors is investigated before proposing a novel design criterion that allows a priori prediction of the deviation to plug flow conversion for single pellet string reactors under isothermal conditions.

In addition, the pressure drop behaviour of the series of considered single pellet string reactors is compared to the Blake-Kozeny equation. By introducing a scaling factor to the outer confining wall within an equivalent diameter expression that depends on the diameter aspect ratio of the reactor, excellent agreement between numerical simulation and pressure drop predictions is obtained.

Finally, the characterisation of single pellet string reactors is extended to cover nonisothermal behaviour. For highly exothermic reactions, reactor runaway is observed to take place at the first catalytic pellet within the string in reactors with wall cooling. Variation of various parameters including reactor geometry and material properties reveals a region where stable reactor operation with near-plug flow behaviour is possible. This region is limited by conditions leading to thermal runaway. As a result, a related design criterion for the operating behaviour of nonisothermal single pellet string reactors is proposed.

Open-source tools can be combined to enable an automated simulation routine covering pre-processing, CFD simulation and post-processing, similar to the functionality of commercial programmes but highly flexible to user requirements. Targeted packing generation such that the outcome resembles the properties of a corresponding real packing is possible, if choosing the appropriate settings. This should draw the attention of researchers to the importance of the packing in reactor modelling. The outcomes of the extensive characterisation of the single pellet string reactor with a conversion behaviour close to plug flow also under nonisothermal conditions underlines its great potential for catalyst testing.

# Kurzzusammenfassung

Katalytische Festbettreaktoren sind das Zugpferd der chemischen Industrie und ihr optimaler Betrieb ist von entscheidender Bedeutung, sei es hinsichtlich der Produktqualität, dem Profit oder Umwelt- und Ressourcenfragen. Hierbei kann eine simulationsbasierte Analyse hinsichtlich der Anlagenoptimierung wertvolle Impulse geben. Je nach zugrundeliegendem Modell sind unterschiedliche Detaillierungsgrade erforderlich. Bei partikel aufgelösten Modellen stellt die zufällige Pelletanordnung innerhalb einer Schüttung eine Herausforderung dar. Um einen Reaktor zu simulieren, müssen hierbei orts aufgelöste Informationen über die Schüttung vorhanden sein, welche aus Experimenten oder numerischen Simulationen stammen können. Ein weiterer Bereich, in dem die Reaktorsimulation wertvolle Einblicke in das Verhalten von Festbettreaktoren geben kann, ist die Vorhersage des Betriebsverhaltens industrieller Anlagen auf Grundlage von Laborexperimenten, möglichst ohne den Zwischenschritt kostspieliger Pilotanlagen.

Die vorliegende Arbeit ist thematisch zweigeteilt. Der erste Teil thematisiert die numerische Packungsgenerierung mit Hauptaugenmerk auf dem Einfluss von Materialeigenschaften auf Zufallsschüttungen von kugelförmigen Partikeln in zylindrischen Umwandungen. Hierbei werden Schüttungen mit moderaten Durchmesserhältnissen von Zylinderwand zu Katalysatorpellet betrachtet. Außerdem wird das Verhalten einer Tablettenschüttung bei Schrumpfung der Einzelpellets analysiert, wie zum Beispiel bei der reduktiven Katalysatoraktivierung in chemischen Reaktoren zu beobachten. Im zweiten Teil wird das Betriebsverhalten von Perlenschnurreaktoren mittels numerischer Strömungsmechanik (CFD) betrachtet. Dies ist ein spezieller Reaktortyp, bei welchem sich Pellets in Rohren mit nur geringfügig größerem Durchmesser übereinander anordnen - sinnbildlich wie Perlen an einer Schnur. Innerhalb der gesamten Arbeit wird für die Modellbildung und Simulation ausschließlich Open-Source-Software verwendet. Dabei wird für die Packungsgenerierung auf Blender™ und LIGGGHTS® zurückgegriffen und für die CFD-Simulationen OpenFOAM® verwendet. Um das Ausführen der wiederkehrenden Schritte zu erleichtern werden die Simulationsabläufe durch Einbettung in Bash- und Pythonskripte automatisiert. Die Verwendung eines solchen automatisierten Simulationsablaufs wird mittels einer kurzen Studie unter Variation der Versuchsanordnung gezeigt. Dabei umfasst jeder Simulationsdurchlauf mehrere Schritte einschließlich der Geometrieerzeugung und Netzgenerierung, der CFD-Simulation sowie abschließender Auswertungsberechnungen.

In der anschließenden detaillierten Betrachtung der numerischen Packungsgenerierung, basierend auf den Gesetzen der Starrkörperphysik, liegt das Hauptaugenmerk auf dem Einfluss der Materialeigenschaften. Es zeigt sich, dass die resultierende Anordnung der

Pellets von sehr losen bis hin zu dicht gepackten Schüttungen reicht. Den größten Einfluss auf die Bettstruktur haben dabei der Reibungskoeffizient und die Stoßzahl, letztere jedoch nur bei Pellets mit rauer Oberfläche. Aus der Analyse der zugehörigen radialen Porositätsprofile wird ein Ausdruck zur Vorhersage der wahrscheinlichen Position des wandnähesten lokalen Porositätsminimums als Funktion des Durchmesserhältnisses von Wand und Pellets abgeleitet.

Als nächstes wird die Pelletschrumpfung in den Algorithmus zur Packungsgenerierung integriert. Die durch Schrumpfung veränderten Packungsstrukturen weisen eine höhere Ordnung in Wandnähe auf. Insbesondere die Auswertung von Druckverlusten über die Packung zeigt die Bedeutung der lokalen Struktur. Bei Verwendung eines Porositätsmittlerwertes über die gesamte Schüttung kommt es zu signifikanten Abweichungen im Vergleich zu den partikel aufgelösten Simulationen.

Die systematische Betrachtung von laminar durchströmten Perlenschnurreaktoren, in denen eine isotherme, irreversible Reaktion hypothetischer erster Ordnung  $A \longrightarrow B$  an der Oberfläche der nicht porösen Katalysatorpellets abläuft, offenbart große Ähnlichkeit zum Umsatz bei idealer Pfropfenströmung, sofern ein günstiger Parametersatz zugrunde liegt. Die Anwendbarkeit existierender Auslegungskriterien für konventionelle Festbettreaktoren wird überprüft bevor ein neuartiges Kriterium für die Auslegung von Perlenschnurreaktoren vorgeschlagen wird, welches eine Vorhersagen über die zu erwartende Umsatzabweichung im Vergleich zur idealen Pfropfenströmung trifft.

Im Anschluss wird das Druckverlustverhalten der betrachteten Perlenschnurreaktoren mit der bekannten Blake-Kozeny-Korrelation verglichen. Führt man einen Skalierungsfaktor zur Gewichtung des Einflusses der begrenzenden Wand in die Berechnung des Äquivalenzdurchmessers in Abhängigkeit der Reaktorgeometrie ein, so kann eine ausgezeichnete Übereinstimmung zwischen numerischer Simulation und Druckverlustkorrelation erzielt werden.

Abschließend wird die Betrachtung der Perlenschnurreaktoren um nichtisotherme Szenarien erweitert. Geht man von wandgekühlten Reaktoren aus, so kann bei hochexothermen Reaktionen ein thermisches Durchgehen im Bereich des vordersten Katalysatorpellets beobachtet werden. Mittels Variationen von Reaktorgeometrie und Materialeigenschaften lässt sich ein klar begrenzter Parameterraum ausmachen, innerhalb dessen ein stabiler Reaktorbetrieb mit einem Umsatz nahe der idealen Pfropfenströmung vorliegt. Parametersätze außerhalb des stabilen Gebiets führen hingegen zu thermischem Durchgehen. Diese Beobachtungen münden in einem Stabilitätskriterium für den Betrieb nichtisothermer Perlenschnurreaktoren.

Die vorgestellten Beispiele zeigen, dass automatisierte Simulationsroutinen über mehrere Simulationsdurchläufe einschließlich Parametervariationen mittels Open-Source-Werkzeugen realisiert werden können. In ihrer Funktionalität ähneln diese Routinen kommerziellen Programmen, weisen jedoch gleichzeitig eine höhere Flexibilität auf. Die Ergebnisse der

durchgeführten Packungsgenerierungen zeigen, dass numerisch erzeugte Zufallsschüttungen durch die verwendeten Parameter beeinflusst werden. Bei überlegter Wahl des Parametersatzes kann die simulierte Schüttung die Eigenschaften einer korrespondierenden realen Schüttung widerspiegeln. Die umfassende Charakterisierung des Perlenschnurreaktors zeigt, dass diese bei geeigneter Auslegung ein Umsatzverhalten nahe der idealen Pfropfenströmung aufweisen und somit für Katalysatortests prädestiniert sind.





# Contents

<b>Abstract</b>	<b>vii</b>
<b>Kurzzusammenfassung</b>	<b>ix</b>
<b>1 Introduction</b>	<b>1</b>
<b>2 Outline of the basic theory</b>	<b>5</b>
2.1 Fixed-bed reactor fundamentals . . . . .	5
2.2 Aspects on conservation laws and balance equations . . . . .	7
2.3 Discretisation in numerical modelling . . . . .	9
<b>3 Literature overview on design criteria for fixed-bed reactors and the SPSR concept</b>	<b>11</b>
<b>4 Scripting as an approach to automated CFD simulation for packed bed catalytic reactor modelling</b>	<b>19</b>
4.1 Introduction . . . . .	21
4.2 Methodology . . . . .	22
4.3 Case study . . . . .	25
4.3.1 Set-up . . . . .	25
4.3.2 Results . . . . .	26
4.4 Conclusion . . . . .	28
<b>5 Influence of material properties on numerically generated random packed beds</b>	<b>29</b>
5.1 Introduction . . . . .	31
5.2 Methodology . . . . .	34
5.2.1 Packing generation . . . . .	34
5.2.2 Evaluation of voidage . . . . .	37
5.3 Case set-up . . . . .	38
5.3.1 Investigation of packing characteristics . . . . .	38
5.3.2 Parameter study on material properties . . . . .	39
5.4 Results and discussion . . . . .	40
5.4.1 Packing characteristics . . . . .	40
5.4.2 Material properties . . . . .	45
5.5 Conclusion . . . . .	53

5.S	Supporting information	55
5.S.1	Verification of sample size by analysis of mean value and standard deviation within one sample data set	55
5.S.2	Statistical analysis of the influence of material properties for beds generated with LIGGGHTS <sup>®</sup>	56
5.S.3	Statistical analysis of the influence of material properties for beds generated with Blender <sup>™</sup>	57
<b>6</b>	<b>Numerical simulation of pellet shrinkage within random packed beds</b>	<b>59</b>
6.1	Introduction	61
6.2	Methodology	61
6.3	Case set-up	63
6.4	Results and discussion	64
6.5	Summary and conclusion	69
6.S	Supporting information	71
6.S.1	Mesh generation	71
6.S.2	Grid-independence study	72
<b>7</b>	<b>Characterisation and design of single pellet string reactors</b>	<b>75</b>
7.1	Introduction	77
7.2	Methodology	80
7.2.1	Geometry	80
7.2.2	Particle positioning with Blender <sup>™</sup>	81
7.2.3	Numerical simulation	82
7.3	Case set-up	83
7.4	Results and discussion	85
7.4.1	Base case single pellet string reactor	85
7.4.2	Single pellet string reactor variations	88
7.4.3	Fixed-bed design criteria	93
7.4.4	Single pellet string reactor design criterion	96
7.5	Conclusion	98
7.S	Supporting information	100
7.S.1	Influence of inlet and outlet configuration and back-diffusion	100
7.S.2	Grid-independence study	102
7.S.3	Influence of particle size of inert fines	103
7.S.4	Influence of gas properties	104
7.S.5	Influence of feed dilution	105
7.S.6	Influence of tracer diffusion	105
7.S.7	Conversion-based trend analysis	108

---

<b>8</b>	<b>Numerical investigation of pressure drop in single pellet string reactors</b>	<b>111</b>
8.1	Introduction . . . . .	113
8.2	Methodology . . . . .	114
8.2.1	Geometry . . . . .	114
8.2.2	Governing equations . . . . .	114
8.3	Case set-up . . . . .	115
8.4	Results and discussion . . . . .	116
8.4.1	Base case . . . . .	116
8.4.2	Parameter study . . . . .	117
8.4.3	Pressure drop correlations . . . . .	117
8.5	Conclusion . . . . .	123
<b>9</b>	<b>Nonisothermal behaviour in reactive single pellet string reactors</b>	<b>125</b>
9.1	Introduction . . . . .	127
9.2	Preliminary considerations . . . . .	131
9.3	Model description and implementation . . . . .	132
9.3.1	Reactor geometry . . . . .	132
9.3.2	Fluid domain . . . . .	133
9.3.3	Catalytic and inert solid domains . . . . .	135
9.3.4	Surface reaction . . . . .	136
9.3.5	Implementation . . . . .	137
9.4	Single pellet string reactor scenarios . . . . .	140
9.4.1	Common reactor properties and assumptions . . . . .	140
9.4.2	Base case . . . . .	142
9.4.3	Variations on the base case . . . . .	142
9.5	Results . . . . .	146
9.5.1	Parameter study . . . . .	146
9.5.2	Adaptation of Benneker criterion . . . . .	165
9.5.3	Criterion on thermal runaway . . . . .	167
9.6	Summary and conclusion . . . . .	168
9.S	Supporting information . . . . .	170
9.S.1	Grid-independence study . . . . .	170
9.S.2	Influence of contact point handling . . . . .	170
<b>10</b>	<b>Summary and outlook</b>	<b>175</b>
	<b>Bibliography</b>	<b>181</b>
	<b>Nomenclature</b>	<b>199</b>
	<b>List of Figures</b>	<b>203</b>

<b>List of Tables</b>	<b>209</b>
<b>List of Publications</b>	<b>211</b>

# 1 Introduction

Fixed-bed reactors are most widely used in chemical industry [1], owing their breakthrough to the discovery and success of solid catalysts [2]. Optimal reactor operation is a vital economic aspect and its constructive and operational simplicity may be a reason for the success of fixed-bed reactors, with a remarkable variety of reactor geometries encountered not only in industry but also at lab scale. This includes fixed-beds with relatively large diameter of the confining wall, used for adiabatic processes, and at the same time reactors with rather small tube diameter to enhance heat transfer to and from the catalytic bed as required for highly endothermic or exothermic reactions [3]. The latter may be arranged such that a large number of reactor tubes forms a so called multitubular reactor. In case of extremely small diameter aspect ratio, that is between the outer confining tube and a diameter characterising the size of the catalytic pellets forming the bed, the resulting special type of fixed-bed reactor is called single pellet string reactor (SPSR), as introduced by Scott et al. [4]. Although this reactor geometry deviates from most established design rules for fixed-bed reactors in an effort to approach ideal plug flow behaviour as close as possible, with a uniform fluid flow through the reactor, it is discussed as a possible means for catalyst testing [5].

While conventional fixed-bed reactors, understood here as those reactors which follow common design criteria as for example that by Mears [6] and later adjusted by Gierman [7] on axial dispersion and that by Chu and Ng [8] on radial dispersion which lead to relatively long reactors with a minimum diameter aspect ratio, respectively, have been extensively studied in the past decades, publications on the single pellet string reactor concept [4] are scarce. However, recent works indicate a renewed interest in the reactor concept [5, 9–16] and evidence is required on its flow hydrodynamics and conversion behaviour before it can be used for reliable catalyst testing and kinetic studies, as this requires the underlying reactor to be free of transport effects [17] or at least to know the influence of the reactor geometry on transport phenomena.

Besides experimental investigations, computational fluid dynamics (CFD) have become an accepted design tool in chemical engineering, and especially for catalytic fixed-beds [18, 19], which is nowadays widely used. Before numerical simulation of the flow, concentration and temperature fields through fixed-bed reactors, information on the arrangement of the pellets within the random packed bed is required. This may be accomplished by digitising experimental data or by means of numerical packing generation, a field rapidly growing in recent years.

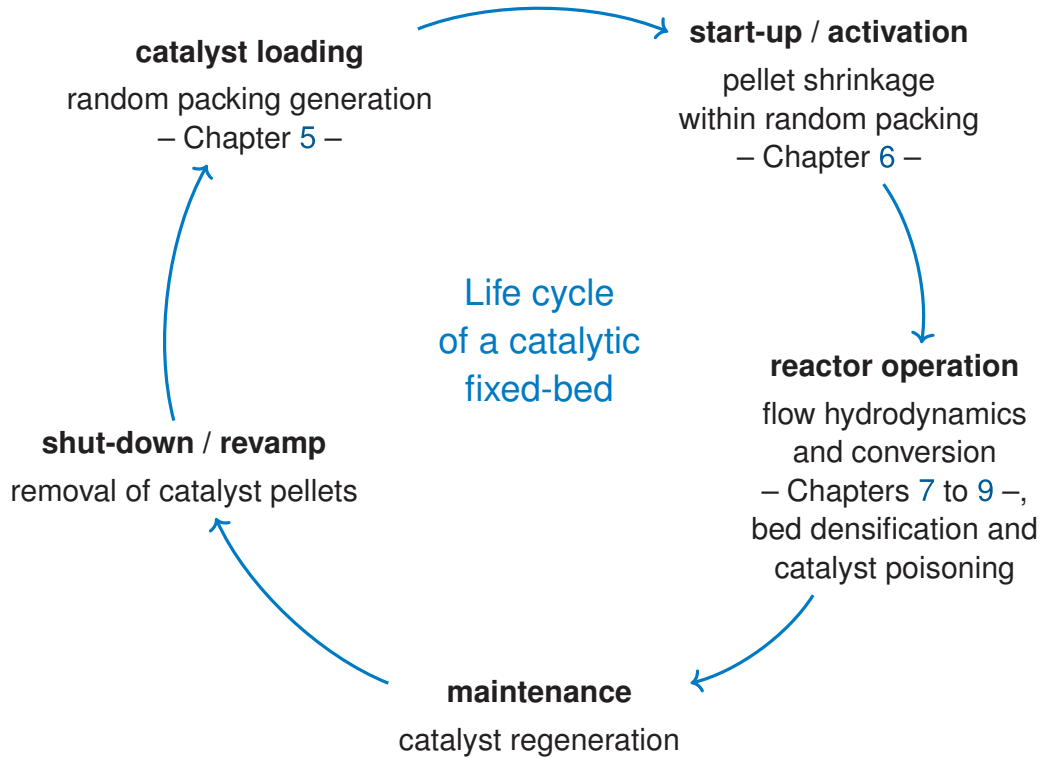


**Figure 1.1:** Generalised life cycle of a catalytic fixed-bed reactor, indicating related chapters within this thesis.

As numerous as the types and applications of fixed-bed reactors are the aspects surrounding the life cycle of a random packing of catalytic pellets as outlined in Figure 1.1. The bed is initially formed by catalyst loading where pellets are introduced into the reactor and settle under the influence of gravity. Often, catalysts are shipped and handled in an oxidised form for safety aspects, thus requiring an activation stage during the start-up of the reactor where the pellets are reduced under controlled conditions to their catalytic form. During this process, the chemical structure of the catalyst pellets undergoes changes which may result in a significant loss of the pellet volume, which in turn affects pellet arrangement within the random packing. This is easily accessible as a reduced bed height, an observation often encountered in industry. During plant operation reaction media pass through the fixed-bed reactor and the equipment may be under vibration, resulting in a densification of the random packing. Also, the catalyst may experience poisoning which influences the conversion behaviour of the catalytic bed. This brings the necessity of catalyst regeneration or replacement during maintenance or even a shut-down of the reactor, respectively.

Within this work, aspects of fixed-bed reactors are investigated by means of numerical modelling and simulation. The emphasis is two-fold, covering packing generation and the influence of pellet shrinkage on the catalytic bed as well as phenomena within the reactor during operation. While packings with moderate diameter aspect ratios are the subject of discussion for details on pellet arrangement within the catalytic bed, the single pellet string reactor is in focus for investigating the flow hydrodynamics and conversion behaviour

---

during reactor operation. Both topics are embedded in an automated simulation framework based on Bash [20] and Python [21] scripting integrating packing generation with LIGGGHTS<sup>®</sup> [22] and Blender<sup>™</sup> [23] as well as CFD simulations of the reactor during operation with OpenFOAM<sup>®</sup> [24].

The remaining chapters within this thesis are organised as follows:

- An introduction on fixed-bed reactor fundamentals as well as general aspects of reactor modelling, covering aspects on conservation laws and discretisation in reactor modelling, are presented in Chapter 2. This part is kept rather short, given that the required background information are covered in each of the following chapters individually.
- A comprehensive literature overview on the single pellet string reactor is presented in Chapter 3. This covers the initial work from Scott, Lee and Papa [4] up to the most recent research in this field.
- Means of simulation automation applied to fixed-bed reactor modelling with open-source software are discussed in Chapter 4. The proposed automated simulation routine covers multiple entire simulation runs from bed generation, CFD simulation to post-processing.
- The influence of material properties on characteristics of random packings are investigated in Chapter 5, giving details on mean and local bed properties. The two software packages, LIGGGHTSS<sup>®</sup> and Blender<sup>™</sup>, based on the distinct element method and contact dynamics, respectively, are compared with regard to the obtained packings of mono-sized spherical pellets within cylindrical containers for set-ups with moderate diameter aspect ratios.
- Chapter 6 demonstrates the feasibility of modelling the volume contraction of catalytic pellets during catalyst activation within a random packing investigating the influence thereof on pellet arrangement and flow hydrodynamics. A bed of an industrial methanol synthesis catalyst in tablet form is considered.
- The investigation of single pellet string reactors of spherical pellets in cylindrical tubes starts with a thorough characterisation of the flow and conversion behaviour of an isothermal, heterogeneously catalysed gas-phase reaction as presented in Chapter 7. This covers a parameter study on the influence of reactor geometry and fluid properties and leads to a novel design criterion for this type of reactor based on reactor geometry, fluid properties and flow velocity, all known a priori.
- The pressure drop through the single pellet string reactors introduced in Chapter 7 is subject of detailed discussion in Chapter 8. Within narrow fixed-bed reactors, the influence of the confining wall should be taken into account. Comparison of the

simulated pressure loss to the Blake-Kozeny equation, which is equivalent to the contribution of laminar flow within the Ergun equation, is made and a geometry-based weighting factor introduced to scale the influence of the confining wall in an equivalent diameter expression.

- The characterisation of single pellet string reactors is extended to include the impact of thermal effects in Chapter 9. A parameter study related to exothermic reactions, covering for example variations of the heat of reaction and activation energy as well as thermophysical properties of the involved fluid and catalyst material reveals regions of thermal runaway and stable reactor operation.
- The thesis ends with a summary of the obtained findings based on the conducted numerical packing generations and CFD simulations and offers thoughts on possible topics for further investigation in Chapter 10.



## 2 Outline of the basic theory

The presented work on fixed-bed reactors is based on numerical simulations only. This includes both, means of random packing generation and reactive flow simulation. Here, an overview on fixed-bed reactor fundamentals is presented followed by common aspects of the conservation laws underlying the numerical models. Afterwards, thoughts on the different types of discretisation encountered in numerical simulation are outlined. This chapter is kept rather short as details on further theoretical background information as well as the relevant literature are covered separately within each of the following chapters.

### 2.1 Fixed-bed reactor fundamentals

As the name suggests, fixed-bed reactors consist of a bed of solid pellets that have settled within an outer confining reactor geometry and are assumed immobile, i.e. fixed in their position within the bed. Fluids, either gases or liquids or a combination of both, pass through the reactor bed. In case of gases passing through the fixed-bed, the flow approximates ideal plug flow behaviour [25] which is characterised by fluids passing the reactor in an orderly manner, especially without back-mixing of fluid elements [25]. This holds especially at turbulent flow conditions of the reacting fluids [26]. In case of ideal plug flow, the residence time is uniform for all fluid elements. However, dead zones and channeling are present as a result of the local bed structure [3, 27] which cause deviations to ideal plug flow, resulting in a distribution of the residence times for the various flow elements. Evaluation of the residence time distribution by experimental or numerical means can be used to determine the deviation to ideal behaviour, indicating bypassing and dead volumes (cf. [27] for details). In the context of fixed-bed reactors, the observed peak broadening in the residence time distribution is attributed to the so called *dispersion*, which may be understood as a diffusion-like process or some degree of back-mixing which is superimposed on plug flow [25, 28] originating from the influence of the local packing arrangement on the fluid flow.

The pressure loss across a packed bed is highly influenced by the size of the pellets, favouring large pellets to reduce pressure drop [3]. Fixed-beds of very small pellets are not feasible due to possible plugging and significant pressure loss [25].

Temperature control in fixed-bed reactors is crucial and challenging as they are often subject to a low heat conductivity within the bed [25] making them prone to hot-spot formation [3]. This may lead to thermal runaway of the reactor [3] and induces radial gradients also in the fluid composition, given the influence of temperature on local conversion [25].

To enhance near-isothermal reactor operation, set-ups with small diameter aspect ratio are preferable [17], as found in multitubular reactors [3]. Other means of temperature control include the dilution of the catalytic bed or of the reactant stream as well as intermediate cooling or heating [3].

There is the necessity for isothermal reactor operation and the absence of transport limitations to obtain reliable kinetic data [17, 26] and for effective catalyst testing [29]. For interpretation of the experimental data, an ideal flow pattern in the underlying reactor is important [26] or at least knowledge of the prevailing flow hydrodynamics [30].

Design criteria, by which the deviation to ideal reactor behaviour in regard to transport limitations and isothermal operation is limited, are extensively available [6, 7, 31–34]. These commonly require the reactor diameter to be significantly larger than the catalyst pellet diameter, i.e. a minimum diameter aspect ratio, as well as a reactor length of about 25 to 100 times the pellet diameter. Especially for laboratory equipment, the resulting large and costly reactor set-ups pose a significant level of hazard as they need substantial gas flow rates. Hickman et al. [35] reviewed best practice rules on the design of fixed-bed reactor set-ups for evaluation of heterogeneous catalyst systems at laboratory scale. Limiting factors for downscaling of catalytic fixed-bed reactors in order to generate meaningful results are discussed by Sie [34, 36].

Mathematical modelling of fixed-bed reactors already evolved as an important discipline in chemical reaction engineering in the mid-20th century, starting with simple pseudo-homogeneous reactor models and nowadays ranging to highly sophisticated heterogeneous reactor models [2, 3]. Latest advances include particle-resolved models based on CFD simulations [19]. In general, reactor models need to capture the phenomena happening in the actual experimental and industrial set-ups. These include the reaction, incorporated via a rate equation, as well as the conservation of mass, heat and momentum which are accounted for by the continuity, energy and momentum equation, respectively [3]. The form of the equations used depends on the level of detail and the complexity of the model. Various scales of reactor models are distinguished, namely the microscale, taking into account phenomena at the catalytic sites, the mesoscale, related to the level of the catalyst pellet with interfacial and intraparticle gradients, and the macroscale, focusing on the flow hydrodynamics as well as the heat and mass transfer within the reactor [3]. Very often, pseudohomogeneous one-dimensional models are being used assuming plug flow in axial direction. Despite the apparent low level of detail, these models may already give valuable hints if interpreted correctly with respect to their limitations. However, if transport phenomena cannot be reduced effectively in the experimental set-up, heterogeneous reactor models may be used which explicitly account for these phenomena [30]. The more detailed heterogeneous reactor models distinguish between the fluid and solid domain. Further, a second dimension can be introduced thus allowing for radial gradients. Within this work pellet resolved CFD models of fixed-bed reactor situations are considered.

Common to all reactor models is that the underlying conservation laws are expressed as balance equations which, depending on the level of detail, are solved with respect to time and space. This requires an appropriate discretisation within the considered domains.

## 2.2 Aspects on conservation laws and balance equations

Newton's three laws of motion describe the fundamental behaviour of objects interacting with forces. If there is no force acting upon an object, it will continue at rest or with its linear motion. On the other hand, if a force is acting upon an object, there will be a change to its state of motion. And, if the force acting on an object is applied by another object, the latter will also experience a force of equal magnitude but opposite direction. These laws are the underlying principles for the numerical simulation of packing generation where pellets, i.e. objects, fall under the influence of gravity, a force, and collide with each other as well as with the container they are falling into, i.e. another object. For numerical packing generation, the conservation of linear and angular momentum, expressed by Newton's second law, is evaluated for each contact between colliding objects. Depending on how these collisions are resolved, this may lead to the classical distinct element method (DEM) as proposed by Cundall and Strack [37] or the contact dynamics (CD) method based on the work by Jean and Moreau [38, 39] as discussed in Chapter 5.

While the interactions of objects related to packing generation are treated as discrete, this is not necessarily the case when looking at fluids in motion. Although the properties of a fluid are also based on collisions, namely at microscopic level between molecules, they are often treated as flow fields considering their macroscopic properties. Two approaches can be followed when looking at fluid flows numerically, either by tracking individual fluid elements, also referred to as fluid particles, as in the Lagrangian approach or following the assumption of a continuum as in the Euler approach. The latter is by far more common within the field of fluid mechanics [40] and shall be followed within this work.

Modelling of fluid motion is based on the solution of conservation principles for the flow variables taken into account across the considered space and time domains. Conservation means that the rate of change of a general flow variable needs to balance with the processes leading to an increase or decrease of that flow variable, such as convection, diffusion or reaction. In words, such a balance equation for a general flow variable  $\phi$  can be expressed as [41]

$$\left[ \begin{array}{l} \text{rate of change of } \phi \\ \text{in the control volume} \\ \text{with respect to time} \end{array} \right] = \left[ \begin{array}{l} \text{net rate of increase of } \phi \\ \text{due to } \textit{convection} \\ \text{into the control volume} \end{array} \right] + \left[ \begin{array}{l} \text{Net rate of increase of } \phi \\ \text{due to } \textit{diffusion} \\ \text{into the control volume} \end{array} \right] + \left[ \begin{array}{l} \text{Net rate of } \textit{creation} \text{ of } \phi \\ \text{inside the control volume} \end{array} \right]. \quad (2.1)$$

Depending on the scope considered for a given flow problem, at least balance equations for mass and momentum are required. In addition, it may be necessary to also include equations for the conservation of energy and the involved chemical species if taking into account heat transfer and reaction.

The mass balance for a species A may be expressed by [3]

$$\left[ \begin{array}{c} \text{amount of A} \\ \text{accumulated} \\ \text{per unit time} \end{array} \right] = \left[ \begin{array}{c} \text{amount of A} \\ \text{introduced} \\ \text{per unit time} \end{array} \right] - \left[ \begin{array}{c} \text{amount of A} \\ \text{leaving} \\ \text{per unit time} \end{array} \right] - \left[ \begin{array}{c} \text{amount of A} \\ \text{converted} \\ \text{per unit time} \end{array} \right] \quad (2.2)$$

where convection and diffusion are considered as possible mechanisms for entering or leaving the system [3]. Developing an equation based on a control volume leads to the mass conservation equation which is often called continuity equation. Derivation of this and further conservation equations are not shown here, but rather the reader is referred to classical text books such as *Transport Phenomena* by Bird, Stewart and Lightfoot [42] or *An Introduction to Computational Fluid Dynamics* by Versteeg and Malalasekera [41].

Applying Newton's second law to a fluid element yields the momentum balance. Within a three dimensional Cartesian coordinate system, the momentum balance may be expressed in words as [3]

$$\left[ \begin{array}{c} \text{variation of} \\ \text{amount of momentum} \\ \text{in direction } i \\ \text{per unit time} \end{array} \right] = \left[ \begin{array}{c} \text{amount of momentum} \\ \text{in direction } i \\ \text{added} \\ \text{per unit time} \end{array} \right] - \left[ \begin{array}{c} \text{amount of momentum} \\ \text{in direction } i \\ \text{removed} \\ \text{per unit time} \end{array} \right] - \left[ \begin{array}{c} \text{effect of pressure and} \\ \text{friction forces on} \\ \text{amount of momentum} \\ \text{in direction } i \\ \text{per unit time} \end{array} \right] \quad (2.3)$$

where  $i = 1, 2, 3$ . When considering Newtonian fluids, where the viscous stress is a linear function of the rate of strain [43], the momentum balance amounts to the well known Navier-Stokes equation [40].

For non-isothermal flow problems, an energy balance needs to be considered. In chemical reactors, it is common to neglect the influence of kinetic, potential and work terms as compared to the heat of reaction and heat transfer [3]. The resulting energy balance may be expressed in words by [3]

$$\left[ \begin{array}{c} \text{variation of} \\ \text{heat content} \\ \text{per unit time} \end{array} \right] = \left[ \begin{array}{c} \text{amount of heat} \\ \text{added} \\ \text{per unit time} \end{array} \right] - \left[ \begin{array}{c} \text{amount of heat} \\ \text{removed} \\ \text{per unit time} \end{array} \right] - \left[ \begin{array}{c} \text{heat effect of the} \\ \text{reaction} \\ \text{per unit time} \end{array} \right]. \quad (2.4)$$

For heat transport, convection with the flow and conduction through the fluid are taken into account as opposed to radiation, which shall not be considered here.

Chemical reaction is considered as source term within the mass and heat balance. Within this thesis, only heterogeneously catalysed reactions, that is reactions taking place at the

surface of a solid catalyst, are considered. Therefore, the effect of the chemical reactions is incorporated into the boundary conditions, which are generally describing the properties of the considered flow variables at the boundaries of the spacial domain.

If the fluid under consideration is incompressible, the described set of conservation equations is sufficient to solve the flow problem including the pressure field. In case of an incompressible fluid, the governing equations need to be extended by an equation of state, relating the pressure field to the local temperature and density [41].

Overall, the governing equations describing fluid motion are a set of partial differential equations with respect to space and time. In order to solve these, boundary and initial conditions are required which describe the behaviour of the dependent flow variables at the boundaries of the spacial domain and within the entire solution domain at the initial point in time [40, 41]. On solid walls, the *no-slip* condition holds which sets the fluid velocity at the wall to the velocity of the wall [41]. In case of a fixed bed, where the packing is assumed to be at rest, this would be a zero velocity. Chemical reactions taking place at a wall result in a defined heat flux as temperature boundary condition [41] and also a source respectively sink to the chemical species involved. Often, the fluid boundaries for incompressible viscous flow scenarios are defined with fixed values for velocity and temperature at the inlet and corresponding zero gradient conditions at the outlet as well as a fixed pressure value at the outlet and a zero gradient condition at the inlet [41].

## 2.3 Discretisation in numerical modelling

Within this work, CFD simulations are performed with OpenFOAM<sup>®</sup> [24] which relies on the finite volume method. Excellent theoretical background information thereon can be found in the OpenFOAM<sup>®</sup> documentation by Greenshields [44–46], an OpenFOAM<sup>®</sup> related book by Marić et al. [47] as well as in the classical textbooks as for example by Ferziger and Perić [48], Versteeg and Malalasekera [41] and Andersson et al. [43] to name but a few.

In order to be able to obtain a solution to the set of continuous governing equations by means of CFD simulation as for example with OpenFOAM<sup>®</sup>, these have to be discretised in three ways. First of all, there is the discretisation of the spacial solution domain into cells. The numerical value of each flow variable is attributed to the centre of each of these cells. Thus, the continuous spacial domain is divided into a finite number of subvolumes [48]. This introduces a discretisation error which would vanish for infinitesimal small cells with cell volumes approaching zero [43]. However, a large number of cells correlates with a long simulation time. Therefore, it is a challenge to find the best compromise between solution accuracy and computational time. Often, optimal meshes are non-uniform, with finer regions at areas where large gradients in the flow variables are expected and a coarser grid in regions with little changes [41]. Defining a satisfying grid is a challenging task at the start of

each CFD simulation. The aim should always be to keep it as coarse as possible but also make it as fine as necessary, especially in regions where the flow variables are subject to steep gradients. Ultimately, the solution should be mesh independent, that is not influenced by the underlying computational grid. This can be checked by comparing the solution on different meshes with varying refinement. Ferziger and Peric [48] as well as Celik et al. [49] propose measures for the discretisation error introduced by the finite grid based on the comparison of solutions on three grids with different refinement levels.

Not only in CFD simulations but also for the numerical packing generation, the solution routine requires a discretisation of the time domain into finite steps, if the considered problem evolves with time. The size of the time step is one of the differences between the distinct element method (DEM) and the contact dynamics (CD) method applied for the packing generation in Chapter 5. Most of the conducted flow simulations are steady-state scenarios, except for evaluating the residence time distributions in the various single pellet string reactor scenarios beginning with Chapter 7.

The third type of discretisation encountered in numerical simulation is that of the underlying set of continuous equations. Within CFD the partial differential governing equations are linearised within each cell of the computational grid [41, 43, 48]. Based on the principle of local conservation and by applying Gauss' law, which allows to transform volume integrals to surface integrals, the partial derivatives can be reduced to linear algebraic equations which are then solved by iterative solution methods [43]. A decision on when to stop the iterative process is commonly based on residuals, which yield a comparison between the values of two successive iterations [41, 48]. In addition to the development of the residuals, it is advisable to monitor the value of specific variables, such as for example the average inlet pressure or the overall conversion for reactive flows, as a function of the iteration number. This combination provides a clear picture on the progress of the iterative solution.



### 3 Literature overview on design criteria for fixed-bed reactors and the single pellet string reactor concept

Certainly, the world would be a different place without the contributions of heterogeneous catalysis, which accounts for a large amount of production in chemical industry. Therefore, the continuous development of ever new and better catalysts but also the optimisation of existing industrial plants is of major importance. This brings with it the need to test the performance of catalysts, preferably at laboratory scale, before introducing these to the industrial units. However, it is advantageous to test the performance at or at least close to industrial conditions already at this stage [29]. When the process conditions shall be those corresponding to commercial operation, the parameters such as space velocity, temperature, pressure, feed composition as well as amount and type of catalyst are fixed while the bed dimensions, that is diameter and length, as well as the size of the catalyst particles may be varied [7]. In order to be able to directly relate the obtained experimental results to industrial sized reactors, the catalyst size should not be changed as not to introduce distorting effects on the apparent activity of the catalyst, the selectivity and its deactivation behaviour [36]. To allow a straightforward interpretation of the results from kinetic experiments, transport effects within the underlying bed should be avoided [17]. As a result, the well established conventional design criteria for catalytic testing require rather long packed bed reactors [6] with tube diameters much larger than the catalyst pellet size [8]. The resulting test reactors are relatively large, rather complex and costly, requiring substantial gas flow rates and therefore they may also pose a significant level of hazard. This is where the single pellet string reactor comes into play, a very special type of fixed-bed reactor where pellets are packed into tubes of only slightly larger diameter. Already in the 1960s this type of reactor was discussed and named *single pellet string reactor* (SPSR) by Scott et al. [4] in 1974, who already emphasised a flow behaviour close to that of conventional packed beds. With its simplicity and potential near plug-flow behaviour, would it be possible to run kinetic experiments and industrial catalyst performance tests based on single pellet string reactor set-ups? Not much has been published on this field since its first appearance, however, recent publications [5, 9–16] renew the interest in this special type of reactor.

The work by Sie [34, 36] gives an extensive overview on the field of catalyst testing at reduced reactor scale for fixed-bed reactor systems with gas phase and trickle-flow

processes. Here, the overarching goal is to obtain a testing environment that allows for the use of industrial sized catalysts in a reactor with flow hydrodynamics close to ideal plug flow conditions as not to affect the observed macrokinetics and thus the reaction rate. The packing arrangement in fixed-bed reactors with a higher local voidage close to the confining wall causes deviations to plug flow which is easily accessible as a spread of the residence time distribution (RTD). Sie investigated experimental set-ups at various scales, concluding that *nanoflow reactors* were suitable for testing industrial sized catalysts under commercially relevant conditions. The described nanoflow reactors are similar in set-up as the single pellet string reactor investigated within this dissertation. Also, Sie already commented on the conventional design criterion on lateral diffusion, concluding that this may be too strict for gas phase reactions within nanoflow reactors given that the mass exchange in these reactors is very fast. To improve the flow hydrodynamics in trickle-flow operation, he puts forth the possibility to dilute the catalyst pellets with inert fines.

Before focusing on the single pellet string reactor concept, a closer look is taken on existing design criteria for fixed-bed reactors, focussing on the effect of radial and axial dispersion. The numerical and experimental investigation of the influence of confining walls on single-phase fluid flow through packed beds with cylinder-to-particle diameter ratios of  $2.5 \leq D/d \leq 40$  by Chu and Ng [8] is often stated regarding radial dispersion. They showed that the significant increase of both apparent permeability and porosity coincide above a value of  $D/d$  between seven and eight. Above a diameter ratio of roughly 25, the confining cylinder was observed to be large enough such that the wall effect on permeability can be neglected. Based on Chu and Ng's work, both  $D/d = 8$  and  $D/d = 25$  are used as design criteria for fixed-bed reactors above which the wall effect does not play a major role on the flow. The deviation to plug flow due to axial dispersion has been considered mainly by Carberry [50], Mears [6] and Gierman [7]. Already in the 1950s, Carberry [50] concluded that the effect of mixing on reaction kinetics is negligible considering first order, isothermal processes in packed beds of practical reactor length to particle diameter ratios  $H/d$ . On the other hand, he indicated that when using short beds and low Reynolds number flow, especially for liquids, axial dispersion must be considered. Mears [6] proposed a general criterion for a minimum reactor length above which axial dispersion effects are no longer significant. For a deviation to the length required for plug flow of less than 5% the inequality given in Eq. (3.1) must hold.

$$\frac{L}{d} < \frac{20n}{Pe_{ax}} \ln \left( \frac{1}{1-X} \right), \quad (3.1)$$

where  $L$  is the bed length,  $d$  the particle diameter,  $n$  the order of reaction,  $Pe_{ax}$  the dimensionless Péclet number<sup>1</sup> based on the axial dispersion coefficient and  $X$  the overall reactor conversion. According to Mears, the minimum bed length required to satisfy this

<sup>1</sup> It should be noted that in the original publication this dimensionless group is depicted as Bodenstein number  $Bo$ .



---

criterion is ten times longer in trickle flow operation as compared to pure gas phase and dilution with small inert particles may be utilised to reduce the deviation from plug flow. This observation is shared by Gierman [7] who concluded the necessity of diluting short catalytic beds with inert fines in trickle-flow operation to improve the flow behaviour. Also, he picked up the criterion on a minimum reactor length introduced by Mears, arguing that it is too strict and hence loosened it by proposing a factor of 8 instead of 20 in Eq. (3.1).

Scott et al. [4] introduced the term *single pellet string reactor* to describe reactors with tube diameters only slightly larger than the particle diameter. They conducted pressure drop measurements as well as tracer pulse dispersion experiments in reactors with cylinder-to-particle diameter ratios of  $1.16 \leq D/d \leq 1.35$  using both porous and non-porous spherical particles. The results showed a reproducible flow behaviour with an axial dispersion behaviour comparable to conventional packed beds, when a minimum reactor length of  $L = 50d$  was used. Excellent agreement for the pressure drop in air flow across beds of non-porous glass and stainless steel spheres could be achieved when using a modified Ergun equation [51] by including the surface of the confining wall in addition to the particle surface in an equivalent diameter. To describe dispersion, Scott et al. [4] used the formulation for packed beds postulated by Edwards and Richardson [52] with parameter values adapted to their experimental data. They could expand the applicability of the axial dispersion correlation to SPSRs using modified Reynolds and Péclet numbers based on the particle diameter.

After these initial publications on SPSRs, there is little documented activity on this type of reactor for a couple of decades. However, just recently there has been an increase in the number of publications. Here, an overview of the available publications is presented in chronological order, without claiming completeness.

Hsiang and Haynes [53] presented work on axial dispersion in fixed-bed reactor geometries with significant wall effect, including SPSR set-ups with  $D/d = 1.13, 1.14, 1.54$  and  $1.8$ . They observed a sufficient packing reproducibility for beds with small cylinder-to-particle diameter ratios and concluded on the applicability of packed bed correlations for SPSRs with diameter aspect ratios of  $1.1 \leq D/d \leq 1.4$  as already proposed by Scott et al. [4]. At larger diameter aspect ratios the observed dispersion was found to exceed the values predicted by common packed bed correlations. Chou and Hegedus [54] achieve very close agreement between experimental data and predictions from a heterogeneous model for the transient diffusion in catalytic particles with two regions of different diffusivities by conducting transient pulse diffusivity measurements in SPSRs with a diameter ratio of  $D/d = 1.4$  and containing 320 particles. Lee and co-workers [55] investigated the use of cylindrical rather than spherical particles in SPSRs with lengths of at least  $290d$  as well as diameter ratios of  $D/d = 1.54$  and  $1.81$ , concluding that for laminar flow the same flow behaviour as observed in conventional packed beds persists. They also observed a pressure drop behaviour following the Ergun equation when using the modifications proposed by Scott et al. [4] and presented a set of coefficient values for the axial dispersion

equation proposed by Edwards and Richardson [52]. To experimentally determine the mass transfer between spherical naphthalene particles and air Tsotsas and Schlünder [56] undertook experiments with SPSRs. Another application of the SPSR was chosen by Sharma et al. [57] for measuring effective diffusion coefficients of spherical and ring-shaped commercial catalysts under non-reacting conditions. In order to eliminate the effect of axial dispersion towards pulse broadening, they estimated axial dispersion using non-porous glass particles in comparable set-ups with diameter ratios in the range of  $1.1 \leq D/d \leq 1.4$  and bed height of at least  $200d$ . Sharma et al. [57] concluded that the magnitude of axial dispersion in the reactor was low compared to diffusion and proposed own values for the coefficients in the correlation proposed by Edwards and Richardson [52]. An analytical investigation of overall porosity and radial porosity profiles for packed beds with aspect ratios of  $D/d \leq 2$  was conducted by Govindarao et al. [58]. Pressure drop experiments by Fand et al. [59] in beds with aspect ratios  $D/d < 1.4$  and flow over a large range of Reynolds numbers ( $0.3 \leq Re \leq 705$ ) led to a new modified empirical correlation for the friction factor used in the Ergun equation. In an investigation of heat transfer in fixed-beds of spheres, Dixon [60] observed a potentially predictable behaviour for set-ups with diameter aspect ratio in the range of  $1 < D/d < 2$ . In later publications, the research direction is rather broad. Besides classical set-ups with spherical pellets in cylindrical confining walls and single-phase flow, other pellet and outer geometry shapes are considered besides multiphase flow, chemical reactions and the influence of diluting the catalytic bed with inert fines. A simulative approach towards the pressure drop and residence time behaviour was presented by Müller et al. [12] for single-phase liquid flow in reactors with spherical particles in cylindrical confining walls of aspect ratio  $D/d = 1.2$ . Mainly 2D but also first 3D simulations were conducted with COMSOL Multiphysics<sup>®</sup> 4.2a [12]. Extra space had to be introduced between the pellets in the 2D simulations to allow for liquid flow through the reactor. The pressure drop results as a function of fluid velocity compared well to the correlations proposed by Reichelt [61] and Cheng [62]. The RTDs were of symmetric and relatively narrow shape, pointing to well developed plug flow. Also, obtained Bodenstein numbers  $Bo = \frac{u_0 L}{D_{ax}}$ , assuming open boundaries regarding dispersion, were of such range as to conclude plug flow behaviour. Guo et al. [63] recently published on experimental pressure drop evaluation in slender packed beds of spheres in cylindrical confining walls with diameter aspect ratios of  $1 < D/d < 3$  using single-phase flow of water. They proposed a modified empirical correlation for the friction factor in the Ergun equation for SPSRs, resulting in a mean deviation between predicted and experimental values of 15%.

Various authors investigated heterogeneously catalysed gas phase reactions in SPSR set-ups with cylindrical pellets or even other shapes of pellets other than spheres [5, 13, 14]. Experiments on the catalytic decomposition of nitrous oxide in SPSRs with cylindrical pellets, where the diameter equals the height, were conducted by Klyushina et al. [14]. A comparison of the rate of the catalytic reaction observed in a reactor of aspect ratio of  $D/d = 1.08$  with a packed bed reactor of aspect ratio  $D/d = 9.8$  showed that the influence

---

of macroscopic phenomena was significantly lower in the SPSR, both reactors fulfilling the Mears criterion. Hence, they concluded the suitability of this reactor type to gain kinetic data on reactions in the gas phase using industrial catalyst pellets. Behnam et al. [13] compared experimental results from endothermic steam methane reforming on 4-hole cylinders with external grooves, where the holes were blocked with cement and which were placed in an ordered string with corresponding simulations conducted with FLUENT 6.3. Excellent agreement could be achieved for temperature and species concentration results. It should be noted that comparably short SPSRs were used, covering 30 particles in the experiment and only 10 particles in the CFD simulation including inert particles at the inlet and outlet in both cases.

A group of researchers at the Delft University of Technology focused on SPSRs with spherical pellets but in confining walls with square cross section. Their publication by Calis et al. [64] describes the pressure drop characteristics in composite structured packings, which are basically composed of a large number of SPSRs in parallel. Comparison was made for laminar and turbulent flow between CFD simulation using CFX-5.3 and an experimental set-up. Again, only few particles were taken into account. For mesh generation, the particles were shrunk by 1 % to avoid contact points. This seems to be common practice for numerical simulation, where the handling of contact points may be critical during mesh generation. The results showed an average deviation of 10 % between the experimentally and numerically determined friction factors in the pressure drop correlation by Ergun, fitting only two CFD simulations for each diameter ratio. Using the original factors from the Ergun equation overpredicted the experimentally obtained friction factor by as much as 80 %. A comparison between local velocity profiles from CFD simulations and laser-Doppler anemometry measurements showed good agreement. Their work on composite structured packings was continued by Romkes et al. [65] including mass and heat transfer. They obtained good agreement between experimental data and CFD simulations for heat and mass transfer characteristics, expressed as Nusselt correlation, for reactors with aspect ratios of  $1 \leq D/d \leq 2$ . Hipolito et al. [11] also worked on SPSRs with square cross section, investigating pressure drop characteristics and RTDs for single-phase and two-phase flow. They concluded that the flow of a single liquid phase does not compare sufficiently to plug flow and hence the axial dispersion model cannot be used. On the other hand, adding a gas phase to the flow significantly improved the flow characteristics towards plug flow. In further experiments, the reactors proved suitable from a hydrodynamics point of view for catalyst testing based on experiments for the fast reaction of selective hydrogenation of allene without mass transfer resistance.

A number of papers have been published by the Lange group from Dresden over the past years looking on two-phase flow problems in SPSRs with spherical particles in cylindrical confining walls [12, 15, 66, 67]. The starting point was made with a simulative approach on single-phase liquid flow by Müller et al. [12], as already introduced above. The work was

continued by Langsch et al. [66] in regard of investigating the SPSR as potential reactor concept for the transfer of fast batch processes to continuous operation. They characterised the hydrodynamics and mass transfer characteristics of reactors with spherical catalyst particles in cylindrical channels with an aspect ratio of  $D/d = 1.76$  for the hydrogenation of  $\alpha$ -methylstyrene, a multiphase reaction. As a result, an empirical correlation for the overall volumetric mass transfer coefficient of hydrogen was proposed and the reactor concept found potentially suitable for application in industry as highly efficient reactor unit. In a subsequent publication, Müller et al. [67] utilised multiple channels in parallel for scale-up of the SPSR with promising results for the selective hydrogenation of cinnamaldehyde. Reactor performance comparable in regard of reaction rate and selectivity to those achieved in batch reactors could be achieved with the proposed multi-channel pellet string reactor, if the liquid velocities were chosen high enough. In their most recent work, Müller et al. [15] investigated the transition from batch to continuous operation of the hydrogenation for the synthesis of diacetone-D-allose using cylindrical catalyst particles in SPSRs with aspect ratios of  $D/d < 1.7$  in concurrent downflow. Beside the high selectivity they pointed out the need of very long beds in order to reach full conversion.

Further work on two-phase flow was published by Kallinikos and Papayannakos [68] showing that the hydrodesulphurisation of the heavy gas oil fraction using a spiral reactor, a diluted bed and a pilot plant lead to similar results, when properly designed. All three reactor types were filled with a commercial catalyst extrudate. The diameter aspect ratio between the confining wall of the spiral reactor and the catalyst extrudates was  $D/d = 1.75$ . Increasing the fluid velocity generally improved reactor performance.

A strategy to improve the isothermal properties of catalytic fixed beds lies in the addition of small inert particles to the catalytic bed. This also avoids wall effects and hence improves plug flow behaviour [7], which brings it into the focus regarding SPSRs. The influence of this dilution as well as of the distribution of catalytic and inert particles on conversion has been investigated with a stochastic model by van den Bleek et al. [69] in the late 1960s. Sie [36] in his paper on reactor miniaturisation put forward the need of adding fine particles in small beds of relatively large industrial catalyst pellets to improve the flow hydrodynamics under trickle-flow operation. The surrounding inert fines are decisive to achieve near plug-flow behaviour while the chemical conversion is dictated by the actual size of the catalytic pellets. Berger et al. [70, 71] re-evaluate the influence of dilution on gas-solid reactions in fixed-bed reactors by experimental studies on the catalytic decomposition of nitrous oxide, an irreversible first order reaction, as well as using a random particle distribution model. For systems with positive reaction order and keeping the space time constant, they concluded a negative effect on conversion by bed dilution with inert fines as a result of local bypassing and improper mixing. A criterion for the maximum dilution in regards of the deviation to plug flow conversion was proposed. Moonen et al. [5] tested the performance of a hydrodesulphurisation catalyst for gas oil in SPSR set-ups, with a tube

---

diameter about the size of the catalytic extrudate diameter, and within bench-scale fixed-bed reactors. In some of the single pellet string configurations and the bench-scale reactor set-ups the catalytic bed was diluted with non-porous inert fines. The two-phase flow was directed upwards in the bench-scale reactor and downwards in the SPSRs. The results showed a high reproducibility for the SPSR set-ups and revealed comparable sulphur levels for the investigated SPSR and bench-scale configurations. An improvement of the plug flow behaviour was observed when adding the fines and near plug flow behaviour could be confirmed for the SPSRs with inert material around the catalytic particles. In contrast to Berger et al. [70, 71], it was argued that the addition of inert fines reduced catalyst bypassing. Also, flow behaviour was observed to be closer to plug flow for longer beds and higher liquid hourly space velocities.

The presented literature indicates a continuous interest in the SPSR concept, with a significant increase in research activities in recent years and first indications that it may well be the reactor of choice for catalyst testing under industrial conditions. However, a thorough characterisation of the flow behaviour in this type of reactor is required, indicating its deviation to ideal plug flow behaviour. As part of this work, focussing on the investigation of fixed-bed reactors by means of numerical simulation, an attempt is made to systematically characterise the behaviour of SPSRs composed of spherical, non-porous catalytic pellets within cylindrical confining walls using computational fluid dynamics (CFD), which has been proposed by Dixon and Nijemeisland [72] as a suitable design tool for fixed-bed reactors. In contrast to Scott et al. [4], the reactor set-ups are not restricted to diameter aspect ratios between tube wall and pellet diameter below 1.4 but to a ratio of  $D/d < 2$ , that is, to reactor set-ups where there are always less than two particles within one radial cross section of the reactor.

In Chapter 7 a first parameter study is presented assuming isothermal reactor operation, investigating the effect of reactor geometry, fluid properties and reactant concentration whilst keeping the space time, defined here as ratio of fluid volume across the catalytic bed to the volumetric flow rate, through the reactors constant. The residence time behaviour of a non-diffusive tracer as well as the conversion of a hypothetical first order irreversible gas-phase reaction at the pellet surface, which is considered both isochoric and isothermal, are evaluated and compared to corresponding plug flow results. The obtained results are used to assess the applicability of common design criteria for fixed-bed reactors to SPSR set-ups and derive a design criterion that indicates the deviation of a SPSR set-up to ideal plug flow conversion based only on a priori known values. The pressure drop in the considered SPSR scenarios is thoroughly discussed in Chapter 8, leading to a modified Ergun-like equation for pressure loss predictions. Finally, the characterisation of SPSRs is extended to nonisothermal scenarios in Chapter 9. The chosen systematic approach of analysing numerous SPSR scenarios with variation in the reactor set-up, the fluid and catalyst material properties, as well as the properties of the heterogeneously catalysed reaction taking place

at the surface of the catalyst pellets allows for a thorough characterisation of this special type of fixed-bed reactor. Based on the simulation results, novel design criteria explicitly for SPSRs are proposed together with a modified pressure loss equation that takes into account the special geometrical set-up of this type of reactor.



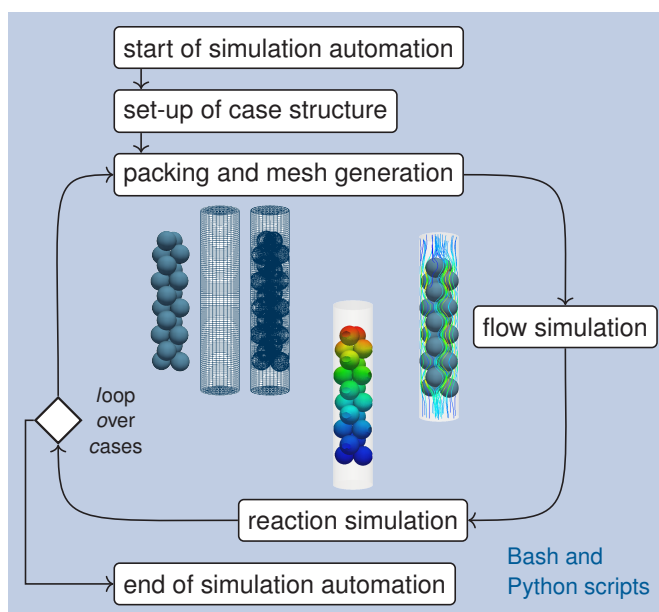
# 4 Scripting as an approach to automated CFD simulation for packed bed catalytic reactor modelling

This chapter was published in a similar form and is reprinted with kind permission from: J. Fernengel, F. Habla and O. Hinrichsen, Scripting as an approach to automated CFD simulation for packed bed catalytic reactor modeling, *Chem. Ing. Tech.* **2018**, *90*, 685–689, DOI 10.1002/cite.201700153. [73]

Copyright 2018 WILEY-VCH Verlag GmbH & Co. KGaA.

## Publication summary

In recent years computational fluid dynamics (CFD) has become a widely applied tool for the simulation of catalytic fixed-bed reactors and numerous authors have contributed towards methods for random packed bed generation and flow simulation. Our approach focuses on an automated simulation routine realized through Bash and Python scripting covering multiple entire simulation runs including preprocessing, simulation as well as post-processing based on open-source software. As an example, the presented routine is demonstrated with a case study on catalytic fixed-bed reactors.



## CRediT author statement

*Johanna Fernengel*: Conceptualisation, Methodology, Software, Formal analysis, Investigation, Visualisation, Writing - Original Draft.

*Florian Habla*: Conceptualisation, Supervision.

*Olaf Hinrichsen*: Project administration, Supervision, Funding acquisition, Writing - Review & Editing.

## Permission/License information



My Orders    My Library    My Profile    Welcome johanna.fernengel.tum@gmail.com    Log out | Help | FAQ

My Orders > Orders > All Orders

### License Details

This Agreement between Mrs. Johanna Fernengel ("You") and John Wiley and Sons ("John Wiley and Sons") consists of your license details and the terms and conditions provided by John Wiley and Sons and Copyright Clearance Center.

[Print](#)   [Copy](#)

License Number	5226561311559
License date	Jan 12, 2022
Licensed Content Publisher	John Wiley and Sons
Licensed Content Publication	Chemie Ingenieur Technik - CIT
Licensed Content Title	Scripting as an Approach to Automated CFD Simulation for Packed Bed Catalytic Reactor Modeling
Licensed Content Author	Olaf Hinrichsen, Florian Habla, Johanna Fernengel
Licensed Content Date	Feb 27, 2018
Licensed Content Volume	90
Licensed Content Issue	5
Licensed Content Pages	5
Type of Use	Dissertation/Thesis
Requestor type	Author of this Wiley article
Format	Print and electronic
Portion	Full article
Will you be translating?	No
Title	From Packing Generation to Single Pellet String Reactor Characteristics: A Numerical Approach to Fixed-Bed Reactors
Institution name	Technical University of Munich
Expected presentation date	Jan 2022
Requestor Location	Mrs. Johanna Fernengel Schwalbenstr. 1  München, 81541 Germany Attn: Mrs. Johanna Fernengel EU828007151
Publisher Tax ID	
Total	<b>0.00 EUR</b>

[BACK](#)



## 4.1 Introduction

Due to their outstanding behaviour and constructive simplicity, fixed-bed reactors play a key role in chemical process engineering. Especially for highly endothermic and exothermic reactions reactors with packed beds of low to medium cylinder-to-particle diameter ratios are widely used. Gaining a deeper insight into local phenomena is of major importance in the design of fixed-bed reactors. A powerful method of growing interest is the use of CFD to obtain information on pressure drop and velocity field, where more recent studies also include temperature and concentration profiles.

Calis et al. [64] demonstrated the applicability of predicting the pressure drop and flow profile of packed bed reactors in a cross-sectional tube with very low tube-to-particle diameter ratios ( $D/d$ ) using a packing algorithm leading to densest random packings and CFX 5.3 by comparison with own experimental data. Simulations by Bai et al. [2] using a coupled discrete element method (DEM) and CFD approach with the commercial packages PFC, Gambit and FLUENT 6.1 to predict the pressure drop at turbulent flow conditions in columns with low  $D/d$  randomly filled with spheres or cylindrical particles agreed well with experimental data.

A different approach to packing generation was followed by Atmakidis and Kenig [74] who utilize ballistic deposition in combination with the Monte Carlo method. Flow simulations of water were carried out with CFX 10.0 using periodic boundary conditions and results for voidage and pressure drop were validated with correlations from literature.

To overcome meshing problems encountered at contact points, Eppinger et al. [75] introduced a method of particle flattening to prevent these points. The simulation routine from bed generation with DEM to flow calculation was conducted with STAR-CCM+. Local voidage profiles and pressure drop results for laminar and turbulent flow in packings with low to medium  $D/d$  ratio were in reasonable agreement with literature values.

Wehinger and Kraume [76] expanded previous work with STAR-CCM+ on fixed-bed reactors by including heat transfer and reaction kinetics. Their work together with co-authors on dry reforming of methane [77] shows excellent agreement of numerical results with own experimental data.

Work focusing on heat transfer in pilot-scale fixed-bed tubes with turbulent air flow based on Fluent simulations is presented by Dixon et al. [78] who implement the packing generation using a soft-sphere algorithm, resulting in tighter packings as compared to common approaches based on hard-sphere models. The obtained packing is validated with literature data. Two approaches to contact point modelling are compared and validated with own experimental data for local temperature profiles.

Simulations on the pressure drop in random packed bed adsorbers presented by Haddadi et al. [79] were based on an in-house DEM code for packing generation and OpenFOAM<sup>®</sup> for meshing and flow simulation and validated experimentally.

An open-source based work flow using Blender<sup>™</sup> for packing generation was put forward by

Boccardo et al. [80]. Mesh generation and laminar flow simulation of water through random packed beds of spheres and cylinders were conducted with OpenFOAM<sup>®</sup> and pressure drop results were in agreement with the Ergun equation.

An aspect common to the reviewed numerical investigations on random packed beds is the structure of the applied simulation routine. At first, the particle positions in the bed are determined followed by some specification of the confining walls. Based on these, a mesh for the subsequent flow simulation has to be generated. In addition to flow simulation, heat transfer and chemical reactions may be considered. The corresponding workload may be embedded in an automated process as is the case when using STAR-CCM+ [75] or can be tackled by means of scripts as reported by Bai et al. [81] for the steps leading from DEM results to mesh generation and by Haddadi et al. [79] for post-processing with ParaView<sup>®</sup>. Also, almost always multiple simulation runs are performed for a stated problem. This implies tedious and time-consuming case set-up typically with a lot of repetition work and little variation to the files.

In this study an automation strategy covering multiple entire simulation runs including pre-processing with parameter variation, geometry set-up and mesh generation, cold-flow and reaction simulation as well as post-processing is developed based solely on open-source software. The random packing is generated with Blender<sup>™</sup> 2.76b [10], mesh generation and simulation are performed with OpenFOAM<sup>®</sup> v2.4.0 [24] whereas ParaView<sup>®</sup> 4.1.0 [82] is used for data analysis and visualization. Whereas part of the used methodology is clearly in accordance with Boccardo et al. [80], the focus here is on the automation of the described routine, explicitly including parameter variations as starting point of individual simulation runs within one routine. Also, a heterogeneous reaction at the catalytic pellet surface is considered in addition. The use of the presented simulation automation is demonstrated with a case study covering three catalytic fixed-bed reactors with low to moderate  $D/d$ .

## 4.2 Methodology

In order to automate an entire simulation routine covering multiple simulation runs including parameter variations, Bash and Python scripts were used. Software packages were integrated via scripting interfaces and a high level of parameterisation within the base files enabled easy parameter variation.

Figure 4.1 shows the structure of the resulting routine. The proposed automated simulation routine consists of four main sections, starting with the set-up of a case structure for the simulation files, followed by a loop over three blocks accounting for the actual simulation-run including packing and mesh generation, flow simulation and reaction simulation. A Bash script was utilized to execute these individual steps. In addition, Python scripts were used

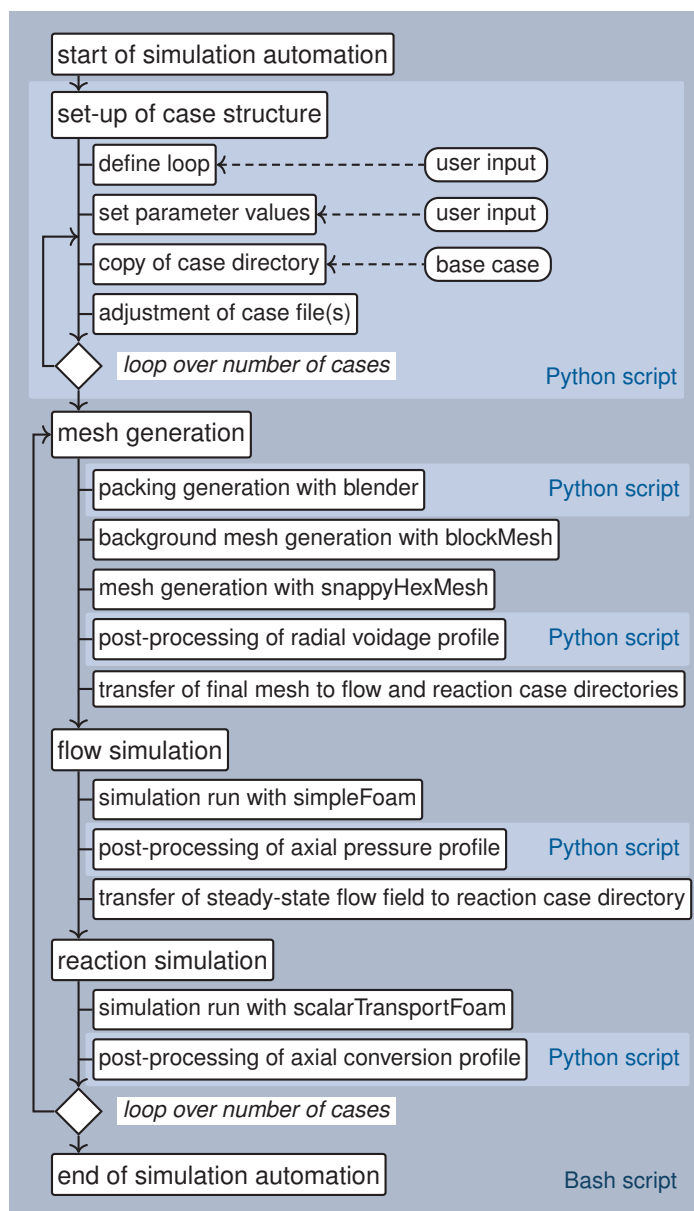


**Figure 4.1:** Flow chart of automated simulation routine.

to perform file manipulations as well as for packing generation with Blender™ and post-processing tasks involving ParaView® functionality.

Since OpenFOAM® cases have a distinctive directory and file structure, a base case directory was set up a priori containing standard files in appropriate directory structure including information on case geometry, parameter values, initial and boundary conditions as well as solver and discretisation settings. Where applicable the base files have been parametrized to a high extend to allow for automated parameter variation.

User input is required prior to starting the simulation routine, defining the number of simulation runs and corresponding sets of parameters. With this information the case structure is set up by means of a Python script in the first step of the routine. For each simulation a directory with unique case name is created by copying and modifying the base case directory according to user input.

Next, a loop over the number of cases is entered which starts with packing and mesh generation. As proposed by Boccardo et al. [80], the individual particle positions within the random packed beds are determined using the open-source animation software Blender™, relying on a rigid-body approach integrated through the Bullet physics library [83]. Based on Blender's Python interface and extensive scripting functionality, packing generation is carried out by a Python script, which is part of the base case and updated according to user input in the very first step of the simulation routine. This file contains information on material properties and rigid-body settings such as friction and restitution, geometry information on particles and confining walls as well as the actual particle deposition and export of the particle surface geometry of the final packing in stereolithographic format. A corresponding cylindrical background mesh with an inlet and outlet length of one particle diameter is set up as a hexahedral mesh with blockMesh. As depicted in Figure 4.2 the final mesh of the flow domain is then obtained from the background mesh, resembling the reactor geometry, and the particle surface geometry of the packing using snappyHexMesh. A Python script with ParaView® functionality is applied to extract data for a radial voidage profile. The mesh generation step ends with transferring the mesh to the case directories for flow and reaction simulation.

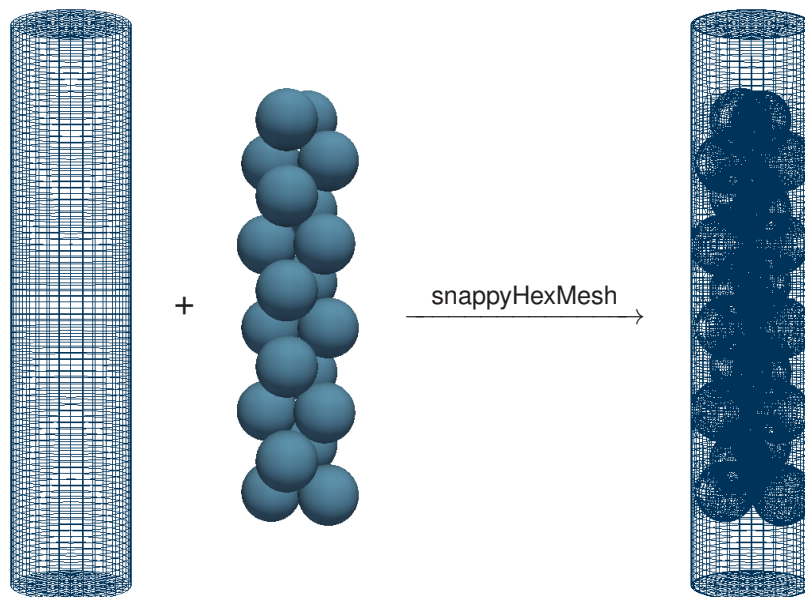


**Figure 4.2:** Principle of mesh generation from hexahedral background mesh and surface with snappyHexMesh, shown for packed bed of spheres in cylindrical confined walls.

Following in the routine are the simulation of the flow field and the subsequent reaction simulation. These are treated separately, assuming that the flow is independent of the reaction. The cold-flow is simulated using simpleFoam, a standard OpenFOAM® steady-state solver. Once the flow simulation has converged within defined residuals, data for an axial pressure profile is extracted and processed by means of a Python script. The obtained flow field inside the packed bed is then transferred to the case directory for reaction simulation.

```
#!/opt/paraviewopenfoam410/bin/pvpython
...
calc = Calculator(Input = packing, ResultsArrayName = radius,
    Function = sqrt(coordsX^2 + coordsY^2))
...
contour = Contour(Input = calc, ContourBy = [POINTS, radius],
    Isosurfaces = [radius])
...
// loop over radii
cylinderArea = 2*radius*math.pi*packingHeight
Contour.Isosurfaces = [radius]
I = IntegrateVariables(contour)
...
porosity = contourArea/cylinderArea
```

**Figure 4.3:** Excerpt of Python script for local voidage evaluation using ParaView<sup>®</sup> functionality.

In the final step an irreversible first order reaction is considered. For species concentration a convection-diffusion equation is solved, using the OpenFOAM<sup>®</sup> solver `scalarTransportFoam` where the reaction is implemented as custom Neumann type boundary condition on the pellet surface as suggested by Maestri and Cuoci [84]. The amount of product formation is directly related to the depletion of reactant on the pellet surface which is, in turn, related to the transport of reactant to the surface by convection and diffusion. By using this simplified approach, the reactions are limited to isovolumetric and isothermal scenarios. When a converged solution has been reached, data is extracted for evaluating axial conversion along the reactor by means of a Python script. This completes the loop for a given case and the simulation routine proceeds with the next or reaches the end.

Details on the radial voidage profile evaluation are given as an example of Python based post-processing with ParaView<sup>®</sup> functionality. The final mesh is reduced in length whereby sections with a height of three times the particle diameter at the bottom and twice the particle diameter at the top of the backed bed are omitted to exclude the ordered bed at the bottom and incomplete layers of particles on top of the packing respectively. The resulting domain is cut into isosurfaces at various radii using ParaView<sup>®</sup>'s contour filter. Setting the area of such isosurfaces into relation to the total area of a corresponding open cylinder gives a measure of voidage. An excerpt of the Python script is shown in Figure 4.3.

The axial pressure and conversion profiles are generated using area-averaged values on slices perpendicular to the reactor length axis.

## 4.3 Case study

### 4.3.1 Set-up

To demonstrate the use of the presented simulation automation, a case study covering three catalytic fixed-bed reactors composed of monosized spherical particles with a diameter of

1 mm in cylindrical confined walls with low to moderate cylinder-to-particle diameter ratios, namely  $D/d = 2, 7.35$  and  $8.41$ , was conducted. The number of catalytic particles was 20 for the first case and 2000 for the remaining cases. Values for the coefficients of friction and restitution were set to 0.3 for packing generation. To obtain the computational mesh of the flow domain a hexahedral background mesh with cylindrical geometry is combined with the packing geometry (compare Figure 4.2). A single phase gas flow with the properties of air at normal temperature and pressure (NTP) was chosen and the uniform inlet velocity adjusted such that a bed Reynolds number of  $Re_{bed} = 1$ , corresponding to laminar flow [85], was achieved. Standard no-slip boundary conditions were used at the cylinder wall and the pellet surface. The pressure at the reactor outlet was set to ambient. The 3-dimensional flow is simulated by evaluating the momentum and continuity equations for an incompressible fluid at steady-state using second-order discretization schemes. An isothermal, isovolumetric, irreversible first order reaction  $A \rightarrow B$  was considered at the catalytic pellet surface with a reaction rate coefficient corresponding to 80% conversion in a comparable plug flow reactor. Species diffusion in the fluid was approximated with the self-diffusion coefficient of nitrogen.

### 4.3.2 Results

With the appropriate user input the simulation routine as outlined in Figure 4.1 was called once and the desired tasks performed accordingly for all three cases. The packing geometry obtained from particle deposition by the rigid-body approach is shown exemplary for the reactor with  $D/d = 2$  in Figure 4.4a, which reveals a repeating pattern with particle positions close to analytical positions for a regular packing with similar diameter ratio. As expected, the corresponding radial voidage profile displayed in Figure 4.5 is in excellent agreement with the analytical solution presented by Govindarao et al. [58]. Results for the radial voidage of the two packed beds with larger  $D/d$  shown in the same figure are well in line with experimental results from Goodling et al. [86]. Numerical values of the mean bed voidage and the packing height related to the particle diameter are given in Table 4.1. Streamlines of the flow across the reactor are exemplarily illustrated for  $D/d = 2$  in Figure 4.4b.

**Table 4.1:** Results of fixed bed reactor simulations.

	$D/d = 2.0$	$D/d = 7.35$	$D/d = 8.41$
bed height-to-pellet diameter ratio, $H/d$ / –	8.3	42.9	33.8
bed voidage excl. inlet and outlet sections, $\varepsilon$ / –	0.54	0.4036	0.4043
overall conversion, $X$ / –	0.687	0.760	0.757

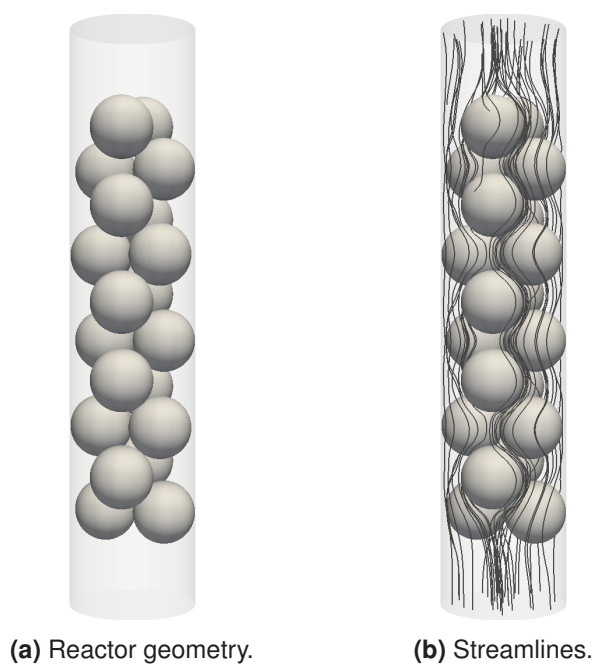


**Figure 4.4:** Packing geometry and flow hydrodynamics for packed bed with  $D/d = 2$ .

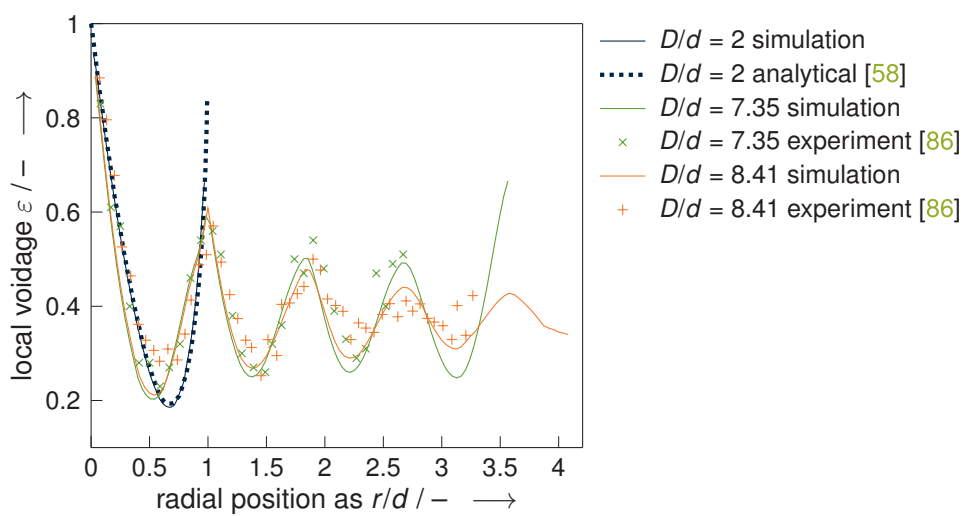


**Figure 4.5:** Radial voidage profiles for packed beds with  $D/d = 2$ , 7.35 and 8.41.



Pressure and conversion results along the reactor axis are given in Figure 4.6. The pressure across the reactor shows a general linear decrease as expected, where the particle layers are visible for the case with  $D/d = 2$ . The overall conversion remains below ideal plug flow conversion with considerably higher values for the packed beds with larger  $D/d$  (refer to Table 4.1 for numerical values). Keeping the bed Reynolds number constant at constant catalytic surface area for the latter two cases results in a significantly longer space time for the reactor with  $D/d = 7.35$  as compared to the case with  $D/d = 8.41$  which may explain the lower conversion in the last case.

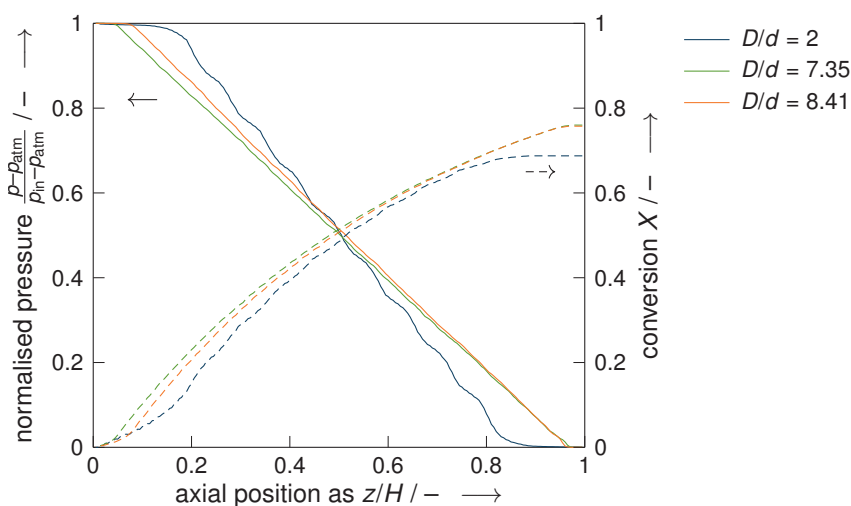


**Figure 4.6:** Area averaged pressure and conversion profiles along the reactor length axis for packed beds with  $D/d = 2, 7.35$  and  $8.41$ .

## 4.4 Conclusion

In this study we presented an automation strategy covering multiple CFD simulations including preprocessing with parameter variation, geometry set-up and mesh generation, cold-flow and reaction simulation as well as post-processing based solely on open-source software. The applicability of the proposed method was demonstrated with a case study covering three catalytic fixed-bed reactors. Our approach transfers the simulation automation known from commercial software to open-source CFD while at the same time including an extensive parameter variation functionality across numerous individual simulation runs. The flexibility of Bash and Python scripting allows for easy adaptability of the proposed routine by including and arranging various simulation components. This provides a convenient framework allowing for time saving and productivity gain in executing open-source CFD studies.

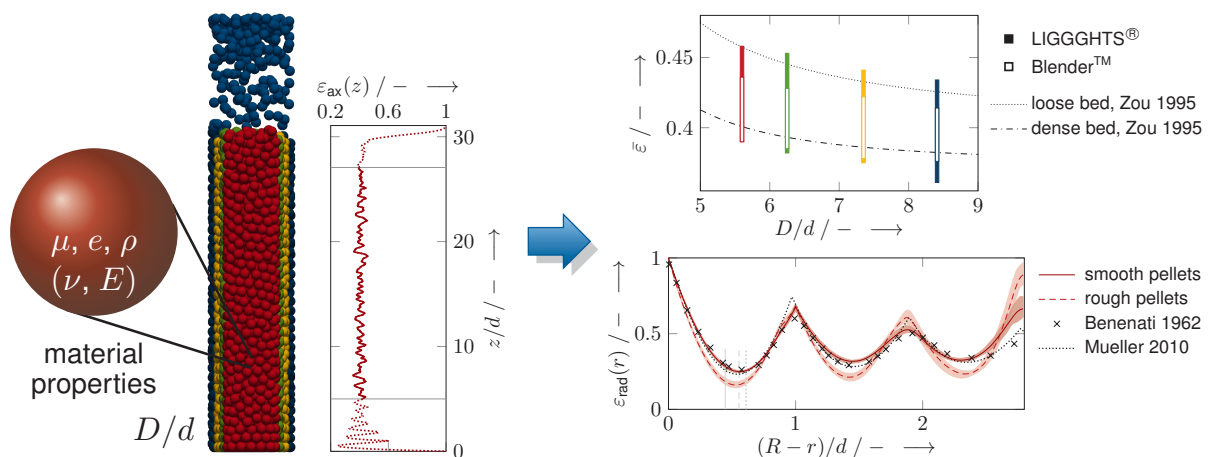


# 5 Influence of material properties on numerically generated random packed beds

This chapter was published in a similar form and is reprinted with kind permission from: J. Fernengel and O. Hinrichsen, Influence of material properties on voidage of numerically generated random packed beds, *Chem. Eng. Sci.* **2021**, *233*, 116406, DOI 10.1016/j.ces.2020.116406. [87]. Copyright 2020 Elsevier Ltd.

## Publication summary

Numerical studies on random packed beds require information on pellet arrangement. Often, the packing structure is taken for granted and not given much attention. This study presents an investigation of the influence of bed height ( $17 < H/d < 164$ ), pellet insertion height ( $40d, 200d$ ) and material properties such as friction ( $0 \leq \mu \leq 1.1$ ) and restitution ( $0.1 \leq e \leq 0.9$ ) on the resulting voidage of beds of spheres in cylindrical containers with diameter aspect ratios of  $5.6 \leq D/d \leq 8.41$ , numerically generated using LIGGGHTS<sup>®</sup> and Blender<sup>™</sup>. The results reveal a wide range of obtained arrangements from loose to dense packings, emphasising the importance of parameter settings in numerical packing generation as the bed structure may have a significant influence, particularly on fluid flow and heat transfer. Though limited to spherical pellets, it is anticipated that the observed trends hold for other pellet and wall geometries.



### CRediT author statement

*Johanna Fernengel*: Conceptualisation, Methodology, Software, Validation, Formal analysis, Investigation, Visualisation, Writing - Original Draft.

*Olaf Hinrichsen*: Project administration, Supervision, Funding acquisition, Writing - Review & Editing.

### Permission/License information

The screenshot shows the RightsLink interface for the article "Influence of material properties on voidage of numerically generated random packed beds". The interface includes a navigation bar with "Home", "Help", and "Live Chat" options, and a user profile for "Johanna Fernengel". The article details section lists the author as Johanna Fernengel and Olaf Hinrichsen, the publication as Chemical Engineering Science, the publisher as Elsevier, and the date as 6 April 2021. Below this, the "Journal Author Rights" section provides a disclaimer and a link to Elsevier's policy page. At the bottom, there are "BACK" and "CLOSE WINDOW" buttons, and a footer with copyright information for the Copyright Clearance Center, Inc.

**CCC | RightsLink®** Home Help Live Chat Johanna Fernengel

**Chemical Engineering Science** Influence of material properties on voidage of numerically generated random packed beds  
Author: Johanna Fernengel, Olaf Hinrichsen  
Publication: Chemical Engineering Science  
Publisher: Elsevier  
Date: 6 April 2021  
© 2020 Elsevier Ltd. All rights reserved.

**Journal Author Rights**  
Please note that, as the author of this Elsevier article, you retain the right to include it in a thesis or dissertation, provided it is not published commercially. Permission is not required, but please ensure that you reference the journal as the original source. For more information on this and on your other retained rights, please visit: <https://www.elsevier.com/about/our-business/policies/copyright#Author-rights>

BACK CLOSE WINDOW

© 2022 Copyright - All Rights Reserved | Copyright Clearance Center, Inc. | Privacy statement | Terms and Conditions  
Comments? We would like to hear from you. E-mail us at [customer-care@copyright.com](mailto:customer-care@copyright.com)

## 5.1 Introduction

Computational fluid dynamics (CFD) simulations have become a widely accepted tool for modelling fixed bed reactors [19, 72, 88] and the number of publications on CFD studies involving random packed beds has been increasing rapidly over the last years, covering topics from flow hydrodynamics and pressure drop behaviour [64, 74, 81, 89–92], to heat transfer problems [93–95] and investigations of reactive packings [77, 84, 96–98]. Other works include contributions on thermal radiation in fixed-bed reactors [99], in packed pebble-bed nuclear reactors [100] and in the field of environmental engineering for groundwater remediation [101–103]. However, little attention is paid to the underlying packing although it may entail significant errors in flow hydrodynamics and therefore also on the results of the subsequent and, to most authors, main research question. Therefore, it is of genuine importance to thoroughly examine the influence factors in the numerical generation of random packings. The general need for more detailed information on packing arrangement and the flow through fixed beds was already demanded by Froment in the early 1970s [2] and especially the interest in numerical packing generation renewed recently by Jurtz et al. [19] in the light of increasing popularity of reactor modelling.

Earlier experimental work on random packed beds, especially on packings of spheres, identified the cylinder-to-particle diameter ratio, or diameter aspect ratio,  $D/d$  as most influential parameter on bed voidage. Other factors, such as packing mode, particle shape, density, friction and restitution, are indicated in literature [86, 104–114]. Based on investigations of packings of equally sized steel balls, Scott [106] observed two well-defined limits enclosing the range of accessible bed voidage, which he called *dense random packing* and *loose random packing*, where the former was obtained by gently shaking the bed. A reduction of bed voidage with decreasing deposition density, that is the number of pellets in the descending cloud, was observed by Macrae and Gray [107]. The packing modes, depending on the method of formation, were extended by Haughey and Beveridge [113] by *very loose random packing*, obtained by settling of a fluidised bed, and *poured random packing*, where spheres were literally poured into a container rather than rolling into place individually which would result in a *loose random packing*. Allen et al. [115] underlined the influence of the packing method on pellet arrangement also for non-spherical and irregularly shaped pellets. Not only the filling speed but also the height from which the pellets are dropped is of importance, resulting in a reduction of bed voidage with increasing pellet insertion height as described by Macrae and Gray [107].

The effect of the pellet characteristics size and shape on the voidage of random packings was put forth by several authors [113, 116, 117], but shall not be detailed here as they are not explored in this study which is limited to spherical pellets.

A thorough experimental investigation of the significance of material properties on packed beds of spheres was performed by Macrae and Gray [107], indicating a possible influence of

surface friction and resilience. The dependence of pellet resilience, expressed by the coefficient of restitution, on impact velocity may be neglected for low impact velocities [118].

Highly influential, but often ignored, is the effect of bed height. As noted by Zou and Yu [119], a reduction in bed height will reduce the mean voidage of the packing. For better comparison of packings, measures should be taken to eliminate the influence of the less densely packed regions at both ends of a packed bed.

Various authors proposed correlations for the mean voidage of random packed beds as a function of the diameter aspect ratio [114, 119–122]. Experimental investigations by Dixon [114] led to a correlation of mean voidage of moderately loose packings of spheres with diameter aspect ratios of  $1 \leq D/d \leq 10$ , eliminating end effects. Using the deposition method by Scott [106], Zou and Yu [119] proposed a correlation for loose and dense packings based on beds of glass and marble balls, however, excluding height effects. Results obtained by de Klerk [120] for loosely packed columns of glass beads with diameter aspect ratios of  $1.7 \leq D/d \leq 19.3$  were found to be in agreement with an earlier work by Leva and Grummer [123]. Correlations for mean bed voidage including a shape factor were proposed by Benyahia and O'Neill [121] for beds with diameter aspect ratios of  $1.5 \leq D/d \leq 50$  based on experiments with spheres, solid cylinders, hollow cylinders and 4-hole cylinders. Ribeiro et al. [122] presented a voidage correlation for random dense packings of monosized glass beads with diameter aspect ratios of  $2 < D/d < 17$  using either water displacement measurements or by recording the height of the packing of a known number of beads.

Often, mean voidage is used to characterise random packings, however, local values may overrule the expected behaviour. Especially in the vicinity of the confining wall, which restricts the pellet arrangement, high local variations in voidage can be observed. As noted by Zou and Yu [119], the influence of the confining wall on random packings of spheres is twofold, that is the *wall effect* from the side wall as well as that originating from the bottom wall and, if applicable, any top wall, also referred to as *thickness* or *height effect*. Investigations on the effect of the surrounding wall are numerous [58, 86, 105, 109, 110, 124–127], leading to the general agreement that there persists an oscillatory voidage profile starting at a value of one at the confining wall, declining until about half a pellet diameter into the bed before rising again in a similar manner. This pattern is repeated but damped in amplitude further into the bed. Experimental studies on this wall effect include but are not limited to the following works: Investigation of radial voidage variations for beds of spheres with diameter aspect ratios of  $D/d = 8.82$  and  $13.67$  by filling the beds with paraffin and determining the voidage in thin concentric rings from the solidified packing arrangement by Roblee et al. [105], a similar investigation based on pouring spherical lead shots into beds with  $D/d = 2.6, 5.6, 14.1, 20.3$  and infinite large bed diameters by Benenati and Brosilow [109] and results put forth by Goodling et al. [86] based on beds of polystyrene spheres in plastic pipes with  $7.35 \leq D/d \leq 16.77$ . Other techniques include

the water displacement method with a rotating cylinder as performed by Ridgway and Tarbuck [124] for beds with diameter aspect ratios of  $7.62 \leq D/d \leq 19.05$  and bed heights of  $15.24 \leq H/d \leq 38.1$ . Later works based on X-ray radiography led to correlations for radial voidage by Mueller [125] for beds of polished plexiglas spheres with a stainless steel microsphere placed at the centre of each sphere and obtained by pouring with resulting beds of height  $H/d = 7.84$  and diameter aspect ratios of  $D/d = 2.02, 3.96, 5.96$  and  $7.99$  as well as by Suzuki et al. [126] for tapped packings of glass beads. Sederman et al. [127] used magnetic resonance imaging to obtain information on radial voidage in random-loose and random-dense beds of spheres with diameter aspect ratios of  $5.6 \leq D/d \leq 19$ . It should be mentioned that no measures to eliminate height effects are reported explicitly in any of these publications.

A semi-analytical expression for radial voidage in random packed beds of mono-sized spheres in cylindrical containers with diameter aspect ratios  $D/d \geq 2.0$  was proposed by Mueller [128], which compares well with experimental data from literature. However, comparison is only made for near integer values of the diameter aspect ratio.

With an increasing number of numerical investigations in the field of fixed-bed reactors, there is the need to obtain information on pellet arrangement in random packings, preferably other than by transferring information from experiments. The challenge in numerical packing generation lies in the random nature of the pellet arrangement within the bed, where pellet positions cannot be described analytically. Therefore, a number of methods aiming at determining these random positions have emerged, including packing generation based on the Monte Carlo method (cf. [129–132]), sedimentation algorithms where spheres are placed sequentially into a container (cf. [133]), simulations based on the discrete element method (DEM) (cf. [75, 81, 118, 134–137]) as well as more recent approaches with rigid body simulations based on contact dynamics (CD) (cf. [80], [138]). Commercial software packages are available for numerical packing generation, as for example DigiDEM™, STAR-CCM+, EDEM® and PFC™ as well as a number of open-source alternatives, such as Yade, ESyS-Particle, LIGGGHTS® and Blender™.

A thorough numerical investigation of the effect of dynamic variables on packings of spheres with a large diameter aspect ratio of  $D/d = 24$  based on DEM simulations has been published by Zhang et al. [118]. They reported a reduced voidage with increasing dropping height and restitution coefficient as well as an increase in voidage with increasing deposition intensity and increasing coefficient of friction; their results are in line with previous experimental findings by Macrae and Gray [107].

Even though CFD based publications report ever new achievements, we have the impression that the underlying packing generation does not get the necessary attention, given the significant influence that local properties of packed beds may have on reactor performance. Recent publications on different methods of numerical packing generation are available

(cf. for example [80, 88, 139, 140]), however, lacking discussion of the influence of related parameters. Often, reported packings are very short and the observed behaviour governed by higher local voidage related to the height effect. The large number of published radial voidage profiles in literature, as opposed to scarcely shown longitudinal voidage profiles, may be understood as an indication thereof. It appears that the numerical packing itself is seldom the main focus of interest but taken as a necessary means for further investigations.

Within this work we want to raise awareness of the impact of various parameters on the arrangement of random packings by numerical investigation of the influence of packing height, pellet insertion height and material properties on the voidage of beds of spheres in cylindrical confining walls with moderate diameter aspect ratio, where the side wall considerably affects the bed voidage. Four diameter aspect ratios are covered, namely  $D/d = 5.6, 6.25, 7.35$  and  $8.41$ , allowing for comparison with experimental data from literature and from within our research group. Packings are generated using the open-source software packages LIGGGHTS<sup>®</sup> and Blender<sup>™</sup> 2.76b based on DEM and contact dynamics, respectively, with focus on the parameter study rather than the underlying numerical methods which have already been published in detail elsewhere.

This chapter is organised as follows: after a short overview of the applied methodologies details are given on the simulation settings and the case set-up. The results section starts with a discussion of the packing characteristics, i.e. bed height and pellet insertion height, leading to the identification of a set-up that is used in the following parameter study on the influence of material properties on mean voidage and the radial voidage profile. Trigonometric considerations are presented resulting in an improved correlation of the position of the first minimum next to the confining wall in radial voidage profiles as a function of the underlying bed geometry.

## 5.2 Methodology

### 5.2.1 Packing generation

Put simply, random packings are obtained by introducing pellets into a container in which they settle under the influence of gravity. Cundall and Strack [37] proposed a numerical model to describe the mechanical behaviour of this dynamic process, the distinct element method (DEM). It assumes that pellets behave as rigid bodies that act independently unless when in contact. The motion of the individual pellets, linear and angular, is evaluated using the Newton-Euler equations, respectively. When colliding, the pellets are allowed to overlap, where the size of the overlap is related to the contact forces. This method requires a small time increment, during which velocities and accelerations are considered constant and disturbances due to interactions do not propagate any further than the direct neighbouring



pellet. In this work, we use the open-source code LIGGGHTS<sup>®</sup> [22, 141] for numerical packing generation based on DEM. For contacts between pellets as well as pellet contacts with the confining wall the Hertz-Mindlin theory is applied, similar to the work of Li et al. [142], Jahani et al. [143], Das et al. [136] and Gong et al. [144] who simulated sandpiles, industrial banana screens under vibration, random packing generation for slender fixed-beds and fusion reactors, respectively. This implies the evaluation of normal forces during contact based on Hertzian theory and using the theory of Mindlin and Deresiewicz for tangential forces. The interested reader may refer to the paper by Džiugys and Peters [145] for a review on numerical simulation of granular matter and to the work of Renzo and Maio [146] for comparison of contact force models common in DEM. For the critical time step, we have chosen to use 20% of the Rayleigh time (cf. [142]), a parameter associated with energy propagation by Rayleigh waves which is dependent on the material properties of the pellets. Pellets are introduced at random positions across the diameter of the confining tube within a section of twice the pellet diameter in height. To decide whether the bed has come to rest, a threshold on the total kinetic energy of the system is used.

Instead of resolving pellet collisions by allowing overlaps, referred to as *soft contact*, the collisions may be considered by the so called *hard contact* model where contacts are not modelled explicitly but rather the effect of the contact by means of momentum exchange based on the conditions just before collision [147] and under consideration of the Coulomb friction model [148]. This allows larger simulation time steps than the soft contact approach used in classical DEM. The contact dynamics (CD) method is based on work by Jean and Moreau, outlined by the authors in [38, 39] and reviewed in detail by Radjai and Richefeu [149]. Here, we use the functionality of the Bullet physics library [83] within the Blender<sup>™</sup> [23] environment for numerical packing generation, as initially proposed by Boccardo et al. [80] and utilised by Partopour and Dixon [138] as well as Flaischlen and Wehinger [140]. Idazi and Bezuijen [147] also simulated granular systems based on the Bullet physics library [147]. Basically, the work flow for treating contacts consists first of all of detecting possible collisions before handling these based on impulse balances and updating pellet velocities. Pellets are introduced similar to the DEM simulations with LIGGGHTS<sup>®</sup> and a threshold on pellet movement is used to decide whether the bed has come to rest. For details on the background and implementation of physics-based simulations the reader may refer to the text book by Erleben et al. [150].

Based on the different approaches for contact modelling in DEM and CD, the material properties taken into consideration vary. While information on density, surface friction and restitution of the involved materials is required in either case, Poisson's ratio and Young's modulus are only taking into account in case of the soft contact model. It should be noted that the coefficients of friction and restitution are properties depending on the characteristics of the two materials interacting in a collision. While in LIGGGHTS<sup>®</sup> these are defined per collision pair, the settings in Blender<sup>™</sup> are related to each collision partner individually

and the resulting coefficients are evaluated by multiplying the values corresponding to the partners involved in the collision. This was stressed by Flaischlen and Wehinger [140] and could be verified with the Bullet source-code.

For a detailed discussion of the differences between classical DEM and the contact dynamics method, the paper by Lim et al. [151] is highly recommended.

### 5.2.1.1 Simulation settings

Within both software environments, comparable settings are established. Mono-sized, spherical pellets are introduced into a cylindrical container at a rate equivalent to pouring at random positions across the tube diameter within a section of twice the pellet height.

The pellets are initially at rest and accelerate due to gravity with  $g = 9.81 \text{ m s}^{-2}$ . For each data point, ten simulation runs are performed to account for the influence of randomness on pellet insertion. The time step  $\Delta t$  is set to a value of 20% of the Rayleigh time in case of DEM simulations with LIGGGHTS<sup>®</sup>, which can be expressed by

$$\Delta t_{\text{DEM}} = 0.2 \frac{\pi r}{0.8766 + 0.163\nu} \sqrt{2\rho \frac{1 + \nu}{E}} \quad (5.1)$$

based on the pellet radius  $r$  as well as its material properties, namely density  $\rho$ , Poisson's ratio  $\nu$  and Young's modulus  $E$ . For simulations based on CD with Blender<sup>™</sup> the time step was set to

$$\Delta t_{\text{CD}} = \frac{1 \text{ s}}{40 \text{ m}} d \quad (5.2)$$

as a compromise between simulation time and accuracy revealed in a pre-study, where  $d$  is the pellet diameter. Simulations are stopped when the bed is at rest, which is determined by a threshold on the total kinetic energy within the packing in LIGGGHTS<sup>®</sup>, set to a value of  $1 \cdot 10^{-8} \text{ J}$ . For simulations with Blender<sup>™</sup> a threshold on the maximum pellet movement between two time steps is implemented with a value of  $1 \cdot 10^{-5} \text{ m}$ , equivalent to  $d/400$ . However, the latter may not always be reached for very smooth (no surface friction) or bouncy (high restitution coefficient) pellets in which case the simulations are stopped after 1000, 1000, 2000 and 4000 time steps for beds with diameter aspect ratios of  $D/d = 5.6$ , 6.25, 7.35 and 8.41, respectively. In these cases, individual pellets at the top of the bed or within cavities were found responsible for missing the set criterion on pellet movement. The simulation frames related to the second stopping criterion were set based on tracking the maximum pellet movement as well as the bed height making sure that no further changes were to be expected when continuing the simulations and thus no significant influences thereof are expected on the final bed.



The material properties of the pellets as well as of the outer confining wall, consisting of a cylindrical tube closed at the bottom by a horizontal plane, are set to the same values.

In Blender™ a number of settings related to the rigid body simulation have to be specified. The pellets, depicted by ico-spheres with five subdivisions, are simulated as *active* rigid bodies of type *dynamic*, implying that their position is controlled by the simulation, whereas the outer confining wall is treated as *active* but not dynamic, as it is to remain fixed in position. The mass of the objects is set according to the specified density. Pellets are treated as spherical objects, assigning the predefined primitive shape *sphere*, which speeds up Bullet's collision algorithm [83, 152]. The collision shape of the outer cylinder and the bottom plane are of type *mesh*, specifying that no changes are considered to the *base* mesh during simulation. As stressed by Fleischlen and Wehinger [140], *friction* and *bounciness* factors are set to the square root of the coefficients of friction and restitution of the two collision partners, respectively. The *collision margin*, defining a possible gap to be left between colliding objects, has to be set to zero in order to obtain realistic packings (cf. Partopour and Dixon [138]). Further, Blender™ allows for *damping of translational* and *rotational* motion of objects, independent of losses during collisions. We understand these parameters as means to apply a drag force originating from interaction with the surrounding fluid. For the sake of comparability with the DEM based simulations with LIGGGHTS®, which do not account for any influence of a surrounding fluid, these are explicitly set to zero, in contrast to a recent publication by Wehinger and Fleischlen [99] who stick to the non-zero standard settings.

### 5.2.2 Evaluation of voidage

The resulting random packings are analysed with respect to local voidage and mean bed voidage. In general, voidage is defined as the ratio of the empty volume between the pellets within a packing to the overall volume enclosed by the outer confining wall over the height of the considered section of the bed. This may be expressed as

$$\bar{\varepsilon} = \frac{V_{\text{void}}}{V_{\text{total}}} = 1 - \frac{V_{\text{solid}}}{V_{\text{total}}} \quad (5.3)$$

where  $V_{\text{void}}$  is the empty, or void, volume between the pellets,  $V_{\text{solid}}$  the joint volume of all pellets and  $V_{\text{total}}$  the total bed volume including pellet volume and the void spaces between the pellets.

To determine local voidage profiles in the longitudinal direction of the bed, Equation (5.3) is applied but limiting the considered bed height to small increments of  $d/100$ . The solid volume in such a slice of the bed is calculated based on the contained pellet segments, using the pellet centre points and radii, whereas the total volume corresponds to the cylinder defined by the diameter of the outer confining wall and the increment in height. A Python

script was used to perform the algorithm for evaluating the longitudinal voidage profile using information on the pellet arrangement of the generated random packed beds.

For evaluation of radial voidage profiles, the approach by Mueller [153] using arc lengths to obtain axially averaged voidage values as a function of radial position is applied. There, the local radial voidage is given by

$$\varepsilon_{\text{rad}}(r) = 1 - \frac{s_{\text{solid}}}{s_{\text{total}}} \quad (5.4)$$

where  $s_{\text{total}}$  is the arc length to radius  $r$  and  $s_{\text{solid}}$  the length thereof, that is occupied by pellets. The arc length intersecting with pellets is determined analytically based on the pellets' centre coordinates and radii. The FORTRAN programme put forth by Mueller [153] has been translated to a Python script, setting longitudinal and radial increments to  $d/100$ .

Mean bed voidages can also be calculated as averages of the local voidage profiles by

$$\bar{\varepsilon} = \frac{\sum_{i=0}^n \varepsilon_{\text{ax},i}}{n} \quad (5.5)$$

where  $\varepsilon_{\text{ax},i}$  is the local axial voidage averaged over the cross section of the  $i^{\text{th}}$  slice of the bed and  $n$  the total number of slices of equal thickness as well as by

$$\bar{\varepsilon} = \frac{\sum_{r=0}^R \varepsilon_{\text{rad}}(r) \cdot r}{\sum_{r=0}^R r} \quad (5.6)$$

based on  $\varepsilon_{\text{rad}}(r)$ , the local radial voidage averaged over the bed length at radial position  $r$ , and weighted by the latter.

## 5.3 Case set-up

The aim of the presented parameter study is twofold, starting with an investigation of the influence of packing characteristics such as packing height, pellet insertion height and height effects on bed voidage to identify settings which allow for an unbiased analysis of the influence of material properties. For both, the pellet insertion rate is modelled equivalent to pouring.

### 5.3.1 Investigation of packing characteristics

To start with, packings with a diameter aspect ratio of  $D/d = 8.41$  are generated using LIGGGHTS<sup>®</sup> with varying number of pellets. The corresponding settings and material properties are provided in Table 5.1. The insertion height  $H_{\text{ins}}$  is adjusted for each scenario such that the pellets are introduced shortly above the expected packing height. Based on

**Table 5.1:** Parameter settings for evaluation of packing characteristics; simulations with LIGGGHTS® only.

pellet diameter, $d$	4 mm
diameter aspect ratio, $D/d$	8.41
number of pellets, $N$	1000, 2000, 3000, 4000, 5000, 6000, 8000 and 10 000
insertion height, $H_{\text{ins}}$	variable acc. to Equation (5.8) or fixed at $165d$
coefficient of friction, $\mu$	0.7
coefficient of restitution, $e$	0.5
density, $\rho$	$8000 \text{ kg m}^{-3}$
Young's modulus, $E$	200 GPa
Poisson's ratio, $\nu$	0.3

the correlation by Benyahia and O'Neill [121] for the mean bed voidage  $\bar{\epsilon}$  as a function of the diameter aspect ratio  $D/d$ , expressed as

$$\bar{\epsilon}_{\text{BON}} = 0.390 + \frac{1.740}{(D/d + 1.140)^2}, \quad (5.7)$$

together with the definition of voidage given in Equation (5.3) and considering an off-set of five pellet diameters on top of the expected bed height, rounded up to the next integer the insertion height amounts to

$$\frac{H_{\text{ins}}}{d} = \left\lceil \frac{2}{3} N \frac{d^2}{D^2} \frac{1}{1 - \bar{\epsilon}_{\text{BON}}} \right\rceil + 5 \quad (5.8)$$

where  $N$  is the number of pellets,  $d$  the pellet diameter and  $D$  the tube diameter. The insertion section has a height of  $2d$ , extending from the calculated insertion height upwards. Pellets are continuously inserted within this section such that the voidage amounts to 0.7, i.e. 30% of the volume is occupied by inserted pellets. This is considered equivalent to pouring, with multiple pellets added to the cylindrical container at a time rather than the subsequent addition of individual pellets. The specified value of 30% of the volume taken by pellets is a result of initial investigations, ensuring a fixed and comparable insertion rate for the investigated diameter aspect ratios. Faster addition could not be reliably maintained as pellets are only introduced if there is no overlap with neighbouring pellets.

In a second set of scenarios the insertion height is kept constant at the level corresponding to the maximum number of considered pellets.

### 5.3.2 Parameter study on material properties

The parameter settings used for evaluating the influence of material properties on bed voidage are provided in Table 5.2, where simulations are performed with both LIGGGHTS® and Blender™. The number of pellets is fixed to yield a resulting bed height of approximately

**Table 5.2:** Parameter settings for variation of material properties, default values highlighted in bold.

parameter	LIGGGHTS <sup>®</sup>	Blender <sup>™</sup>
pellet diameter, $d$		4 mm
diameter aspect ratio, $D/d$	5.6, 6.25, 7.35 and 8.41	
number of pellets, $N$	812, 1020, 1430 and 1891	
insertion height, $H_{\text{ins}}$		$40d$ and $200d$
coefficient of friction, $\mu$	0, 0.1, 0.3, 0.5, <b>0.7</b> , 0.9 and 1.1	
coefficient of restitution, $e$	0.1, 0.3, <b>0.5</b> , 0.7 and 0.9	
density, $\rho$	1000, 3000, 5000, <b>8000</b> and 10 000 kg m <sup>-3</sup>	
Young's modulus, $E$	1, 10, 100 and <b>200</b> GPa	-
Poisson's ratio, $\nu$	0.2, <b>0.3</b> , 0.4 and 0.5	-

$30d$  and pellets are inserted from two different heights, namely  $40d$  and  $200d$ . As before, the pellet insertion rate is specified such that the voidage amounts to 0.7 within the insertion section. Variations of the material properties include coefficients of friction between zero and 1.1 as well as coefficients of restitution between 0.1 and 0.9, where a value of *zero* would correspond to a perfectly inelastic collision and a value of *one* to a perfectly elastic collision. The density is reduced down to 1000 kg m<sup>-3</sup> resembling light materials such as wood and increased up to 10 000 kg m<sup>-3</sup> representing metals. Young's modulus and Poisson's ratio are only taken into account in the DEM simulations with LIGGGHTS<sup>®</sup>. The lower end considered for Young's modulus of 1 GPa is in the range of polymer plastics and the upper end with 200 GPa related to steel. The range of investigated Poisson's ratios corresponds to isotropic materials [154]; the value of the base case of 0.3 may generally be used for metals [155].

Unless explicitly stated otherwise, only one parameter is varied at a time while the remaining parameter settings are kept to the base case settings equivalent to the material properties provided in Table 5.1 with a coefficient of friction of  $\mu = 0.7$ , a coefficient of restitution of  $e = 0.5$ , a density of  $\rho = 8000$  kg m<sup>-3</sup> and for simulations with LIGGGHTS<sup>®</sup> a value of the Young's modulus of  $E = 200$  GPa and a Poisson's ratio of  $\nu = 0.3$ .

## 5.4 Results and discussion

### 5.4.1 Packing characteristics

To start with, a simulation set-up has to be established which allows for an unbiased comparison of the subsequent parameter study on the influence of material properties on pellet arrangement in random packed beds and the resulting mean bed voidage. Especially, this requires an understanding of the influence of bed height. Figure 5.1a depicts a side-view of a packing obtained by numerically placing 1000 spherical pellets into a cylindrical

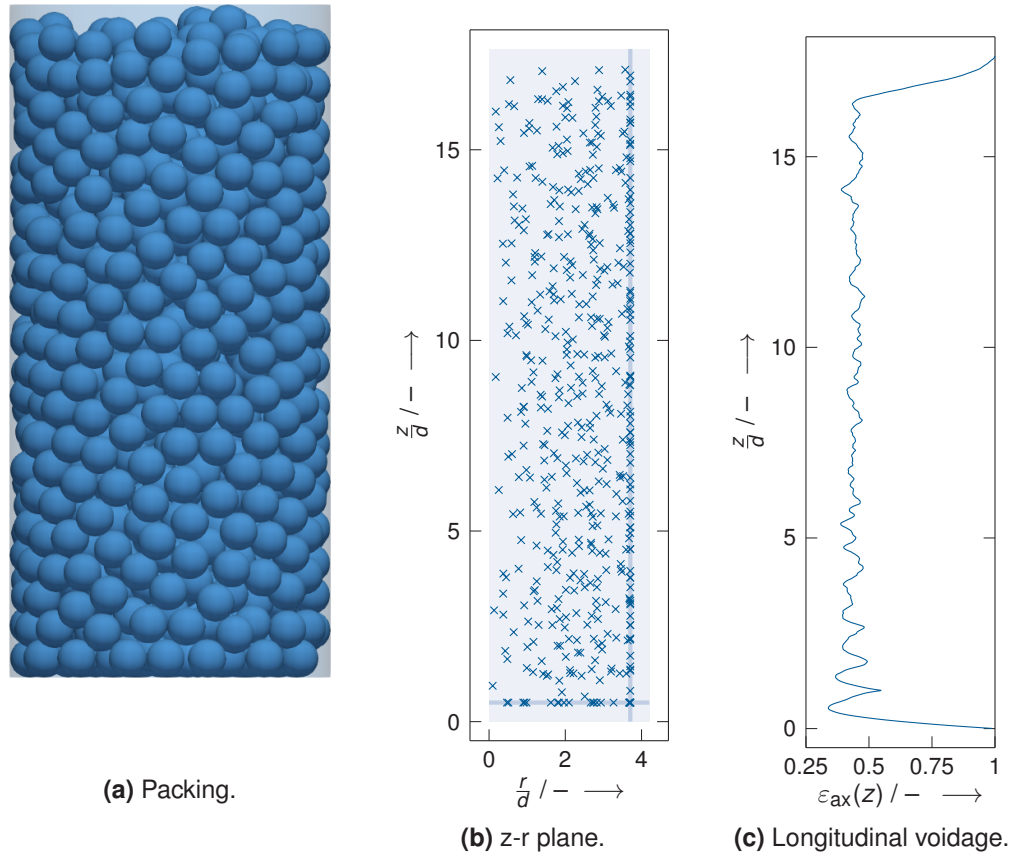


**Figure 5.1:** 2D view of packing obtained by simulation with LIGGGHTS<sup>®</sup> for bed with  $D/d = 8.41$ ,  $N = 1000$  and  $H_{\text{ins}} = 18d$  (a), together with corresponding position of pellet centre points in plane spanning bed height and radius (b) as well as longitudinal voidage profile (c).

container with diameter aspect ratio  $D/d = 8.41$  under the influence of gravity, indicating the random nature of the resulting packing. However, the arrangement obeys a common structure with regard to pellets touching the outer confining wall, that is at the bottom of the bed and at the side wall. This local structure is underlined by the scatter plot shown in Figure 5.1b of pellet centre points within a plane spanning the radius of the bed and the bed's height, where a distance of half a pellet diameter ( $d/2$ ) is indicated. Further into the bed, this order of the first row of pellets adjacent to the wall is lost. Evaluating the local bed voidage in longitudinal direction of the bed, that is averaging voidage in thin slices perpendicular to the length axis, reveals three regions of the bed as can be seen from Figure 5.1c. Starting at the bottom, the voidage decreases from a value of *one*, where the pellets are touching the confining wall, until reaching a global minimum at a distance of half a pellet diameter from the wall. From there, voidage increases until the next row of pellets starts occupying the space between the row of pellets closest to the bottom, resulting in a further reduction of voidage. This behaviour is repeated further into the bed, however, losing order in the voidage profile with increasing distance from the bottom. Within the bed, voidage is fluctuating about a mean value until finally the bed ends where voidage increases back to *one*.

The more ordered packing arrangement at the bottom of the bed and the looser packing at the top have been discussed by a number of authors, including Rutgers [108] who referred to it as *top-bottom effect*, Haughey and Beveridge [113] discussing *end effects*, Dixon [114] pointing out *base plane end effects* and Zou and Yu [119] indicating a *top-bottom wall effect* or *thickness effect*. The latter explicitly excluded sections with a height of  $3d$  from top and bottom of the bed, respectively, for evaluation of the overall packing density. Reyes and Iglesia [129] excluded sections of  $5d$  from both ends when investigating mean voidage values of packings with heights of about  $H/d \approx 60$ .

The influence of the number of pellets on mean bed voidage is subject of Figure 5.2. In a first set of simulations, pellets were inserted at a distance of five times the pellet diameter ( $5d$ ) above the expected bed height based on the mean voidage correlation as a function of the diameter aspect ratio  $D/d$  by Benyahia and O'Neill [121]. Each data point represents the mean value of ten individual simulations and the magnitude of the error bars refers to one standard deviation to both directions. As can be seen from Figure 5.2a, the resulting bed voidage is found to decrease with increasing number of pellets which is consistent with experimental results by Zou and Yu [119]. However, for shorter beds, i.e., those composed of less pellets, the influence of the reduced voidage within the sections at the very ends of the bed on the bed's mean voidage are more pronounced. It is found that the influence of these end effects can be successfully ruled out by excluding sections of  $5d$  from the bottom and  $4d$  from the top of the packing, which is in line with previous publications. Still, the observed trend of voidage reduction with increasing number of pellets within the bed persists when excluding the less dense sections at the very bottom and top end of the bed, respectively. Within this set-up, the insertion height of pellets forming shorter packings is lower as compared to that of longer beds. Therefore, this indicates the influence of the insertion height resulting in lower bed voidages when pellets are introduced at greater insertion height, which is in line with the experimental findings of Macrae and Gray [107].

In a second step, the set-up was adjusted to maintain a fixed insertion height corresponding to that of the case with 10 000 pellets. Again, when taking into account the entire bed, the mean voidage decreases with increasing pellet number, whereas excluding top and bottom sections results in the intended effect where bed voidage is no longer a function of pellet number. This holds for beds with pellet numbers up to about 5000 pellets, above which the data in Figure 5.2b indicates a slight increase of mean bed voidage with pellet number.

Although counter-intuitive at first, this is in line with Figure 5.2a indicating an increase in bed voidage with reduced insertion height. If the insertion height is considerably larger than the resulting bed height, the influence of the number of pellets, or the bed height, on bed voidage is negligible when excluding top and bottom sections of the bed. On the other hand, the reduced apparent insertion height for the upper part of longer beds results in a noticeable increase of the overall mean bed voidage, though less significant than when varying the insertion height. This is in line with Figure 5.3 showing the mean bed voidage in



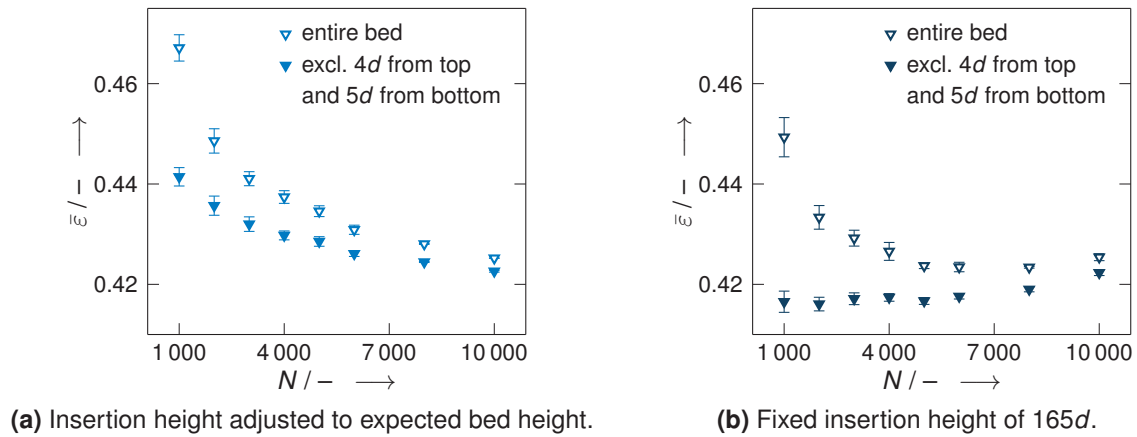


**Figure 5.2:** Influence of pellet number, insertion height and voidage evaluation on mean bed voidage for beds with  $D/d = 8.41$ .

sections across the beds considered in Figure 5.2b. The sections are chosen such that the very bottom of the beds up to a height of  $5d$  and the top sections of  $4d$  height are excluded from the analysis. In addition to the reduced mean bed voidage for the topmost sections of the longest considered beds as a result of reduction to the falling height of the pellets by the growing bed it can also be seen that the mean bed voidage at comparable height within the beds is independent of the bed height on top of the considered section, i.e. the lower sections of the bed are not compressed by layers on top of them. Consequently, the influence of insertion height is expected to fully disappear when adjusted during packing generation keeping a fixed distance between the upper end of the bed and the region of pellet insertion. Within this study, where the effect of varying material properties shall be investigated rather than height effects in very long beds, two fixed insertion heights are considered and the number of pellets set to an expected bed height of  $30d$ , which

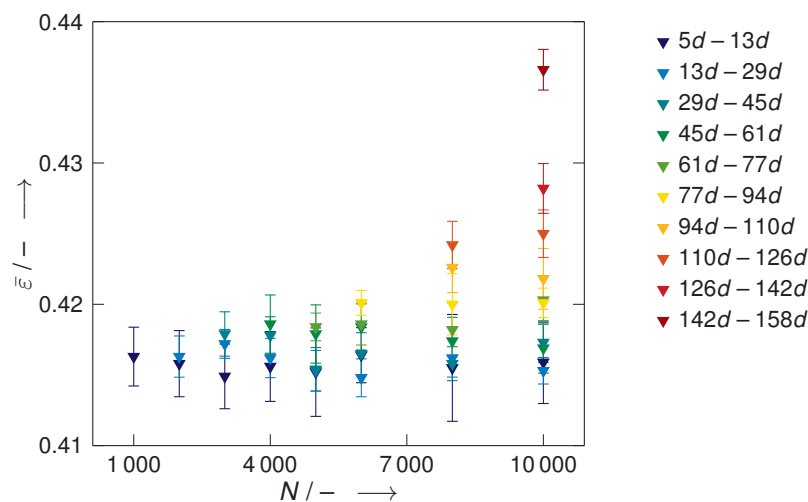


**Figure 5.3:** Variation of mean bed voidage in sections along the bed height for beds with  $D/d = 8.41$  and a fixed insertion height of  $165d$ ; section positions measured from packing bottom.

corresponds to 1891 pellets for beds with a diameter aspect ratio of  $D/d = 8.41$  based on the correlation by Benyahia and O'Neill [121].

Statistical analysis using the toolbox *bioinfokit* [156] for Python indicated only a small variation in the population variances and insignificant differences in the population means for the two data sets considering an adjusted insertion height but with different evaluation aspects of the mean bed voidage (cf. Figure 5.2a) with  $F(1, 14) = 2.94$ ,  $p = 0.108$ . On the contrary, the deviation in population means can be considered significant when comparing of the two data sets shown in Figure 5.2b with  $F(1, 14) = 12.9$ ,  $p = 0.00292$ . A final comparison of the two data sets where topmost and bottommost sections of the bed were excluded for evaluation of the mean bed voidage show a significant deviation in population means comparing beds generated from varying insertion heights to those generated with a fixed insertion height as well as a large variation between the corresponding population variances ( $F(1, 14) = 28.1$ ,  $p = 0.000111$ ).

To verify that ten individual simulation runs per data point are sufficient to properly account for the influence of randomness within the packing generation algorithm, the development of the mean value and the standard deviation in the evaluated mean bed voidage are considered. The data point of beds with  $D/d = 8.41$  made of 1000 pellets generated from a fixed insertion height of  $165d$  (cf. Figure 5.2b for  $N = 1000$ ) and excluding top and bottom sections for the evaluation of the mean bed voidage is taken as an example. As a result, a fluctuation of the mean value of bed voidage about a common value is revealed while the standard deviation appears to come close to a plateau with increasing number of considered data points (cf. supporting information for figure). This indicates that the expected standard distribution of simulation results based on the influence of randomness in the packing generation algorithms can be represented by evaluating ten samples out of the total, countless, population. In addition, an analysis of variance (ANOVA) (cf. for example Ostertagová and Ostertag [157] for details) was carried out to verify the usage of ten simulations per data point a posteriori based on eight sets of data with ten individual simulations. The parameter set of the simulations corresponds to beds with  $D/d = 8.41$  made of 1000 pellets generated from a fixed insertion height of  $165d$  with LIGGGHTS™ (cf. Figure 5.2b for  $N = 1000$ ). Top and bottom sections of the beds were excluded for the evaluation of the mean bed voidage. The sole difference between the analysed simulations is the random number used in the packing generation routine. The result indicates comparable scattering of the data points between the groups, i.e. comparable population variances, and no significant difference in the population means ( $F(7, 72) = 0.759$ ,  $p = 0.623$ ), justifying that ten simulations per data point are sufficient to account for the influence of randomness within the packing generation algorithm.

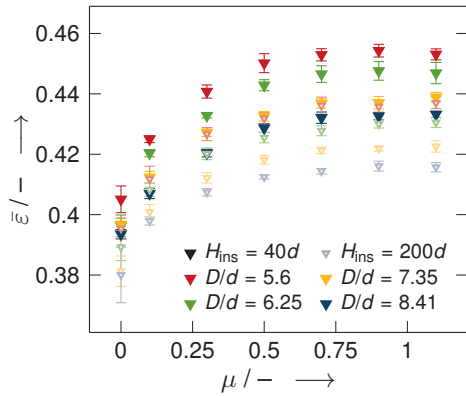


### 5.4.2 Material properties

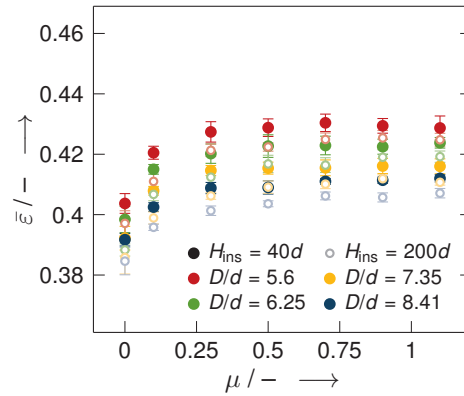
The influence of the material properties friction, restitution and density on mean bed voidage of random packings with moderate diameter aspect ratios of  $D/d = 5.6, 6.25, 7.35$  and  $8.41$  as obtained by numerical simulation with LIGGGHTS<sup>®</sup> and Blender<sup>™</sup> are depicted in Figure 5.4. Again, each data point corresponds to ten individual simulations, showing the mean value with error bars of the size of one standard deviation to both directions. This ensures that the influence of randomness in the pellet insertion is taken into account and does not distort the simulation results. As expected, the overall resulting mean bed voidages are larger with decreasing diameter aspect ratio of the bed and lower pellet insertion heights. Also, rough particles result in beds with higher voidage as compared to smooth pellets where beds are more dense, that is the mean bed voidage increases with the coefficient of friction as evident from Figures 5.4a and 5.4b. This general trend is consistent with the observations by Zhang et al. [118] simulating beds with a much larger diameter aspect ratio of  $D/d = 24$ . A closer comparison between the results obtained with the two considered software packages reveals similar values for smooth pellets whereas the mean bed voidages are higher for larger coefficients of friction when simulated with LIGGGHTS<sup>®</sup>. This is in line with Boeing and Bräunl [158] who found the Bullet physics engine, by which numerical packing generation is included within the Blender<sup>™</sup> environment, to underestimate the effect of friction. With both considered software packages, a plateau is reached for higher values of the coefficient of friction. However, for beds simulated with Blender<sup>™</sup>, the mean bed voidage levels off already at about  $\mu = 0.3$  whereas for simulations with LIGGGHTS<sup>®</sup> the voidage keeps increasing up to a value of approximately  $\mu = 0.7$ . The observed levelling off of mean bed voidages for larger coefficients of friction is not evident from the simulation results published by Zhang et al. [118].

Variations of the coefficient of restitution are shown in Figures 5.4c and 5.4d based on simulations with LIGGGHTS<sup>®</sup> and Blender<sup>™</sup>, respectively. For reasons of clarity, results are only displayed for beds with a diameter aspect ratio of  $D/d = 5.6$  but including two different values of the coefficient of friction, corresponding to smooth and rough pellets. As depicted, the resilience of the pellet material has only limited influence, if any, when pellets are smooth, which seems plausible as the packing arrangement is already very dense. This is different when considering a higher coefficient of friction, where bed voidage decreases with increasing coefficient of restitution. This is in line with Zhang et al. [118] who argued that less energy is available for pellet rearrangement at smaller coefficients of restitution as more kinetic energy is dissipated during collision, thus leading to looser packings. Again, the obtained mean bed voidages are in general higher at the lower pellet insertion height and when simulated with LIGGGHTS<sup>®</sup>.

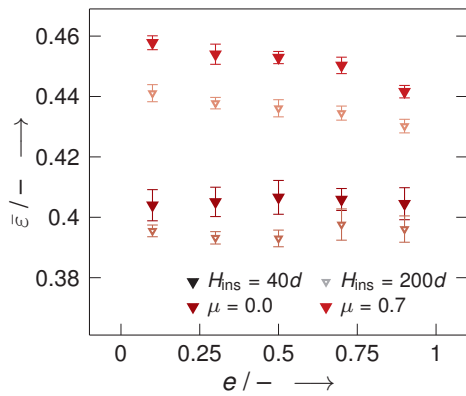
As can be seen from Figures 5.4e and 5.4f, there is no significant influence of pellet density visible on mean bed voidage over the considered range from  $1000 \text{ kg m}^{-3}$  to  $10\,000 \text{ kg m}^{-3}$ .



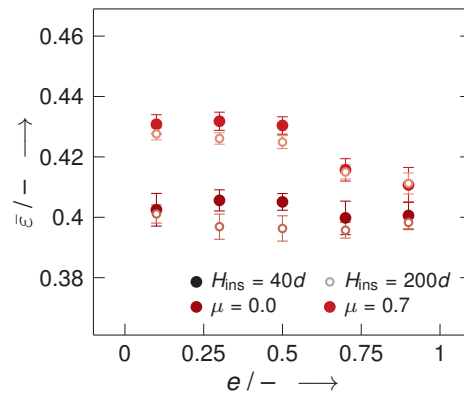
(a) Coefficient of friction, LIGGGHTS®.



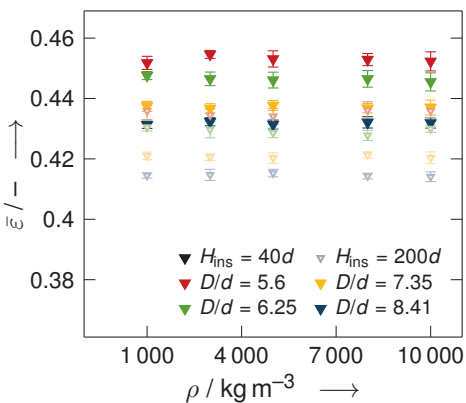
(b) Coefficient of friction, Blender™.



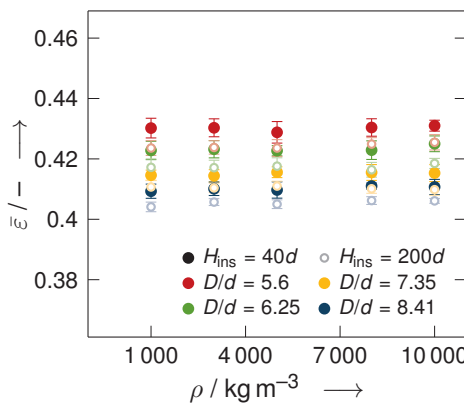
(c) Coefficient of restitution, LIGGGHTS®.



(d) Coefficient of restitution, Blender™.



(e) Density, LIGGGHTS®.



(f) Density, Blender™.

**Figure 5.4:** Influence of material properties on mean bed voidage for packings with  $H/d \approx 30$  based on parameter default values as detailed in Table 5.2 unless specified otherwise; reduced by  $5d$  from bottom and  $4d$  from top of packing for voidage evaluation.

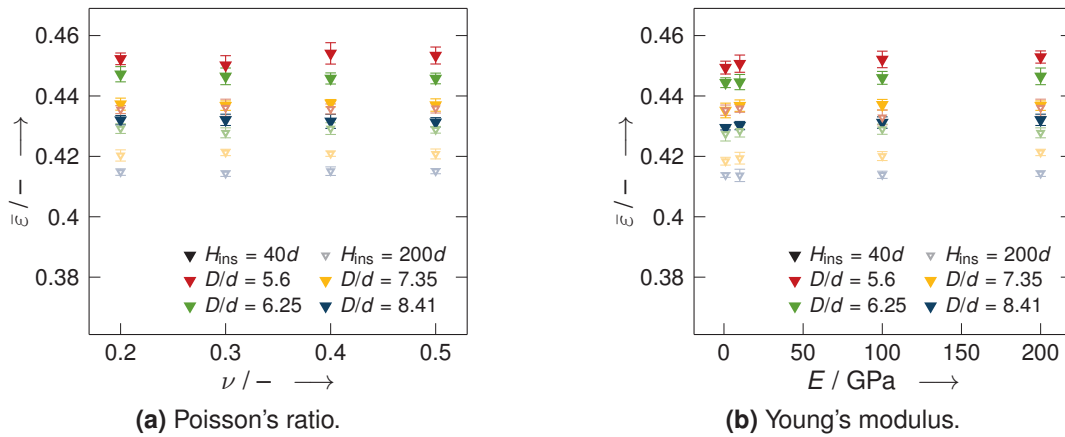


**Figure 5.5:** Influence of Poisson's ratio and Young's modulus on mean bed voidage for packings with  $H/d \approx 30$  based on parameter default values as detailed in Table 5.2 unless specified otherwise and simulated with LIGGGHTS<sup>®</sup>; reduced by  $5d$  from bottom and  $4d$  from top of packing for voidage evaluation.

Simulations based on DEM further account for Poisson's ratio and Young's modulus of the considered material. The data displayed in Figures 5.5a and 5.5b indicates no distinct influence of either of the two material properties within the investigated range of values.

Statistical analysis of beds with  $D/d = 5.6$  based on ANOVA and the post hoc Tukey-Kramer test indicate a similar level of influence for both the coefficient of friction and the coefficient of restitution on mean bed voidage, where the latter is limited to rough pellets. On the other hand, there is only limited influence of the coefficient of restitution for smooth pellets as well as of the pellet density, Poisson's ratio and Young's modulus. This holds for both considered insertion heights and numerical packing generation tools. Details of the performed statistical analyses can be found in the supporting information.

Although this investigation has been limited to mono-sized spherical pellets, it is anticipated that the observed trends are generally valid also for other pellet shapes. Numerical data by Jurtz et al. [159] as well as experimental data by von Seckendorff et al. [160] indicate an even higher influence of friction on the mean bed voidage of cylindrical pellets as compared to spherical pellets.

#### 5.4.2.1 Influence of diameter aspect ratio

As already seen from the depicted results for the various material properties, the overall bed voidage is larger for smaller diameter aspect ratio packings. The influence of the diameter aspect ratio on mean bed voidage is well discussed in literature. For low to moderate diameter aspect ratios, bed voidage decreases with increasing diameter aspect ratio before levelling off and remaining constant for large diameter beds. This is a result of the influence of the confining wall on the local pellet arrangement, which fades away after about four to five pellet diameters into the bed. Numerous correlations for the mean bed voidage based

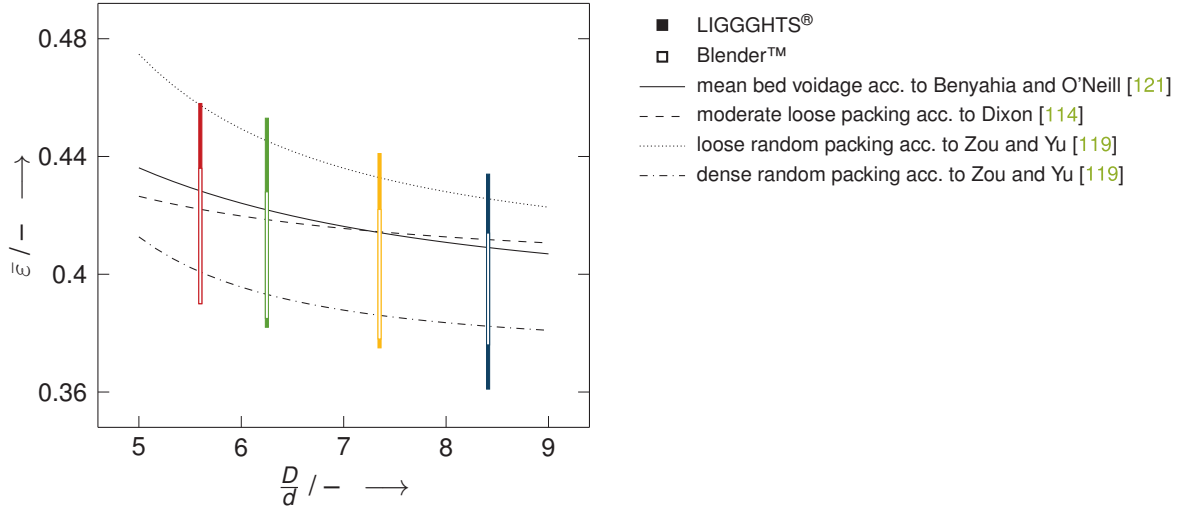


**Figure 5.6:** Range of obtained mean bed voidage as a function of diameter aspect ratio in comparison to literature correlations.

solely on the diameter aspect ratio can be found in literature, including for example the correlation by Benyahia and O'Neill (cf. Equation (5.7)). Based on various means, including pellet insertion rate or packing densification, a wide range of bed voidages can be obtained where the difference in packing densities for dense random packing and loose random packing is roughly 6% [106]. Dixon [114] proposed the following correlation for the mean voidage of *moderate loose packings*:

$$\bar{\varepsilon} = 0.40 + 0.05 \left( \frac{d}{D} \right) + 0.412 \left( \frac{d}{D} \right)^2 \quad (5.9)$$

whereas Zou and Yu [119] provided two sets of correlations, enclosing the full range of mean voidage between dense and loose packing arrangement, of which the ones relevant to the diameter aspect ratios of beds considered in this work are:

$$\bar{\varepsilon} = \begin{cases} 0.372 + 0.002 \left( \exp \left\{ 15.306 \frac{d}{D} \right\} - 1 \right), & D/d \geq 3.95, \text{ dense random packing} \\ 0.400 + 0.010 \left( \exp \left\{ 10.686 \frac{d}{D} \right\} - 1 \right), & D/d \geq 3.9, \text{ loose random packing.} \end{cases} \quad (5.10)$$

The stated equations by all three authors are based on the diameter aspect ratio only and do not take into account any other information on bed generation or material properties. A comparison between these correlations and the wide spectrum of results obtained by varying the material properties is provided in Figure 5.6. It can be seen that the simulation results are covering the full range of mean bed voidage based on the literature correlations. This is interesting as the insertion ratio is kept constant similar to pouring conditions which would lead to looser packings in general. However, reducing the coefficient of friction also results in a densification of the packing. As seen before, similar values can be obtained with both simulation packages for dense packings whereas the most loose packings obtained

with Blender™ take values below the correlation by Zou and Yu [119] while even looser beds are generated when simulating with LIGGGHTS®.

#### 5.4.2.2 Local voidage profiles

So far, investigations on the simulated beds have been based on values of the mean bed voidage, excluding sections of  $4d$  and  $5d$  from top and bottom of the packing, respectively. Given the wide range of obtained bed voidages, the question arises on how this relates to the local pellet arrangement. Therefore, radial voidage profiles of beds of the considered four diameter aspect ratios are shown in Figure 5.7 including very dense ( $\mu = 0$ ) and most loose ( $\mu = 0.7$ ) beds based on the simulations with LIGGGHTS®. Radial voidage profiles are generated for the ten individual simulations corresponding to each scenario using the method proposed by Mueller [153] based on the centre point coordinates of the pellets in the bed and excluding sections of  $4d$  and  $5d$  from top and bottom of the packing, respectively. Plotted are the resulting mean radial voidage profile together with the absolute range of the obtained profiles. For all four diameter aspect ratio beds, the depicted radial voidage profiles follow the expected trend. Starting with a maximum value at the touching points between pellets and the confining wall, the voidage declines until reaching a minimum at approximately half a pellet diameter away from the wall. From there, the voidage increases up to a sharp maximum where the second ring of pellets from the wall starts to contribute to the local voidage. These oscillations continue further away from the confining wall with a damped amplitude. However, extreme values may be observed in the centre of the bed. Some common aspects of the obtained radial voidage profiles shall be discussed in detail in the following.

The position of the first minimum was found to be roughly half a pellet diameter from the confining wall. This is a result of the ordering influence of the wall where pellets touching the wall have their centre points at half a pellet diameter into the bed. In case of a plane wall, such as the base plane closing the cylindrical tube at the bottom, the line of sphere centre points coincides with the position of the minimum in the local voidage distribution (cf. Figure 5.1). When the confining wall is curved, the minimum is shifted away from the wall as the maximum local pellet density moves with the line of sphere contacts [124]. Benenati and Brosilow [109] give the following expression for the position of the first minimum from the wall  $\varepsilon_{\min}$  in terms of pellet diameters:

$$\frac{\delta}{d} = 0.5 + \left(\frac{D}{d} - 1\right) - \sqrt{\left(\frac{D}{d} - 1\right)^2 - 1}. \quad (5.11)$$

This position is indicated in Figure 5.7 as orange dashed line (---). However, for most of the depicted scenarios this prediction does not compare well with the position of the first minimum which is often found to be closer to the wall, leaving room for improvement. Considering the geometry of the outer confining wall and the adjacent pellets, two hypothetical

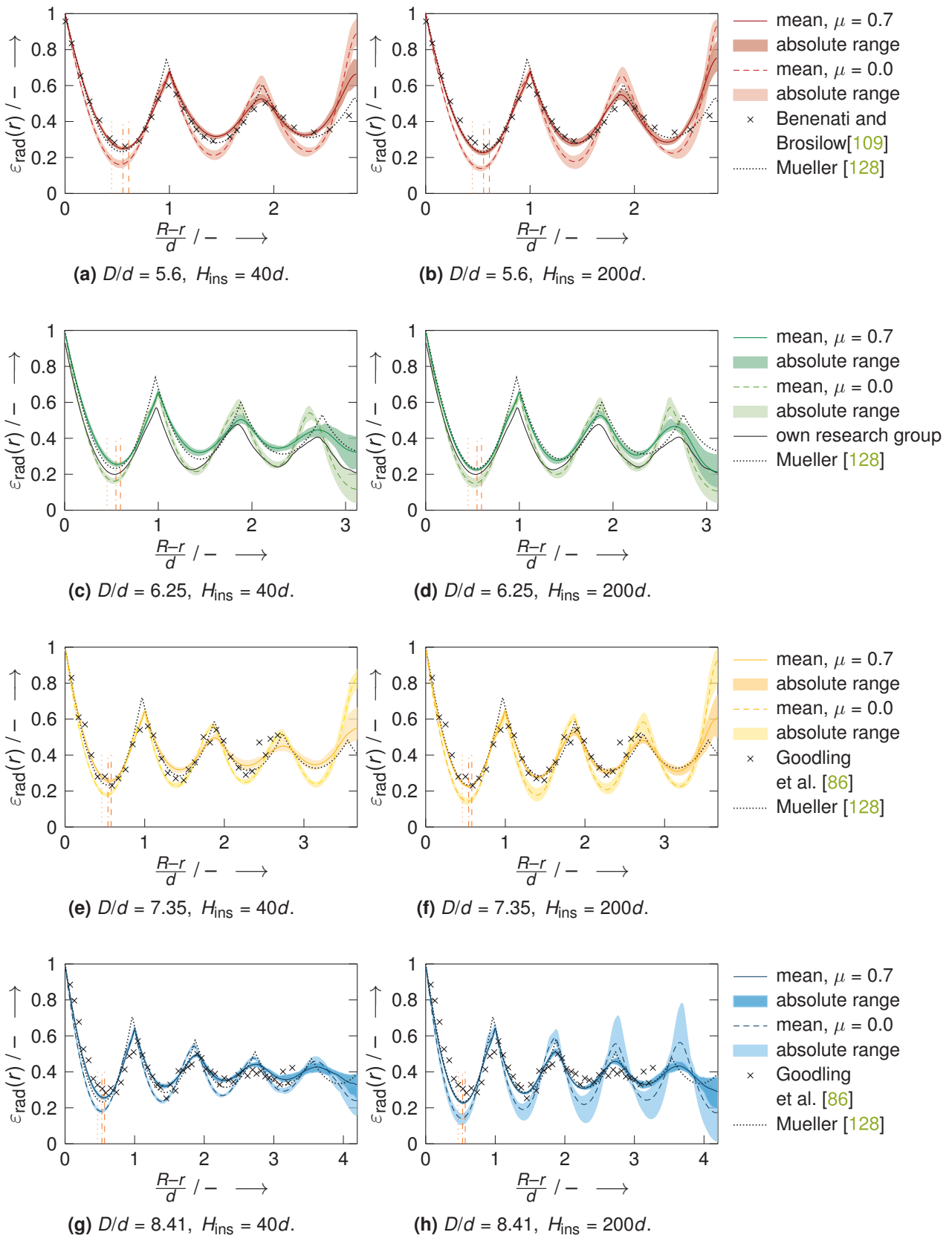


**Figure 5.7:** Radial voidage profiles for beds simulated with LIGGGHTS<sup>®</sup>, excluding  $5d$  and  $4d$  from bottom and top of packing, respectively; orange lines indicating position of local minimum closest to the wall acc. to Benenati and Brosilow [109] (---) as well as analytical positions acc. to Equation (5.12) (-.-) and Equation (5.13) (.....).

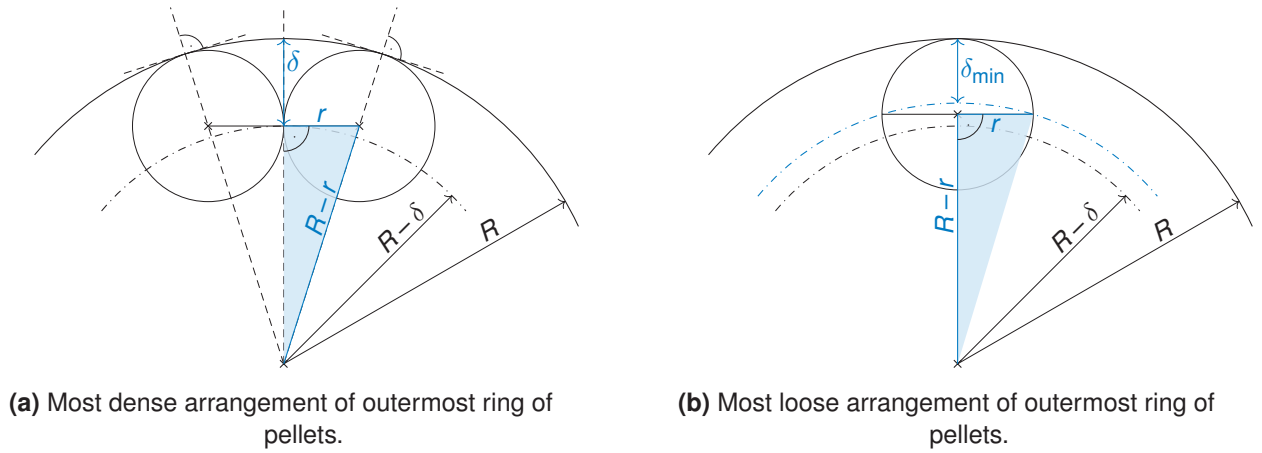


**Figure 5.8:** Trigonometrical considerations leading to analytical position of local minimum in radial voidage profile next to the confining wall.

scenarios of pellet arrangement within the first ring of pellets next to the wall are established, corresponding to the extreme situations of most dense and most loose packing. The related sketches given in Figure 5.8 provide insight into the trigonometric set-up, based on which the position of the first minimum is derived. In the most dense arrangement neighbouring pellets within the outermost ring are touching each other and the wall. It can easily be seen from Figure 5.8a that the theoretical position of the first minimum is equivalent to the line of sphere contacts as reported by Ridgway and Tarbuck [124]. Trigonometrical considerations based on the highlighted right triangle yield the following expression for the distance of the first minimum in the radial voidage profile:

$$\frac{\delta}{d} = \frac{1}{2} \left( \frac{D}{d} - \sqrt{\left( \frac{D}{d} - 1 \right)^2 - 1} \right). \quad (5.12)$$

On the other hand, when the bed arrangement is less dense, neighbouring pellets may not be touching each other. This circumstance shifts the position of the first minimum closer to the confining wall. The corresponding limiting case is posed by one single pellet that is touching the wall, as depicted in Figure 5.8b, where the highest pellet density is found at a distance of

$$\frac{\delta}{d} = \frac{1}{2} \left( \frac{D}{d} - \sqrt{\left( \frac{D}{d} - 1 \right)^2 + 1} \right) \quad (5.13)$$

from the wall. Both scenarios are highly unlikely to be encountered, the most dense arrangement requiring a full outermost ring of pellets which is only feasible for certain diameter aspect ratios and the least dense arrangement being a constructed case based on one pellet only which is strictly speaking not a packed bed. However, the first minimum cannot be closer to the wall than given by Equation (5.13) and is expected somewhere near the position obtained from the most dense arrangement. As anticipated, both of the proposed



expressions as well as that of Benenati and Brosilow [109] tend to half a pellet diameter for large diameter aspect ratios. The observed first minima in Figure 5.7 are indeed closer to the position predicted by a most dense arrangement within the outermost ring of pellets, indicated by an orange dash dotted line (---), than the position put forth by Benenati and Brosilow (---). The hypothetically closest position of the first minimum to the wall, as expressed by Equation (5.13), is indicated by an orange dotted line (.....).

The position of the sharp maximum less than one pellet diameter from the confining wall, as visible in all scenarios shown in Figure 5.7, is a result of the intertwining of the first and second ring of pellets from the wall, that is, the pellets of the second ring are placed between two adjacent pellets of the first ring. Further into the bed, the strong order of the pellet arrangement close to the confining wall is lost and the subsequent maxima are smoother. The first maximum is shifted further to the wall with increasing diameter aspect ratio for similar trigonometric reasons as considered for the first minimum.

For beds with large diameter aspect ratio, the oscillatory shape of the radial voidage is flattened out further into the bed. However, at moderate diameter aspect ratios, the profile may experience interference with the opposite wall. From the simulated beds, the cases with diameter aspect ratios of  $D/d = 5.6$  and  $7.35$  (cf. Figures 5.7a, 5.7b, 5.7e and 5.7f) show a very pronounced maximum in the centre of the packing, originating from an open channel. On the contrary, the simulation results of beds with diameter aspect ratios of  $D/d = 6.25$  and  $8.41$  (cf. Figures 5.7c, 5.7d, 5.7g and 5.7h) indicate a minimum voidage in the centre of the packing, corresponding to a stack of pellets.

Within the beds of all four considered diameter aspect ratios and from both pellet insertion heights, the extrema in the radial voidage profile depicted in Figure 5.7 are generally more pronounced for smooth pellets. This holds especially for the first minimum and also the other extrema but, remarkably, not for the first maximum, which remains at a similar value, also at varying pellet insertion height which tends to further pronounce the values of the extrema.

The simulation results depicted in Figure 5.7 are compared with experimental data from literature as well as the semi-analytical correlation for the radial voidage as proposed by Mueller [128]. Overall, the semi-analytical expression captures the oscillating nature of the voidage profile which is damped with increasing distance to the wall. However, all maxima are sharp rather than becoming smoothed out from the second maximum onwards and the oscillation continues as if unaffected by the condition specific to the centre of the packing. Apart from that, the semi-analytical expression is closer to the simulation results obtained for looser packings, possibly owing to the fact that the empirical parameters were determined by fitting to experimental data available from literature [128] which tends to be obtained by pouring of material with significant surface friction and no further densification, thus resulting in rather loose packings.



As evident from Figures 5.7a and 5.7b, the radial voidage profiles corresponding to the simulated beds with a diameter aspect ratio of  $D/d = 5.6$  show only limited variation with the insertion height and the radial profiles for the pellets with considerable surface friction are in excellent agreement with the experimental data by Benenati and Brosilow [109] who poured spherical lead shot into cylindrical containers, except for the centre of the bed where the simulated voidage is higher than the experimental result. In case of beds with diameter aspect ratio  $D/d = 6.25$ , illustrated in Figures 5.7c and 5.7d, comparison is made with experimental data of pellet positions performed in our research group for a bed of spherical polyoxymethylene pellets of 4 mm diameter within a cylindrical container, amounting to a bed height of about  $H/d \approx 23$ . The radial profile has been obtained by the same method as for the simulated beds following Mueller [153], excluding top and bottom sections of the bed. This experimental result is in closer agreement with the more dense packing arrangement obtained by numerical simulation which is in line with the experimental set-up where the insertion height was well above the resulting bed height and filling conditions comparable to pouring. Interestingly, the values of the minima are very similar but the maxima shifted to lower values throughout the entire profile. The remaining set-ups with diameter aspect ratios of  $D/d = 7.35$  and  $8.41$ , shown in Figures 5.7e to 5.7h, are compared to experimental data by Goodling et al. [86] who poured precision polystyrene spheres into plastic pipes. Due to their experimental method of evaluating the radial voidage profile by cutting thin annular rings from the solidified bed, no data is available for the centre of the bed. The experimental data appears closest to the simulation results obtained with rough pellets and from greater insertion height for both diameter aspect ratios. Though visible for all set-ups depicted in Figure 5.7, the difference between the two considered insertion heights is most pronounced for the beds with  $D/d = 8.41$ . As evident from Figure 5.7g corresponding to an insertion height of  $H_{\text{ins}} = 40d$ , the range of values observed for both smooth and rough pellets is quite narrow. For the larger insertion height of  $H_{\text{ins}} = 200d$ , this still holds for the profiles corresponding to rough spheres where the minima are shifted to slightly lower values, as illustrated by Figure 5.7h. However, the radial voidage profiles of smooth spheres inserted at greater height cover a much larger range of values and the extrema are generally more pronounced except for the first maximum.

## 5.5 Conclusion

Numerical generation of random packed beds with moderate diameter aspect ratio was found to be capable of yielding the full range of packing modes from very loose to highly dense. It was found to be of genuine importance to exclude the top and bottom most sections of the beds for an unbiased resulting mean bed voidage as these sections are less dense than the remainder of the bed. The influence of the pellet insertion height was detailed and a parameter study on the effect of material properties on mean voidage and local radial voidage performed considering two fixed insertion heights. From the simulation

results, the structure of random packed beds tends to be of higher order when pellets are smooth and introduced from greater heights, resulting in a lower overall mean bed voidage. Overall, the two properties coefficient of friction as well as the coefficient of restitution, but limited to rough pellets, appear to be the most influential material properties on the mean bed voidage. This is underlined by statistical analysis of the simulation results. The wide range of obtained results for local and mean bed voidage indicates the importance of choosing the conditions for random packing generation as this may have an impact on any further simulations of flow through those beds. Also, beds generated with Blender™ were found to underestimate the effect of friction yielding beds with lower voidage as compared to those generated with LIGGGHTS®. In addition, the position of the first minimum was determined from trigonometric considerations, leading to closer agreement with the simulation results as to the position proposed by Benenati and Brosilow [109].

The simulation results were found to be in general agreement with the experimental study by Macrae and Gray [107] and a related numerical investigation by Zhang et al. [118] both considering beds of spheres in cylindrical containers but for large diameter aspect ratios of  $D/d \geq 24$  where the effect of the confining wall becomes negligible.

The performed systematic investigation of the influence of bed height, pellet insertion height and material properties provides insight into the effect of these parameters on the voidage of the resulting random packed beds. The wide range of obtained pellet arrangements emphasises the influence and importance of the parameter settings in numerical packing generation of which researchers using this method as a means to easily obtain packing structures which are taken as a starting point for further research should be aware of. To our opinion there does not exist a parameter setting that leads to the *representative bed*. Rather, the combination of a chosen packing mode, including filling density and insertion height, and a set of material properties lead to a specific numerical packing. By carefully choosing these parameters, the numerically generated bed may become a better representation of its *real* counterpart.

This investigation was limited to mono-sized spherical pellets dropped into cylindrical containers. Care should be taken when analysing results based on random beds with moderate diameter aspect ratio, keeping in mind the various parameters influencing the character of the bed and how these might influence any subsequent simulation results. Future work may reevaluate the effect of bed height, pellet insertion height and material properties on beds of other shapes of pellets and confining wall geometries, though it is a reasonable assumption that the observed trends will generally remain valid. Also, it would be of great interest to investigate both spatial and temporal distributions of contact forces relevant in the packing generation process as well as the energy within the system as a function of the various influence factors.

## 5.S Supporting information

Statistical analysis is performed using the Python package *bioinfokit* by R. Bedre [156]. For details on the analysis of variance (ANOVA) the reader is referred to standard text books or the article by Ostertagová and Ostertag [157] as an example.

### 5.S.1 Verification of sample size by analysis of mean value and standard deviation within one sample data set

Ten individual simulation runs which differ solely in the random number used within the packing generation algorithm are taken as the basis of each of the shown data points within the manuscript. The mean value thereof is indicated with one standard deviation as error bars to both sides. An a priori sample size determination would lead to a much larger value than the performed ten simulations per data point, given that the population size, i.e. the number of possible arrangement of pellets within the random packing, is countless. Therefore, explicitly choosing a number of ten has been more of a pragmatic choice rather than a statistically proven value. However, analysing the situation a posteriori reveals that the mean value of bed voidage fluctuates about a common value while the standard deviation appears to come close to a plateau as can be seen from Figure 5.9. This indicates that the expected standard distribution of simulation results based on the influence of randomness in the packing generation algorithms can be represented by evaluating ten samples out of the total, countless, population.

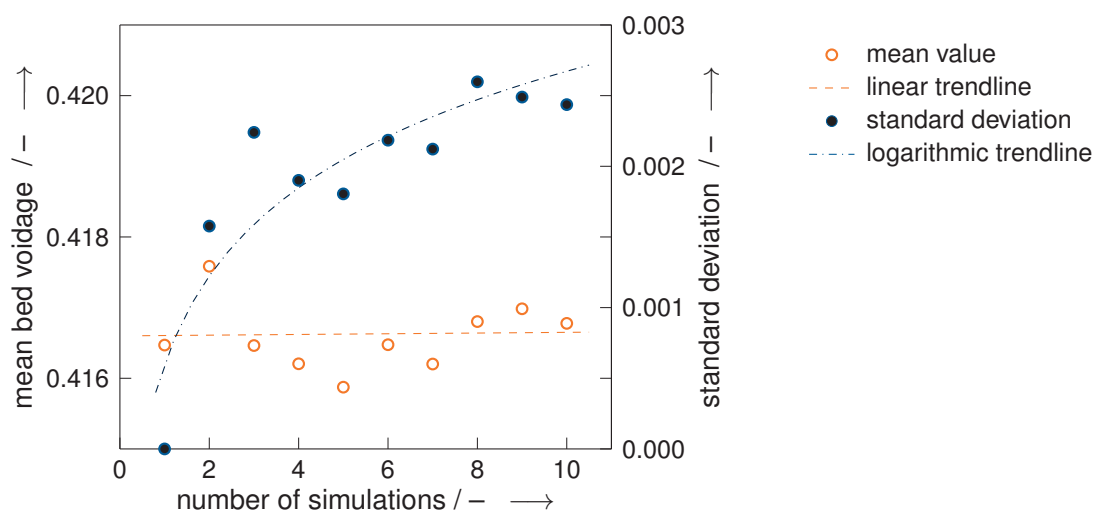


**Figure 5.9:** Development of mean and standard deviation with increasing number of simulations per data point.

## 5.S.2 Statistical analysis of the influence of material properties for beds generated with LIGGGHTS®

### 5.S.2.1 Insertion height of 40d

Exemplary, statistical analysis is performed for beds with  $D/d = 5.6$ , for which the variation in the coefficient of restitution is included in the manuscript. An ANOVA of the six groups considered - namely one on the variation of the coefficient of friction ( $\mu$ ), two on the variation of the coefficient of restitution ( $e$ ) for two different values of the coefficient of friction and one each on the variations of the density ( $\rho$ ), Poisson's ratio ( $\nu$ ) and Young's modulus ( $E$ ) - results in a considerably low  $p$ -value which leads to the clear rejection of the underlying null hypothesis of equal means amongst the groups ( $F(5, 24) = 18.2, p = 1.77 \cdot 10^{-7}$ ). A post hoc Tukey-Kramer test indicates that there is no significant deviation among each other for the three groups  $\rho$ ,  $\nu$  and  $E$ . The detailed ANOVA on these three groups as a follow-up underlines this indication showing only low scatter in variances and no significant deviation in the group means ( $F(2, 10) = 1.59, p = 0.25$ ). An ANOVA of the three remaining groups indicates significant differences ( $F(2, 14) = 18.4, p = 0.000121$ ) which can be associated to direct comparison of groups with varying coefficient of restitution at no friction ( $p = 0.001$  for both combinations with  $e(\mu=0)$ ) while there is no significant difference indicated between groups  $\mu$  and  $e(\mu=0.7)$  ( $p = 0.320$ ). Individual comparison of the groups  $\mu$  and  $e(\mu=0.7)$  indicate similar variances and no significant difference in the group means ( $F(1, 10) = 1.61, p = 0.233$ ). This suggests a similar level of influence of both coefficient of friction and coefficient of restitution at considerable levels of friction on the mean bed voidage. A reduced consideration of only the two groups with varying coefficient of restitution with sole difference in the coefficient of friction indicates a large difference in variances and a highly significant difference in the group means ( $F(1, 8) = 280, p = 1.64 \cdot 10^{-7}$ ). This emphasises the strong influence of the coefficient of friction on

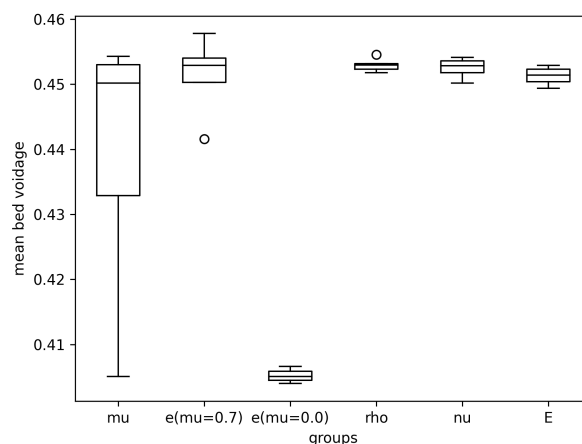


**Figure 5.10:** Boxplot of group data considered for ANOVA of packed beds with  $D/d = 5.6$  and an insertion height of  $40d$  as generated with LIGGGHTS®. Whiskers restricted to 1.5 times the interquartile range, data outside this range shown as outlier.

the mean bed voidage and also its effect on how influential the coefficient of restitution is on the mean bed voidage. The boxplot depicted in Figure 5.10 considering all six groups visualises the reported findings.

### 5.S.2.2 Insertion height of 200d

An analogue evaluation of beds of  $D/d = 5.6$  generated with LIGGGHTS<sup>®</sup> but from an insertion height of  $H_{ins} = 200d$  leads to similar conclusions. As a summary, the corresponding boxplot is depicted Figure 5.11.

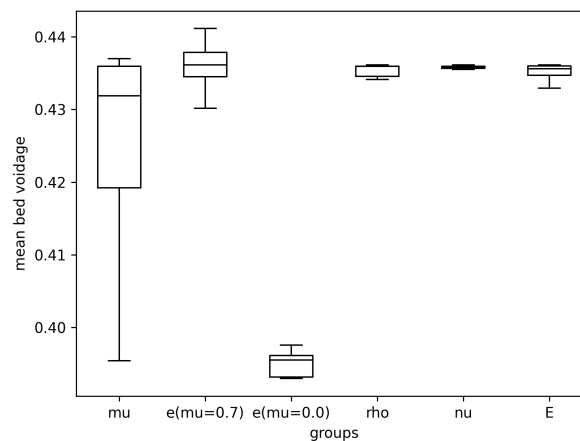


**Figure 5.11:** Boxplot of group data considered for ANOVA of packed beds with  $D/d = 5.6$  and an insertion height of  $200d$  as generated with LIGGGHTS<sup>®</sup>. Whiskers restricted to 1.5 times the interquartile range, data outside this range shown as outlier.

## 5.S.3 Statistical analysis of the influence of material properties for beds generated with Blender<sup>™</sup>

### 5.S.3.1 Insertion height of 40d

Again, a one-way ANOVA was performed for the different groups considered in bed generation with Blender<sup>™</sup> for beds with  $D/d = 5.6$  and an insertion height of  $H_{ins} = 40d$ , where the number of groups is reduced to four, covering one group on the influence of the coefficient of friction ( $mu$ ), two groups on the influence of the coefficient of restitution at two different values of the coefficient of friction ( $e(mu=0.7)$  and  $e(mu=0.0)$ ) and one group on the influence of the pellet density ( $rho$ ). The initial ANOVA reveals significant differences in the group means ( $F(3, 18) = 13.5, p = 0.000075$ ). Considering the boxplot of the situation shown in Figure 5.12 it follows that there is little scattering of the data points within group  $rho$  and it is concluded that the pellet density thus has no significant influence on the overall mean bed voidage. A Tukey-Kramer post hoc test indicates significant differences for all direct comparisons with the group  $e(mu=0.0)$  ( $p = 0.001$ ) and on the other hand no significant differences between groups  $mu$  and  $e(mu=0.7)$ . Detailed comparison between the latter two groups indicates variation in the group variances and insignificant variation

in the group means ( $F(1, 10) = 0.00174, p = 0.968$ ). Reduced comparison of the two groups with variation in the coefficient of restitution at different values of the coefficient of friction indicates significantly different group means ( $F(1, 8) = 21.3, p = 0.00173$ ). As with the LIGGGHTS<sup>®</sup> simulations, this indicates the substantial influence of the coefficient of friction as well as of the coefficient of restitution, however restricted to rough pellet surfaces, whereas the influence of the coefficient of restitution for smooth pellets as well as the influence of the pellet density on mean bed voidage are low. The corresponding boxplot as depicted in Figure 5.12 visualises the discussed results.

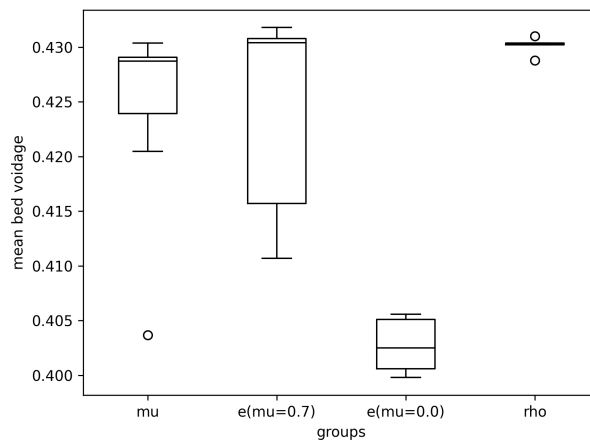


**Figure 5.12:** Boxplot of group data considered for ANOVA of packed beds with  $D/d = 5.6$  and an insertion height of  $40d$  as generated with Blender<sup>™</sup>. Whiskers restricted to 1.5 times the interquartile range, data outside this range shown as outlier.

### 5.S.3.2 Insertion height of $200d$

An analogue evaluation of beds of  $D/d = 5.6$  generated with Blender<sup>™</sup> but from an insertion height of  $H_{ins} = 200d$  leads to similar conclusions. As a summary, the corresponding boxplot is shown in Figure 5.13.

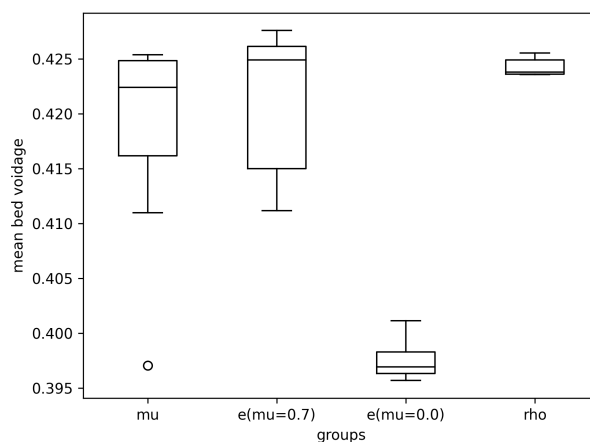


**Figure 5.13:** Boxplot of group data considered for ANOVA of packed beds with  $D/d = 5.6$  and an insertion height of  $200d$  as generated with Blender<sup>™</sup>. Whiskers restricted to 1.5 times the interquartile range, data outside this range shown as outlier.

# 6 Numerical simulation of pellet shrinkage within random packed beds

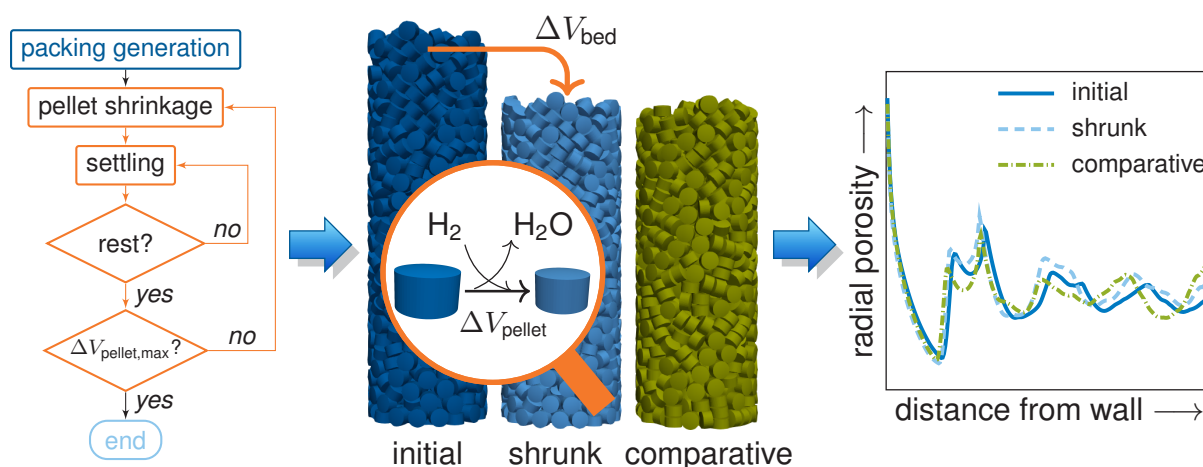
This chapter was published in a similar form and is reprinted (adapted) with permission from:

J. Fernengel, R. Weber, N. Szesni, R. W. Fischer and O. Hinrichsen, Numerical Simulation of Pellet Shrinkage within Random Packed Beds, *Ind. Eng. Chem. Res.* **2021**, *60*, 6863–6867, DOI 10.1021/acs.iecr.0c05307. [161]

Copyright 2021 American Chemical Society.

## Publication summary

Catalytic pellets may experience volume contraction during reductive activation. Although known and easily accessible as reduced bed height within industrial fixed-bed reactors, the effects on bed structure are lacking discussion. A simulation routine is presented to predict the effects of pellet shrinkage within random packings on pellet arrangement and flow hydrodynamics, using Blender™ for pellet deposition and shrinkage and OpenFOAM® for flow simulation. After pellet shrinkage, packings show a high mean voidage and values for pressure drop below expectation. The feasibility of simulating pellet shrinkage within random packings is demonstrated, indicating its potential for reactor simulation.





## CRedit author statement

*Johanna Fernengel*: Conceptualisation, Methodology, Software, Formal analysis, Investigation, Visualisation, Writing - Original Draft.

*René Weber*: Investigation.

*Normen Szesni*: Project administration.

*Richard W. Fischer*: Project administration, Funding acquisition.

*Olaf Hinrichsen*: Project administration, Supervision, Funding acquisition, Writing - Review & Editing.

## Permission/License information

The screenshot shows the CCC RightsLink interface. At the top, there are navigation links for Home, Help, and Live Chat, along with a user profile for Johanna Fernengel. The main content area displays the title of the paper, the author list (Johanna Fernengel, René Weber, Normen Szesni, et al), the publication information (Industrial & Engineering Chemistry Research, American Chemical Society), and the date (May 1, 2021). Below this, a message states: "PERMISSION/LICENSE IS GRANTED FOR YOUR ORDER AT NO CHARGE". This message is followed by a list of conditions for the permission, including that it covers both print and electronic formats, allows for adaptation of figures and tables, requires appropriate credit to be given, and is a one-time permission. At the bottom of the message box, there are "BACK" and "CLOSE WINDOW" buttons. The footer of the page contains copyright information for 2022 and contact details for the Copyright Clearance Center, Inc.



## 6.1 Introduction

The synthesis of methanol is one of the most important examples of heterogeneous catalysis [162]. Commercial methanol synthesis catalysts contain CuO/ZnO/Al<sub>2</sub>O<sub>3</sub> as main components [163], which are utilised in catalytic fixed-bed reactors [164]. The catalysts are supplied as precursor in oxide state as cylindrical pellets or tablets [162]. Prior to plant operation, these have to be activated by reduction, mostly with hydrogen diluted in an inert gas, during which copper oxide is reduced to metallic copper [163, 165], releasing a significant amount of oxygen as water. This is accompanied by a volume contraction of the catalyst pellets, which causes shrinkage of the random packed catalyst bed [163], visible as reduced bed height. Although the volume contraction during activation of metal oxide catalyst by reduction is known, there is a lack of literature contributions on pellet shrinkage and its effect on packed bed structure. Available literature includes shrinkage of single pellets [166], pellet shrinkage within fluidised beds [167] and within fixed beds [168, 169] however excluding pellet resolved bed arrangements. Also, considerations on bed consolidation phenomena in chromatographic columns under compression have been made with respect to local packing variations [170]. Recent considerations of changes to the bed structure under compression have been studied in relation to fragmentation of catalyst pellets [171]. To predict the influence of pellet shrinkage within random packings on bed arrangement and flow hydrodynamics, this work introduces a simulation routine that accounts for settling of pellets into random packed beds under gravity, shrinkage of the individual catalyst pellets within the bed and the bed's response. Blender™ [23] is used for simulation of pellet deposition and shrinkage, the flow through the catalyst bed is obtained with OpenFOAM® [24]. Two scenarios of tablet shrinkage within random packed beds are considered and analysed with focus on bed voidage, local voidage profiles and pressure loss along the bed.

## 6.2 Methodology

The challenge in numerical packing generation lies in the absence of an analytical solution for the pellet positions within the bed. Therefore, means of pellet positioning, based for example on collision detection and the laws of physics, have to be applied. Commercial software packages, such as DigiDEM™ STAR-CCM+, EDEM® and PFC™, are available as well as LIGGGHTS® and Blender™ as open-source alternatives, the latter of which is applied here. Packing generation with Blender™ (cf. Boccardo et al. [80] as well as Partopour and Dixon [138]) relies on the Bullet Physics Library [83], enabling rigid body simulations. The motion of rigid objects of any shape is evaluated using the Newton-Euler equations, assuming the standard isotropic Coulomb friction model for point contacts between bodies and applying an impulse-momentum law at the moment of contact (cf.

Bender et al. [148] for details). Blender™ has a Python™ interface which allows for use of scripts to define simulation routines.

Figure 6.1 displays a simplified flowchart of the bed generation routine with subsequent pellet shrinkage. Parameter input is required covering pellet shape, dimensions before and after shrinkage, material properties and number, geometry of the confining wall and details on the filling procedure. The tablet shape is approximated by a surface mesh of a cylindrical base which is curved on both sides. The pellet input is implemented as random within a fixed insertion section across the diameter of the confining cylindrical wall with a filling density comparable to pouring. After settling of the random packing, implemented as threshold value for the maximum change in pellet position between subsequent simulation time steps, the pellets are shrunk in radial and longitudinal direction at their current position within the bed by scaling the pellet dimensions. The continuous nature of the shrinkage process has to be discretised for the simulation. Therefore, a number of discrete shrinkage steps is used, chosen based on a pre-study such that the influence on the simulation results is negligible. Fewer shrinkage steps noticeably reduced the resulting bed voidage which may be due to additional momentum transfer by the induced collisions between the pellets, whereas a larger value only increased simulation time. The scaling factors follow a geometric series. After each of the discrete shrinkage steps, where the pellet geometry is scaled, the bed is allowed to settle again. When the bed has come to rest the next volume contraction is

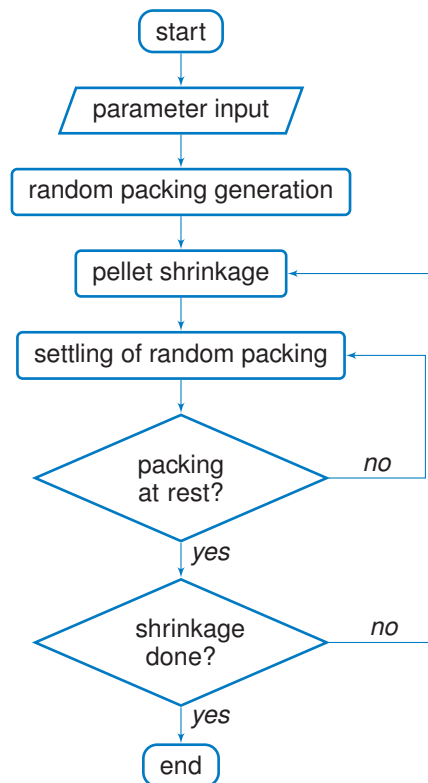


**Figure 6.1:** Simplified flowchart of random packing generation including routine for pellet shrinkage and settling of the bed.

applied to the pellets. This is repeated until the final pellet size has been reached and the resulting arrangement used for the flow simulation.

Mesh generation and flow simulation are performed with OpenFOAM<sup>®</sup> v4.1. The parameters for meshing with `snappyHexMesh` were adjusted based on a grid independency study, including the resolution of the cylindrical background mesh, refinement next to pellet surfaces and contact points and layer addition adjacent to surfaces (cf. supporting information). CFD simulations of an incompressible, isothermal, steady-state, laminar flow are performed with `simpleFoam`.

## 6.3 Case set-up

Two cases of pellet shrinkage during catalyst activation within a tubular fixed-bed are considered with different sets of arbitrary shrinkage values. The catalyst pellets are industrial standard sized tablets of  $6 \times 4$  mm. Only a section of the bed height is considered, though sufficiently long to investigate the effect of shrinkage on the bed structure. Therefore, 1000 tablets are filled into a cylindrical DN 40 standard pipe. Three beds are generated for each case: (1) one bed where the tablets are deposited under gravity, equivalent to catalyst loading, (2) one bed after pellet shrinkage based on the configuration obtained under (1), thus corresponding to the catalyst bed after activation, and (3) one bed for comparison obtained by deposition of pellets with dimensions corresponding to those of the shrunk tablets. Cold flow simulations are conducted for all obtained beds. The set of parameters

**Table 6.1:** Parameters for bed generation and flow simulation.

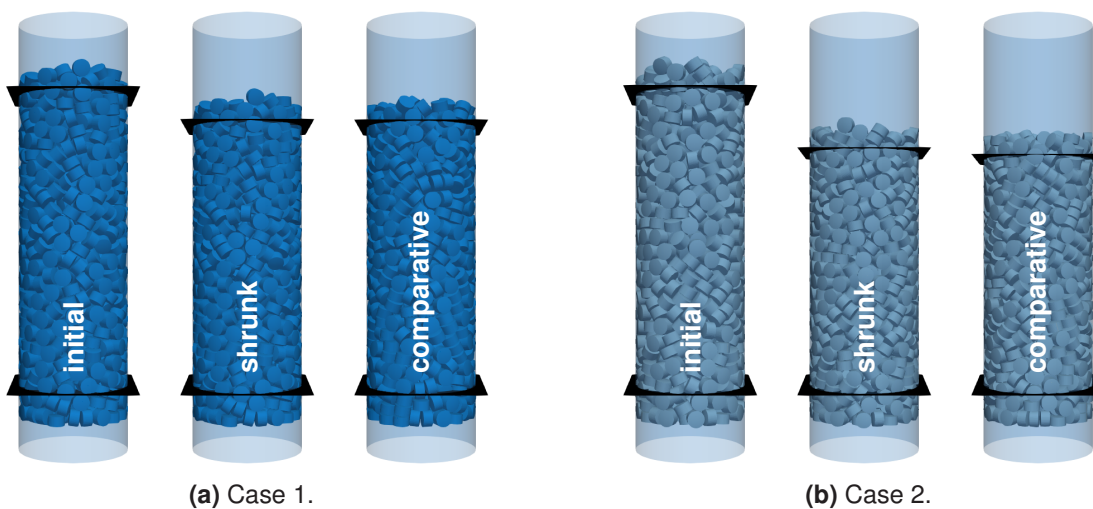
	Case 1	Case 2
Pellet deposition		
tablet diameter, $d$	6 mm	
tablet height, $h$	4 mm	
tube diameter, $D$	40.3 mm	
coefficient of friction, $\mu$	0.1	
coefficient of restitution, $e$	0.5	
number of pellets, $N$	1000	
time step, $\Delta t$	$1.5 \cdot 10^{-4}$ s	
threshold on pellet movement, $\Delta s$	$0.01d$	
Pellet shrinkage		
radial shrinkage, $\Delta r_p = \frac{d_{ini} - d_{shr}}{d_{ini}}$	2.5 %	5 %
height shrinkage, $\Delta h_p = \frac{h_{ini} - h_{shr}}{h_{ini}}$	5 %	10 %
number of shrinkage steps, $N_{shr}$	250	
Flow simulation		
superficial velocity, $u_0$	$0.01 \text{ m s}^{-1}$	
kinematic viscosity, $\nu$	$1.529 \cdot 10^{-5} \text{ m}^2 \text{ s}^{-1}$	
fluid density, $\rho$	$1.189 \text{ kg m}^{-3}$	

used for bed generation, pellet shrinkage and flow simulation are provided in Table 6.1. The low coefficient of friction resembles the smooth tablet surface and poses a limiting case to the shrinkage scenario, where pellet movement is least hindered. The set flow velocity ensures laminar conditions with particle Reynolds numbers of  $Re_p \approx 3.3$ .

## 6.4 Results and discussion

The pellet arrangement within the random packings of both cases is depicted in Figure 6.2. As expected, the beds obtained after pellet shrinkage and the comparative beds are shorter than the corresponding initial packings. Comparison of the bed heights (cf. Table 6.2) reveals a shrinkage of roughly 9% and 17% in total bed height, in the respective scenario, which compares well with the corresponding volumetric pellet shrinkages of 9.7% and 18.8%, respectively. Details of the simulation results are discussed for *Case 2*, where shrinkage is more pronounced.

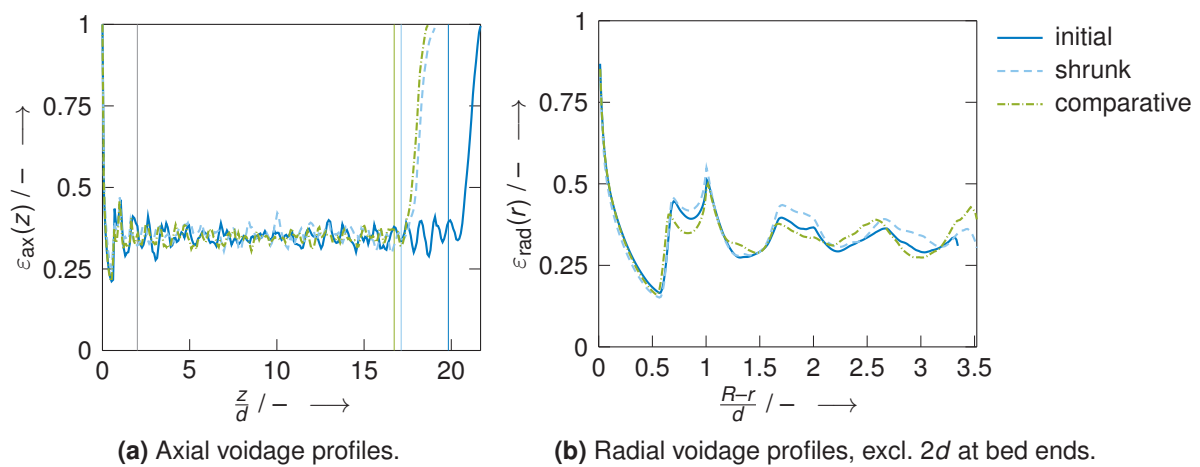
Figure 6.3a shows the axial voidage profile, indicating a strong local order in pellet arrangement at the bottom of the bed. By definition, the local voidage takes a value of *one* at the touching *points* or *lines* between bottom wall and rounded tablets. From there, local voidage declines steeply for a length of half a tablet diameter into the bed, where it reaches a global minimum. Further into the bed, the voidage profile shows three distinct local maxima, at distances of one tablet height, one tablet diameter and twice the tablet height from the bottom, respectively. From there on, the profile exhibits fluctuations around a mean value before increasing to *one* within a height of about one tablet diameter, corresponding to the top-most layer of tablets in the bed. While the general trends are similar for initial, shrunk and comparative bed, the initial bed is higher also based on the diameter of the underlying tablets. In the following, sections of twice a tablet diameter are excluded from both ends of



**Figure 6.2:** Packings as obtained by simulation. Planes enclosing bulk packing, cylindrical tubes indicating considered flow domain.

**Table 6.2:** Properties of simulated beds. Voidage and pressure values based on reduced bed excl. sections of  $2d$  from both ends.

	Case 1	Case 2
Initial packing		
bed height	13.06 cm	13.10 cm
mean bed voidage	0.348	0.350
pressure drop per unit length	12.02 Pa m <sup>-1</sup>	11.91 Pa m <sup>-1</sup>
Shrunk packing		
bed height	11.90 cm	10.90 cm
mean bed voidage	0.352	0.355
pressure drop per unit length	11.92 Pa m <sup>-1</sup>	12.06 Pa m <sup>-1</sup>
Comparative packing		
bed height	11.89 cm	10.67 cm
mean bed voidage	0.349	0.347
pressure drop per unit length	12.22 Pa m <sup>-1</sup>	14.15 Pa m <sup>-1</sup>

**Figure 6.3:** Local voidage profiles for *Case 2*.

the beds to omit the influence of end effects (cf. Figure 6.2 for indication of cut-off sections). The reduced height of shrunk and comparative beds is accompanied by a larger diameter aspect ratio of tube to tablet diameter  $D/d$  as evident from Figure 6.3b. The local order of tablets in the vicinity of the outer confining wall is similar to that observed at the bottom of the bed. However, the local radial voidage is below *one* indicating touching *areas* between tablets and tube wall where tablets align with the curvature of the tube, followed by an initial steep decline, related to tablets whose front sides are oriented towards the wall, until reaching a global minimum at a distance of just more than half a tablet diameter from the wall. At this position, both, tablets with front sides and cylindrical sides facing the wall, fully contribute to the solid fraction and the off-set further away from the confining wall is a result of the tube curvature. The following steep increase in radial voidage is related to tablets touching the tube wall with their front side. After a light decline, the voidage increases further to a local maximum at just more than one tablet diameter from the wall. The following maxima are damped in magnitude and voidage oscillates around a mean value. Comparing the three beds reveals somewhat more pronounced extrema near the wall for the shrunk bed, indicating a higher order in tablet arrangement. This is also evident from Figure 6.4, showing a scatter plot of tablet midpoints within the cross-section of the confining tube. Significant are the two outer rings of midpoints at a distance of about half a tablet height and half a tablet diameter from the wall. Their position is governed by the tablet's height-to-diameter ratio ( $h/d$ ) and the diameter aspect ratio ( $D/d$ ). The off-set in position of the outermost ring is stronger as tablets facing the confining wall with their front side are more affected by the tube curvature.

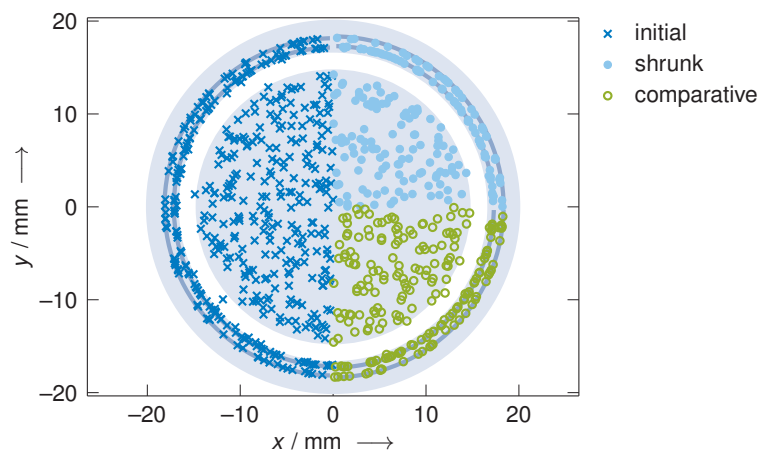


**Figure 6.4:** Tablet midpoints for *Case 2*, excluding  $2d$  at bed ends.

A closer look on pellet displacement and change in pellet orientation due to shrinkage within the packed bed may give an indication for the only minor variation in radial voidage and tablet midpoint positions. Figure 6.5a displays the average change of the pellets vertical and radial position normalised by the initial tablet diameter as a function of the pellets' initial radial position. As a results of shrinkage, pellets move significantly downwards. In contrast, radial displacement of the pellets is considerably small. As expected, the general trend is

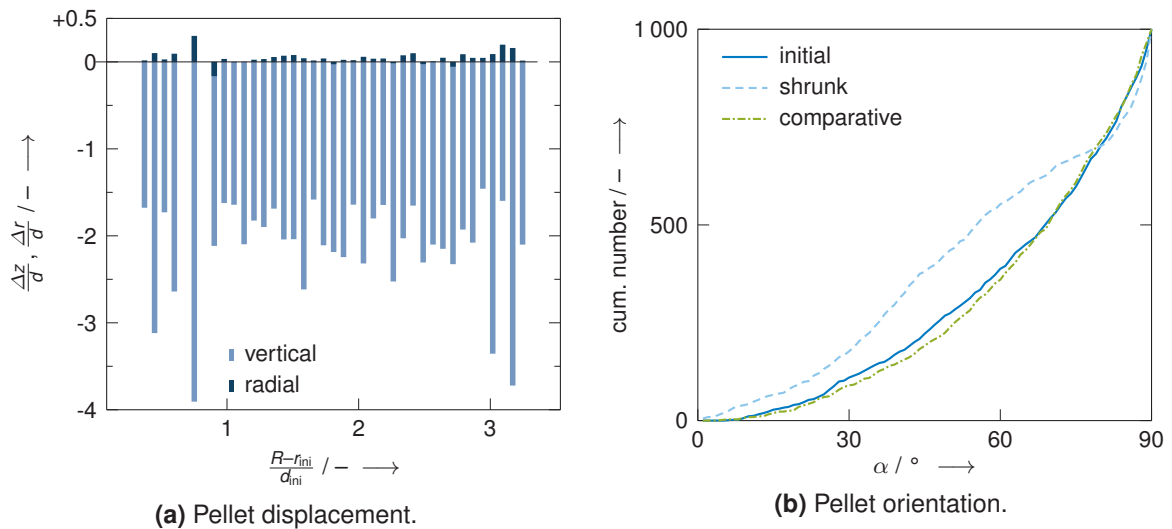


**Figure 6.5:** Effect of shrinkage on pellet arrangement for *Case 2*.

for pellets to move towards the confining wall (positive displacement in Figure 6.5a), as  $D/d$  is increased by pellet shrinkage. However, some pellets are pushed towards the centre of the bed. The region between the first and second ring of pellets from the confining wall is worth taking a closer look. While the largest radial movement of pellets towards the wall corresponds to tablets within the outermost ring, the most significant radial movement away from the wall corresponds to pellets within the second ring of tablets from the tube wall. This relative movement of pellets away from each other increases the gap between tablet midpoints in this region for the shrunk bed, cf. Figure 6.4, and results in the increased local radial voidage at just less than one tablet diameter from the tube wall, cf. Figure 6.3b. At the same time, pellet orientation changes as evident from Figure 6.5b, where an angle of  $0^\circ$  corresponds to tablets laying horizontally while an angle of  $90^\circ$  represents tablets standing upright. Both angle distributions for initial and comparative bed follow a convex function indicating a high number of rather upright oriented pellets. Contrary, the angle distribution for the shrunk bed is concave over a large range, thus more tablets have a rather horizontal alignment, but an even steeper convex slope at the very end of the range. Overall, the changes in pellet displacement and orientation induced by shrinkage indicate that vacant space in radial direction is occupied by pellet rotation rather than displacement.

The mean bed voidages in Table 6.2 reveal a slight deviation in value for the initial beds, which may be attributed to the influence of randomness in the packing generation algorithm. The considered beds are with  $D/d \approx 7$  in a range where voidage is generally expected to decrease with increasing  $D/d$  [121]. However, variation in  $D/d$  is small. *Case 1* shows similar values for initial and comparative bed voidage, whereas for *Case 2* the expected decrease is observed. Both shrunk beds show larger mean voidages than the corresponding initial and comparative beds. Considering their origin, this comes as no surprise: reducing the insertion height of pellets and high filling speeds increase bed voidage [107] by reducing both kinetic energy and time left for a pellet to take a new position before being hindered



by neighbouring pellets. Here, insertion height is at a minimum, considering shrinkage and settling within the bed, and filling speed at a maximum, charging the pellets from within the initial bed.

The pressure losses for *Case 2* are compared in Figure 6.6 showing the highest overall pressure drop across the initial bed. However, this is governed by bed length rather than an indication of the beds' resistance against flow which is highest for the comparative bed based on the pressure gradient (cf. also Table 6.2). For both initial beds, the values of pressure drop per unit length differ by less than 1%, as do the mean bed voidages. The highest pressure drops per unit length correspond to the comparative beds whereas the values for the shrunk beds are closer to the initial beds. Figure 6.7 compares the simulated pressure drops with those expected using the correlation by Eisfeld-Schnitzlein [172], indicating also tablet diameters and mean bed voidages. The correlation predicts a near linear increase of pressure drop per unit length from initial over shrunk to comparative bed, based on the pellet dimensions and observed bed voidages. Clearly, the simulated pressure drop across the shrunk bed violates this pattern with a value close to that of the initial bed. This underlines the influence of local pellet arrangement which can only be accounted for insufficiently within the correlation relying on overall bed properties.

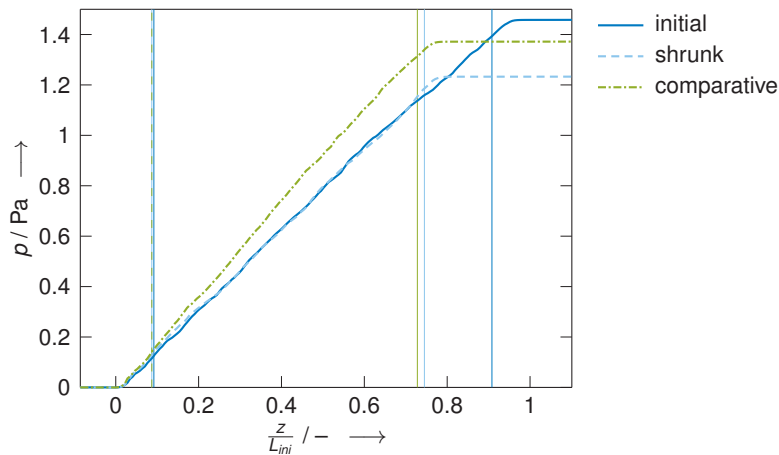


**Figure 6.6:** Area-averaged pressure losses for *Case 2*. Lines indicate positions used for evaluating pressure drop per unit length.



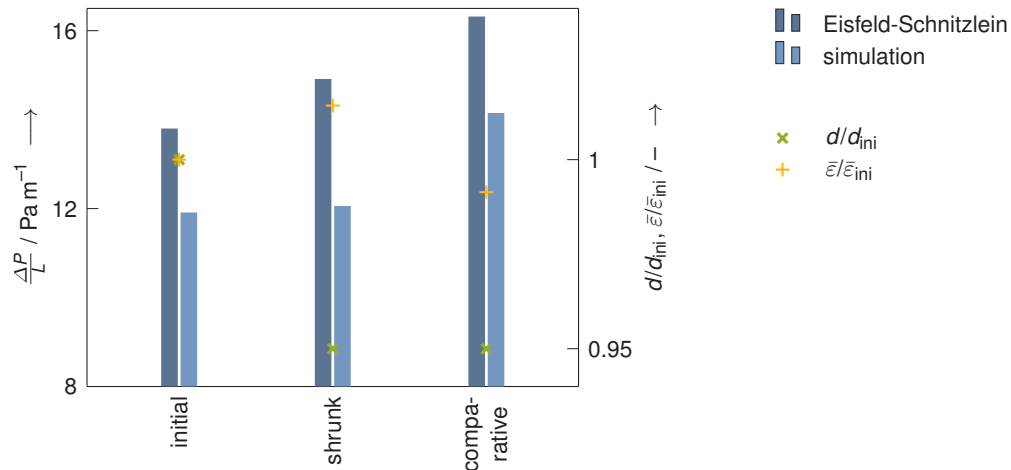


**Figure 6.7:** Comparison of simulated pressure drops for *Case 2* with Einfeld-Schnitzlein [172] correlation.

## 6.5 Summary and conclusion

In summary, catalyst pellets may experience volume contraction during activation, as for example CuO/ZnO/Al<sub>2</sub>O<sub>3</sub> catalysts used in methanol synthesis. A simulation routine was proposed to investigate the influence of pellet shrinkage within packed beds, covering random packing generation, pellet shrinkage within the bed and the related settling of the pellets. Influences of bed structure on the hydrodynamics of a steady-state, laminar flow were studied using CFD.

Two scenarios with different pellet shrinkages were considered with three beds each, one *initial bed* wherein the pellets experience a number of subsequent shrinkage and settling steps resulting in a *shrunk bed* and a *comparative bed* obtained by deposition of pellets with the dimensions after shrinkage. Analysis of axial voidage profiles led to the exclusion of sections of twice a tablet diameter from top and bottom of the beds to eliminate end effects. The radial voidage profiles revealed a higher order near the wall for the shrunk bed. The obtained mean bed voidages were such that the shrunk beds are least dense and the corresponding pressure losses per unit length lower than expected. A closer look on the effect of shrinkage on pellet arrangement revealed a region of low voidage between the first and second ring of pellets from the tube wall, underlining the importance of considering local packing structures in numerical simulations rather than solely relying on average bed properties.

It should be noted that the presented values for pressure drop are related to air at normal conditions. Absolute values were not of interest at this stage and interpretation of the presented results should not be overstated but merely demonstrate the feasibility and indicate the potential of simulating pellet shrinkage within random packings as a contribution towards a better understanding of reactor behaviour by means of numerical simulation. Also, to widen the range of applicability a custom friction model should be implemented

when considering materials with higher coefficient of friction as this is underestimated by Blender™ as compared to DEM code (cf. Chapter 5). The proposed shrinkage routine may be embedded in a more complex simulation framework, taking into account conversion and heat transfer, and allowing for example individual pellet shrinkages based on local temperature or conversion by closer coupling with CFD simulations. Also, bed densification by vibration may be considered.

## 6.S Supporting information

### 6.S.1 Mesh generation

The OpenFOAM<sup>®</sup> utilities *blockMesh* and *snappyHexMesh* are used to first generate a cylindrical background mesh, corresponding to the region covered within the cylindrical reactor tube, from which the pellet arrangement of the catalytic packed bed as obtained by simulation with Blender<sup>™</sup> is removed in a second step.

The cylindrical background mesh is set up such that there are 100 cells across the diameter of the tube. The cell length in longitudinal direction, i.e. along the reactor length axis, is adjusted accordingly to give cells as close to ideal as possible.

All three sub-routines of *snappyHexMesh*, namely *castellatedMesh*, *snap* and *addLayers*, are applied which perform cell splitting in the vicinity of specified surfaces, removal of the cells within the pellets (i.e. only fluid phase considered), smoothing of the mesh by snapping to specified surfaces and finally addition of cell layers adjacent to specified surfaces. Please note that mesh generation was initially conducted for turbulent flow simulations which require a higher level of mesh resolution close to surfaces. These meshes have been re-used for the presented laminar flow simulations.

The main settings for the three *snappyHexMesh* steps performed are as follows:

- 1.) Mesh refinement around surfaces and removal of mesh within pellets

```
castellatedMeshControls
{
  ...
  nCellsBetweenLevels 1;
  refinementSurfaces
  {
    pellets
    {
      level (1 1);
      gapLevelIncrement 2;
    }
  };
  resolveFeatureAngle 1;
  refinementRegions
  {
    pellets
    {
      mode distance;
      levels ((0.00006 2) (0.0006 1));
    }
  };
  ...
}
```

## 2.) Snapping of mesh points close onto surfaces

```
snapControls
{
  nSmoothPatch 3;
  tolerance 0.8;
  nSolverIter 10;
  nRelaxIter 5;
  // Feature snapping
  nFeatureSnapIter 10;
  implicitFeatureSnap false;
  explicitFeatureSnap true;
  multiRegionFeatureSnap false;
}
```

## 3.) Addition of layers adjacent to specified surfaces

```
addLayersControls
{
  relativeSizes true;
  layers
  {
    "pellets"
    {
      nSurfaceLayers 1;
    }
    "walls"
    {
      nSurfaceLayers 2;
    }
  }
  expansionRatio 1.0;
  finalLayerThickness 1.0;
  minThickness 0.2;
  nGrow 0;
  ...
}
```

### 6.S.2 Grid-independence study

The procedure followed to quantify the uncertainty introduced by spacial discretisation of the computational domain is based on the routine proposed by the Fluids Engineering Division of ASME [49].

A mesh independency study was conducted for the comparative bed of *Case 2* as this is the shortest bed considered and hence likely to result in a computational grid with the lowest total number of cells amongst the six considered bed arrangements. The parameter being varied is the number of cells across the diameter of the background mesh generated with

*blockMesh* and therefore the average cell size within the background mesh. The respective number of cells across the cylindrical reactor tube is 100, 50, 25 from fine to coarse. Details of the three considered meshes and the calculations leading to the error estimates based on Celik et al. [49] are summarised in Table 6.3. The pressure drop per unit length of packed bed is considered as variable  $\phi$ .

**Table 6.3:** Mesh details and discretisation error calculations.

<i>Case 2, comparative bed</i>	
$N_1$	39 327 755
$N_2$	12 979 055
$N_3$	3 897 999
$r_{21}$	1.444
$r_{32}$	1.484
$\phi_1$	14.1489
$\phi_2$	13.7000
$\phi_3$	13.8382
$p$	3.403
$\phi_{\text{ext}}^{21}$	14.329
$e_a^{21}$	3.17 %
$e_{\text{ext}}^{21}$	1.26 %
$GC_{\text{fine}}^{21}$	1.59 %

The settings underlying the finest grid ( $N_1$ ) have been used in the simulations leading to the results presented in this manuscript. Due to reasons of computational feasibility two coarser meshes have been considered in the grid independence study. This leads to an uncertainty for the fine grid solution, which can be expressed by the grid convergence index  $GC_{\text{fine}}^{21}$ , amounting to less than 1.6%.

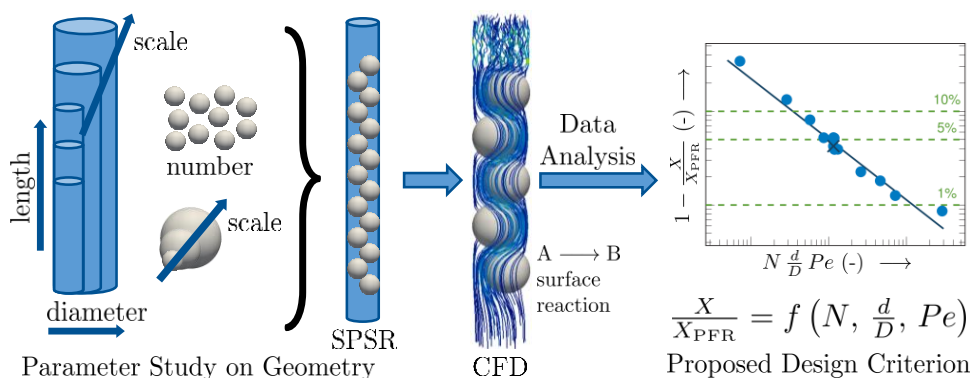


# 7 Characterisation and design of single pellet string reactors

This chapter was published in a similar form and is reprinted with kind permission from: J. Fernengel, L. Bolton and O. Hinrichsen, Characterisation and design of single pellet string reactors using numerical simulation, *Chem. Eng. J.* **2019**, *373*, 1397–1408, DOI 10.1016/j.cej.2019.03.114. [173]. Copyright 2019 Elsevier B.V.

## Publication summary

The concept of single pellet string reactors (SPSR), where particles are packed in tubes of only slightly larger diameter, has been subject of recent studies which demonstrate a renewed interest in this reactor concept, including its use for catalyst testing. However, there remains the need for a thorough characterisation of the reactor performance. In this study, an attempt is made to systematically investigate the flow and conversion behaviour of SPSRs consisting of spherical, non-porous particles in cylindrical confining walls using computational fluid dynamics (CFD). A parameter study with variations on reactor geometry is conducted considering laminar flow and an isothermal, irreversible hypothetical first order reaction taking place at the catalytic particle surface. In addition to reaction simulation, the residence time behaviour is investigated based on numerical tracer experiments. The results showed that conversion close to plug flow can be achieved with SPSRs using favourable parameter settings. Conversion was found to be enhanced in reactors at larger scale, with smaller cylinder-to-particle diameter ratio and with a larger number of catalytic particles. The applicability of existing design criteria for conventional fixed-bed reactors is evaluated. Based on the observations a design criterion for SPSRs is proposed which allows prediction of the deviation to plug flow conversion based on reactor geometry, fluid properties and flow velocity.



### CRedit author statement

*Johanna Fernengel*: Conceptualisation, Methodology, Software, Formal analysis, Investigation, Visualisation, Writing - Original Draft.

*Leslie Bolton*: Supervision, Project administration, Funding acquisition, Writing - Review & Editing.

*Olaf Hinrichsen*: Project administration, Supervision, Funding acquisition, Writing - Review & Editing.

### Permission/License information

The screenshot displays the CCC RightsLink interface. At the top left is the logo for CCC RightsLink. On the right side of the header, there are navigation links for Home, Help, and Live Chat, along with a user profile for Johanna Fernengel, which includes options for Account Info and Sign Out. The main content area features a card for the article "Characterisation and design of single pellet string reactors using numerical simulation". The card includes a thumbnail of the journal cover, the author names (Johanna Fernengel, Leslie Bolton, Olaf Hinrichsen), the publication (Chemical Engineering Journal), the publisher (Elsevier), and the date (1 October 2019). Below the article details is a section titled "Journal Author Rights" with a paragraph of text explaining the author's rights and a link to Elsevier's copyright policies. At the bottom of the interface, there is a footer with copyright information and contact details for the Copyright Clearance Center.

**CCC RightsLink** Home Help Live Chat Johanna Fernengel

Account #: 3001987060  
Account Info  
Sign Out

**Characterisation and design of single pellet string reactors using numerical simulation**  
Author: Johanna Fernengel, Leslie Bolton, Olaf Hinrichsen  
Publication: Chemical Engineering Journal  
Publisher: Elsevier  
Date: 1 October 2019  
© 2019 Elsevier B.V. All rights reserved.

**Journal Author Rights**  
Please note that, as the author of this Elsevier article, you retain the right to include it in a thesis or dissertation, provided it is not published commercially. Permission is not required, but please ensure that you reference the journal as the original source. For more information on this and on your other retained rights, please visit: <https://www.elsevier.com/about/our-business/policies/copyright#Author-rights>

BACK CLOSE WINDOW

© 2022 Copyright - All Rights Reserved | Copyright Clearance Center, Inc. | Privacy statement | Terms and Conditions  
Comments? We would like to hear from you. E-mail us at [customer-care@copyright.com](mailto:customer-care@copyright.com)



## 7.1 Introduction

Heterogeneous catalysis accounts for a large amount of production of the chemical industry and the development of new catalyst systems as well as the optimisation of existing units is of great importance. Especially, there is a need for testing the performance of commercial catalysts at industrial process conditions but preferably at smaller scale [29]. To replicate commercial process conditions at small scale, it is necessary to operate with the same space velocity, temperature, pressure, feed composition and catalyst, but to use shorter or narrower catalyst beds possibly containing smaller catalyst particles [7]. In order to obtain information which may be directly related to industrial sized reactors, it is preferable to use the catalyst in exactly the same form as in the industrial sized reactor, so as not to introduce distorting effects on the apparent activity of the catalyst, the selectivity and its deactivation behaviour [36]. Therefore, conventional design criteria for catalytic testing result in long packed bed reactors [6, 7] with tube diameters much larger than the catalyst pellet size [8], as otherwise poor axial and radial dispersion within the bed would be expected, which make it difficult to interpret results of kinetic experiments. These criteria lead to relatively large and costly reactors which require substantial gas flow rates and may pose a significant level of hazard. On the contrary, a reactor concept where pellets are packed into tubes of only slightly larger diameter came up in the 1960s and was named *single pellet string reactor* (SPSR) by Scott et al. [4] in 1974 who already described the similarity of the reactor's flow behaviour to conventional packed beds. However, are SPSRs suitable for kinetic experiments and industrial catalyst performance testing? Recent publications [5, 14, 15] demonstrate a renewed interest in this reactor concept, including its use for catalyst testing.

A comprehensive overview on the fundamental issue of downscaling of fixed-bed reactors was presented by Sie [36]. The central goal was, and still is today, to find a suitable small reactor operating with industrial sized catalysts and thereby showing a hydrodynamic behaviour sufficiently close to ideal plug flow to have a negligible effect on the macrokinetics and hence the reaction rate. Deviations from plug flow arise mainly due to an uneven voidage distribution in the reactor packing, visible as a spread of the residence time distribution (RTD). Based on experiments, Sie concluded that reactors below the scale of microreactors can be used for testing industrial catalysts yielding data comparable to commercial operation. Although named *nanoflow reactor*, he therewith already indicated the applicability of SPSRs. Experiments by Scott et al. [4] in reactors with cylinder-to-particle diameter ratios of  $1.16 \leq D/d \leq 1.35$  using both porous and non-porous spherical particles showed a reproducible flow behaviour with an axial dispersion comparable to conventional packed beds. From then onwards, publications on SPSRs have been infrequent, with an increase in number just recently. In the following a brief outline of available literature contributions is given, with no claim to completeness, starting in chronological order.

Work on axial dispersion in the presence of significant wall effects was conducted by Hsiang and Haynes [53], who reported sufficient packing reproducibility and confirmed the observation by Scott et al. [4] that packed bed correlations are applicable for SPSR with cylinder-to-particle diameter ratios of  $1.1 \leq D/d \leq 1.4$ . Above these diameter ratios the dispersion exceeded the values expected from the correlations. Lee et al. [55] investigated the use of cylindrical particles in SPSRs concluding that for laminar flow the same flow behaviour as observed in conventional packed beds persists. Sharma et al. [57] concluded from measuring effective diffusion coefficients of commercial catalysts that the magnitude of axial dispersion in SPSRs was low compared to diffusion. Dixon [60] reported a potential predictable behaviour for beds with aspect ratios of  $1 < D/d < 2$  as a result of heat transfer experiments with beds of spheres.

More recent work on SPSRs evolves in different research directions, including single-phase reactions in beds with spherical particles in cylindrical confined walls as well as other particle and outer geometry shapes, multiphase flow, reaction and bed dilution with inert fines.

Pressure drop and residence time simulations with COMSOL Multiphysics<sup>®</sup> 4.2a were presented by Müller et al. [12] for liquid flow in reactors with spherical particles in cylindrical confining walls of aspect ratio  $D/d = 1.2$ , concluding near plug flow behaviour.

An increasing amount of research activity can be recognised on heterogeneously catalysed gas phase reactions in beds with cylindrical or other shaped pellets. Klyushina et al. [14] investigated the catalytic decomposition of nitrous oxide using an industrial catalyst of equilateral cylindrical shape. Comparing the rate of the catalytic reaction observed in a SPSR with  $D/d = 1.08$  and a packed bed reactor with  $D/d = 9.8$  they concluded the suitability of SPSRs to gain kinetic data. A comparative study between simulation with FLUENT 6.3 and experimental results was conducted by Behnam et al. [13] on endothermic steam methane reforming using cylindrical particles with external grooves in an ordered string with excellent agreement for temperature and species concentration results.

SPSRs with spherical particles and square cross section of the confining walls were the subject of research at Delft University of Technology, starting with a publication by Calis et al. [64] on a simulative (CFX-5.3) and experimental investigation of pressure drop in composite structured packings (effectively composed of a large number of SPSRs in parallel). This work was continued by Romkes et al. [65] obtaining good agreement between experimental data and computational fluid dynamics (CFD) simulations for heat and mass transfer characteristics. Other work on SPSRs with square cross section was published by Hipolito et al. [11] on the selective hydrogenation of allene which concluded that the reactors are suitable for catalyst testing.

Over the past years, numerous studies have been published by the Lange group at Dresden on two-phase flow in SPSRs with spherical particles in cylindrical confining walls, the simulative paper by Müller et al. [12] on single-phase liquid flow marking the starting point. Langsch et al. [66] investigated the SPSR's potential as reactor concept for the transfer of fast batch processes to continuous operation studying the hydrogenation of  $\alpha$ -methylstyrene. A scale-up of the SPSR by parallelisation of multiple channels showed promising results for the selective hydrogenation of cinnamaldehyde [67]. Müller et al. [15] investigated the transition from batch to continuous operation of the hydrogenation for the synthesis of diacetone-D-allose using cylindrical catalyst particles in SPSRs in concurrent downflow. Further work on two-phase flow was published by Kallinikos and Papayannakos [68] showing that the hydrodesulphurisation of heavy gas oil on commercial catalyst extrudates in a spiral reactor, a diluted bed and a pilot plant lead to similar results.

One approach which has been used to improve the isothermal properties of catalytic fixed beds is the addition of small inert particles to the catalytic bed. This avoids wall effects and hence improves plug flow behaviour [7], which makes it an important consideration for SPSRs. The influence of dilution on conversion has been investigated with a stochastic model by van den Bleek et al. [69] in the late 1960s. Sie [36] put forward the need of adding fine particles in small beds of relatively large industrial catalyst particles for hydrodynamic reasons when operating with trickle-flow. The surrounding inert fines ensure near-plug flow hydrodynamics while the catalytic conversion is dictated by the actual size of the catalytic particles. Berger et al. [70, 71] re-evaluated the influence of dilution on gas-solid reactions in fixed-bed reactors by experimental studies on the catalytic decomposition of nitrous oxide and using a random particle distribution model. Moonen et al. [5] tested the performance of a hydrodesulphurisation catalyst for gas oil in SPSRs, with a tube diameter about the size of the catalytic extrudate diameter, and bench-scale fixed bed reactors. Some SPSR configurations and the bench-scale reactor were diluted with non-porous inert fines. The results revealed comparable sulphur levels with high reproducibility of the SPSRs.

The literature presented above shows the ongoing interest in SPSRs over decades. The recent increase in research activities related to this reactor may result in its more widespread adoption for catalyst testing. Nonetheless, there is the need for a thorough characterisation of the SPSR, leading to design criteria relating reactor performance to ideal plug flow behaviour.

In this work, an attempt is made to systematically characterise SPSRs of spherical, non-porous particles in cylindrical confining walls by CFD simulations. A parameter study on the reactor geometry is conducted whilst keeping the space time constant. As opposed to Scott et al. [4] we do not restrict the cylinder-to-particle diameter ratio to  $D/d < 1.4$  but regard reactors with a diameter ratio of  $D/d < 2$  as SPSRs. Residence time behaviour as well as the conversion of a hypothetical first order irreversible gas-phase reaction at the pellet surface are evaluated and compared to corresponding plug flow results. The applicability of

common design criteria for conventional fixed-bed reactors to SPSRs is discussed, covering criteria on axial dispersion, radial dispersion, external mass transfer limitations and bed dilution. Finally, a design criterion is derived for which SPSRs show a behaviour close to ideal plug flow.

## 7.2 Methodology

The numerical study on the SPSR is based on a heterogeneous reactor model, using CFD for flow evaluation, reaction simulation and investigation of residence time behaviour. As the inside of the pellets is of no interest within this study, only the fluid phase is simulated whereas the solid phase is incorporated through the mesh and appropriate boundary conditions. Mesh generation and CFD simulations are performed with OpenFOAM<sup>®</sup> v2.4.0 [24]. The simulation routine covering geometry set-up, mesh generation, flow simulation, reaction simulation and tracer propagation as well as certain post-processing steps is automated using Bash and Python scripts to allow for easy parameter variation (cf. [73]).

### 7.2.1 Geometry

Under ideal conditions, spherical particles in a SPSR rest on top of each other and on alternating sides of the reactor. Thus, the particle position can be described mathematically. When adding fines to the system, the positions cannot be described analytically any more and the software Blender<sup>™</sup> 2.76b [23] is used for generating a geometrical arrangement inside the SPSR. The reactor length is determined by the cylinder-to-particle diameter ratio as well as the number and size of particles. In addition, some space upstream including a short bed of inert fines and downstream of the catalytic particles is introduced.

#### 7.2.1.1 Analytical particle position

The position of spherical particles within a SPSR with a cylindrical confining wall can be expressed as a function of the pellet diameter  $d$  and the cylinder diameter  $D$  based on trigonometric relations. The centre point coordinates of the  $i^{\text{th}}$  particle are given by Equations (7.1) to (7.3).

$$x_i = (-1)^i \left( \frac{D-d}{2} \right) \quad (7.1)$$

$$y_i = 0 \quad (7.2)$$

$$z_i = \frac{d}{2} + (i-1) \sqrt{d^2 - (D-d)^2}. \quad (7.3)$$

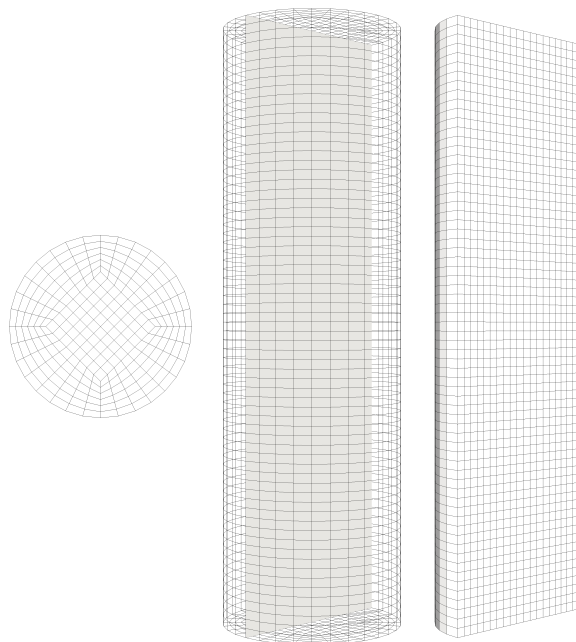


**Figure 7.1:** General structure of background mesh; top view, front view and cross-section as indicated in front view (from left to right).

The corresponding height  $H$  of a bed with a total number of  $N$  particles can be evaluated as

$$H = d + (N - 1)\sqrt{d^2 - (D - d)^2}. \quad (7.4)$$

## 7.2.2 Particle positioning with Blender™

When the particle position cannot be described analytically, we use the open-source software Blender™ as first proposed by Boccoardo et al. [80]. The algorithm for particle deposition and settling into a bed relies on collision detection and resolution based on rigid body physics, which is made available through integrating the Bullet Physics Library [83]. Further insight into rigid body simulations can be found in [148].

### 7.2.2.1 Mesh generation

The fluid domain surrounding the particles in the SPSR is meshed using the utility *snappyHexMesh* as supplied with OpenFOAM®. For this a cylindrical background mesh representing the inner diameter and the height of the reactor tube is generated with *blockMesh*, another utility supplied with OpenFOAM®. The general structure applied for the background mesh is shown in Figure 7.1. Information on particle size and position are entered into the *snappyHexMesh* routine either as analytical values or via a stereolithographic file. The mesh generation algorithm starts with cell refinement of the background mesh close to particle surfaces and the removal of cells within particles. Then, mesh points close to the particle surfaces are moved onto these. Finally, layers of mesh cells are introduced adjacent to

surfaces to improve mesh quality and for further mesh refinement close to the particles as well as the wall region.

### 7.2.3 Numerical simulation

It is assumed that the flow field is independent of the reaction. This allows using a segregated solution where a cold flow is simulated prior to the reaction. The residence time is evaluated with a virtual tracer experiment based on the cold flow.

#### 7.2.3.1 Flow simulation

We assume an isothermal flow of a single phase, viscous and incompressible Newtonian fluid at steady-state in a 3D domain. The corresponding governing equations are the continuity equation as provided in Equation (7.5) and the momentum balance stated in Equation (7.6),

$$\nabla \cdot \mathbf{u} = 0 \quad (7.5)$$

$$\nabla \cdot (\mathbf{u}\mathbf{u}) = -\frac{1}{\rho} \nabla p + \nu \nabla^2 \mathbf{u}, \quad (7.6)$$

where  $\mathbf{u}$  is the velocity vector,  $\rho$  the fluid density,  $p$  the pressure and  $\nu$  the kinematic viscosity.

The standard OpenFOAM<sup>®</sup> solver *simpleFoam* is applied to compute the flow through the reactor setting steady-state conditions and treating the flow as laminar. A Dirichlet boundary condition is set as velocity inlet condition. No-slip boundary conditions are set for the velocity at the pellet surfaces as well as at the reactor wall whereas a zero-gradient condition is defined at the outlet. The pressure at the outlet is set to atmospheric; all other pressure boundary conditions are implemented as zero-gradient conditions.

#### 7.2.3.2 Reaction simulation

A hypothetical first order irreversible reaction  $A \longrightarrow B$  is considered to take place at the catalytic particle surface. Further, the reaction is assumed isothermal and isochoric. The transport of passive species in an incompressible flow by convection and diffusion under steady-state is described by

$$\nabla \cdot (\mathbf{u} Y) - \nabla \cdot (\mathcal{D} \nabla Y) = 0, \quad (7.7)$$

where  $Y$  is the mass fraction of the passive species and  $\mathcal{D}$  the molecular diffusion coefficient of the species within the fluid. In the OpenFOAM<sup>®</sup> simulation this is realised using the standard solver *scalarTransportFoam*.

The heterogeneous surface reaction is introduced into the reactor model as Neumann type boundary condition on the catalytic particles by defining a concentration dependent depletion gradient at the particle surface. As put forward by Maestri and Cuoci [84], the flux of the reactant across the pellet surface equals the rate of depletion due to the heterogeneous reaction. This can be expressed using Fick's law of diffusion and the rate equation for an irreversible first order reaction by

$$-\mathcal{D} \nabla Y_p = k Y_p, \quad (7.8)$$

where  $k$  is the reaction rate coefficient and  $Y_p$  the mass fraction of the reactant at the particle surface. The remaining boundary conditions are set as Dirichlet condition at the inlet and zero-gradient conditions at non-catalytic surfaces and the reactor outlet.

### 7.2.3.3 Simulation of residence time behaviour

The RTD over the string of particles is evaluated with a numerical step tracer experiment. Therefore, the transient transport of a passive tracer species through the SPSR by convection and diffusion is considered.

$$\frac{\partial Y}{\partial t} + \nabla \cdot (\mathbf{u} Y) - \nabla \cdot (\mathcal{D} \nabla Y) = 0 \quad (7.9)$$

For the simulation of the tracer experiments, the solver *scalarTransportFoam* is used. To omit the reactor entrance and exit length, the step input of the tracer is explicitly set at the catalytic bed entrance and the tracer response sampled directly downstream of the last particle. The residence time distribution functions  $E(t)$  are evaluated based on the resulting cumulative distribution curves by

$$E(t) = \frac{d}{dt} \left[ \frac{Y(t)}{Y_0} \right]_{\text{step}}, \quad (7.10)$$

where  $Y(t)$  is the tracer mass fraction at the catalytic bed exit at time  $t$  and  $Y_0$  is the mass fraction of tracer at the inlet.

## 7.3 Case set-up

All of the SPSR variations introduced in the following are evaluated in regard to conversion as a function of axial position and RTD. The particles are spherical and non-porous, the confining walls of cylindrical shape. A single phase laminar gas flow is considered with a constant space time of 1 s over the string of particles. Here, space time is defined as

$$\tau = \frac{V_f}{\dot{V}} \quad (7.11)$$



with  $\dot{V}$  being the volumetric flow and  $V_f$  the fluid volume occupying the catalytic bed. Based on the reactor geometry, the resulting superficial velocity  $u_0$  for each SPSR can then be expressed as

$$u_0 = \frac{V_f}{A_t \tau} = \frac{H - \frac{NV_p}{A_t}}{\tau} = \frac{d + (N-1)\sqrt{d^2 - (D-d)^2} - \frac{2Nd^3}{3D^2}}{\tau}, \quad (7.12)$$

where  $V_p$  is the particle volume and  $A_t$  the cross sectional area of the empty reactor tube. In case of filling the void space surrounding the catalytic particles with inert fines, the total volume of fines is added to the volume of catalytic particles in the equation above. The assumption of laminar flow is based on the particle Reynolds number  $Re_p$ . The physical properties of the considered gas flow are those of nitrogen for both reactants and products. These are especially:

- self-diffusion coefficient of  $\mathcal{D} = 1.72 \cdot 10^{-5} \text{ m}^2 \text{ s}^{-1}$  (760 mmHg, 0 °C) [174]
- kinematic viscosity of  $\nu_a = 1.529 \cdot 10^{-5} \text{ m}^2 \text{ s}^{-1}$  (1 bar, 20 °C).

A tracer with non-diffusive properties is used for the numerical residence time experiments.

For simulating the catalytic surface reaction, the feed is composed of pure reactant. The heterogeneous reaction rate constant  $k$  is set to a value corresponding to 80 % conversion in a comparable plug flow reactor with identical specific surface area and space time. Based on the SPSR geometry, the specific surface area  $a$  can be expressed by

$$a = \frac{NA_p}{V_f} = \frac{Nd^2}{\frac{1}{4}HD^2 - \frac{1}{6}Nd^3}, \quad (7.13)$$

where  $A_p$  is the surface area of one catalytic particle. The reaction rate constant  $k$  can be evaluated analytically using the following expression for plug flow conversion  $X_{\text{PFR}}$ :

$$X_{\text{PFR}} = 1 - e^{-\tau ka}. \quad (7.14)$$

The base case scenario (*scenario a*) consists of a string of 20 catalytic particles with a diameter of  $d = 0.8 \text{ mm}$  in a cylindrical tube of  $D = 1.0 \text{ mm}$  inner diameter. The fluid has the properties of nitrogen as specified above and pure reactant is introduced at the reactor inlet. There are no inert fines surrounding the catalytic particles but a short bed of inert fines with a height of  $1d$  and fines of  $0.2d$  diameter positioned upstream of the catalytic bed to enforce near-plug flow behaviour in order to prevent back-mixing in the entry zone and replicate the likely practical arrangement (cf. supporting information for influence of in-/outlet configuration). The variations on this base case include a reactor in which the particles are stacked right on top of each other along the axis of the reactor



**Table 7.1:** Geometry settings of single pellet string reactor scenarios.

case	$N$	$d$ in mm	$D$ in mm	$D/d$	$d/d_{\text{fines}}$	scenario
-	-	-	-	-	-	-
a	20	0.8	1.0	1.25	-	base case
b	20	0.8	1.0	1.25	-	stacked particles
c1	20	1.2	1.5	1.25	-	scaling
c2	20	1.6	2.0	1.25	-	
d1	20	0.8	0.9	1.125	-	diameter ratio variation
d2	20	0.8	1.2	1.5	-	
d3	20	0.8	1.4	1.75	-	
e1	5	0.8	1.0	1.25	-	particle number
e2	10	0.8	1.0	1.25	-	
e3	50	0.8	1.0	1.25	-	
e4	100	0.8	1.0	1.25	-	
f	20	0.8	1.0	1.25	5	inert fines

rather than touching the cylinder wall on alternating sides (*scenario b*), two reactors where the base case geometry is scaled by factors of 1.5 and 2.0 respectively (*scenario c*), three reactors with varying cylinder-to-particle diameter ratio where the particle diameter is kept constant while adjusting the cylinder diameter (*scenario d*) and four reactors with varying number of catalytic particles, ranging from  $N = 5$  to  $N = 100$  (*scenario e*). Also, filling the void space between the catalytic particles with inert fines of considerably smaller diameter is considered (*scenario f*). The properties of the SPSR variations are summarised in Table 7.1. Considering especially the scenario with varying particle number, it should be noted that the heterogeneous reaction rate constant is re-evaluated for each scenario based on a corresponding plug flow conversion of 80%. Hence the analytical solution of the rate constant  $k$  is inversely proportional to the number of pellets in the reactor.

## 7.4 Results and discussion

### 7.4.1 Base case single pellet string reactor

A grid-independence study has been conducted based on overall bed conversion, details of which are included in the supporting information. The resulting geometry as well as sections of the final mesh are shown in Figure 7.2. The final mesh consists of roughly 4.5 million cells, with additional refinement towards the particle surfaces and the cylinder wall.

The specification of a constant space time of 1 s across the catalytic bed results in a particle Reynolds number of  $Re_p = 0.45$  for the base case, which can be approximated as laminar flow.

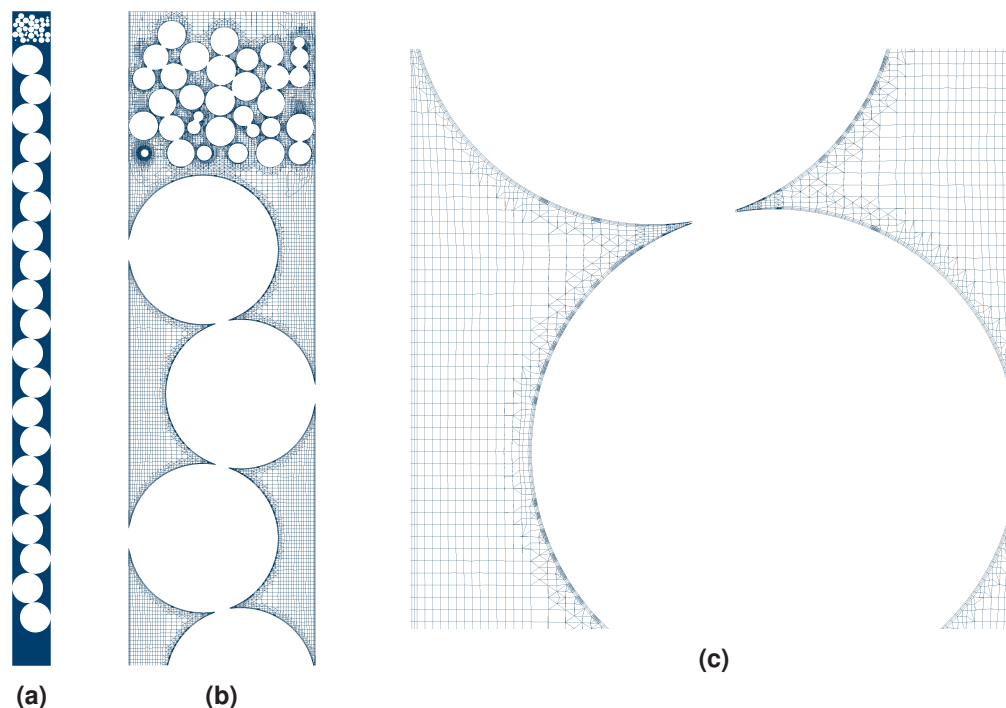


**Figure 7.2:** Lateral cuts through geometry (a) and final mesh of flow domain (b and c) for base case SPSR (*scenario a*).

Figure 7.3 shows the resulting flow field within the reactor, revealing the heterogeneous nature of the flow surrounding the catalytic particles. Consistently high velocity values are located in the region between catalytic particles and reactor wall, alternating in location through the reactor with the particle position. The inert bed at the reactor entrance imposes the desired near plug flow behaviour there.

Displayed in Figure 7.4 is the resulting RTD of a non-diffusive tracer over the catalytic bed, that is omitting the inlet section with the inert bed and the short empty tube at the outlet. The curve shows a sharp gradient and a following maximum after about half the defined space time of 1 s. This is similar to convective behaviour in laminar flow reactors. On top of this, the pulse is broadened by dispersion resulting from the inherent character of the SPSR. For comparison, the RTD of a non-diffusive tracer corresponding to ideal plug flow takes the shape of a Dirac delta function at the reactors space time. When superimposing the influence of tracer diffusion, the peak is broadened, less asymmetric and the maximum shifted further towards the space time of the reactor (cf. supporting information), leading to the same conclusion as obtained by Sharma et al. [57] that the magnitude of axial dispersion in SPSRs is low compared to diffusion.

Finally, the conversion of the hypothetical first order irreversible reaction taking place at the surface of the catalytic particles is presented in Figure 7.5. The overall reactor conversion with a value of 76.6% is close to the corresponding ideal plug flow conversion of 80%. Subfigure 7.5b depicts the conversion per pellet for the 20 catalytic particles within the bed based on the average concentration on each pellet and that on the previous pellet,

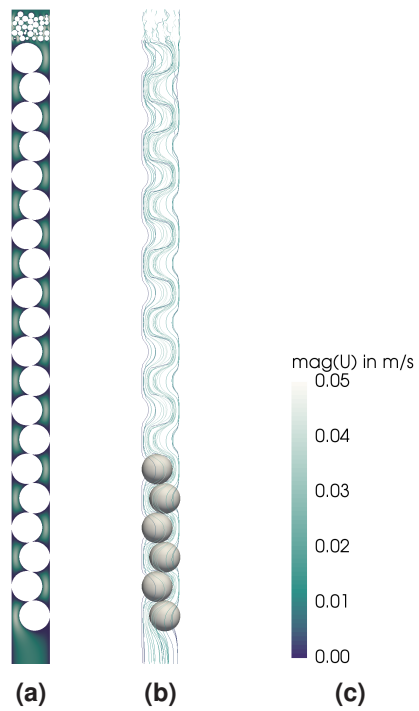


**Figure 7.3:** Flow field inside base case SPSR (*scenario a*) shown in lateral cut through the reactor (a) and as streamline plot (b). Scale adjusted to catalytic section, geometry of bottom six spheres shown for visualisation.

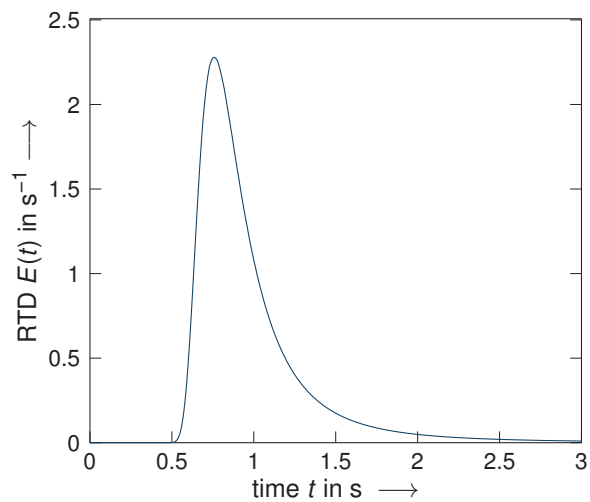


**Figure 7.4:** Residence time distribution for base case SPSR (*scenario a*).

thus taking into account the reduced reactant concentration through the bed. The apparent conversion on the first pellet is considerably higher than on the following pellets. Here, the inlet concentration is used for evaluating the conversion on the first pellet, hence attributing any effects on conversion due to back-mixing in the vicinity and upstream of that particle to the first pellet resulting in the observed artefact (cf. supporting information). Further downstream the conversion per particle remains at a similar level, decreasing towards the end of the catalytic bed. A significant reduction in conversion can be seen for the last two pellets. This section may be understood as outlet length, where the flow conditions deviate to within the bed, resulting in a shorter local residence time per pellet as the deflection of the flow is reduced due to the lack of subsequent pellets.

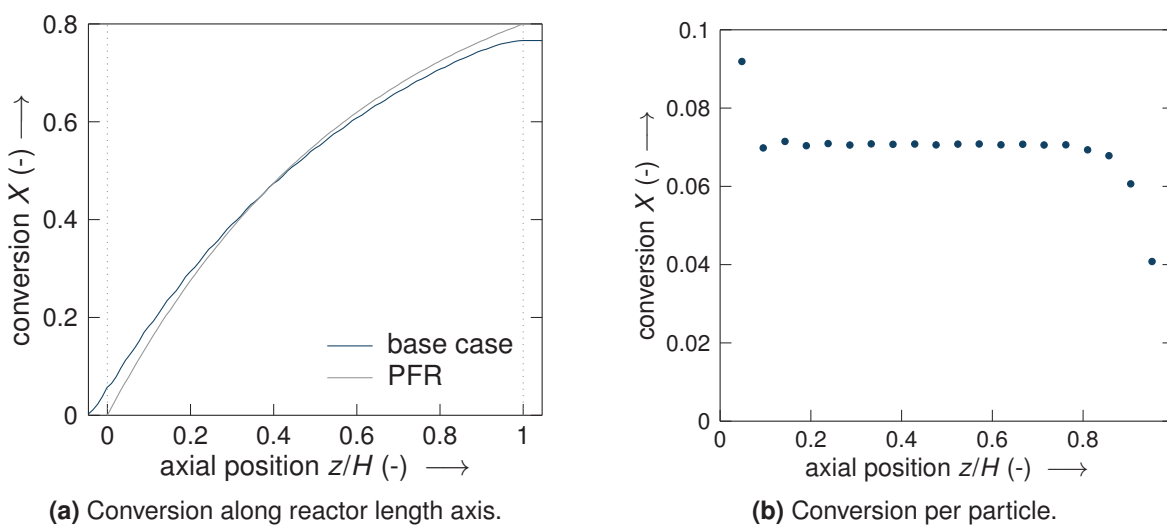


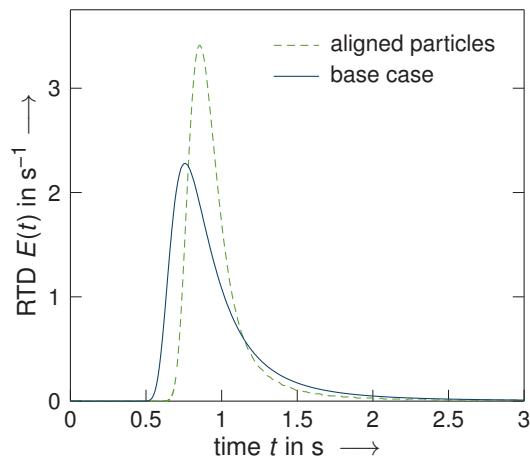
**Figure 7.5:** Conversion in base case SPSR (*scenario a*). Particle based conversion values shown at centre point position of corresponding particles.

## 7.4.2 Single pellet string reactor variations

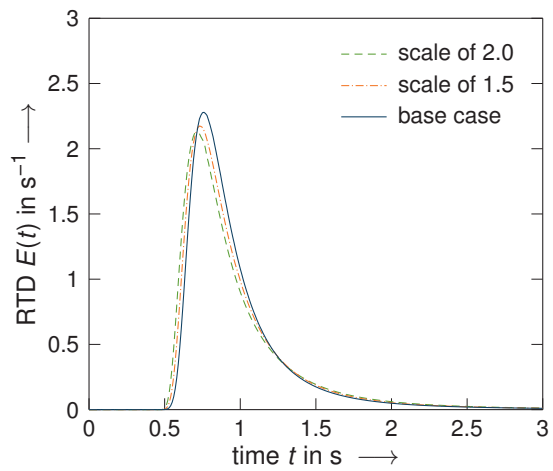
First, the residence time behaviour of the various SPSR scenarios is discussed, where the corresponding distributions can be found in Figure 7.6. Subfigure 7.6a reveals that when the particles are strictly aligned on top of each other the RTD is narrower and shifted towards later times as compared to the base case scenario. This may be a result of the local voidage distribution in the radial cross-sections of the reactor, which is more ordered due to the rotational symmetry of the set-up. Thus, *scenario b* is closer to the ideal plug flow behaviour than the base case. As can be seen from Subfigure 7.6b, the general shape of the RTDs is very similar for reactors at different scales. However, a lower maximum position and an earlier and sharper increase of the curve, corresponding to less ideal behaviour, can be identified with increasing scale factor. More variation in the residence time behaviour can be observed when changing the cylinder-to-particle diameter ratio as indicated in Subfigure 7.6c. A behaviour closest to plug flow with the most narrow distribution and shifted furthest to later times can be observed for the SPSR with the

smallest diameter aspect ratio ( $D/d = 1.125$ ), where the particles are only slightly smaller than the confining cylindrical wall. On the other hand, the RTD for the SPSR with the largest diameter aspect ratio ( $D/d = 1.75$ ) shows a shape similar to one expected for laminar flow reactors. The flow in this set-up is dominated by channelling and an increase in dead volumes, resulting in little radial mixing expressed by the highly asymmetric RTD with a sudden increase and slow decrease in slope. In between, the RTDs show the lowest maximum and the broadest distribution for the set-up with a cylinder-to-particle diameter ratio of  $D/d = 1.5$ . Although a constant space time has been set for all SPSR variations, the mean residence time increases with decreasing cylinder-to-particle diameter ratio. The general trend of a more ideal behaviour with decreasing diameter aspect ratio persists when superimposing tracer diffusion (cf. supporting information). A clear trend can be identified for the residence time behaviour of SPSR with varying number of catalytic particles. As illustrated by Subfigure 7.6d, the distributions become narrower and the maxima shifted further towards the plug flow solution of a Dirac delta function at 1 s with increasing particle number. As shown in Subfigure 7.6e, the fastest fluid fraction takes longer to pass through the SPSR when adding fines to the void space surrounding the catalytic bed. The RTD is shifted to the right, has a lower minimum and an appearance closer to a bell shape. The behaviour is closer to plug flow as compared to the base case scenario, which is in line with Moonen et al. [5].

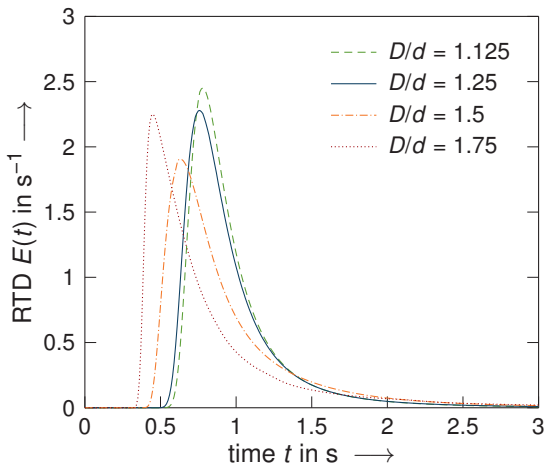
Secondly, the conversion in the considered SPSR variations is presented in Figure 7.7. The conversion along the reactor's longitudinal axis is very close to the base case behaviour when the particles in the string are stacked on top of each other as shown in Subfigure 7.7a, where the overall conversion is slightly higher with a value of 76.9% as compared to 76.6% for the base case scenario. Subfigure 7.7b reveals an increase in conversion with increasing scale factor. The overall reactor conversion amounts to 78.2% when scaling the base case geometry by a factor of 1.5 and to 78.6% when scaling by a factor of 2.0. Both conversion along the reactor and overall bed conversion are very similar for SPSRs with cylinder-to-particle diameter ratios between  $D/d = 1.125$  and 1.5, with a maximum value of 76.9% for the overall bed conversion for  $D/d = 1.125$ , as can be seen in Subfigure 7.7c. Deviations are found for the set-up with  $D/d = 1.75$  with a considerably lower bed conversion. This correlates with the trend that the RTD is closest to plug flow for SPSR with smaller diameter aspect ratio. The reduced conversion for the SPSR with highest cylinder-to-particle diameter ratio considered indicates an increase in channelling in this reactor. A plot of the overall bed conversion as function of the cylinder-to-particle diameter ratio as detailed in Subfigure 7.8a reveals a decreasing conversion with increasing diameter aspect ratio with stronger slope towards larger diameter aspect ratios. The data in Subfigure 7.7d shows a strong influence of conversion on the number of catalytic particles in the SPSR. In general, conversion increases with particle number. The scenarios with five and ten catalytic particles are too short to achieve conversion close to that of plug flow, but with 50 particles the conversion approaches that of plug flow. Using even more



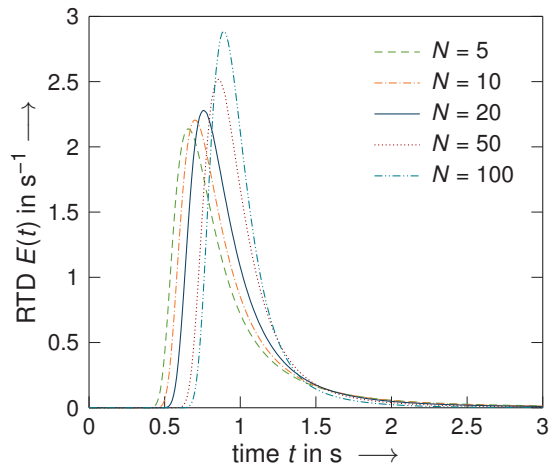
(a) Variation in particle arrangement (scenario b).



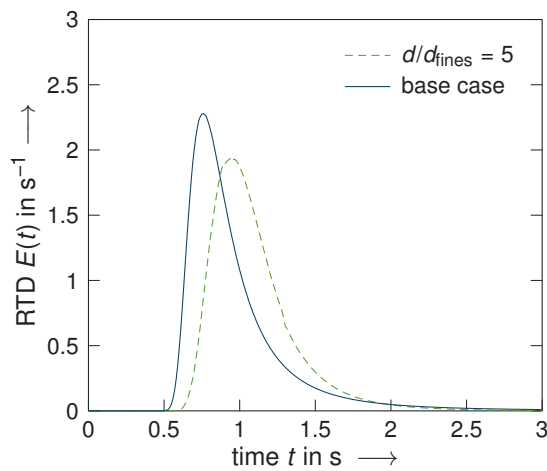
(b) Variation in scale (scenario c).



(c) Variation in diameter ratio (scenario d).



(d) Variation in particle number (scenario e).

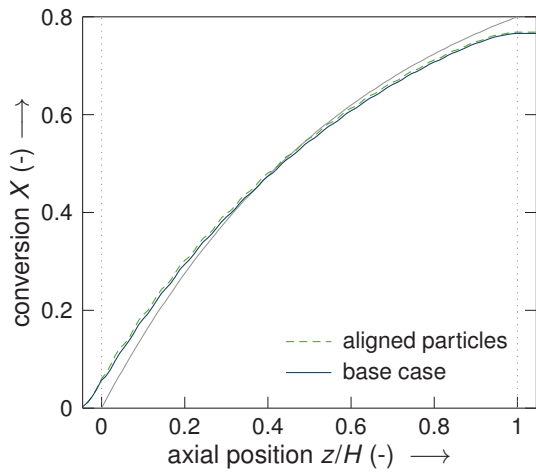


(e) Addition of inert fines (scenario f).

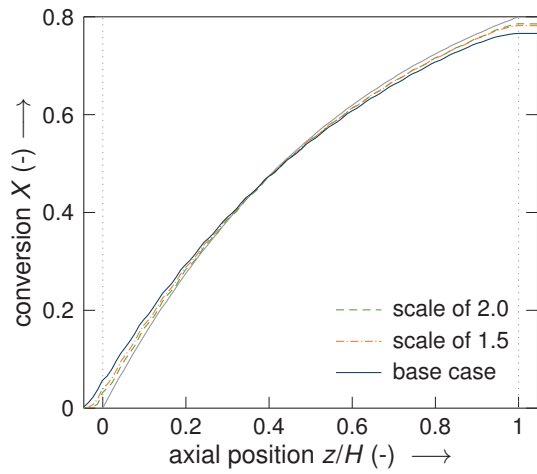
**Figure 7.6:** Residence time distributions for SPSR scenarios.

particles brings no significant further improvement. The maximum conversion achieved with 100 catalytic particles is 79.3%. This can also be seen in Figure 7.8b displaying the overall bed conversion as a function of the particle number. Below 20 particles in a string there is a strong downturn on conversion whereas above 20 particles a high number of additional particles is required for considerable improvement in conversion. This is consistent with the observation by Scott et al. [4] that about 30 to 50 particles are required such that end effects may be neglected when analysing the axial dispersion behaviour of SPSRs. Also Moonen et al. [5] concluded that the flow behaviour in SPSRs is closer to plug flow for longer beds. The influence of the number of catalytic particles on the overall bed conversion is much stronger than the influence of the cylinder-to-particle diameter ratio as can be concluded from Figure 7.8. According to Subfigure 7.7e, adding inert fines to the system reduces the overall bed conversion. This may be due to shielding of the catalytic surface area by the fines such that molecular diffusion within the fluid flow is hindered. Simulations with a smaller fine diameter revealed a further reduction in conversion (cf. supporting information). Similar results were obtained by Berger et al. [70, 71] for fixed-bed systems with positive reaction order arguing that bed dilution with inert fines increased local bypassing and facilitated improper mixing. Contrary, Moonen et al. [5] achieved higher conversion when adding inert fines reasoning with reduced catalyst bypassing, but using catalyst extrudates in SPSRs.

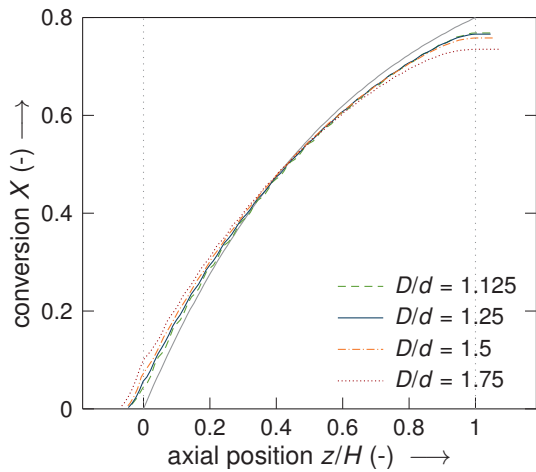
Simulations of the base case with varying fluid properties, namely molecular diffusion and viscosity, as well as feed dilution revealed that only diffusion has a noticeable influence on conversion (cf. supporting information).



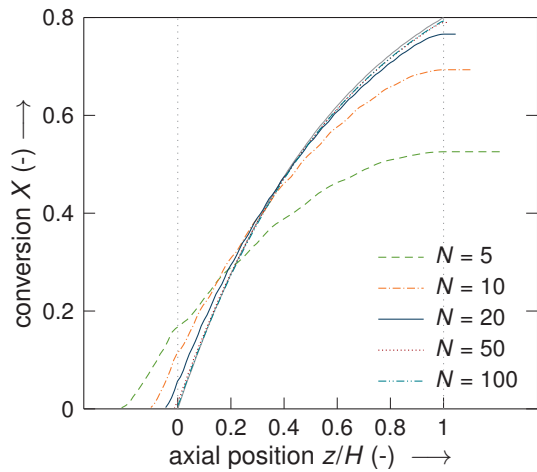
(a) Variation in particle arrangement (scenario b).



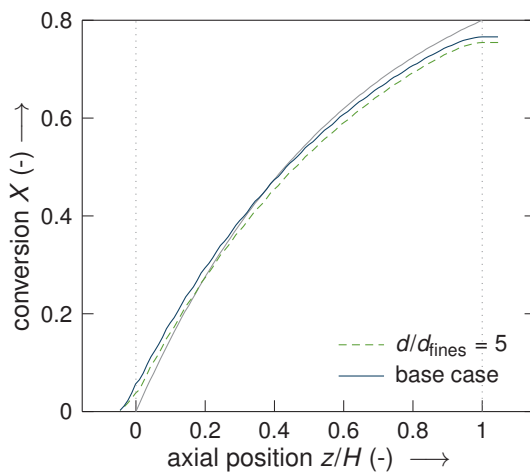
(b) Variation in scale (scenario c).



(c) Variation in diameter ratio (scenario d).



(d) Variation in particle number (scenario e).



(e) Addition of inert fines (scenario f).

**Figure 7.7:** Conversion along the reactor for SPSR scenarios. PFR conversion (—) shown for comparison.



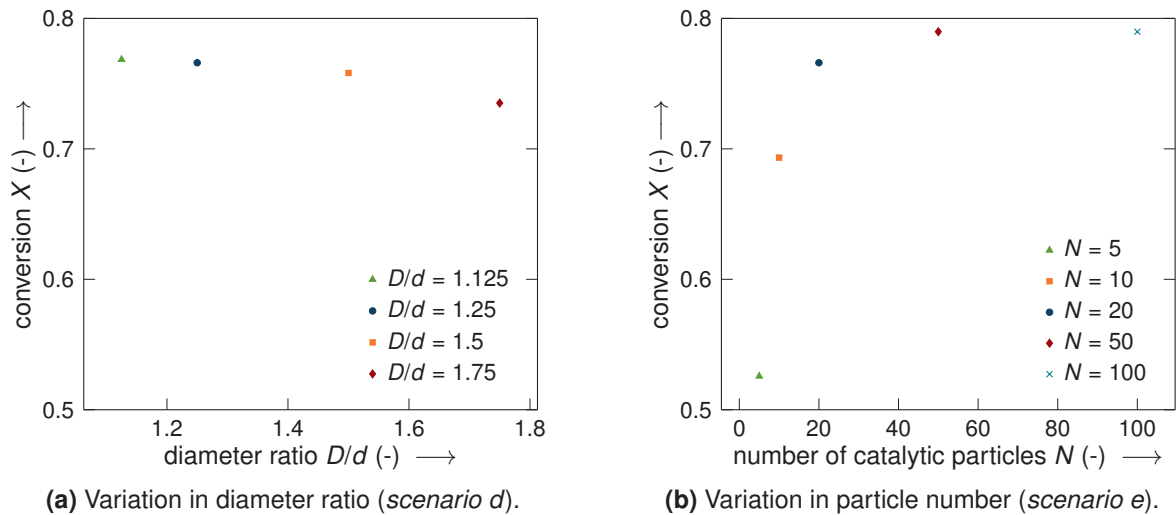


**Figure 7.8:** Influence of cylinder-to-particle diameter ratio and particle number on overall reactor conversion.

### 7.4.3 Fixed-bed design criteria

The extent of deviation of real fixed-bed reactors from plug flow is often described by a single parameter: either the number of stages  $N_{TIS}$  in a corresponding tanks-in-series model, or the dispersion coefficient  $D_{ax}$  which indicates the degree of axial dispersion superimposed on ideal plug flow using the dispersion model [27]. Both parameters can be determined from the residence time distribution. Here, the evaluation is based on the tanks-in-series model using the method of moments to determine the mean residence time as well as the corresponding standard deviation. According to Elgeti [175], the parameters in the two models are related by  $u_0 H/D_{ax} = 2(N_{TIS} - 1)^\dagger$ . In all cases of reactions with simple kinetics, the overall conversion is lower than the ideal plug flow conversion (as shown for this work in Figure 7.9).

Mears [6] developed a criterion for the deviation of fixed-bed reactor operation from plug flow for single-phase and trickle-flow operation in isothermal reactors and assuming power law reaction rates based on the lengths required to achieve the same conversion. This criterion is rather conservative and was loosened by Gierman [7], resulting in the following condition for reactors such that their required length deviates less than 5% from the length required to achieve the same conversion in ideal plug flow:

$$\frac{u_0 H}{D_{ax}} > 8n \ln \left( \frac{1}{1-X} \right) \quad (7.15)$$

The results of applying this criterion to the simulated SPSR scenarios are shown in Figure 7.10. Overall, the SPSRs are in the range of the criterion, with the base case being just off satisfying the inequality. The general trend observed earlier that the deviation to plug flow

<sup>†</sup> It should be noted that in the original publication the dimensionless group  $u_0 H/D_{ax}$  is depicted as Bodenstein number  $Bo$ . Care should be taken regarding the ambiguous usage of  $Pe$  and  $Bo$  in literature.

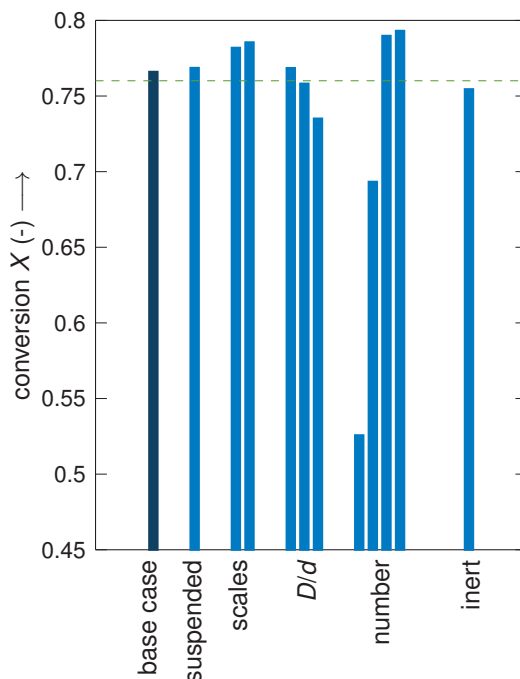


**Figure 7.9:** Overview of overall bed conversion results for simulated SPSR scenarios; dashed line indicating 5% deviation in conversion as compared to ideal plug flow behaviour.

is reduced by decreasing cylinder-to-particle diameter ratio and increasing particle number is reflected. In contrast, the criterion is easily satisfied for the scenario with inert fines although its conversion remains below the base case conversion. Also, the scenario with only five catalytic particles satisfies the criterion but deviates strongly from plug flow conversion. The overall conversion appears to be overruled by the dispersion results, evaluated from the RTDs shown in Figure 7.6 as obtained with a non-diffusive tracer. However, to assess reactor performance using a diffusive tracer is more realistic. This shifts the behaviour further towards plug flow leading to larger values of the dimensionless group  $u_0 H/D_{ax}$  (cf. supporting information) and thus favouring the compliance with the above criterion on axial dispersion.

For random packed beds with small cylinder-to-particle diameter ratio, the effect of the confining wall has noticeable impact on bed voidage and permeability. Chu and Ng [8] have shown that below a value of  $D/d = 8$  a significant increase in bed voidage results from the influence of the confining walls whereas above values of  $D/d = 25$  the voidage and permeability are near constant. As a result, choosing a value of  $D/d > 8$  or  $D/d > 25$  for fixed-bed reactors is a criterion commonly used to neglect radial gradients. Clearly, this criterion in either form does not hold true for SPSRs which by definition have a cylinder-to-particle diameter ratio of less than two.

Carberry [33] puts forth considerations regarding interface gradients, such as concentration gradients between the bulk phase and the catalytic particle surface. Based on the ratio between observed reaction rate and maximum possible reaction rate in a heterogeneous

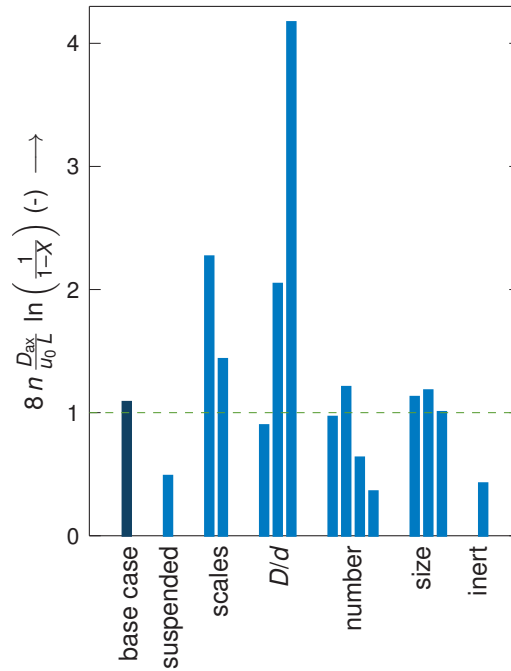


**Figure 7.10:** Evaluation of axial dispersion criterion in the form proposed by Gierman [7] for simulated SPSRs; dashed line indicating threshold value.

system, called Carberry number  $Ca$ , external mass transfer limitations may be neglected if [163]

$$\frac{R^{obs}}{k_f a_v c_0} < \frac{0.05}{|n|}, \quad (7.16)$$

where  $R^{obs}$  is the observed global rate of reaction,  $k_f$  the interface mass transfer coefficient,  $a_v$  the area per unit volume of catalyst,  $c_0$  the initial bulk concentration of reactant and  $n$  the reaction order. The observed global rate of reaction is evaluated dividing the concentration difference over the reactor by the total residence time including inlet and outlet sections. The interface mass transfer coefficient can be obtained from the Schmidt number  $Sc = \nu/\mathcal{D}$  and the particle Reynolds number  $Re_p$  by the correlation of Wakao and Funazkri [176]:

$$Sh = 2 + 1.1 Sc^{1/3} Re_p^{0.6}, \quad (7.17)$$

where the Sherwood number is defined as  $Sh = k_f d/\mathcal{D}$  with the diffusion coefficient  $\mathcal{D}$ . The Carberry numbers are evaluated accordingly for the simulated SPSR scenarios, which easily satisfy the criterion as can be seen from Figure 7.11. This is as expected, since the reaction under consideration is a heterogeneously catalysed gas phase reaction.

The dilution of catalyst beds with inert fines is common practice in laboratory experiments. Van den Bleek et al. [69] were the first to quantitatively describe the influence of dilution on conversion using a mathematical model. They proposed using the relative decrease of conversion due to the dilution  $\Delta$  as a measure of deviation. Berger et al. [70, 71] further

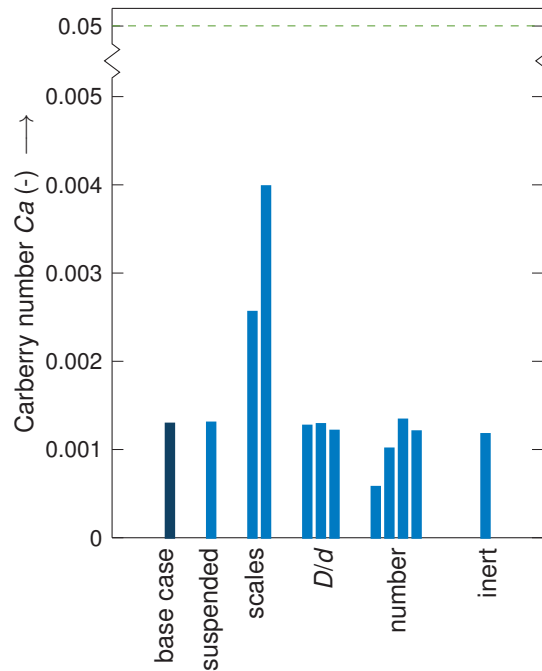


**Figure 7.11:** Evaluation of Carberry criterion on external mass transfer limitations [163] for simulated SPSRs; dashed line indicating threshold value.

developed this concept of *dilution effect* resulting in the following expression, relating the effect of dilution on conversion to observable reactor and reaction parameters:

$$\Delta = \left( \frac{b}{1-b} \right) \left( \frac{d}{L} \right) \left( \frac{X_{\text{dil}}}{2} \right) n \quad (7.18)$$

where  $b$  is the dilution factor described by the volume of inert material as a fraction of total volume of solids and  $L$  the total length of the reactor. Setting the accepted deviation in conversion to 5% results in the following maximum allowed bed dilution

$$b < \frac{1}{1 + 10 X_{\text{dil}} d L}. \quad (7.19)$$

This inequality is met by the simulated SPSR scenario with inert particles filling the void space between the catalytic pellets as well as by the additional scenarios shown in the supplementary information.

#### 7.4.4 Single pellet string reactor design criterion

The simulation results have been analysed for trends in the data spanning over all simulated SPSR variations with the aim to derive a criterion to predict the deviation to plug flow conversion. The major influence of the cylinder-to-particle diameter ratio  $D/d$  and of the number of particles in the catalytic bed  $N$  emphasised by the RTD and conversion plots acts as a starting point. As can be seen from Subfigure 7.12a, a logarithmic relation can be identified between the deviation to plug flow conversion, expressed as  $1 - \frac{X}{X_{\text{PFR}}}$ , and a

measure of bed length divided by the cylinder-to-particle diameter ratio,  $N d^2/D$ . A positive aspect of using the product of particle number and particle diameter as measure of bed length lies in the thereby included consideration of reactor scale. However, taking only into account the reactor geometry would leave aside any influence of the fluid properties and velocity. The Péclet number, defined as ratio of advective to diffusive transport by

$$Pe = \frac{u_0 d}{\mathcal{D}}, \quad (7.20)$$

is therefore incorporated into the considerations. The diffusion coefficient, rather than the dispersion coefficient, is used as it is a pure material property and thus known *a priori*. The resulting plot is shown in Subfigure 7.12b. In logarithmic presentation, a linear relation is revealed between the deviation to plug flow conversion as a function of the number of particles, the cylinder-to-particle diameter ratio and the Péclet number. Fitting a linear regression to the data results in the following expression:

$$\log \left\{ 1 - \frac{X}{X_{\text{PFR}}} \right\} = -0.647 \cdot \log \left\{ N \frac{d}{D} Pe \right\} - 0.65 \quad (7.21)$$

which may act as a design criterion to numerical and experimental set-ups. Minimum values for  $N \frac{d}{D} Pe$  related to deviations to plug flow conversion of less than 1%, 5% and 10% are provided in Table 7.2.

It should be noted that the relation shown in Figure 7.12 is established based on SPSR scenarios with a corresponding PFR conversion of 80%. However, simulations of the base case scenario using reaction rate coefficients corresponding to PFR conversion values of 20% and 50% revealed that the correlation is still valid, as would have been expected.

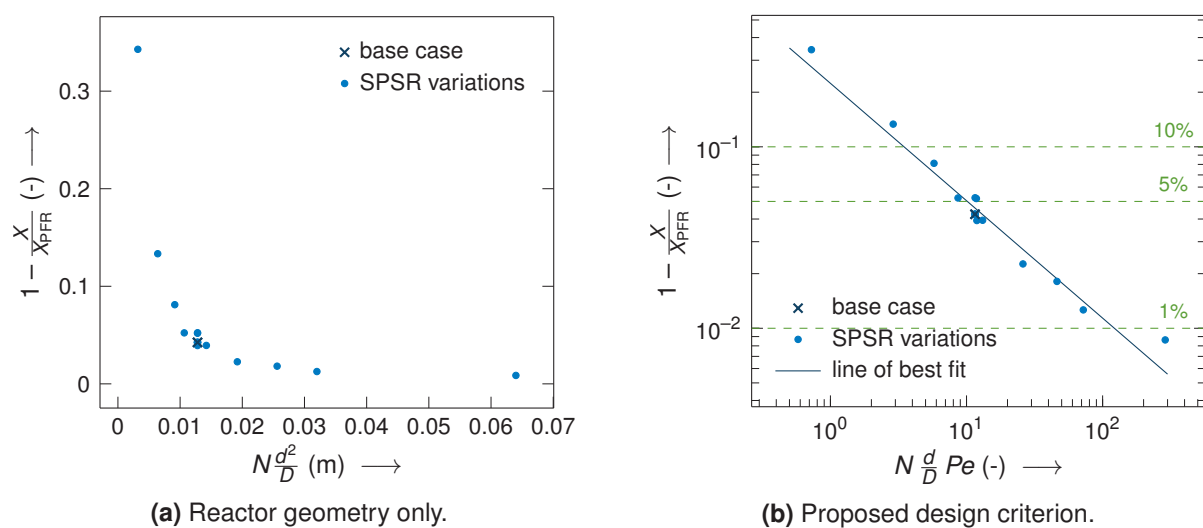


**Figure 7.12:** Trend analysis showing deviation to plug flow conversion as function of particle number, cylinder-to-particle diameter ratio and Péclet number.

**Table 7.2:** Threshold values of proposed design criterion based on particle number, cylinder-to-particle diameter ratio and Péclet number for deviations to plug flow conversion of less than 1 %, 5 % and 10 %.

$1 - \frac{X}{X_{\text{PFR}}}$	$N_D^d Pe$
1 %	> 122
5 %	> 10
10 %	> 3.5

A second trend can be identified relating the amount of conversion on the first particle of a catalytic SPSR compared to the overall bed conversion and the total number of particles to the deviation to plug flow conversion. However, this trend does not pose a suitable criterion to be used for designing SPSRs as neither the conversion on the first particle nor the overall bed conversion are known *a priori*. Refer to the supporting information for further details.

## 7.5 Conclusion

The concept of SPSRs has been studied sporadically over the last few decades, with recent publications focusing on the application of SPSRs for catalytic testing [5] and a possible reactor concept for transferring processes from batch to continuous operation [15]. In this paper we presented a comprehensive characterisation of the flow and conversion behaviour of various SPSR scenarios based on numerical simulation where it was assumed that flow and reaction are independent of each other. This study specifically considered a heterogeneously catalysed, isothermal and isomolar gas-phase reaction with no change in gas density over spherical catalyst particles. The conversion in a SPSR with only 20 catalytic particles of 0.8 mm diameter and a cylinder-to-particle diameter ratio of  $D/d = 1.25$ , as defined in the base case, was found to be close to ideal plug flow conversion. The parameter study conducted revealed that conversion deviating less than 5 % from plug flow can be achieved easily. In general, the conversion of an isothermal, irreversible, heterogeneously catalysed gas phase reaction in SPSRs was considerably closer to plug flow at larger scale, with decreasing cylinder-to-particle diameter ratio and with increasing number of catalytic particles. Similar trends were obtained regarding the flow behaviour in the laminar regime using a non-diffusive numerical tracer to evaluate the corresponding RTDs. Increasing the size (scale) of the reactor gives a closer approach to plug flow conversion, despite apparently yielding a less plug flow like RTD. Likewise, adding inert fines to the free space surrounding the catalyst particles gives a more plug flow like RTD, yet reduces overall bed conversion.

The applicability of existing design criteria for fixed-bed reactors was evaluated. The SPSR scenarios considered were within the range of the criterion on axial dispersion by Gierman

[7]. By definition, the criterion on neglecting radial dispersion by Chu and Ng [8] is not applicable to SPSRs as a matter of their geometry. External mass transfer limitations expressed by the Carberry criterion [33, 163] were not significant as expected for heterogeneous gas phase reactions. The decrease of conversion as a result of bed dilution with inert fines was found to be less than 5%, thus complying with the corresponding criterion by Berger et al. [70, 71].

A clear relationship could be deduced from the simulation results, relating the deviation to plug flow conversion to the reactor geometry, the flow velocity and the diffusion coefficient. On the basis of this observation, we have proposed a novel criterion for the design of SPSRs, which to our knowledge is the first of its kind. The correlation stated in Eq. (7.21) enables a straightforward and accurate a priori prediction of the deviation to plug flow conversion based only on the reactor geometry, fluid properties and the flow velocity.

In general, we have shown that a suitably designed SPSR can closely approach plug flow kinetic behaviour, and the concept is therefore a suitable system for kinetic experiments.

The assumption of isothermal conditions as well as the fact that both reactants and products are considered having the properties of nitrogen are to be mentioned as clear limitations of this study. Further work is planned on understanding further aspects of the SPSR behaviour, particularly the influence of thermal effects due to reaction, the influence of the shape of catalyst particles as well as liquid and mixed-phase reactants.

## 7.S Supporting information

### 7.S.1 Influence of inlet and outlet configuration and back-diffusion

The following three configurations are considered for the reactor sections upstream and downstream of the string of catalytic particles regarding geometry set-up and velocity inlet boundary condition:

- (1) empty inlet and outlet sections of  $2d$  length upstream and downstream of the catalytic bed in combination with a parabolic velocity profile for the inlet flow
- (2) inert bed of  $1d$  length with fines of  $0.2d$  diameter upstream and downstream of the catalytic bed and additional empty pipe sections of  $0.05d$  length between in-/outlet and inert beds as well as between inert beds and catalytic bed in combination with a constant inlet flow velocity
- (3) empty inlet and outlet sections of  $0.05d$  length upstream and downstream of the catalytic bed, such that the pellets do not touch the boundaries, in combination with a constant inlet flow velocity

The corresponding geometries are depicted in Figure 7.13.

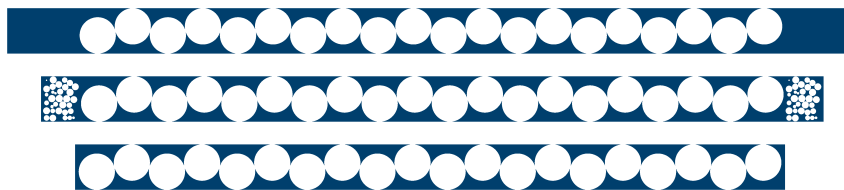


**Figure 7.13:** Slice along longitudinal axis of inlet and outlet geometry set-ups with empty tube sections of  $2d$  length, inert beds of  $1d$  length and virtually no inlet and outlet sections (top to bottom).

The conversion achieved in each of the set-ups using base case settings is shown in Figure 7.14, where the axial position is normalised such that the catalytic bed stretches from zero to one on the horizontal axis. A considerable amount of back-diffusion upstream of the catalytic bed is visible for the case with long empty inlet of  $2d$  length as well as for the case with inert particles. Maximum conversion results are obtained by the reactor with an inert packing at the front and back of the reactor, followed by the case with a  $2d$  inlet and outlet length and finally the case with just a constant inlet velocity and very short inlet and outlet lengths. A scenario based on the first inlet/outlet configuration but with reduced diffusion coefficient reduces the amount of back-mixing upstream of the catalytic bed as illustrated by Figure 7.15 and indicates molecular diffusion as the cause for the observed effect.

To appropriately reflect the situation in the laboratory, the geometry with inert packing is used in the following with Dirichlet boundary conditions for velocity and concentration at the



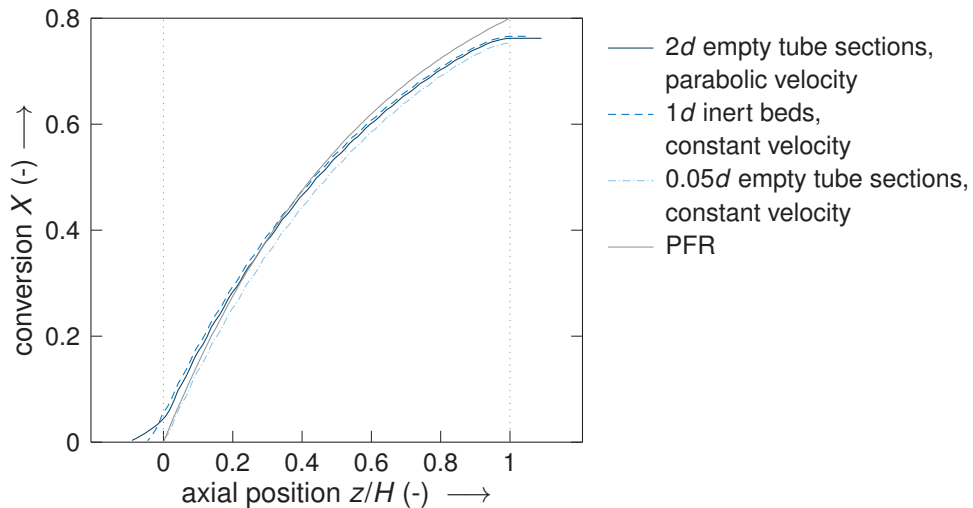


**Figure 7.14:** Conversion results for SPSR *scenario a* with varying in-/outlet geometry and velocity inlet boundary condition.

flow inlet, thus corresponding to plug flow. This is in line with Carberry [50] who stressed that entrance effects in shallow beds may be overcome by placing so called *dummy beds* upstream of the catalytic bed.

Since the outlet variations above do not have an influence on the overall bed conversion, no inert packing downstream of the catalytic bed will be considered but an empty outlet with the same total length as the inlet, i.e., of  $1.1d$  length.

The chosen inlet and outlet configurations, including boundary conditions and the bed of inert fines upstream of the catalytic bed, are based on a pragmatic view of what is likely to be practically achievable.

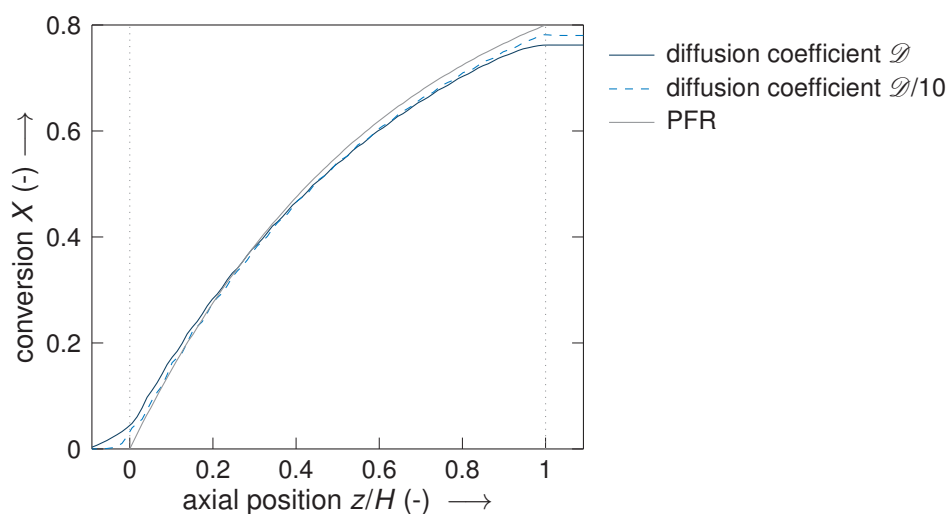


**Figure 7.15:** Effect of reduced diffusion coefficient on bed conversion for SPSR of *scenario a* with  $2d$  empty inlet and outlet length and parabolic inlet velocity.

## 7.S.2 Grid-independence study

The conversion in a SPSR of *scenario a* but reduced to only five catalytic pellets was compared for different mesh settings. Three background meshes with different levels of cell refinement were used, corresponding to a number of cells across the cylinder diameter between 25 and 100. In addition, the *snappyHexMesh* settings adjusting the refinement level at the catalytic particle surface and between adjacent surfaces including walls were varied, where a value of one corresponds to halving a background cell in all three dimensions of space, thus resulting in eight cells. Details on the combination of settings chosen for each mesh are presented in Table 7.3. The surface of the inert particles in the short bed at the reactor entrance is less refined than the catalytic particles. Here, no reaction is taking place and the region is generally of less interest.

**Table 7.3:** Key parameters of meshes considered in grid-independence study.

mesh	edge length of hex. cells <sup>1</sup> in mm	<i>snappyHexMesh</i> surface refinement	<i>snappyHexMesh</i> gap level increment
0	0.04	1	3
1	0.04	2	1
2	0.04	2	2
3	0.04	2	3
4	0.02	1	1
5	0.02	1	2
6	0.02	1	3
7	0.02	2	1
8	0.02	2	2
9	0.01	1	1
10	0.01	1	2

<sup>1</sup> average edge length of hexahedral-dominant background mesh

The conversion along the reactor axis resulting on each mesh are compared in Figure 7.16. From Subfigure 7.16a it can be seen that the overall bed conversion amounts to little more than 50%, which is far away from the corresponding plug flow conversion of 80% used to specify the reaction rate constant. Apart from this the figure shows limited variation in the result depending on the mesh used. The close-up of the reactors far downstream section in SubFigure 7.16b reveals the grid dependency of the shown axial conversion results. Meshes 0 to 3, based on the coarsest background mesh, appear to be too coarse to correctly capture the particle surface. A general trend of increasing reactor performance with increasing gap level refinement settings, resulting in an increased catalytic surface area in the simulation, can clearly be identified. When the mesh elements between the particles become smaller, the catalytic surface increases as the 'gap' located around to the particle touching points get smaller (cf. Figure 7.2). The interplay between this effect and the gradual elimination of the numerical diffusion with further grid refinement results

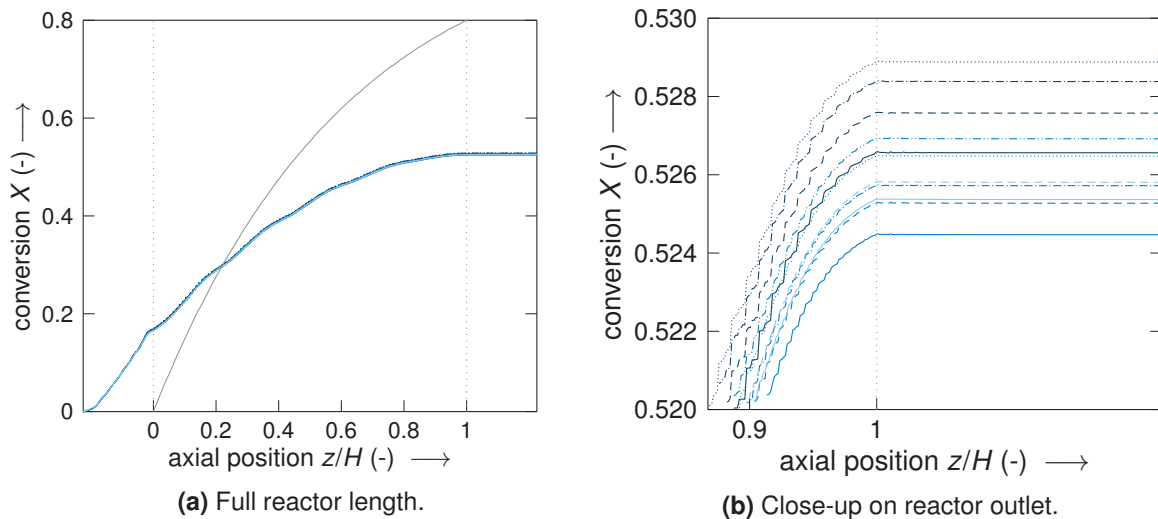


**Figure 7.16:** Conversion across the reactor for SPSR of *scenario a* with reduced particle number of  $N = 5$  using meshes with different refinement according to Table 7.3; marking by line style: mesh 0 (—), mesh 1 (---), mesh 2 (---), mesh 3 (---), mesh 4 (—), mesh 5 (---), mesh 6 (---), mesh 7 (---), mesh 8 (---), mesh 9 (—) and mesh 10 (---). PFR conversion shown for comparison (—).

in the observed reactor performances. Nonetheless it should be noted that the deviation in overall bed conversion is less than 1% for all meshes shown. As a compromise between the increased simulation time with a finer mesh and the conversion results revealed with the grid-independence study, the settings corresponding to *mesh 5* in Table 7.3 are used in the parameter study.

### 7.S.3 Influence of particle size of inert fines

To investigate the effect of the size of fines on conversion, a reduced set-up where only the first five catalytic particles are simulated is considered for reasons of simulation time. Therefore, the space time is reduced accordingly to  $\tau = 0.25$  s and the corresponding plug flow conversion used to determine the reaction rate coefficient lowered to  $X_{\text{PFR}} = 0.2$ . The size of inert material upstream of the catalytic bed is kept constant; only the size of inert fines filling the void space between the catalytic pellets is varied. The results of this reduced set-up varying the diameter of the fines is shown in Figure 7.17. As expected, it reveals a further reduction in conversion when reducing the diameter of the inert fines.

While this implies that a closer adherence to plug flow conversion is achieved in the absence of small inert particles, the reader should note that in a system other effects not considered here, such as heat, may have a larger impact, possibly leading to a different observation.

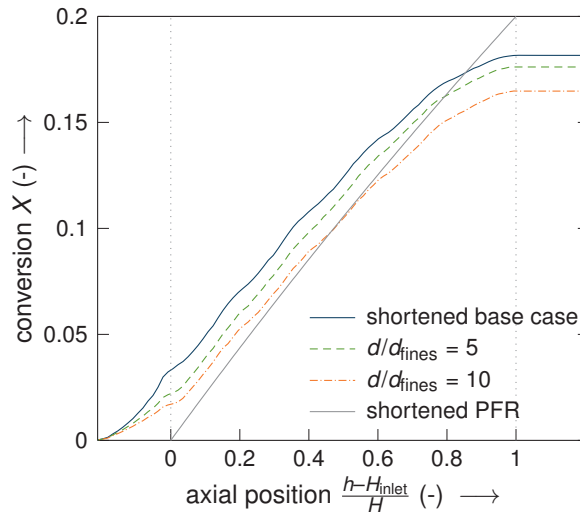


**Figure 7.17:** Comparison of conversion in SPSRs where the void space is filled with fines of different size with shortened base case, considering only the first five pellets, and corresponding PFR conversion.

#### 7.S.4 Influence of gas properties

The fluid viscosity has only limited influence on the RTD. Evidence for this is provided in Figure 7.18. Only reducing the kinematic viscosity by a factor of as much as 25 results in a noticeable effect, namely a lower maximum and a slightly earlier increase of the distribution curve. Residence time distributions for the SPSR scenarios with variation in reactant concentration are not shown as there is no influence on the fluid flow and hence on the residence time behaviour.

Figure 7.19 shows that the fluid viscosity does not have any visible influence on reactor conversion.

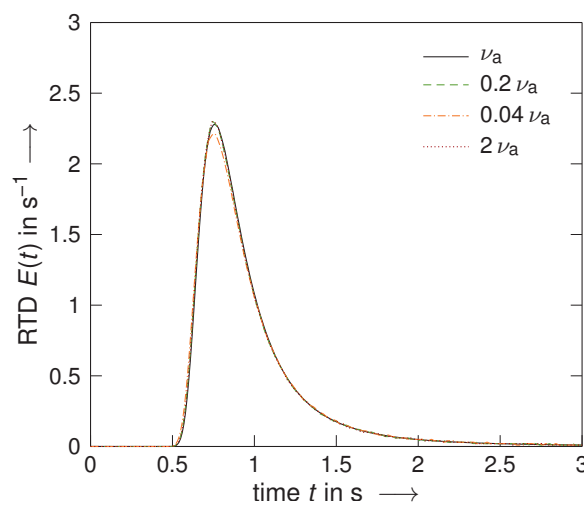


**Figure 7.18:** Residence time distributions for SPSR with variation in fluid viscosity.

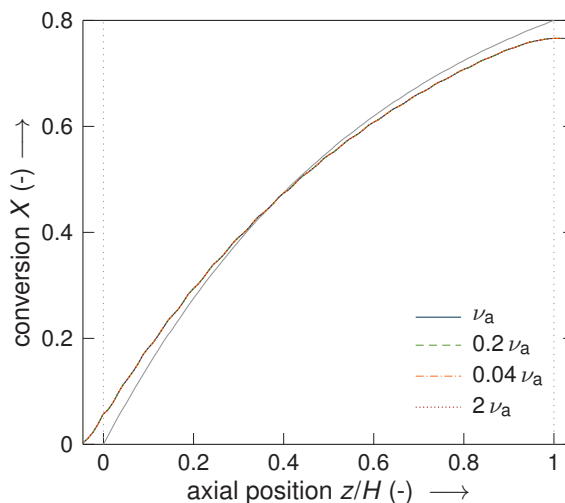


**Figure 7.19:** Conversion along the reactor for SPSR scenario with variation in gas viscosity. PFR conversion (—) shown for comparison.

### 7.S.5 Influence of feed dilution

Since the fluid is considered to have the properties of nitrogen, there is no influence of feed dilution on the flow and the residence time behaviour. Therefore, only the influence on conversion is considered when investigating the influence of feed dilution. The results presented in Figure 7.20 show that feed dilution does not have any visible influence on reactor conversion.

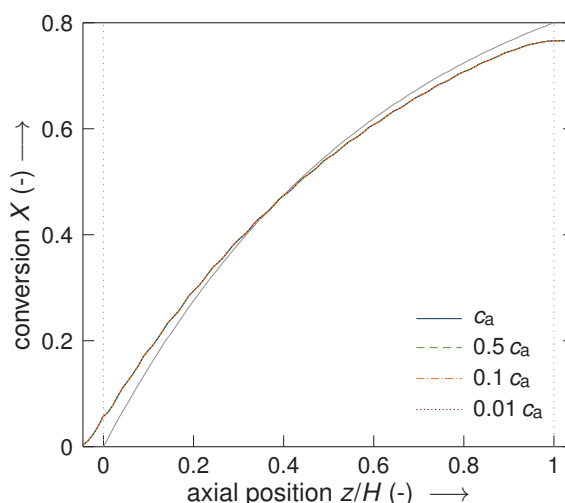


**Figure 7.20:** Conversion along the reactor for SPSR scenarios with variation in reactant concentration,  $c_a$  corresponding to pure feed. PFR conversion (—) shown for comparison.

### 7.S.6 Influence of tracer diffusion

By using a non-diffusive tracer to investigate the residence time behaviour of the various SPSR scenarios we were able to uncouple the effect of dispersion based on the inherent character of the reactor from the influence of molecular diffusion of the tracer. Thus,

the nature of the flow came to the fore. However, a diffusive tracer is more realistic and should be used when assessing for example the axial dispersion criterion according to Gierman [7].

Figure 7.21 shows the RTDs resulting from numerical tracer experiments with both diffusive and non-diffusive properties, where the value of the self-diffusion coefficient of nitrogen [174] is used for the diffusive tracer (cf. conversion simulations presented in the paper). The RTD obtained with the non-diffusive tracer shows a sharp increase at about half the space time across the catalytic bed before reaching its peak value significantly before the reactor's space time followed by a more gentle decline. This asymmetrical curve essentially reflects the RTD of ideal laminar flow through a pipe, thus indicating a laminar character of the flow through the string of catalytic particles. Therefore, this provides an initial sign that there is little dispersion in the considered SPSR base case resulting from flow hydrodynamics, i.e., excluding tracer diffusion. In contrast, a Dirac pulse at the reactor's space time would correspond to ideal plug flow hydrodynamics, indicating no spread in the distribution and a single mean residence time matching the reactor's space time. Including tracer diffusivity leads to an RTD with a broader peak which is however far more symmetric and the maximum is shifted considerably closer towards the reactor's space time as compared to the non-diffusive tracer result. With increasing deviation to plug flow hydrodynamics, the maxima of the obtained distributions are shifted towards earlier times, that is further away from the corresponding space time, and exhibit a more asymmetric shape. This holds true for both tanks-in-series model and axial dispersion model (cf. [25, 27]). Apart from the apparent peak broadening, indicating that most of the dispersion seems to come from diffusion, the latter distribution corresponding to the diffusive tracer closer resembles plug flow with substantial axial dispersion.

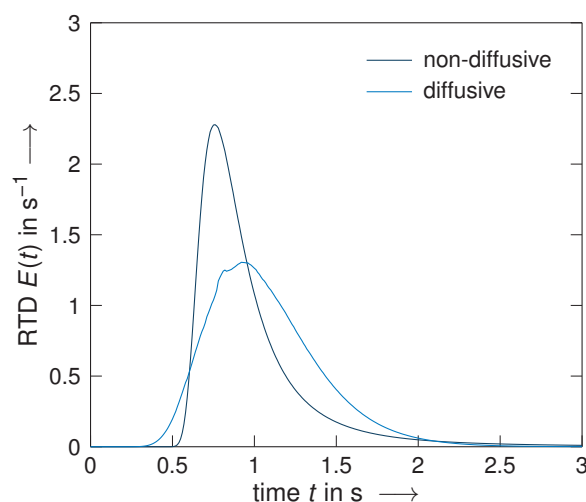


**Figure 7.21:** Comparison of residence time behaviour of base case SPSR (*scenario a*) with diffusive and non-diffusive tracer.

In order to demonstrate the influence of tracer diffusivity on the parametric studies, an example is provided here. Figure 7.22 depicts the residence time behaviour obtained both

with a non-diffusive and a diffusive tracer for SPSRs with varying diameter aspect ratio. In case of using a diffusive tracer, the residence time behaviour is closer to plug flow at smaller cylinder-to-particle diameter ratios (SubFigure 7.22b), which is in line with the trend concluded from simulations using a non-diffusive tracer (SubFigure 7.22a). However, evidence on the laminar character of the flow for SPSRs with a larger diameter aspect ratio is lost when superimposing tracer diffusion, implying that the contribution of molecular diffusion towards axial dispersion is higher than the contribution from flow hydrodynamics. This is in line with Sharma et al. [57] who concluded that the contribution of axial dispersion to pulse broadening is low in single pellet string reactors.

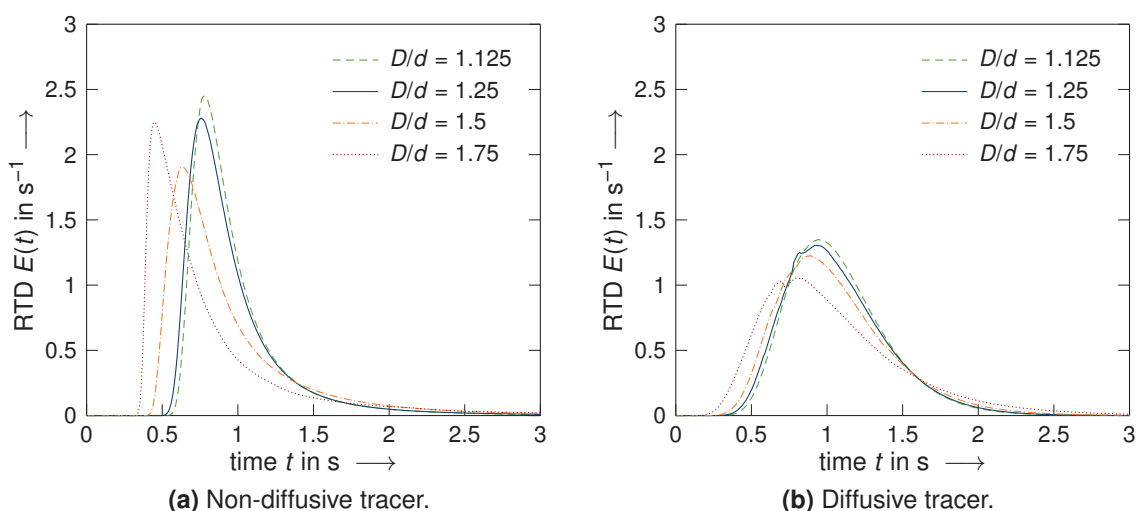


**Figure 7.22:** Comparison of residence time distributions for SPSRs with varying diameter aspect ratio using a non-diffusive and a diffusive tracer.

In an attempt to benchmark the reactors' residence time behaviour against plug flow, we use the dispersion model. However, its intended use is for small deviations from plug flow. The limitations of using this model become apparent when dealing with flow close to laminar conditions where in the extreme case of a laminar flow reactor the tracer is transported by convection only, thus the shape of the RTD is a result of the parabolic velocity profile only. In order to capture this asymmetric shape, applying the conversion model leads to high dispersion values, which is seriously misleading. Therefore, care should be taken when interpreting the values of the dimensionless group  $u_0 H/D_{ax}$  obtained from the RTDs, as shown in Table 7.4. These are consistently larger in case of using a diffusive tracer which indicates the shift in the residence time behaviour towards plug flow. However, the values do not reflect the increase in dispersion when including tracer diffusion.

Regarding the axial dispersion criterion by Gierman [7], an increasing value of the dimensionless group  $u_0 H/D_{ax}$  means that the criterion is met more easily, which is the case when including tracer diffusion.

**Table 7.4:** Comparison of dimensionless group  $u_0 H/D_{ax}$  obtained from RTDs with non-diffusive and diffusive numerical tracers.

case	$D/d$	$u_0 H/D_{ax}$ from RTD with non-diffusive tracer	$u_0 H/D_{ax}$ from RTD with diffusive tracer
d0	1.125	13.20	18.34
a	1.25	10.94	16.46
d1	1.5	5.91	12.65
d2	1.75	3.38	6.93

### 7.S.7 Conversion-based trend analysis

A trend can be identified relating the conversion across the first particle of a catalytic SPSR and the total number of particles to the deviation to plug flow conversion. As shown in the corresponding paper the conversion across the first particle is considerably higher than across the particles in the remaining bed, as a result of back-mixing upstream of the catalytic bed. A first plot of the deviation to plug flow conversion as function of the conversion on the first particle normalised with the overall bed conversion for all considered SPSR scenarios reveals that these two quantities can be related. In a logarithmic presentation of this relation, a linear trend is distorted mainly by the data points corresponding to the scenarios with lowest deviation to plug flow conversion, namely the SPSR scenarios with 50 and 100 particles. In an attempt to improve the correlation, the deviation to plug flow conversion is divided by the number of catalytic particles in the reactor. This leads to a linear relation when plotted in a double-logarithmic diagram, shown in Figure 7.23. The corresponding linear regression of best fit is

$$\log \left\{ \frac{1}{N} \left( 1 - \frac{X}{X_{\text{PFR}}} \right) \right\} = 2.05 \cdot \log \left\{ \frac{X_1}{X} \right\} - 0.73. \quad (7.22)$$

As a result, the overall bed conversion in a SPSR is closer to plug flow when the conversion is evenly distributed between the particles and especially when the conversion across the first particle is similar to that across the others. The largest discrepancy from this trend corresponds to the SPSR scenario where the space between the catalytic particles is filled with inert fines. Maximum values of the conversion on the first particle related to overall bed conversion corresponding to deviations to plug flow conversion of less than 1%, 5% and 10% are stated in Table 7.5 for SPSRs with 20 and 50 catalytic particles accordingly. However, it should be noted that this trend does not pose a suitable criterion to be used for designing SPSRs as neither the conversion on the first particle nor the overall bed conversion are known *a priori*.



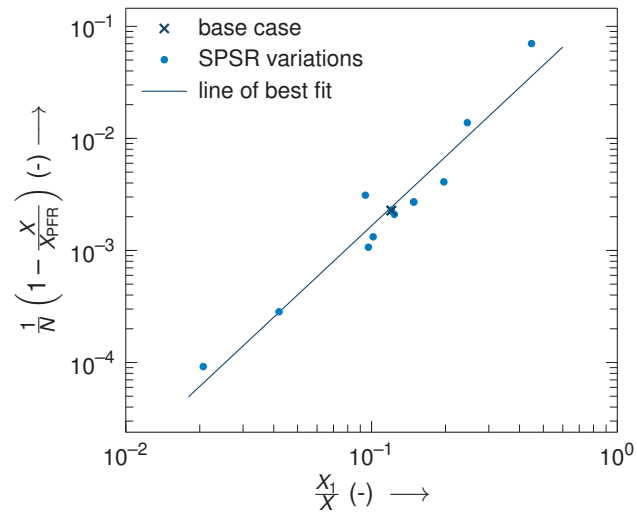


**Figure 7.23:** Trend analysis showing deviation to plug flow conversion as function of conversion on first pellet normalised with overall bed conversion.

**Table 7.5:** Threshold values of conversion on first particle normalised with overall bed conversion for deviations to plug flow conversion of less than 1%, 5% and 10% for SPSR with 20 and 50 catalytic particles.

$1 - \frac{X}{X_{\text{PFR}}}$	$\frac{X_1}{X}$ for $N = 20$	$\frac{X_1}{X}$ for $N = 50$
1 %	< 5.6 %	< 3.6 %
5 %	< 12 %	< 8 %
10 %	< 17 %	< 11 %

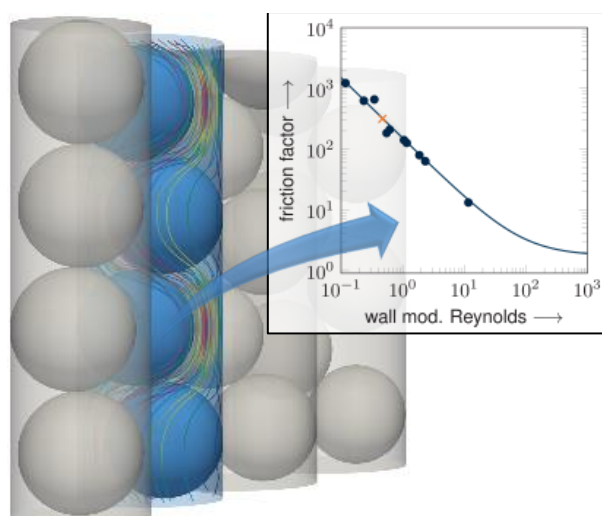


# 8 Numerical investigation of pressure drop in single pellet string reactors

This chapter was published in a similar form and is reprinted with kind permission from: J. Fernengel, L. Bolton and O. Hinrichsen, Numerical investigation of pressure drop in single pellet string reactors, *Chem. Eng. Technol.* **2020**, 43, 172–178, DOI 10.1002/ceat.201900372. [177]. Copyright 2019 WILEY-VCH Verlag GmbH & Co. KGaA.

## Publication summary

In narrow fixed bed reactors the influence of the confining wall on pressure drop cannot be neglected. Here, the pressure drop in single pellet string reactors, a limiting case of fixed bed reactors with a cylinder-to-particle diameter ratio below two, is studied using computational fluid dynamics simulations. Deviations to the Ergun, and more specifically Blake-Kozeny, equation are evident though the general trend is met. A geometry-based weighting factor is introduced to scale the influence of the confining wall in an equivalent diameter expression. Agreement between numerical simulation and pressure drop predictions from correlation are thereby improved significantly.



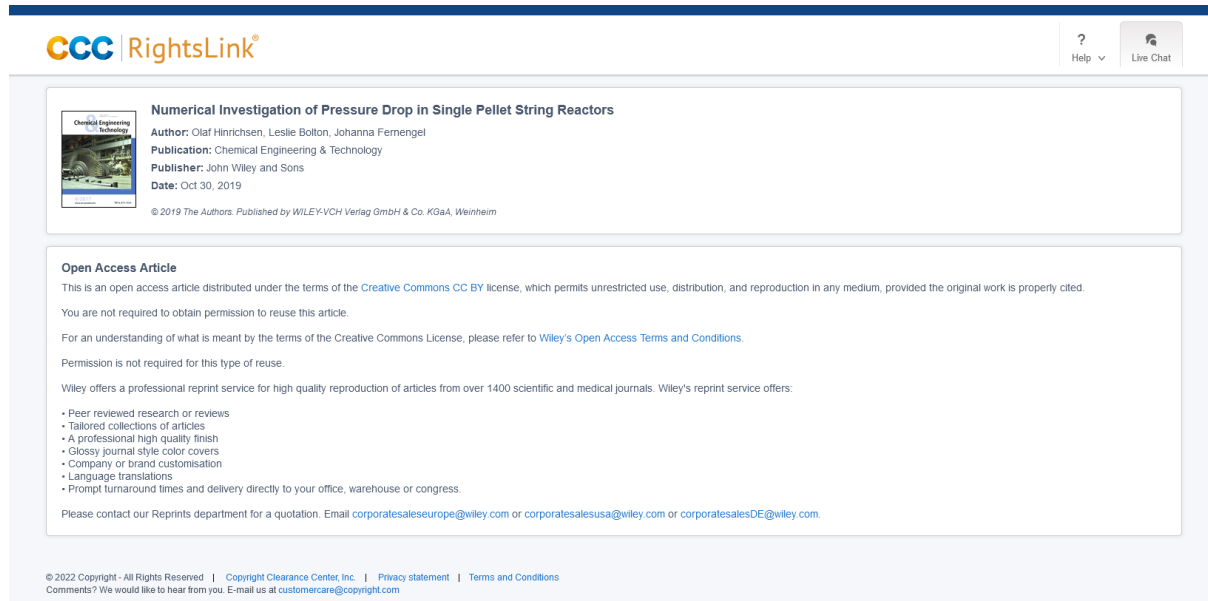
## CRedit author statement

*Johanna Fernengel*: Conceptualisation, Methodology, Software, Formal analysis, Investigation, Visualisation, Writing - Original Draft.

*Leslie Bolton*: Supervision, Project administration, Funding acquisition, Writing - Review & Editing.

*Olaf Hinrichsen*: Project administration, Supervision, Funding acquisition, Writing - Review & Editing.

## Permission/License information



The screenshot shows the RightsLink interface for the article "Numerical Investigation of Pressure Drop in Single Pellet String Reactors". At the top left is the CCC RightsLink logo. On the right, there are links for "Help" and "Live Chat". The article title is displayed prominently. Below the title, the author information is listed: "Author: Olaf Hinrichsen, Leslie Bolton, Johanna Fernengel", "Publication: Chemical Engineering & Technology", "Publisher: John Wiley and Sons", and "Date: Oct 30, 2019". A copyright notice follows: "© 2019 The Authors. Published by WILEY-VCH Verlag GmbH & Co. KGaA, Weinheim".

**Open Access Article**

This is an open access article distributed under the terms of the [Creative Commons CC BY](#) license, which permits unrestricted use, distribution, and reproduction in any medium, provided the original work is properly cited.

You are not required to obtain permission to reuse this article.

For an understanding of what is meant by the terms of the Creative Commons License, please refer to [Wiley's Open Access Terms and Conditions](#).

Permission is not required for this type of reuse.

Wiley offers a professional reprint service for high quality reproduction of articles from over 1400 scientific and medical journals. Wiley's reprint service offers:

- Peer reviewed research or reviews
- Tailored collections of articles
- A professional high quality finish
- Glossy journal style color covers
- Company or brand customisation
- Language translations
- Prompt turnaround times and delivery directly to your office, warehouse or congress.

Please contact our Reprints department for a quotation. Email [corporatesaleseurope@wiley.com](mailto:corporatesaleseurope@wiley.com) or [corporatesalesusa@wiley.com](mailto:corporatesalesusa@wiley.com) or [corporatesalesDE@wiley.com](mailto:corporatesalesDE@wiley.com).

© 2022 Copyright - All Rights Reserved | [Copyright Clearance Center, Inc.](#) | [Privacy statement](#) | [Terms and Conditions](#)  
Comments? We would like to hear from you. E-mail us at [customercare@copyright.com](mailto:customercare@copyright.com)

## 8.1 Introduction

Establishing pressure drop-flow rate relations for fixed-bed reactors has been subject of research since decades and still is today [178]. Within the wide range of fixed-bed dimensions found in industry, the single pellet string reactor (SPSR) is an exception, where pellets are packed into tubes of only slightly larger diameter. Although already introduced in the 1970s by Scott et al. [4], it has not attracted much attention until recent publications indicated a renewed interest in this reactor concept, including its use for catalyst testing [5, 14, 15]. In a previous publication, Fernengel et al. [173] characterized conversion and residence time behaviour in single pellet string reactors using numerical simulation and derived a design criterion comparing the reactor's performance to ideal plug-flow. Here, the pressure drop behaviour of the presented SPSR variations is elaborated and discussed in the light of common literature correlations.

In his landmark article, Ergun [51] reviewed factors influencing pressure loss of flow through random packed beds, namely fluid properties and velocity, as well as the bed-related properties voidage and particle characteristics and proposed a correlation which remains most widely used for packed-bed pressure drop. Therein, the pressure drop is split into two additive terms related to viscous and kinetic losses, each with an empirical constant, commonly referred to as first and second Ergun coefficient, respectively. For laminar flow, viscous losses are predominant, reducing the Ergun equation to the first term, that is the Blake-Kozeny equation [179, 180].

However, the Ergun equation does not account for pressure loss due to the confining wall, which gains importance with decreasing cylinder-to-particle diameter ratio. Modifications of the Ergun equation by using equivalent diameters as characteristic length [4, 181], adjustment to the Ergun coefficients [59, 61, 172] and a new empirical correlation [63] have been proposed to remedy this shortcoming with various success, as detailed later. In this work, a numerical investigation of pressure drop in single pellet string reactors based on computational fluid dynamics (CFD) simulations is presented. First, the pressure drop across an SPSR of spherical particles along the reactor length axis is shown in detail for a base case scenario. The influence of fluid viscosity, flow velocity, diameter aspect ratio and pellet size on the pressure drop of laminar flow through single pellet string reactors is discussed and the results are compared to correlations from literature. Finally, a weighting factor is introduced to the equivalent diameter expression proposed by Scott et al. [4] scaling the influence of the confining wall's surface and thus improving the agreement between simulation and an Ergun-based pressure drop correlation.

## 8.2 Methodology

The simulations are based on a heterogeneous reactor model, incorporating the solid particles through the mesh with appropriate boundary conditions. The fluid is assumed incompressible due to negligible density changes and low flow velocities. Mesh generation and fluid simulation are performed using snappyHexMesh and simpleFoam as provided with OpenFOAM<sup>®</sup> v2.4 [24].

### 8.2.1 Geometry

Within an SPSR, the spherical particles are stacked on top of each other touching the wall on alternating sides (cf. Figure 8.1). The resulting particle positions can be described analytically based on the particle diameter  $d$  and the cylinder diameter  $D$  by Equations (8.1) and (8.2), when the  $z-x$  plane spans through the particle midpoints such that  $y_i = 0$ :

$$x_i = (-1)^i \left( \frac{D-d}{2} \right) \quad (8.1)$$

$$z_i = \frac{d}{2} + (i-1) \sqrt{d^2 - (D-d)^2} \quad (8.2)$$

The length  $H$  of the string of  $N$  particles is then given by

$$H = d + (N-1) \sqrt{d^2 - (D-d)^2}. \quad (8.3)$$

A short bed of inert fines is placed upstream of the catalytic pellet string to closely resemble possible experimental set-ups, enforcing near-plug flow and thus preventing back-mixing in the entry zone. The particle positions within this random inert packing are obtained using Blender<sup>™</sup> 2.76b [23].

### 8.2.2 Governing equations

Laminar flow of incompressible isothermal fluids at steady-state is described by the equations of continuity and motion as stated in Equations (8.4) and (8.5), respectively, where  $\mathbf{u}$  is the velocity vector,  $\rho$  the fluid density,  $p$  the pressure and  $\nu$  the kinematic viscosity.

$$\nabla \cdot \mathbf{u} = 0 \quad (8.4)$$

$$\nabla \cdot (\mathbf{u}\mathbf{u}) = -\frac{1}{\rho} \nabla p + \nu \nabla^2 \mathbf{u} \quad (8.5)$$

Standard boundary conditions for internal flow problems [41] are used setting a constant velocity normal to the inlet with  $|\mathbf{u}| = u_0 = \text{const.}$  and a fixed outlet pressure  $p_{\text{out}} = p_{\text{atm}}$ .

No-slip is defined at wall and particle surfaces ( $u_s = 0 \text{ m s}^{-1}$ ); the remaining boundaries are set to zero gradient normal to the boundary ( $\partial/\partial n = 0$ ).

### 8.3 Case set-up

Both inert and catalytic particles are considered spherical and non-porous with a smooth surface, the confining wall is a cylindrical tube. Nitrogen is passed through the reactor at ambient conditions. A constant space time  $\tau$ , defined here as the ratio of the fluid volume  $V_f$  surrounding the catalytic particles to the volumetric flow rate  $\dot{V}$ , is maintained across the catalytic bed. The resulting superficial velocity  $u_0$  then depends on the reactor geometry, amounting to

$$u_0 = \frac{\dot{V}}{A_t} = \frac{V_f}{A_t \tau} = \frac{H - \frac{V_p}{A_t}}{\tau} = \frac{d + (N-1) \sqrt{d^2 - (D-d)^2} - \frac{2Nd^3}{3D^2}}{\tau} \quad (8.6)$$

with  $A_t$  being the reactor's empty cross-sectional area and  $V_p$  the total volume of catalytic pellets.

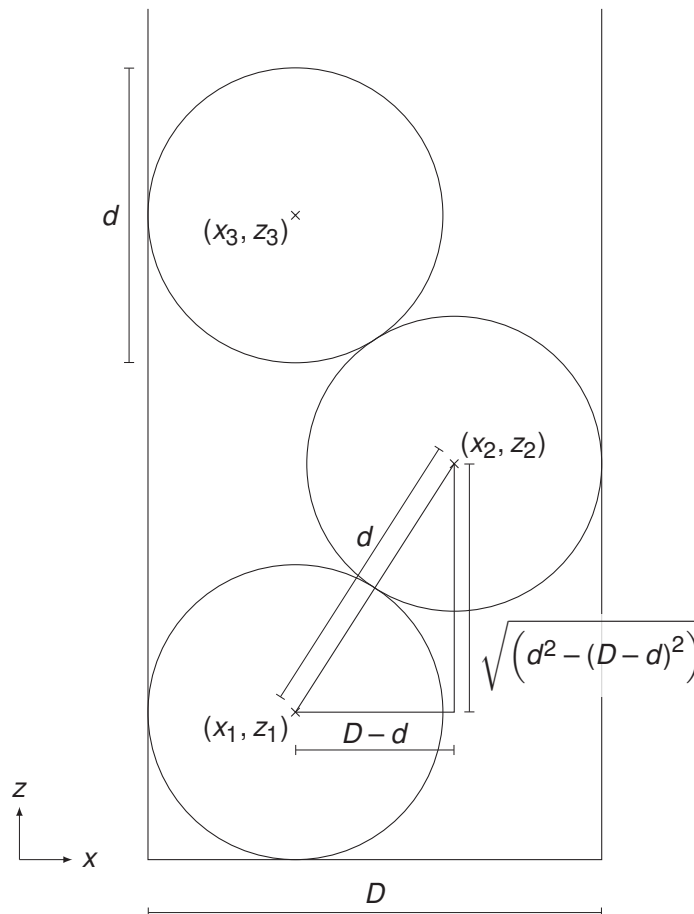


**Figure 8.1:** Bottom section of a SPSR showing trigonometric expressions used for analytical pellet positions.

**Table 8.1:** Geometry and fluid properties of considered single pellet string reactors.

Case	Number of particles $N / -$	Particle diameter $d / \text{mm}$	Cylinder diameter $D / \text{mm}$	Viscosity
A	20	0.8	1.0	$\nu$
B1	20	0.8	1.0	$0.2\nu$
B2	20	0.8	1.0	$0.04\nu$
B3	20	0.8	1.0	$2\nu$
C1	5	0.8	1.0	$\nu$
C2	10	0.8	1.0	$\nu$
C3	50	0.8	1.0	$\nu$
C4	100	0.8	1.0	$\nu$
D1	20	0.8	0.9	$\nu$
D2	20	0.8	1.2	$\nu$
D3	20	0.8	1.4	$\nu$
E1	20	1.2	1.5	$\nu$
E2	20	1.6	2.0	$\nu$

In order to evaluate the influence of fluid viscosity, flow velocity and reactor geometry variations are performed on a base case set-up, consisting of 20 catalytic pellets of  $d = 0.8$  mm diameter arranged as single pellet string in a confining cylindrical tube of inner diameter  $D = 1.0$  mm and a short bed of inert fines with a diameter of  $d/5$  placed upstream. A fluid with a viscosity of  $\nu = 1.529 \cdot 10^{-5} \text{ m}^2 \text{ s}^{-1}$  and a density of  $\rho = 1.2506 \text{ kg m}^{-3}$  passes the catalytic bed with a space time of 1 s, thus expecting laminar flow through the reactor. Properties of the considered reactor variations are provided in Table 8.1.

## 8.4 Results and discussion

### 8.4.1 Base case

As a result of the flow simulation, it can be seen from Figure 8.2 that the inert bed at the reactor entrance accounts for a substantial part of the pressure drop, whereas the slope of the pressure curve is significantly lower within the catalytic bed. The individual particles can be identified by the wavy shape of the curve which indicates the heterogeneous nature of the flow surrounding the catalytic pellets. The pressure drop is larger at regions with smaller free cross-sectional area.

In the following, only the pressure drop over the length of the catalytic pellet string is considered, that is between axial positions zero and one as indicated in Figure 8.2.



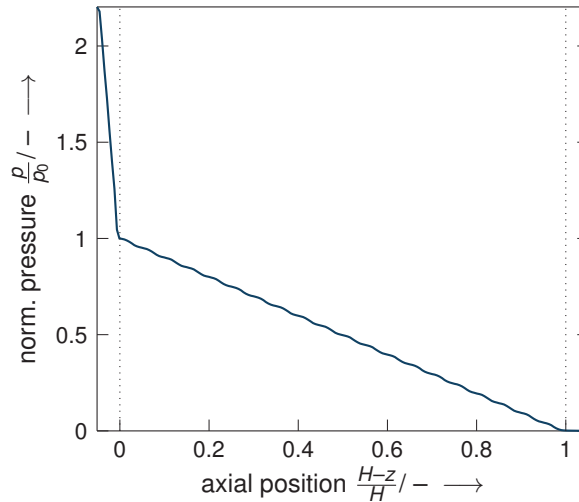


**Figure 8.2:** Normalised average cross-sectional pressure for the base case SPSR as function of axial position.

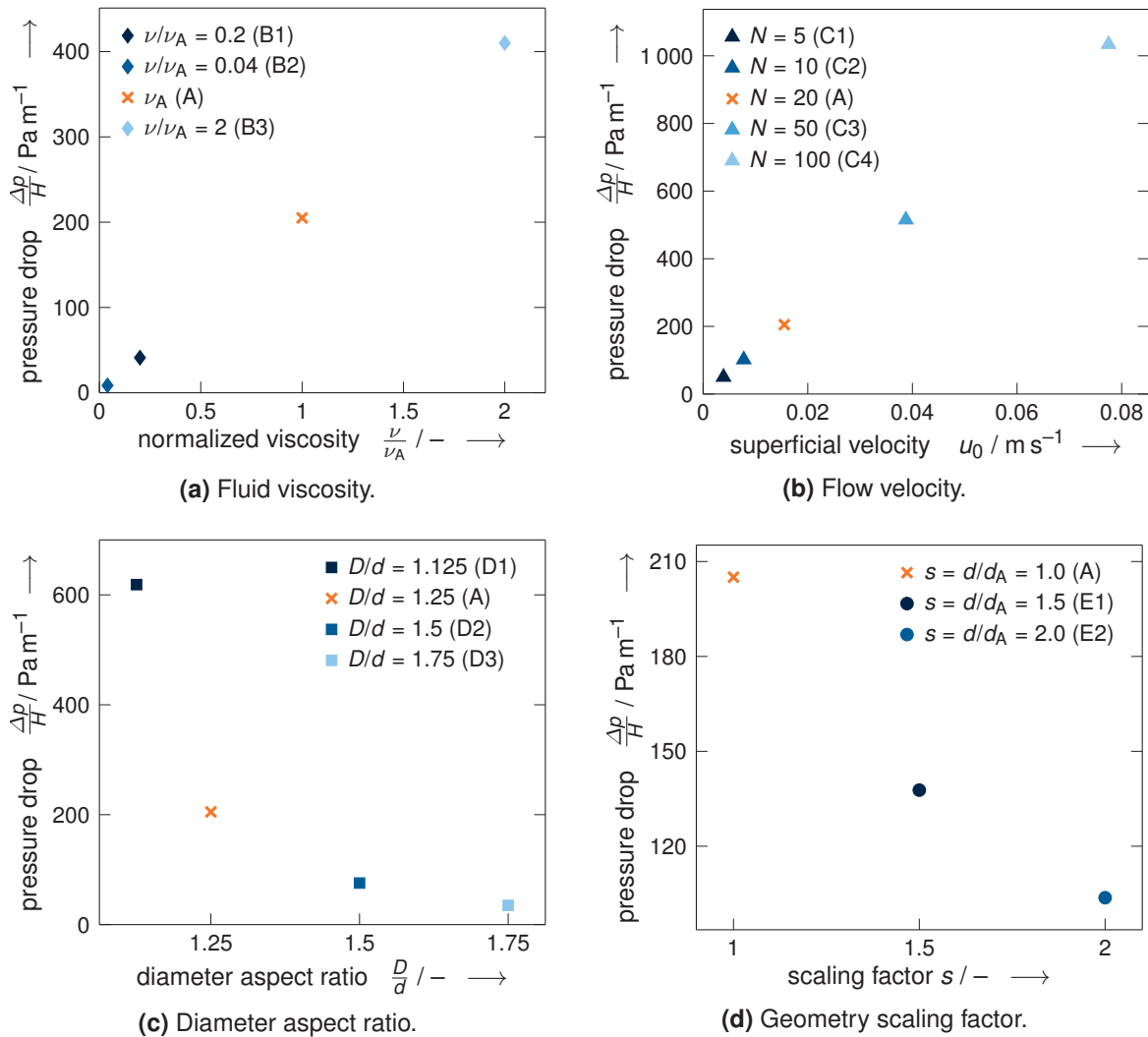
### 8.4.2 Parameter study

Figure 8.3a shows a linear relation between pressure drop and fluid viscosity, as expected for laminar flow where viscous energy losses are predominant. Similarly, the linear relation observed between pressure drop and fluid velocity obtained by varying the number of pellets in the string (cf. Equation (8.6)) as displayed in Figure 8.3b indicates laminar flow. From Figure 8.3c it can be concluded that the pressure drop over the pellet string decreases with increasing diameter aspect ratio where the decline is reduced towards higher aspect ratios. This trend is as expected as there are two main flow paths prevailing in SPSRs, one meandering around the pellets crossing from one side of the bed to the other and the second passing the particles in a straight manner perpendicular to the plane through the pellet centres. These flow channels adjacent to the pellet string are more pronounced with increasing diameter aspect ratio, leading to higher bed voidages for the considered reactor geometries. It should be noted that voidage and diameter aspect ratio are not related linearly with a voidage maximum at [58]. Figure 8.3d suggests a decrease in pressure drop with increasing scaling factor  $s$ .

### 8.4.3 Pressure drop correlations

When introducing the SPSR concept, Scott et al. [4] achieved excellent agreement between experimental pressure drop results in air flow through SPSRs with glass and stainless steel spheres and the Ergun equation by including the surface of the confining wall in addition to the particle surface in an equivalent diameter expression. Following this approach, the simulated pressure drops across the SPSRs are compared to the Ergun equation [51] given by

$$\frac{\Delta p}{H} = 150 \frac{(1 - \bar{\epsilon})^2}{\bar{\epsilon}^3} \frac{\nu u_0}{d^2} + 1.75 \frac{1 - \bar{\epsilon}}{\bar{\epsilon}^3} \frac{\rho u_0^2}{d} \quad (8.7)$$



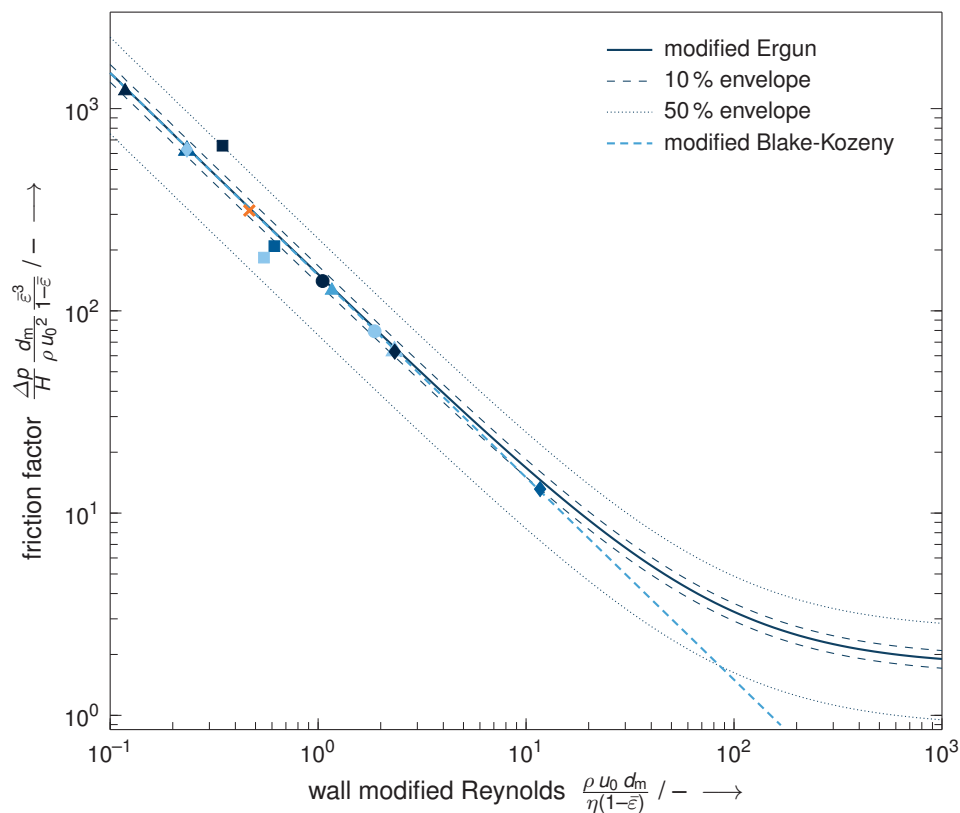
**Figure 8.3:** Influence of fluid viscosity, flow velocity, diameter aspect ratio and geometry scaling factor on pressure drop.

where  $\Delta p/H$  is the pressure drop across the bed per unit length,  $\bar{\epsilon}$  is the mean bed voidage and  $\eta$  means the dynamic viscosity of the fluid. The first term in Equation (8.7) describes the viscous losses which are decisive at laminar flow whereas the second term accounts for inertial losses that dominate at turbulent conditions. As proposed by Scott et al. [4] and successfully applied by Lee et al. [55], a modified equivalent diameter including the wall surface  $S_w$  in addition to the total pellet surface  $S_p$  is used as characteristic length. This modified equivalent diameter  $d_m$  is defined by

$$d_m = \frac{6 V_p}{S_p + S_w} \quad (8.8)$$

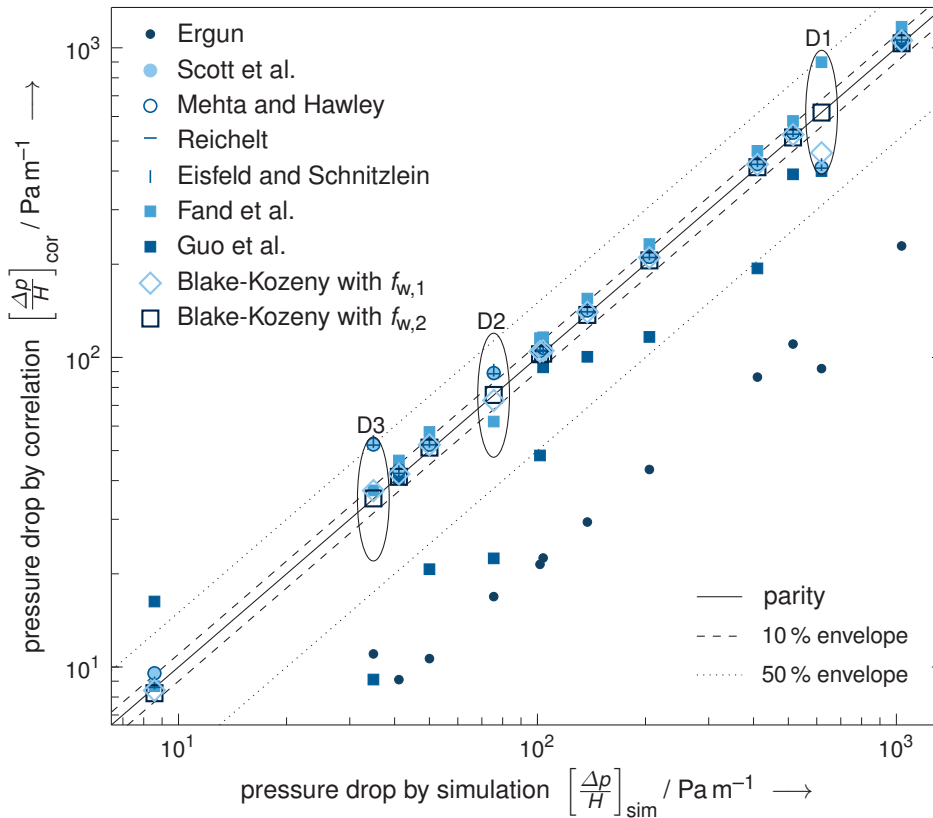
where  $V_p$  is the total pellet volume.

Figure 8.4 indicates that the obtained simulation results compare well with the Ergun equation using the modified equivalent diameter, with most values deviating less than 5%. Systematic deviations are observed for variations of the diameter aspect ratio. It should be noted that the considered single pellet string reactors are mainly within the laminar regime with wall modified Reynolds numbers below 2.4, just missed by the case with lowest viscosity with a value of 11.7, where the inertial term is negligible. This reduces Equation (8.7) to the first term which is the Blake-Kozeny equation [179, 180].



**Figure 8.4:** Comparison of pressure drop across SPSR variations with Ergun [51] and Blake-Kozeny [179, 180] equation using a modified equivalent diameter [4]; symbols and colour coding as in Figure 8.3.

Figure 8.5 compares pressure drop predictions by common literature correlations with the obtained simulation results. It is evident that the original Ergun equation [51] underestimates the pressure drop by far, which is expected as it excludes the influence of the confining wall. Using the equivalent diameter proposed by Scott et al. [4] shifts the predicted values markedly closer to parity. However, values for single pellet string reactors with diameter aspect ratios other than  $D/d = 1.25$  differ significantly.



**Figure 8.5:** Comparison of simulation results for pressure drop per unit length in SPSRs with literature and own correlations. Variations in diameter aspect ratio marked to ease allocation.

A similar approach, using a hydraulic radius as characteristic length, was proposed by Mehta and Hawley [181] based on experiments but with larger aspect ratio packed beds of spheres ( $7 \leq D/d \leq 91$ ). Reichelt [61] further refined this correlation by introducing a dependency of the second Ergun coefficient on the diameter aspect ratio, by which the range of validity could be increased down to  $D/d > 1.7$ . Eisfeld and Schnitzlein [172] fitted Reichelt's correlation to experimental data available from literature, resulting in slightly different values of the numerical constants. The predicted pressure drops according to Mehta and Hawley [181] lead to nearly equivalent though not identical results as obtained with the modification by Scott et al. [4], with imperceptible changes when adopting the adjustments proposed by Reichelt [61] as well as those by Eisfeld and Schnitzlein [172]. The results of the described four modifications to the Ergun equation are virtually the same, with mean deviations of 11.2%, 11.2%, 9.5% and 12.1% to the obtained simulation results, respectively.

Another modification of Reichelt's approach was followed by Fand et al. [59] with correlation equations for both Ergun coefficients as function of the diameter aspect ratio. However, this correlation leads to larger mean deviations of 14.5% when compared to the simulation results.

A new empirical correlation for pressure drop in packed beds with  $1 < D/d < 2$  was presented recently by Guo et al. [63] based on experimental work. Although explicitly proposed for SPSR geometries, this correlation shows larger deviations from the simulation results than the other cited correlations.

The observed relation between the observed simulation results and the various literature correlations is in line with earlier publications based on both simulative and experimental work. Müller et al. [12] presented simulations of SPSRs of spheres and  $D/d = 1.2$  with COMSOL Multiphysics® 4.2a showing good agreement with the correlation by Reichelt [61]. Comparison between experimental data and simulations with CFX-5.3 for pressure drop across SPSRs with spherical particles and square cross section of the confining wall was published by Calis et al. [64]. The results showed an average deviation of 10% between experimentally and numerically determined Ergun coefficients, when fitting two CFD simulations for each diameter aspect ratio. Hipolito et al. [11], who studied single and two-phase flow in SPSRs with similar geometry, achieved good agreement between a modified Ergun equation with parameters fitted to their experimental data based on the formulation by Lee et al. [55] which is essentially as proposed by Scott et al. [4] previously.

Here, four correlations based on the Ergun equation that include the effect of the confining wall [4, 61, 172, 181] were found capable of predicting the pressure drop mostly well within an envelope of 10% deviation but with outliers deviating by about 50%. Significant deviations correspond to SPSRs with variations of the diameter aspect ratio, marked with D1, D2 and D3 in Figure 8.5 accordingly. This leaves room for improvement to the pressure drop correlation.

Since the obtained data points are within the laminar flow region, the proposed correlation is based on the Blake-Kozeny equation. Due to the observation that the Ergun related correlations apart from Fand et al. [59] overestimate the pressure drop for large diameter aspect ratio SPSRs whereas for very small values the pressure drop is underestimated, a weighting factor  $f_w$  is introduced to the surface of the confining wall in the modified equivalent diameter expression, resulting in

$$d_m = \frac{6 V_p}{S_p + f_w S_w}. \quad (8.9)$$

In a first attempt, marked as Blake-Kozeny with  $f_{w,1}$  in Figure 8.5, the diameter aspect ratio of the SPSR is simply related to the base case value of  $D/d = 1.25$  such that the weighting factor becomes

$$f_{w,1} = \frac{1.25 d}{D}. \quad (8.10)$$

This shifts the predicted pressure drops further towards parity, with most values well within the 10% envelope, while the SPSR with smallest considered diameter aspect ratio still shows a more significant deviation.

Further, the optimal weighting factors are evaluated for each considered single pellet string reactor set-up individually which are then used to fit an empirical equation as function of the diameter aspect ratio, resulting in

$$f_{w,2} = 0.736 \frac{D}{d} - 14.7 \left(1 - \frac{d}{D}\right)^{3.74} + 4.8 \left(\frac{D}{d}\right)^{-17.5} \quad \text{for } 1.125 \leq \frac{D}{d} \leq 1.75. \quad (8.11)$$

The terms in the equation have been chosen to resemble the dependency on the diameter aspect ratio and the voidage of the single pellet string reactor geometry. By this, the mean deviation of the obtained correlation, marked as Blake-Kozeny with  $f_{w,2}$  in Figure 8.5, to the simulated pressure drop is noticeably reduced to 0.8% with one outlier corresponding to the case with lowest considered viscosity with a deviation of 4%.

The values of the optimal individual weighting factors as well as both proposed expressions are presented in Figure 8.6, from which it is evident that the contribution of the confining wall is more pronounced at very low diameter aspect ratios, where the free cross-sectional area is constricted most. Here, large parts of the wall surface area are in contact with the gas flowing at its maximum velocity, whereas some parts of the pellets are situated in stagnant flow regions, i.e., close to touching points with other pellets or the wall, and therefore cannot

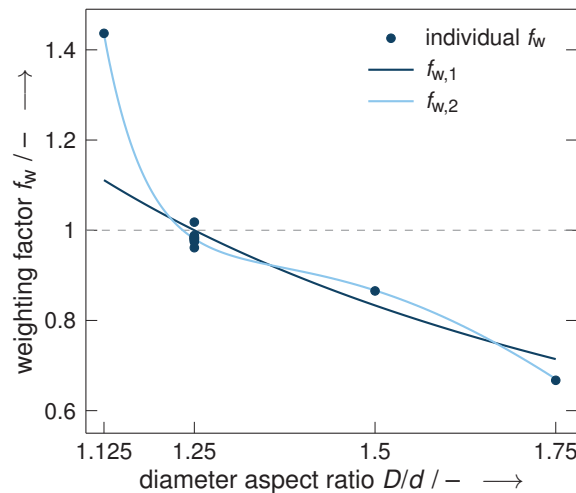


**Figure 8.6:** Wall surface weighting factor as function of diameter aspect ratio.

generate pressure drop. With increasing diameter aspect ratio two flow channels develop in the plane perpendicular to where the particles touch the wall on alternating sides which goes along with a reduced flow velocity in these channels resulting in less pressure drop. Hence the need to include the wall surface area with a weighting factor as function of diameter aspect ratio in the Blake-Kozeny equation.

## 8.5 Conclusion

The simulated pressure drop across single pellet string reactors follows the expected trends when varying fluid viscosity, flow velocity, diameter aspect ratio and reactor scale. Ergun-based correlations can be used to describe the pressure drop behaviour when considering the influence of the confining wall. As it seems, our choice of the base case geometry coincides with a good agreement to the pressure drop correlations by chance. Following the approach by Scott et al. [4] and introducing a weighting factor to the surface of the confining wall in the equivalent diameter formulation excellent results were obtained in combination with the Blake-Kozeny equation. Using a straightforward factor based solely on the diameter aspect ratio in comparison to the base case already resulted in a significant increase in accuracy. Further improvement could be achieved with a more elaborated empirical expression for the weighting factor as a function of the diameter aspect ratio containing five fitted parameters. This allows improved predictions of the pressure drop in SPSRs as compared to the correlations available from literature. However, the proposed formulations of the weighting factor are based on a limited number of SPSR variations. Further simulations to the existing parameter study are planned to confirm and possibly extend the range of validity, potentially covering turbulent flow scenarios.





# 9 Nonisothermal behaviour in reactive single pellet string reactors

---

This chapter was published in an earlier version as Eurokin project report:

J. Fernengel, L. Bolton and O. Hinrichsen, Pellet-String Reactor Gas-Solid Systems. Phase II, Eurokin 2019. [182]

Inclusion of this chapter would not have been possible without the kind permission of the consortium members.

---

## Report summary

The numerical investigation of single pellet string reactors (SPSR), a special type of fixed bed reactor, as presented in Chapters 7 and 8, is extended to include the impact of thermal effects. The nonisothermal behaviour of heterogeneously catalysed gas-phase reactions in single pellet string reactors of spherical pellets in cylindrical tubes is investigated by means of CFD simulations. Thermal runaway is observed when varying the heat of reaction. Results of a parameter study reveal a region where stable operation is possible based on heat of reaction, activation energy, reactor scale, corresponding plug flow conversion, fluid heat capacity and thermal conductivity of the catalyst material – all a priori known values. The height of the inert bed, number of simulated pellets and temperature-dependency of the diffusion coefficient showed only minor influence. As a result, a novel criterion on the thermal runaway in single pellet string reactors is proposed.

## CRedit author statement

*Johanna Fernengel*: Conceptualisation, Methodology, Software, Formal analysis, Investigation, Visualisation, Writing - Original Draft.

*Leslie Bolton*: Supervision, Project administration, Funding acquisition, Writing - Review & Editing.

*Olaf Hinrichsen*: Project administration, Supervision, Funding acquisition, Writing - Review & Editing.



## 9.1 Introduction

A key issue in the operation of fixed bed reactors with exothermal reactions remains the heat management. An imbalance between the heat originating from reactant conversion by an exothermal reaction and its removal may lead to a number of undesirable consequences, from difficulties in maintaining the product quality [183] due to influence on equilibrium conversion and selectivity [2], damages to the catalyst or the construction material [1] and safety issues [184]. Also, degradation of heat sensitive products might occur [185]. Therefore, to improve heat transfer out of catalytic fixed beds, it is advisable to reduce the reactor diameter in case of exothermic reactions to facilitate heat removal to the reactor wall as noted in the 1970s by Froment [2] or introduce inert particles with high thermal conductivity as heat dissipating diluent as patented recently by Simanzhenkov et al. [186]. When an increase in operating temperature by various means such as changes in the operating conditions, as for example the feed temperature, composition and throughput, cooling temperature or the catalyst properties, cannot be controlled any longer by built-in cooling mechanisms, the enhancement of the reaction rate due to the increased temperature will worsen the situation and may ultimately lead to thermal runaway.

Single pellet string reactors, as limiting case of fixed-bed reactors with a diameter ratio between outer confining wall and catalytic particles below two, are expected to show excellent heat transfer characteristics and shall therefore be investigated in this chapter in regard of their nonisothermal behaviour.

Numerous publications have addressed thermal runaway, starting with Bilous and Amundson [183] who coined the phrase *parametric sensitivity* as a region, where reactor operation is very sensitive to the parameters of the system, or, using the definition by Emig et al. [187], a region where small changes in the parameters lead to large variations in the state variables.

The contribution by Emig and co-workers [187] on the sensitivity of a fixed-bed reactor for the synthesis of vinyl acetate catalysed by zinc acetate supported on activated carbon is one of the few experimental studies available in literature. Based on their experimental data, the authors fitted the parameters of a two-dimensional pseudohomogeneous reactor model and concluded that it would be the method of choice to use appropriate models for a priori runaway prediction based on the rate of temperature rise and the maximum temperature in the hot spot rather than using early sensitivity diagrams by various authors.

Bauman and Varma [188] obtained good agreement between experiments of CO oxidation on commercial cylindrical pellets with CuO catalyst supported on  $\gamma$ -alumina in a diluted fixed-bed with constant wall temperature and a corresponding heterogeneous reactor model for the reactor sensitivity when varying the flow rate and the inlet temperature.

Based on experimental results and a corresponding two-dimensional heterogeneous reactor model, Anastasov [189] concluded that there is practically no risk of an uncontrolled

hot spot leading to reactor runaway for the oxidation of o-xylene to phthalic anhydride over an industrial  $V_2O_5 - TiO_2$  catalyst.

Reactor models have been used extensively to study parametric sensitivity and runaway in tubular reactors with and without catalytic beds. Based on the numerical predictions of temperature and concentration profiles along the reactor, a number of runaway criteria have been proposed. Bilous and Amundson [183] investigated the parametric sensitivity of unpacked quasiisothermal tubular reactors using a 1D homogeneous reactor model with constant wall temperature regarding changes in feed concentration and wall temperature on product concentration and reactor temperature profiles along the reactor. A one-dimensional pseudohomogeneous reactor model was implemented by van Welsenaere and Froment [190] to describe exothermic reactions in fixed-bed tubular reactors with constant wall temperature and derived two criteria for runaway from the analysis of intrinsic properties of the temperature profile along the reactor, namely the point of inflection in the temperature profile occurring before the maximum point and the temperature at the maximum, where the resulting criteria are limited to the underlying set-up used for the reactor model. A more general plot to distinguish between stable operation and runaway for an irreversible first-order exothermal reaction within the gas-phase inside a tubular reactor was proposed based on a one-dimensional model based on dimensionless parameters for heat generation and heat removal by Oroskar and Stern [191]. Incorporating explicitly the effective radial heat and mass transport in a two-dimensional pseudohomogeneous reactor model, Emig et al. [187] obtained good agreement between simulation results and the experimental data used for parameter fitting. Later work with pseudohomogeneous reactor models include that of Balakotaiah and Luss [192] who derived an explicit runaway criterion for catalytic reactors with inter- and intraparticle transport resistances. Maria and Stefan [193] obtained satisfactory agreement for a reactor sensitivity analysis with a one-dimensional pseudohomogeneous adiabatic model but with more complex reaction kinetics for the vapour-phase nitrobenzene hydrogenation yielding satisfactory results for runaway prediction as compared to the *generalised sensitivity criterion* put forth by Morbidelli and Varma [194].

The main problem with pseudohomogeneous reactor models for fixed-bed reactors remains in the lack of distinguishing between fluid and solid temperature within the bed. What matters in heterogeneous reactors is the particle temperature due to its direct influence on reaction rate, selectivity and catalyst degradation [195]. Therefore, Morbidelli and Varma [195] stressed that all criteria available in literature at that time which have been based on pseudohomogeneous models show similar deviation in predicting reactor sensitivity as compared to the experimental data by Emig et al. [187]. Also, the use of one-dimensional models should be questioned as Carberry and White concluded that it requires a two-dimensional description of the temperature field while a one-dimensional description of mass transport is sufficient [196].

An initially one-dimension heterogeneous plug-flow model of fixed-bed catalytic reactors with internally isothermal particles but including the effect of interparticle mass and heat transfer by Morbidelli and Varma [195] was extended by the same authors to two dimensions including intraparticle mass transfer [197] thus improving the agreement with the experimental data by Emig et al. [187]. Raghaven [184] concluded on the basis of a two-dimensional heterogeneous reactor model looking at the oxidation of benzene and o-xylene to maleic anhydride and phthalic anhydride, a series-parallel reaction, that the latter reaction is more likely to cause thermal runaway due to an extreme sensitivity to variations in temperature and feed composition. However, this is not in line with the experimental findings of Anastasov [189]. A one-dimensional heterogeneous model of a cooled tubular catalytic reactor taking into account the influence of interparticle and intraparticle transport limitations but assuming isothermal catalyst particles was used to calculate stability boundaries by Balakotaiah et al. [198]. They extended their work to more complex reaction systems such as parallel and consecutive networks but with homogeneous models for continuously stirred tank reactors. Quina and Ferreira [199] investigated the runaway behaviour of fixed-bed reactors for the partial oxidation of methanol to formaldehyde over iron/molybdenum-oxide catalysts based on the *generalised parametric sensitivity* by [194] using three different models – a one-dimensional pseudohomogeneous reactor model as well as a one-dimensional and a two-dimensional heterogeneous model – concluding that the side reaction of formaldehyde oxidation had to be taken into account as driving force for thermal runaway as a result of its high activation energy. The use of a less active first bed zone was identified to reduce the parametric sensitivity of the studied system and thus stabilise the reactor operation [199].

Herskowitz and Hagan [200] proposed a runaway criterion suitable for any kinetic single-reaction system based on the  $\alpha$  model for wall-cooled fixed-bed reactors with good agreement to the experimental data by Emig et al. [187]. The  $\alpha$  model [201] is a special one-dimensional model based on the asymptotic analysis of a two-dimensional model for tubular reactors under the assumption that the adiabatic temperature change is much larger than the temperature variation within a cross section of the reactor.

Data mining techniques have been successfully applied by Varga et al. [202] to forecast the runaway of a second-order reaction in an industrial catalytic fixed-bed reactor using a heterogeneous reactor model to formulate the underlying linguistic rules.

Hot spot formation and reactor runaway remain up-to-date topics, as for example depicted by Gruber et al. [203] who optimise the geometry of a wall coated microreactor for the methanation of carbon dioxide in the light of the thrive for power to gas technologies targeting minimum hot spot temperatures using a one-dimensional reactor model and 3D simulations with Ansys<sup>®</sup> Fluent. Considering a one-dimensional ideal plug-flow reactor model, Kummer and Varga [204] recently defined two new criteria to indicate runaway conditions. The authors suggest that it may not be sufficient to apply one of the criteria

available from literature nor one of their own but rather to rely on a combination of the proposed criteria. This sums up nicely the situation on runaway criteria, where there is not the one most suitable criterion for all set-ups and which remain a topic of interest based on a number of reasons from process optimisation closer to critical operating conditions or novel processes and reactor concepts to facilitate for example power to gas from volatile energy sources.

However, it must be stressed that any of the criteria available from literature can only be as good as the underlying model predicts the reactor's behaviour, where heterogeneous reactor models are to be preferred over homogeneous models especially since the latter do not distinguish between fluid and solid temperature.

Despite the vast amount of criteria published to predict thermal runaway conditions, these are of limited importance given the highly specific set-ups found in industrial applications and experimental set-ups with single test tubes are often used to determine the range of parametric sensitivity prior to the operation of multitubular reactors [1]. These must not be operated in regions with high parametric sensitivity as non-uniform conditions throughout the tubes may lead to runaway in individual tubes [1].

Reactor runaway can be detected by analysing the product composition [1], monitoring the fluid temperature or the bed temperature. A comparison of temperature control strategies to prevent thermal runaway during ethane hydrogenolysis in fixed-bed reactors led to the conclusion that a control based on the temperature of the fluid at the reactor exit, as often used in industry, was too slow to protect the bed against runaway whereas a control based on the average solid temperature in the bed allowed an earlier detection of conditions within the sensitive region and were found to be effective to prevent runaway [205].

Apart from runaway, thermal effects may have substantial influence on reactor behaviour in real reacting systems and cannot be neglected. Changes in the gas density, induced for example by temperature variations, may result in buoyancy effects which are known to have significant influence on the flow behaviour in macroscopic fixed-bed reactors [206].

Single pellet string reactors have been introduced and thoroughly characterised regarding the deviation of their conversion and residence time behaviour to ideal plug-flow in Chapter 7 and details on pressure have been discussed in Chapter 8. However, these chapters have been limited to isothermal operation only. So far, neither the parametric sensitivity of single pellet string reactors nor the deviation to ideal behaviour in case of nonisothermal conditions have been subject of investigation. Therefore, the study presented in Chapters 7 and 8 is extended to exothermic reactions, dealing with thermal effects encountered in heterogeneously catalysed gas-phase reactions within single pellet string reactors. Buoyancy effects based on changes in the gas molecular weight due to the reaction are excluded from this study and special emphasis is laid on the heat transfer behaviour.

A temperature dependent reaction rate was implemented for the heterogeneously catalysed gas phase reaction considered at the surface of the catalytic pellets. In order to resolve local temperature and concentration gradients substantial mesh refinement was required as compared to the previous isothermal study (cf. Chapter 7). To obtain feasible simulation set-ups, this required a reduction in the number of simulated catalyst pellets within the string. Also, when taking into account thermal effects, the catalytic pellets were resolved to include thermal conductivity. This required a closer look at contact point handling, that is the touching points between pellets as well as between pellets and the surrounding wall.

At an early stage, it was found that temperature increases caused by thermal runaway were far more important than buoyancy effects, with the exothermic heat of reaction and the activation energy being the main parameters driving this behaviour. The interplay between heat release due to the reaction and heat removal proved decisive for reactor stability. Therefore, the aim of this study was extended to identify a region where stable operation of exothermal reactions in single pellet string reactors is feasible, taking into account variations in heat of reaction, activation energy, reaction rate coefficient, reactor scale, number of catalytic pellets in the single pellet string reactor as well as thermophysical properties.

This chapter is organised as follows: after addressing a preliminary consideration based on the preceding phase considering isothermal SPSRs in Section 9.2, the reactor model and its implementation are presented in Section 9.3. This is followed by details on the set-up of the considered single pellet string reactor scenarios in Section 9.4. The results of the base case scenario as well as those of a case with significant thermal effects are examined at the beginning of Section 9.5 before illustrating the outcomes of the performed parameter variations. Based on the outlined simulation results, an analogy to the Benneker criterion on thermal effects in fixed-bed reactors [206] is presented. Finally, a criterion to determine a region where stable reactor operation is possible without thermal runaway is proposed. A summary and conclusion are provided in Section 9.6.

## 9.2 Preliminary considerations

The high mesh refinement required to capture steep local temperature and concentration gradients makes it impractical to simulate entire single pellet string reactors as performed for the parameter study in Chapter 7. Therefore, preliminary considerations were taken into account to decide which reactor region should be considered. Also, evaluating the influence of thermal effects on the residence time distribution in the reactors was omitted due to reasons of practicability.

Since the original attempt was to capture buoyancy induced flows, these would be related to the region of highest heat generation. In term, this corresponds to a region with high



reactant concentration and an accelerated reaction rate coefficient due to high local temperatures. Highest reactant concentration can be found at the reactor inlet and, despite possible cooling effects of the inlet stream, the highest temperatures are expected within the upper section of the pellet string.

Going back to the conversion results of the base case single pellet string reactor set-up in Chapter 7, shown in Figure 7.5b on page 88, there is an increased conversion associated with the first pellet in the string which was traced back to be caused by back-diffusion.

Hence, the highest temperature gradients will normally be present in the vicinity of the first catalytic pellet in the single pellet string and the simulation domain was limited to the first 2.5 pellets.

### 9.3 Model description and implementation

The research question of investigating thermal effects in SPSRs makes it necessary to fully include the catalytic pellets within the simulation domain. As opposed to the investigation of isothermal single pellet string reactor set-ups in Chapter 7, the catalytic pellets were meshed to allow for thermal transport within the solid. For simplicity, however, the inert bed upstream of the pellet string was only included as boundary condition to the fluid domain and not fully resolved. The simulation domain can thus be divided into three regions, namely fluid, catalytic solid and inert solid, the modelling and simulation of which is the focus of this section.

#### 9.3.1 Reactor geometry

Within the single pellet string of catalytic pellets, the ideal pellet positions can be expressed analytically by

$$x_i = (-1)^i \cdot \left( \frac{D-d}{2} \right) \quad (9.1)$$

$$y_i = 0 \quad (9.2)$$

$$z_i = (i-1) \cdot \sqrt{d^2 - (D-d)^2} + \frac{d}{2} \quad (9.3)$$

where  $d$  is the pellet diameter,  $D$  the diameter of the confining cylindrical wall and  $i$  the pellet index variable. Figure 9.1 shows the pellet arrangement at the bottom of a SPSR with trigonometric relations leading to the analytical pellet positions.

As in Chapter 7, there is a short bed of fine inert particles upstream of the catalytic string of pellets. The arrangement within this bed is random, which requires means of packing generation.



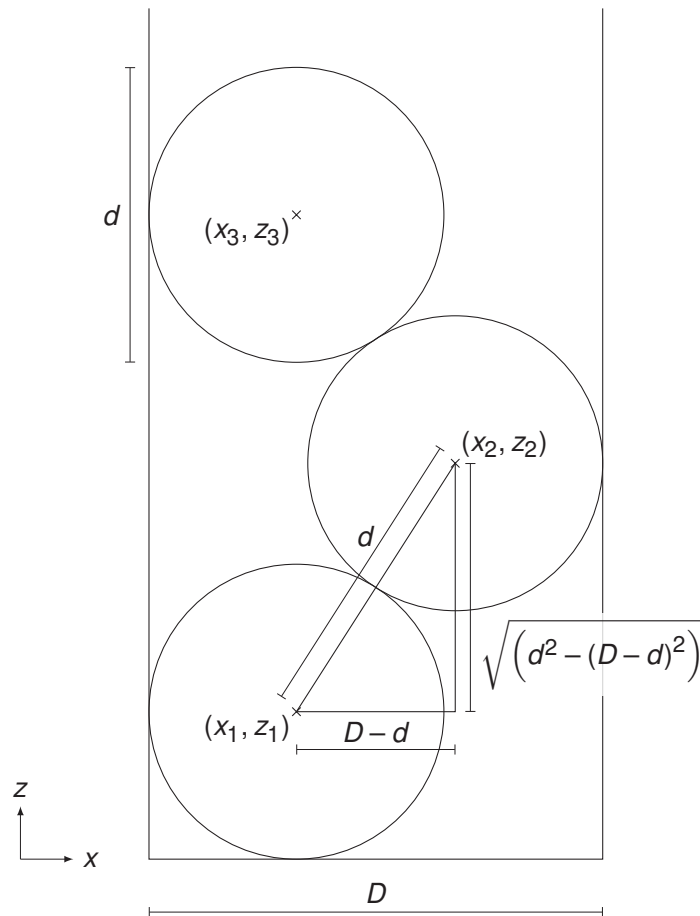


**Figure 9.1:** Schematic view of bottom three pellets in SPSR with trigonometric relations required for analytical pellet positions.

### 9.3.2 Fluid domain

The single phase flow of a pure nonisothermal, compressible Newtonian fluid, with no change in composition, was considered. To describe the flow behaviour, the conservation of mass, momentum and energy were considered at steady state. The equation of continuity for the fluid [41, 42] reads

$$\nabla \cdot (\rho \mathbf{u}) = 0 \quad (9.4)$$

where  $\rho$  is the fluid density and  $\mathbf{u}$  the fluid velocity, and the equation of motion amounts to [42]

$$\nabla \cdot (\rho \mathbf{u} \mathbf{u}) = -\nabla p - \nabla \cdot \boldsymbol{\tau} + \rho \mathbf{g} \quad (9.5)$$

where  $p$  is the static pressure,  $\boldsymbol{\tau}$  the viscous stress tensor and  $\mathbf{g}$  the gravitational acceleration. For Newtonian fluids the viscous stress tensor can be expressed by Newton's Law of viscosity [42, 48]:

$$\boldsymbol{\tau} = -\eta \left( \nabla \mathbf{u} + (\nabla \mathbf{u})^T \right) + \frac{2}{3} \eta (\nabla \cdot \mathbf{u}) \mathbf{I} \quad (9.6)$$

where  $\eta$  is the dynamic viscosity and  $\mathbf{I}$  the unit tensor, neglecting the influence of the dilatational viscosity as often done in CFD [42].

Species movement as a result of Fickian diffusion and convection was considered by the passive scalar transport equation at steady state

$$\nabla \cdot (\rho \mathbf{u} Y) - \nabla \cdot (\rho \mathcal{D} \nabla Y) = 0 \quad (9.7)$$

where  $Y$  is the mass fraction and  $\mathcal{D}$  the diffusion coefficient.

The enthalpy based conservation of energy leads to [42]

$$\nabla \cdot (\rho \mathbf{u} h) + \nabla \cdot \left( \rho \mathbf{u} \frac{|\mathbf{u}|^2}{2} \right) - \nabla \cdot (\alpha \nabla h) = \rho \mathbf{g} \cdot \mathbf{u} + \nabla \cdot (\boldsymbol{\tau} \cdot \mathbf{u}) \quad (9.8)$$

considering convective and conductive transport as well as mechanical source terms, where  $h$  is the specific enthalpy and  $\alpha$  the thermal diffusivity of the fluid. Thermal radiation is not considered in this study. The heat of reaction related to the heterogeneous surface reaction taking place at the surface of the catalytic pellets was taken into account as a source term at the interface between *fluid* and *catalytic solid*.

In order to solve for the unknowns in the conservation equations as function of space and time, further fluid relations need to be considered, namely the thermal and caloric equation of state, as well as information on possible temperature dependence of the fluid's transport properties, viscosity, molecular diffusivity and thermal conductivity.

The fluid was assumed to behave as a perfect gas, following the ideal gas law [207]:

$$\rho = \frac{p M}{R T} \quad (9.9)$$

where  $M$  is the molecular weight of the gas and  $R$  the ideal gas constant. Also, the fluid shall be calorically perfect [207], such that the specific heat capacity  $c_p$  is temperature independent.

$$c_p \neq c_p(T) \rightarrow c_p = \text{constant} \quad (9.10)$$

Further simplifications were met regarding transport properties. In a first attempt, the dynamic viscosity  $\eta$  was considered constant, as was the Prandtl number  $Pr$ , defined as

$$Pr = \frac{\nu}{\alpha} = \frac{\eta C_p}{\kappa_f}, \quad (9.11)$$

where  $\kappa_f$  is the thermal conductivity of the fluid.

As an alternative, the dynamic viscosity  $\eta$  was evaluated using Sutherland's formula [208]

$$\eta = \eta_{ref} \left( \frac{T}{T_{ref}} \right)^{1.5} \frac{T_{ref} + S}{T + S} \quad (9.12)$$

where  $\eta_{ref}$  is the dynamic viscosity at reference temperature  $T_{ref}$  and  $S$  the Sutherland constant. In this case, the modified Eucken correlation [209] was used to express the thermal conductivity of the fluid by

$$\kappa = \eta M (1.32c_p + 0.45R). \quad (9.13)$$

The self-diffusion coefficient  $\mathcal{D}$  was assumed constant apart from one scenario, where the temperature dependency is expressed by [27, 210]

$$\mathcal{D} = \mathcal{D}_{ref} \left( \frac{T}{T_{ref}} \right)^{1.75} \frac{\rho_{ref}}{\rho}. \quad (9.14)$$

As the pressure difference across the considered simulation domain is low, its influence on the diffusion coefficient was not considered locally. However, the effect of higher overall gas pressure on properties is included.

### 9.3.3 Catalytic and inert solid domains

Both types of solid domains accounted for in this study, namely catalytic and inert, were considered to be non-porous with no species diffusion within these domains. Therefore, the heterogeneous chemical reaction was limited to the catalytic surface only.

Heat transport was taken into account within the catalytic solid domain, where heat generation is present due to the reaction.

According to Fourier's law of heat conduction [42], the heat flux  $\mathbf{q}$  is proportional to the thermal conductivity  $\kappa$  and the temperature gradient  $\nabla T$

$$\mathbf{q} = \kappa \nabla T \quad (9.15)$$

assuming that the material behaves isotropically, that is the thermal conductivity is independent of the direction.

The inert solid domain was assumed to act as an insulator with no heat conduction.

### 9.3.4 Surface reaction

A heterogeneously catalysed, hypothetical first order irreversible reaction was considered at the surface of the catalytic pellets within the SPSR. Preliminary discussions whether to take into account a reaction distributed through the catalytic pellets instead lead to the conclusion that the outcomes would be broadly similar. The surface reaction acts as a source term to both species transport and heat balance. A power law model was used to determine changes to the species concentration, where the specific reaction rate follows the Arrhenius equation. Thus the temperature dependency of the reaction rate constant  $k$  can be expressed by [27]

$$k(T) = k(T_0) \exp \left\{ \frac{E_a}{R} \left( \frac{1}{T_0} - \frac{1}{T} \right) \right\} \quad (9.16)$$

where  $k(T_0)$  is the reaction rate constant at the reference temperature  $T_0$  and  $E_a$  the activation energy.

Assuming a first order irreversible reaction  $A \rightarrow B$  at the catalyst surface gives the following relation for reactant depletion, which has to be balanced by transport of species through the boundary layer by diffusion:

$$-\mathcal{D} \nabla Y = k(T) Y_{\text{cat}} \quad (9.17)$$

where  $Y_{\text{cat}}$  is the mass fraction of reactant at the catalytic surface.

The heat released due to the reaction then amounts to

$$q = -\Delta H k(T) \frac{\rho}{M} Y_{\text{cat}} \quad (9.18)$$

with heat of reaction  $\Delta H_{\text{rxn}}$  and molar mass of the reactant  $M$ . This expression was integrated into the energy boundary condition, a Cauchy type boundary condition coupling the temperature fields in the catalytic solid domain and the fluid domain. At the interface, the temperature of both domains must be equal, that is  $T_{\text{cat}} = T_{\text{f}} = T$ , and the heat fluxes must balance. Therefore, conduction was taken into account through the solid and the fluid boundary layer as well as the heat flux due to the reaction:

$$\kappa_{\text{S}} \nabla T_{\text{S}} + \kappa_{\text{f}} \nabla T_{\text{f}} = -\Delta H k(T) \frac{\rho}{M} Y_{\text{cat}} \quad (9.19)$$

where  $\kappa_{\text{S}}$  and  $\kappa_{\text{f}}$  are the heat conductivities of the catalytic solid and the fluid respectively.

### 9.3.5 Implementation

As in phase 1 of the project, a heterogeneous reactor model was used to implement the SPSR. However, dropping the assumption of isothermal conditions, we did not restrict the simulation domain to the fluid phase but fully included the catalytic solid pellets in addition. The flow field is no longer independent of the reaction, which has an impact on the energy balance and thus the temperature dependent reaction rate. Therefore, a cold-flow simulation was no longer feasible. This added complexity to the simulation demanding higher mesh refinement. Investigation of residence time behaviour was dropped for reasons of excessive computational time. This reduced the simulation routine to geometry generation, mesh generation and reactive flow simulation.

As before, the CFD simulations were implemented in OpenFOAM<sup>®</sup> v4.1 [24]. Where pellet positions could not be described analytically, the software Blender 2.76b [23] was used for random bed generation (cf. for example [80, 140, 211]). Data analysis and visualisation were performed with ParaView 5.6.0-RC1 [82]. Details on the implementation of the reactive flow in SPSRs are provided in the following.

#### 9.3.5.1 Geometry and mesh generation

Considering both fluid and solid domains with thermal conductivity within the catalytic solids requires strategies for contact point handling. Figure 9.2 shows common approaches found in literature. Here, different methods were used to account for the contact between catalytic pellets and between catalytic pellets and the confining wall, using bridges and caps respectively (cf. inserts in Figure 9.3).

The geometry was obtained with Blender 2.76b [23], covering both inert and catalytic pellets. The inert bed required means of random packing generation, whereas for the analytically positioned catalytic pellets means of contact point modification were necessary. Small cylinders were introduced between the centre points of the catalytic pellets, with a diameter equivalent to a tenth of the corresponding pellet diameter.

In addition, a slice of a hundredth of the diameter of the confining wall was removed over the string of catalytic pellets next to the confining wall. This introduces a gap between the catalytic pellets and the confining wall, corresponding to the scenario *caps* for contact point treatment as shown in Figure 9.2. The final geometry covering the random inert pre-bed as well as the catalytic pellet string with bridges between adjacent catalytic pellets and caps between catalytic pellets and the confining wall was exported as stereolithography file.

Based on this arrangement of inert and catalytic pellets, the mesh was prepared with *snappyHexMesh*, an OpenFOAM<sup>®</sup> tool. A cylindrical background mesh with the dimensions of the confining wall was constructed with *blockMesh*. The length of the cylinder allows room for the inert packing surrounded by short empty tube sections of  $0.05d$  and the 2.5 catalytic

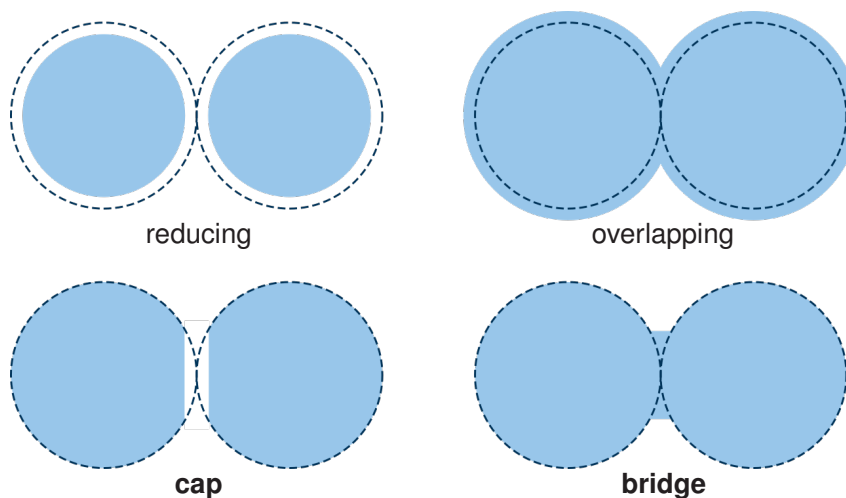


**Figure 9.2:** Common strategies of contact point handling, after Dixon et al. [212]; methods used in this study indicated by bold font.

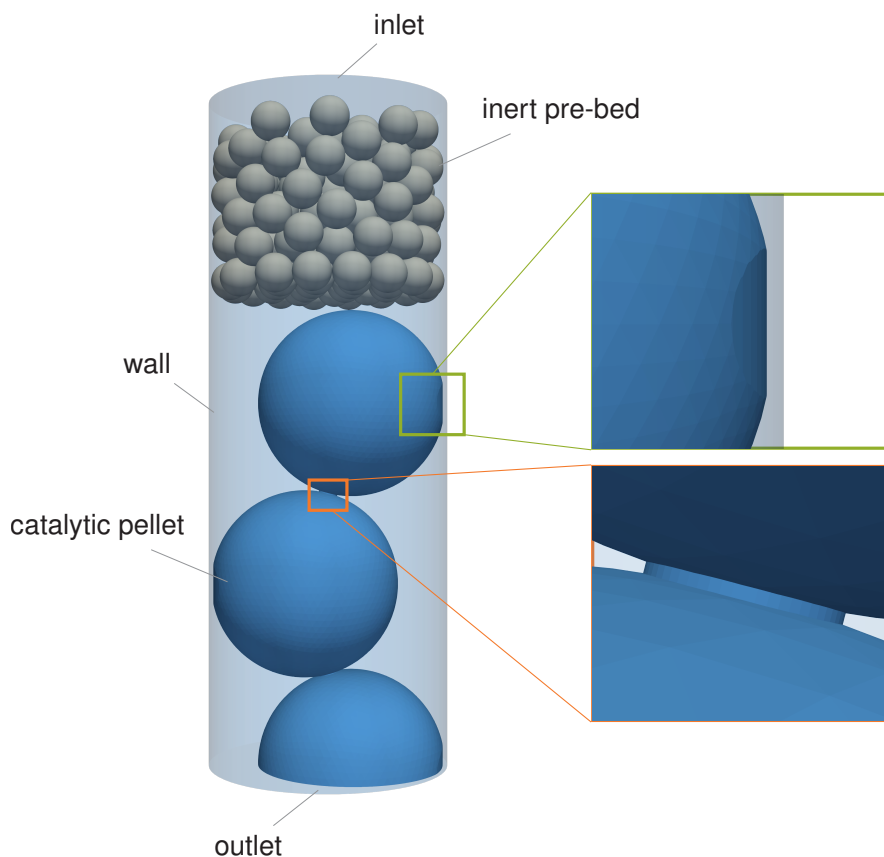


**Figure 9.3:** Geometry set-up showing top section of a SPSR including an inert pre-bed with labelling of boundaries. Inserts show contact point treatment between catalytic pellets and confining wall (top) and between adjacent catalytic pellets (bottom).

pellets. A schematic view of the set-up is shown in Figure 9.3. Two separate meshes were constructed, one for the catalytic pellets and one for the fluid domain. The inert pre-bed is incorporated as holes to the fluid domain. The mesh was designed with further cell refinement compared to the background mesh towards surfaces and insertion of additional cell layers adjacent to surfaces.

### 9.3.5.2 Reactive flow simulation

The laminar reactive flow through the SPSR was simulated using the standard OpenFOAM® solver *chtMultiRegionSimpleFoam*. This allows evaluation of buoyant flow of Newtonian fluids and heat conduction within the solids, coupled by conjugate heat transfer between solid and fluid regions [46]. The solver was set to steady-state and customised by adding an equation for passive species transport (cf. Eq. (9.7)). A heterogeneously catalysed gas phase reaction was considered to take place at the surface of the catalytic pellets by appropriate boundary conditions for temperature coupling and reactant depletion at the interface between catalytic pellets and fluid domain.

#### 9.3.5.2.1 Boundary conditions

Standard flow boundary conditions for an internal flow problem were used, defining an inlet flow and constant pressure at the outlet [41]. A no-slip boundary condition was defined at walls and pellet surfaces. Special conditions were set at catalytic surfaces for temperature and species concentration.

The inlet boundary conditions for pressure, velocity, species concentration and temperature are:

$$\frac{\partial p_{\text{in}}}{\partial n} = 0, \quad |\mathbf{u}_{\text{in}}| = u_0 = f(\tau), \quad Y_{\text{in}} = \text{const.} \quad \text{and} \quad T_{\text{in}} = \text{const.} \quad (9.20)$$

The corresponding boundary conditions at the outlet were set to:

$$p_{\text{out}} = \text{const.}, \quad \frac{\partial u_{\text{out}}}{\partial n} = 0, \quad \frac{\partial Y_{\text{out}}}{\partial n} = 0 \quad \text{and} \quad \frac{\partial T_{\text{out}}}{\partial n} = 0. \quad (9.21)$$

A no-slip condition to the velocity was set at the confining wall as well as at the inert and catalytic pellet surfaces and the pressure was approximated with a zero gradient normal to these surfaces:

$$u_{\text{inert}} = u_{\text{cat}} = 0 \quad \text{and} \quad \frac{\partial p_{\text{surf}}}{\partial n} = 0. \quad (9.22)$$

Zero gradients were also enforced for species mass fraction and temperature at the confining wall and the surface of the inert pellets in the pre-bed:

$$\frac{\partial Y_{\text{inert}}}{\partial n} = 0 \quad \text{and} \quad \frac{\partial T_{\text{inert}}}{\partial n} = 0. \quad (9.23)$$

At catalytic surfaces, the boundary condition for the species mass fraction reflects the reactant depletion due to the hypothetical first order irreversible reaction  $A \rightarrow B$  as expressed by Eq. (9.17), which was implemented in a custom boundary condition.

The corresponding temperature boundary condition specifies both the temperature value at the interface, which has to match the temperature in the adjacent solid and fluid domain, and the temperature gradient, containing conduction to the attached domains and a source term related to the surface reaction:

$$T_{\text{cat}} = T_{\text{s}} = T_{\text{f}} \quad \text{and} \quad \kappa_{\text{s}} \nabla T_{\text{s}} + \kappa_{\text{f}} \nabla T_{\text{f}} = -\Delta H k(T) \frac{\rho}{M} Y_{\text{cat}}. \quad (9.24)$$

This boundary condition was implemented based on *turbulentTemperatureRadCoupled-Mixed* for the temperature at the interface between fluid and catalytic solid.

### 9.3.5.2.2 Initial conditions

To start with, the flow field was initialised with *potentialFoam*, while the pressure, temperature and reactant concentration fields were set to uniform values representing the inlet values of the variables respectively. Where applicable, simulation results of related scenarios were used as starting point for further simulations, as for example the isothermal base case result for mildly exothermic reactions, which in turn were used for cases with higher exothermicity and so on.

## 9.4 Single pellet string reactor scenarios

### 9.4.1 Common reactor properties and assumptions

Within this project, the non-isothermal behaviour of single phase gas flow through single pellet string reactors with a heterogeneously catalysed surface reaction were investigated using CFD simulation, especially by evaluating the conversion within the reactor. The inlet velocity  $u_0$  of the fluid was set to a value resembling a space time over the catalytic bed of  $\tau = 1$  s, which can be expressed as a function of reactor geometry as

$$u_0 = \frac{\dot{V}}{A_{\text{t}}} = \frac{V_{\text{f}}}{A_{\text{t}}\tau} = \frac{L - \frac{V_{\text{p}}}{A_{\text{t}}}}{\tau} = \frac{d + (N-1)\sqrt{d^2 - (D-d)^2} - \frac{2Nd^3}{3D^2}}{\tau} \quad (9.25)$$



where  $\dot{V}$  is the volumetric flow rate,  $A_t$  the cross sectional area of the empty reactor tube,  $V_f$  the fluid volume surrounding the catalytic bed,  $\tau$  the space time,  $V_p$  the total volume of pellets in the catalytic bed,  $d$  the pellet diameter,  $D$  the cylinder diameter and  $N$  the number of catalytic pellets. The temperature of the inlet stream as well as the temperature of the confining wall were fixed to

$$T_{\text{in}} = T_w = 293 \text{ K.} \quad (9.26)$$

The considered flow scenario resembles an internal flow problem. Here, a fixed pressure value equal to atmospheric pressure was specified at the reactor outlet, that is the outflow boundary:

$$p_{\text{out}} = 1 \text{ atm.} \quad (9.27)$$

The reaction  $A \rightarrow B$  at the catalytic surface was assumed irreversible and of hypothetical first order, with the physical properties of nitrogen for both reactant and product gas. These are:

- molecular weight  $M = 28.0134 \text{ g mol}^{-1}$
- specific heat capacity  $c_p = 1040 \text{ J kg}^{-1} \text{ K}^{-1}$
- dynamic viscosity  $\eta = 1.912 \cdot 10^{-5} \text{ kg m}^{-1} \text{ s}^{-1}$
- Prandtl number  $\text{Pr} = 0.725$

For all considered scenarios, it was assumed that pure reactant is entering the reactor at the inlet, such that

$$Y_{\text{in}} = 1. \quad (9.28)$$

Both inert and catalytic pellets were treated as non-porous solids with the following set of thermophysical properties, that were assumed constant:

- thermal conductivity  $\kappa_s = 1 \text{ W m}^{-1} \text{ K}^{-1}$
- specific heat capacity  $c_p = 440 \text{ J kg}^{-1} \text{ K}^{-1}$
- density  $\rho = 1845 \text{ kg m}^{-3}$

The heterogeneous reaction rate coefficient  $k$  was set to a value corresponding to a conversion of 80 % in a comparable isothermal plug flow reactor at inlet temperature with equal

specific surface area  $a$  and space time. The specific area of a SPSR can be expressed by

$$a = \frac{A_{cat}}{V_f} = \frac{Nd^2}{\frac{1}{4}HD^2 - \frac{1}{6}Nd^3} \quad (9.29)$$

based on the reactor geometry and the conversion in a plug flow reactor  $X_{PFR}$  can be evaluated analytically using

$$X_{PFR} = 1 - e^{-\tau ka}. \quad (9.30)$$

### 9.4.2 Base case

The base case set-up is identical to phase I of the project with a SPSR consisting of 20 spherical catalytic pellets of  $d = 0.8$  mm diameter resting on top of each other and to alternating sides touching the cylindrical confining wall of diameter  $D = 1.0$  mm. However, only the initial part of this reactor - the first 1.5 or 2.5 pellets - was actually simulated, since these determine whether the reactor is stable or not. Upstream of this catalytic string of pellets is a short pre-bed made of inert spherical particles with a diameter of  $d/5$  over a length of the diameter of one catalytic pellet,  $d$ . The fixed space time of  $\tau = 1$  s over the catalytic string of pellets results in a superficial inlet velocity of  $u_0 = 8.6906 \cdot 10^{-3}$  m s<sup>-1</sup>. The reaction is considered isothermal, that is with heat of reaction  $\Delta H = 0$  kJ mol<sup>-1</sup>, with a reaction rate constant corresponding to 80 % conversion in a comparable plug flow reactor amounting to  $k = 2.73184 \cdot 10^{-4}$  m s<sup>-1</sup>. The activation energy is fixed at  $E_a = 50$  kJ mol<sup>-1</sup>. For the physical properties of the fluid and solids the values are set to those defined in the section above.

### 9.4.3 Variations on the base case

A parameter study was conducted starting from the base case scenario including variations on the heat of reaction, the length of the inert pre-bed, the number of simulated catalytic pellets at fixed reactor length, three scenarios with varying activation energy, different geometry scale of the reactor set-up, varying number of catalytic pellets within the single pellet string and hence the reaction rate in the part of that reactor which is simulated, double pressure as compared to the base case, varying conversion in the corresponding isothermal plug flow reactor to determine the reaction rate constant as well as varying thermophysical properties of fluid and catalytic solid and a scenario with temperature-dependent diffusion coefficient.

The first parameter to be varied was the *heat of reaction*, given its direct impact on heat generation and thus density variations within the reactor. Only exothermic reactions were considered, starting with moderate values of the heat of reaction with  $\Delta H = -16$  kJ mol<sup>-1</sup>,

doubling the values up to  $\Delta H = -256 \text{ kJ mol}^{-1}$ . Intermediate values were subsequently introduced in addition to this geometric series to capture transition effects.

This was followed by a short investigation of any effect that the *inert bed length* might have, covering two set-ups with double the length of the inert pre-bed of the base case, that is with inert particles of  $d/5$  diameter and a total pre-bed length of  $L_{\text{inert}} = 2d$ . One simulated case corresponds to isothermal operation whereas the other case takes an exothermal reaction with a heat of reaction of  $\Delta H = -224 \text{ kJ mol}^{-1}$  into account.

To examine the influence of the *number of simulated pellets*, a series of simulations covering heats of reaction from  $\Delta H = 0$  to  $-256 \text{ kJ mol}^{-1}$  was conducted for the base case geometry but simulating only the inert pre-bed and the first 1.5 catalytic pellets in the string. Two simulations were performed, one isothermal and one with a heat of reaction of  $\Delta H = -224 \text{ kJ mol}^{-1}$ , where the simulation domain covers  $N_{\text{sim}} = 3.5$  catalytic pellets in addition to the inert pre-bed.

Next, a series of set-ups with heats of reaction from  $\Delta H = -32$  to  $-128 \text{ kJ mol}^{-1}$  was studied from two higher values of the *activation energy* as compared to the before, namely  $E_a = 100 \text{ kJ mol}^{-1}$  and  $E_a = 150 \text{ kJ mol}^{-1}$ . It should be noted that the number of simulated catalytic pellets was reduced to  $N_{\text{sim}} = 1.5$  from here on.

The influence of *reactor scale* was included by two simulation series, with geometry scaling factors of 1.5 and 2.0, covering heats of reaction from  $\Delta H = 0$  to  $-128 \text{ kJ mol}^{-1}$  and  $\Delta H = 0$  to  $-64 \text{ kJ mol}^{-1}$ , respectively. For the inert pre-bed the pellet diameter was adjusted to  $d/5$  and the bed length to  $d$  depending on the diameter of the catalytic pellets considered, with a pre-bed diameter matching the inner diameter of the confining wall.

The *number of pellets in the SPSR* has direct influence on the inlet velocity and the value of the reaction rate constant. Here, variations to the number of catalytic pellets were considered between  $N = 5$  and 100, otherwise keeping the base case geometry. Two simulations were conducted for each set-up, one isothermal and the other with a heat of reaction of  $\Delta H = -64 \text{ kJ mol}^{-1}$ .

Then, the effect of *doubling the notional gas pressure* was investigated by a series of simulations covering heats of reaction from  $\Delta H = 0$  to  $-224 \text{ kJ mol}^{-1}$ .

Further, simulations of the SPSR base case geometry considering an isothermal and an exothermal reaction with  $\Delta H = -64 \text{ kJ mol}^{-1}$  were used to evaluate the influence of the reaction rate constant on reactor performance by adjusting the value of the *corresponding plug flow conversion* in a range of  $X_{\text{PFR}} = 0.2$  to 0.95.

To round off the SPSR scenarios, the influence of varying transport coefficients was tackled. A set-up considering an exothermal reaction with  $\Delta H = -64 \text{ kJ mol}^{-1}$  was used to investigate variations to the fluid's *heat capacity* between  $c_p = 104$  and  $2080 \text{ J kg}^{-1} \text{ K}^{-1}$  and

variations to the *thermal conductivity* of the catalytic pellets from  $\kappa = 0.05$  to  $2 \text{ W m}^{-1} \text{ K}^{-1}$ . The effect of allowing a temperature-dependent diffusion coefficient was studied with a series of simulations where the heat of reaction was allowed to vary from  $\Delta H = 0$  to  $-320 \text{ kJ mol}^{-1}$ .

Table 9.1 provides a summary of the considered parameter variations with relevant values for reactor geometry and material properties.

**Table 9.1:** Geometry and thermophysical properties of considered single pellet string reactor variations.

Scenario	$N$ -	$N_{\text{sim}}$ -	$d$ mm	$D$ mm	$H_{\text{inert}}$ mm	$\Delta H$ kJ mol <sup>-1</sup>	$E_a$ kJ mol <sup>-1</sup>	$p$ atm	$X_{\text{PFR}}$ -	$C_p$ J kg <sup>-1</sup> K <sup>-1</sup>	$\kappa_f$ W m <sup>-1</sup> K <sup>-1</sup>
base case	20	2.5	0.8	1.0	0.8	0	50	1.0	0.8	440	1.0
heat of reaction	20	2.5	0.8	1.0	0.8	0 to -256	50	1.0	0.8	440	1.0
inert bed length	20	2.5	0.8	1.0	1.6	0 and -224	50	1.0	0.8	440	1.0
number of simulated pellets	20	1.5	0.8	1.0	0.8	0 to -256	50	1.0	0.8	440	1.0
	20	3.5	0.8	1.0	0.8	0 and -224	50	1.0	0.8	440	1.0
activation energy	20	1.5	0.8	1.0	0.8	32 to -128	100	1.0	0.8	440	1.0
	20	1.5	0.8	1.0	0.8	32 to -128	150	1.0	0.8	440	1.0
reactor scale	20	1.5	1.2	1.5	0.8	0 to -128	50	1.0	0.8	440	1.0
	20	1.5	1.6	2.0	0.8	0 to -64	50	1.0	0.8	440	1.0
number of pellets in SPSR	5 to 100	1.5	0.8	1.0	0.8	0 and -64	50	1.0	0.8	440	1.0
double pressure	20	1.5	0.8	1.0	0.8	0 to -224	50	2.0	0.8	440	1.0
corresponding PFR conversion	20	1.5	0.8	1.0	0.8	0 and -64	50	1.0	0.2 to 0.95	440	1.0
heat capacity	20	1.5	0.8	1.0	0.8	0	50	1.0	0.8	104 to 2080	1.0
thermal conductivity	20	1.5	0.8	1.0	0.8	0	50	1.0	0.8	440	0.05 to 2
$T$ -dependent diffusion coefficient	20	1.5	0.8	1.0	0.8	0 to -320	50	1.0	0.8	440	1.0
$T$ -dependent dynamic viscosity	20	2.5	0.8	1.0	0.8	-64 to -256	50	1.0	0.8	440	1.0

## 9.5 Results

In this section, the simulation results are presented for the conducted parameter study on conversion behaviour of exothermic reactions in SPSRs. Details on the computational grid, the flow field and the reactant depletion within the reactor, which yields to the conversion along the reactor length axis, are provided for the base case scenario. This is followed by an investigation of the influence of the heat of reaction with visualisation of reactant depletion and temperature within the simulation domain. For most other scenarios, only the influence of the considered parameter on the outlet conversion is considered, with some additional insights where required for discussion. Also, convergence monitoring is illustrated for one set-up. The simulation results are analysed for possible correlations, beginning with parallels drawn to a criterion by Benneker et al. [206] looking at the enhancement of axial dispersion in fixed bed reactors due to density induced free convection currents. Finally, a criterion on thermal runaway for exothermic reactions in SPSRs is established.

### 9.5.1 Parameter study

#### 9.5.1.1 Base case

Mesh generation of the fluid and catalytic solid domain with *snappyHexMesh* results in hexahedra-dominated grids. Settings resulting in a base case mesh with roughly 4.8 million and 2.5 million cells for fluid and solid domain, respectively, were chosen with cell refinement and layer addition at surface boundaries. A grid-independence study following the procedure by [49] revealed a mesh related uncertainty of less than 1%. Details thereto can be found in Appendix 9.S.1 to this chapter. A planar cut through the mesh is shown in Figure 9.4 together with three details showing the mesh structure at the catalytic surface, the region between catalytic surface and adjacent wall introduced by the contact point handling and close to a touching point between two catalytic pellets.

The results of flow and reactant concentration obtained by the computational fluid dynamics simulation of the isothermal base case scenario are shown in Figure 9.5. As can be seen from the streamline plot in Figure 9.5a, the inert pre-bed imposes a near plug flow with higher maximum flow velocities than in the remaining flow domain. The meandering nature of the flow around the catalytic pellets in the single pellet string arrangement, as obtained in Chapter 7, is clearly recognisable. Reactant depletion along the reactor length axis due to the chemical reaction at the surface of the catalytic pellets is visible in the profile plot through the plane of catalytic pellet centre points as well as in the corresponding contour plot both shown in Figure 9.5b, where the contours are a distance of  $\Delta Y = 0.02$  apart. These figures also reveal a significant amount of back-mixing into the inert pre-bed.

Figure 9.6 compares the conversion along the reactor length axis based on area averaged values to ideal plug flow behaviour. In this plot, the position of the first two catalytic pellets

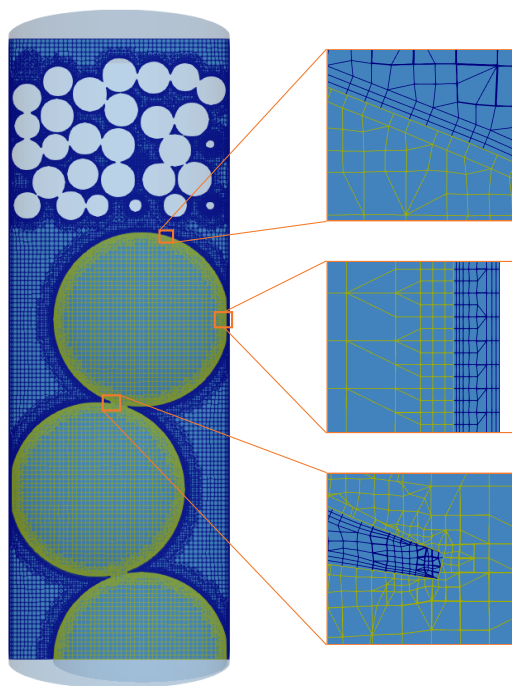


**Figure 9.4:** Space mesh for fluid and catalytic solid domain. Inserts show mesh details at solid-fluid interphase (top), between catalytic pellets and confining wall (centre) and close to contact point between adjacent catalytic pellets (bottom).

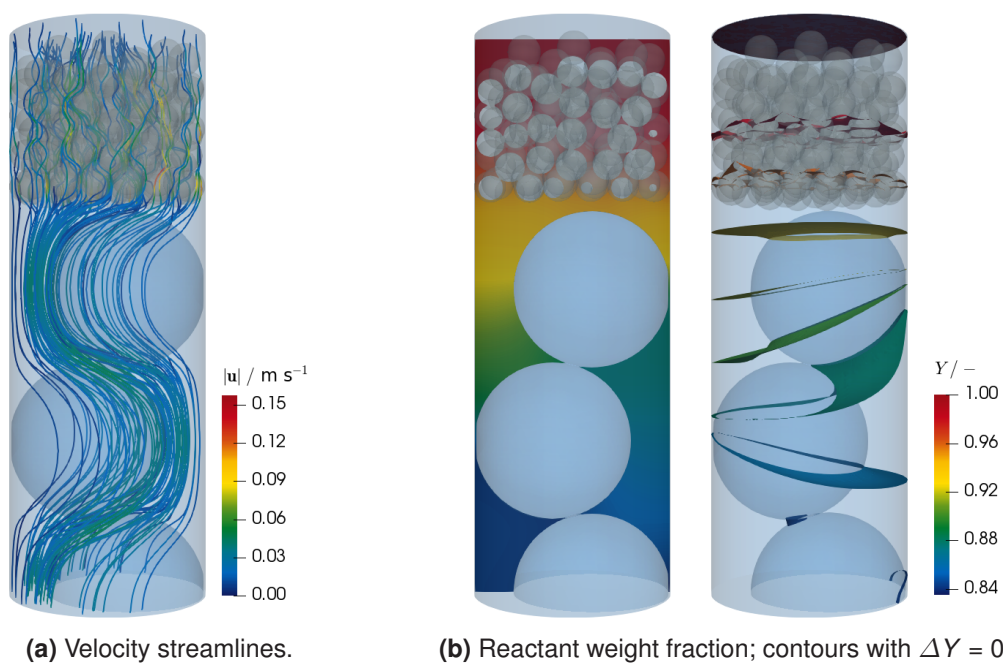


**Figure 9.5:** Visualisation of simulation results for base case isothermal SPSR.

is reflected by the form of the curve, as are the back-mixing into the inert pre-bed and the influence of the condition at the outflow boundary. The conversion values are above ideal plug flow at the beginning of the reactor, an observation that was attributed to back-mixing as a result of molecular diffusion in Chapter 7.

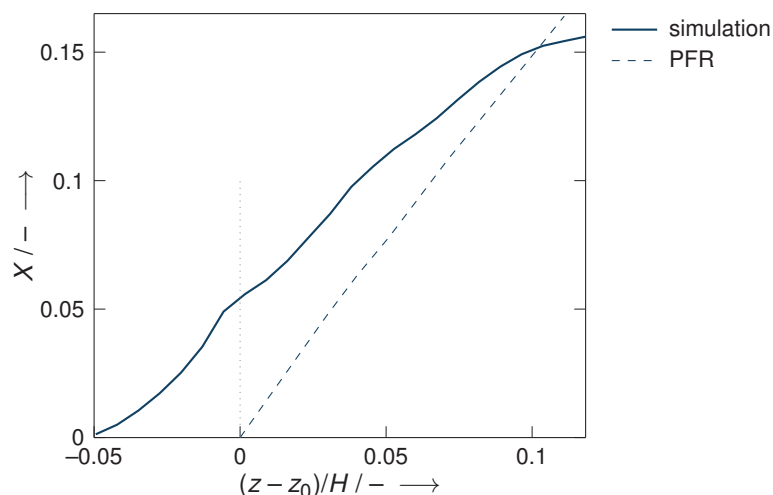


**Figure 9.6:** Conversion along the reactor length axis in base case isothermal SPSR.

### 9.5.1.2 Heat of reaction

A series of simulations is conducted considering an exothermic reaction at the surface of the catalytic pellets with increasing heat of reaction. Figure 9.7 reveals details on the conversion behaviour of a hypothetical first order, irreversible, heterogeneously catalysed gas phase reaction inside the single pellet string reactor by visualising isosurfaces representing the amount of reactant. It should be noted that the colour bars corresponding to the first four shown scenarios are the same. From the depicted results it can be seen that the reactant depletion, or the conversion, increases gradually with exothermicity until conversion is so strong that the reactant is consumed within a fraction of the reactor.

This observation correlates with the temperature profile in the reactor, as shown for the plane through the centre points of the catalytic pellets in Figure 9.8. As expected by definition, the isothermal case is linked to a constant temperature throughout the reactor (cf. 9.8a). Increasing the heat of the exothermic reaction results in heat release, as can be seen for the following scenarios. Although the colour bars have individual ranges, the qualitative course of the temperature distribution is similar for the scenarios with heats of reaction of  $\Delta H = -64 \text{ kJ mol}^{-1}$  and  $\Delta H = -128 \text{ kJ mol}^{-1}$ , where a narrow range of maximum temperatures is surrounding the catalytic surfaces throughout the reactor and declining temperatures towards the isothermal reactor wall. The region of maximum temperatures is reduced by further increasing the heat of reaction, eventually resulting in a locally restricted hot spot at the upstream side of the first catalytic pellet.



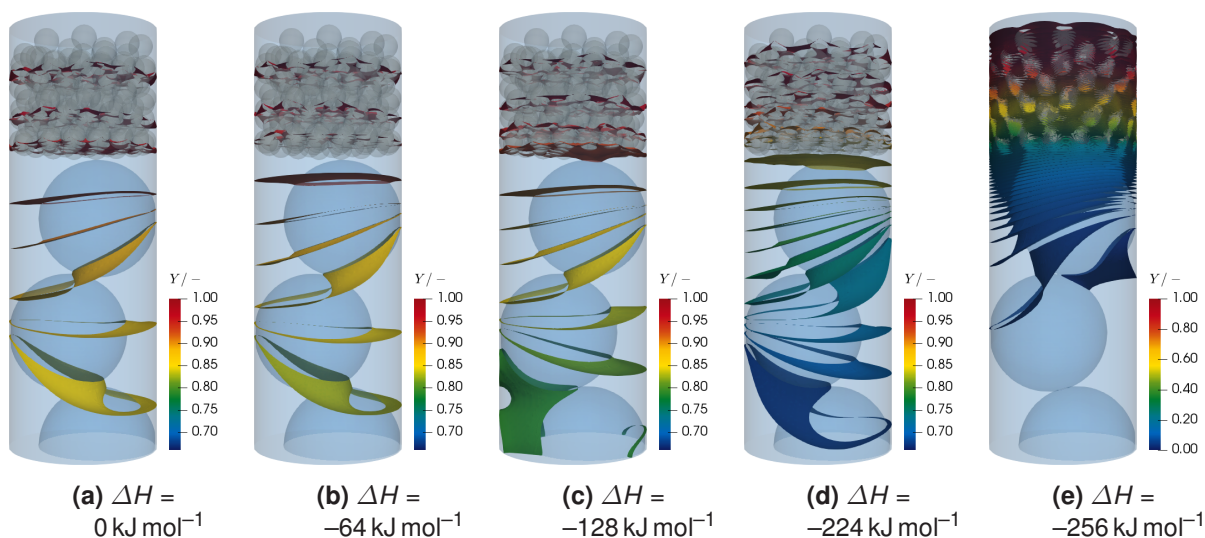


**Figure 9.7:** Reactant weight fraction in SPSR scenarios with varying heat of reaction, contours from  $Y = 0.99$  downwards in steps of  $\Delta Y = 0.02$ .

From these profiles, buoyancy effects do not appear to be a problem in reactor stability. The key issue for reactor operation is the need to get the heat away, so that the conversion and correspondingly regions of maximum temperature are spread along the catalytic surface more evenly rather than forming local hot spots. There is no mechanism by which the hot spot can be moved further down the reactor with the chosen set-up. Therefore, the temperature at the uppermost catalytic pellet is crucial for SPSR operation with exothermic surface reaction.

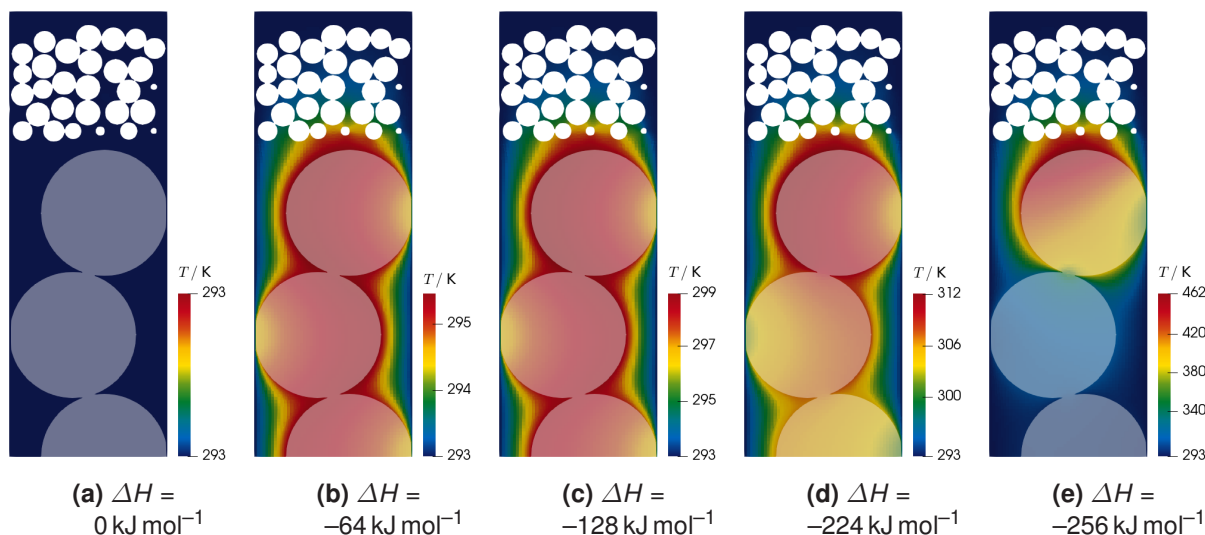


**Figure 9.8:** Temperature profiles in plane through centre points of catalytic pellets for varying heat of reaction.

A quantitative representation showing the influence of the heat of reaction on the maximum temperature along the reactor length axis is provided in Figure 9.9. As concluded from Figure 9.8, it is evident from Figure 9.9a that the maximum temperatures lie within a narrow range for low values of the heat of reaction. The two set-ups with heat of reaction of  $\Delta H =$

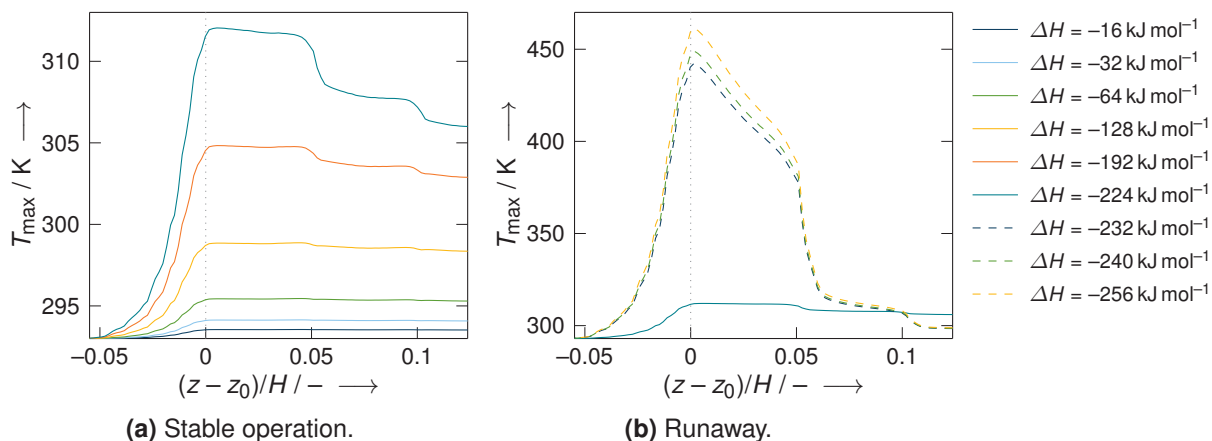


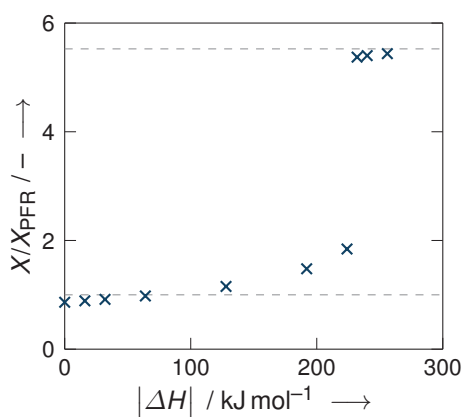
**Figure 9.9:** Parametric sensitivity of the maximum temperature in a SPSR along the reactor length axis with respect to the heat of reaction for a hypothetical first order, irreversible, heterogeneously catalysed gas phase reaction. Dotted line indicating top of catalytic bed.

$-16$   $\text{kJ mol}^{-1}$  and  $\Delta H = -32$   $\text{kJ mol}^{-1}$  reveal a near constant maximum temperature along the simulated part of the catalytic bed with values only slightly above the inlet temperature. Increasing the heat of reaction to  $\Delta H = -64$   $\text{kJ mol}^{-1}$  and  $\Delta H = -128$   $\text{kJ mol}^{-1}$  gradually adds more details to the profile, namely temperature plateaus corresponding to the individual catalytic pellets. Also, the maximum temperature surrounding the first catalytic pellet rises and a decreasing temperature is visible down the pellet string where the temperature decline is located around the touching points between the catalytic pellets. These trends are even more pronounced at higher values of the heat of reaction. However, temperature variations appear within the plateaus, especially for  $\Delta H = -224$   $\text{kJ mol}^{-1}$ . Further increasing the heat of reaction by as little as  $8$   $\text{kJ mol}^{-1}$  to  $\Delta H = -232$   $\text{kJ mol}^{-1}$  results in a very sensitive response with significant changes to the maximum temperatures within the reactor as illustrated by Figure 9.9b. First of all, the maximum temperature rises sharply and is located at the top of the uppermost catalytic pellet in the string. From there on, the temperature decreases rapidly already along this first catalytic pellet. A steep slope is visible between the first and the second catalytic pellet which brings the maximum temperatures down to values in the range of the SPSR exhibiting stable operation with  $\Delta H = -224$   $\text{kJ mol}^{-1}$ . In the vicinity of the third catalytic pellet the temperature is further decreased. At higher heats of reaction, the shape of the plot remains but with changes to the maximum temperature. The reactor sensitivity to changes in the heat of reaction is well summarised by the two plots in Figure 9.9, indicating moderate response of the maximum temperature up to a transition value above which the reactor behaviour changes tremendously.

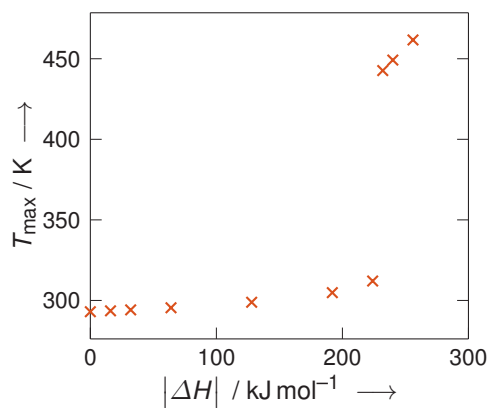
A common assumption found in literature is that the catalytic pellets are treated as internally isothermal [195, 198]. The results depicted in Figures 9.8b, 9.8c and 9.9a, corresponding to moderate exothermicity, where the SPSRs show a non-sensitive behaviour, reinforce this assumption. However, at higher heats of reaction leading to local hot spot formation and runaway this is no longer the case as illustrated especially by Figures 9.8d, 9.8e and 9.9b.

The observed changes to the reactor behaviour can be related to rate enhancement by temperature increases (cf. Arrhenius equation, Eq. (9.16)). Heat is released by the exothermic surface reaction, which in turn results in a higher reaction rate due to the increased temperature. This accelerates the reaction up to runaway at high values of the heat of reaction. The effects of variations to the heat of reaction on conversion and temperature throughout the reactor as visualised in Figures 9.7, 9.8 and 9.9 are summarised and extended by further data points in Figure 9.10. It is evident from Figure 9.10a that reactor conversion increases with exothermicity, where the dashed lines in the figure correspond to isothermal ideal plug flow conversion and full reactant depletion. Also, the data points reveal a jump in conversion at a certain heat of reaction, beyond which the reactant is consumed almost completely. This is accompanied by a similar shape of the maximum temperature in the reactor as a function of increasing exothermicity, shown in Figure 9.10b. The reactor outlet temperature, included in Figure 9.10c, follows the shape of the maximum temperature up to the sudden steep increase in maximum temperature and conversion before showing an abrupt decrease. This is in line with the hot spot formation at the first catalytic pellet, leaving only little reactant. Thus, the heat generation downstream of the first pellet stagnates and is overruled by the cooling effect of the confining walls which remain at fixed coolant temperature.

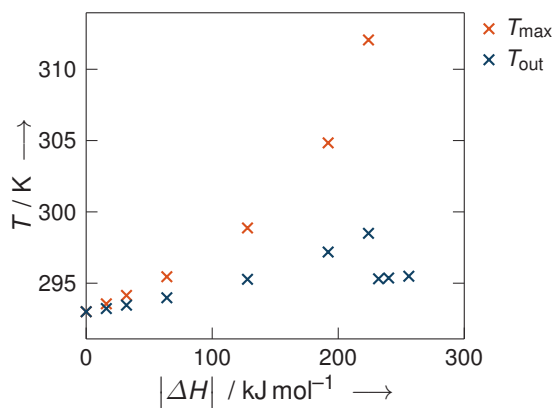
For an investigation of the influence of contact point handling on the simulated reactor behaviour the reader is referred to Appendix 9.S.2 at the end of this chapter.



(a) Normalised reactor outlet conversion; dashed lines indicating isothermal PFR conversion and full reactant depletion.



(b) Hot spot temperature.

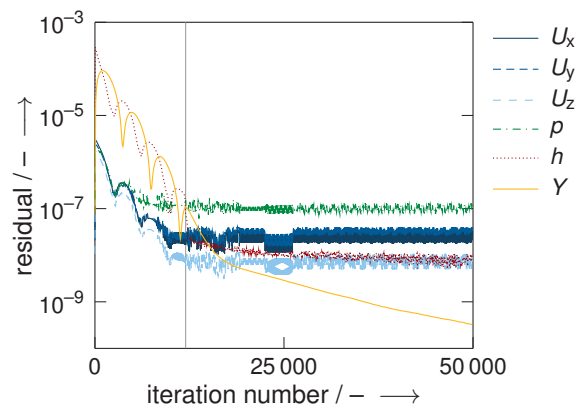


(c) Reactor outlet temperature.

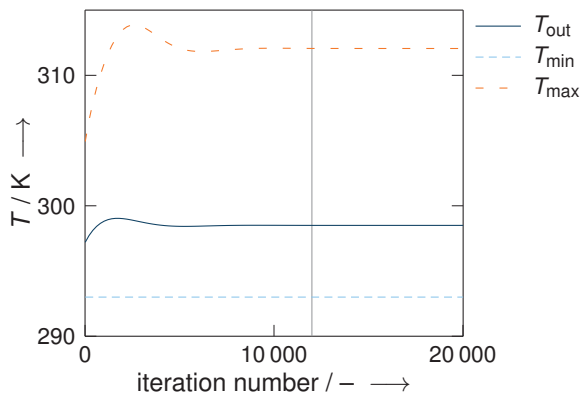
**Figure 9.10:** Influence of increasing heat of reaction for exothermic reactions on SPSR conversion and reactor temperatures.

## Convergence

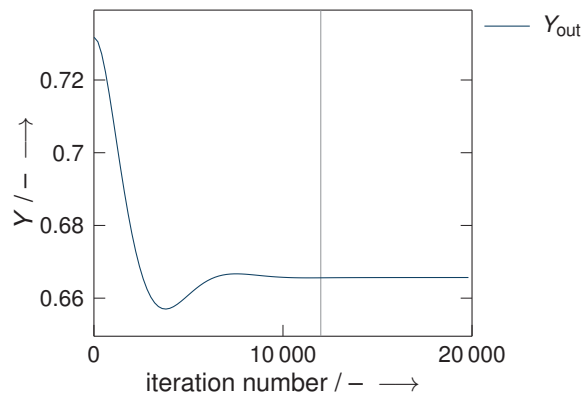
Before proceeding with the parameter study, a short discussion of convergence monitoring shall be included. Residuals of pressure, velocity, enthalpy and reactant weight fraction as well as the target quantities temperature and amount of reactant are tracked over the number of solver iterations. Figure 9.11 shows as an example the resulting curves for the scenario with a heat of reaction of  $\Delta H = -224 \text{ kJ mol}^{-1}$ . As illustrated by the residual plot in Figure 9.11a pressure converges first, followed by velocity, enthalpy and species. Inspection of the evolution of minimum and maximum reactor temperature as well as average outlet temperature with the number of iterations shown in Figure 9.11b reveals value overshoots for maximum and outlet temperature while the minimum temperature remains at the inlet and coolant temperature. In contrast, the evolution of the reactant weight fraction depicted in Figure 9.11c undershoots before levelling off after about 12 000 iterations. At this point, the monitored temperatures appear to have reached constant values and residuals of the shown variables in Figure 9.11a are all roughly below  $1 \cdot 10^{-7}$ . The simulation could have been stopped at this point. Other set-ups show similar convergence behaviour and simulations were stopped when target values levelled off and residuals were considerably small.



(a) Residual reduction pattern.



(b) Target value evolution - temperature.



(c) Target value evolution - reactant fraction.

**Figure 9.11:** Convergence monitoring for SPSR of the scenario *heat of reaction* with  $\Delta H = -224 \text{ kJ mol}^{-1}$ .

### 9.5.1.3 Height of inert pre-bed

Two cases are considered with a longer pre-bed height of twice the catalytic pellet diameter, one isothermal and the second exothermic with a heat of reaction of  $\Delta H = -224 \text{ kJ mol}^{-1}$ . The simulation results are presented in Figure 9.12 together with the data for SPSRs with a pre-bed of  $1d$  length as shown before in Figure 9.10a. The isothermal case shows a mildly increased conversion as compared to the base case pre-bed length. This could possibly be linked to more back-mixing into the longer pre-bed thus causing a higher conversion. On the other hand, the conversions of the exothermic case match for both set-ups with different pre-bed length. The conversion enhancing effect due to back-diffusion into the longer pre-bed seems to be opposed by some effect. Possibly, this may be attributed to the additional heat exchange enabled by a larger wall section surrounding the pre-bed which acts as a heat sink, lowering the temperature in the reactor and therefore also the conversion. However, the observed effect is marginal and appears to be rather negligible in the overall setting.

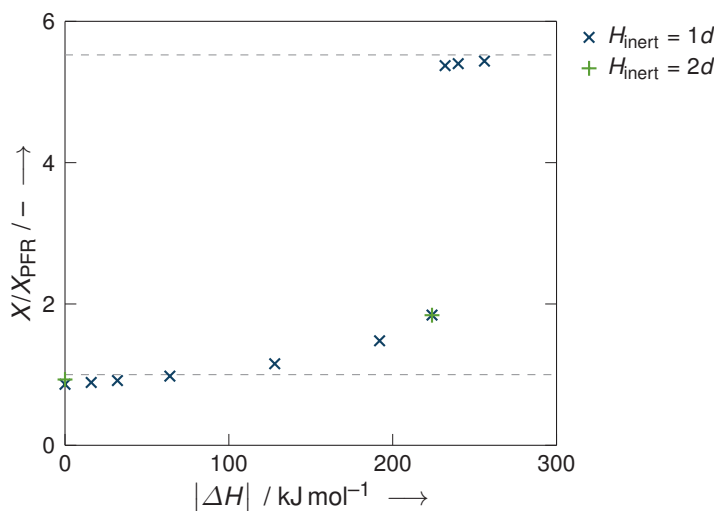


**Figure 9.12:** Influence of inert pre-bed height on SPSR conversion; dashed lines indicating isothermal PFR conversion and full reactant depletion.

### 9.5.1.4 Number of simulated pellets

Simulating the entire SPSR with a mesh refinement sufficient for capturing temperature and species gradient is not reasonable regarding simulation times. Also, from the preliminary considerations in Chapter 9.2 it should be sufficient to include only the upper part of the catalytic pellet string. This is verified by the reactor behaviour observed for varying heat of reaction (cf. Section 9.5.1.2), indicating that the temperature at the first catalytic pellet within the single pellet string arrangement is crucial for reactor operation. The question remaining is how far the number of considered catalytic pellets can be reduced without distorting the results by the influence of the outlet boundary condition. Therefore, simulations covering the first 1.5 and 3.5 catalytic pellets are performed with otherwise identical settings to the scenario with varying heat of reaction performed with 2.5 catalytic pellets.

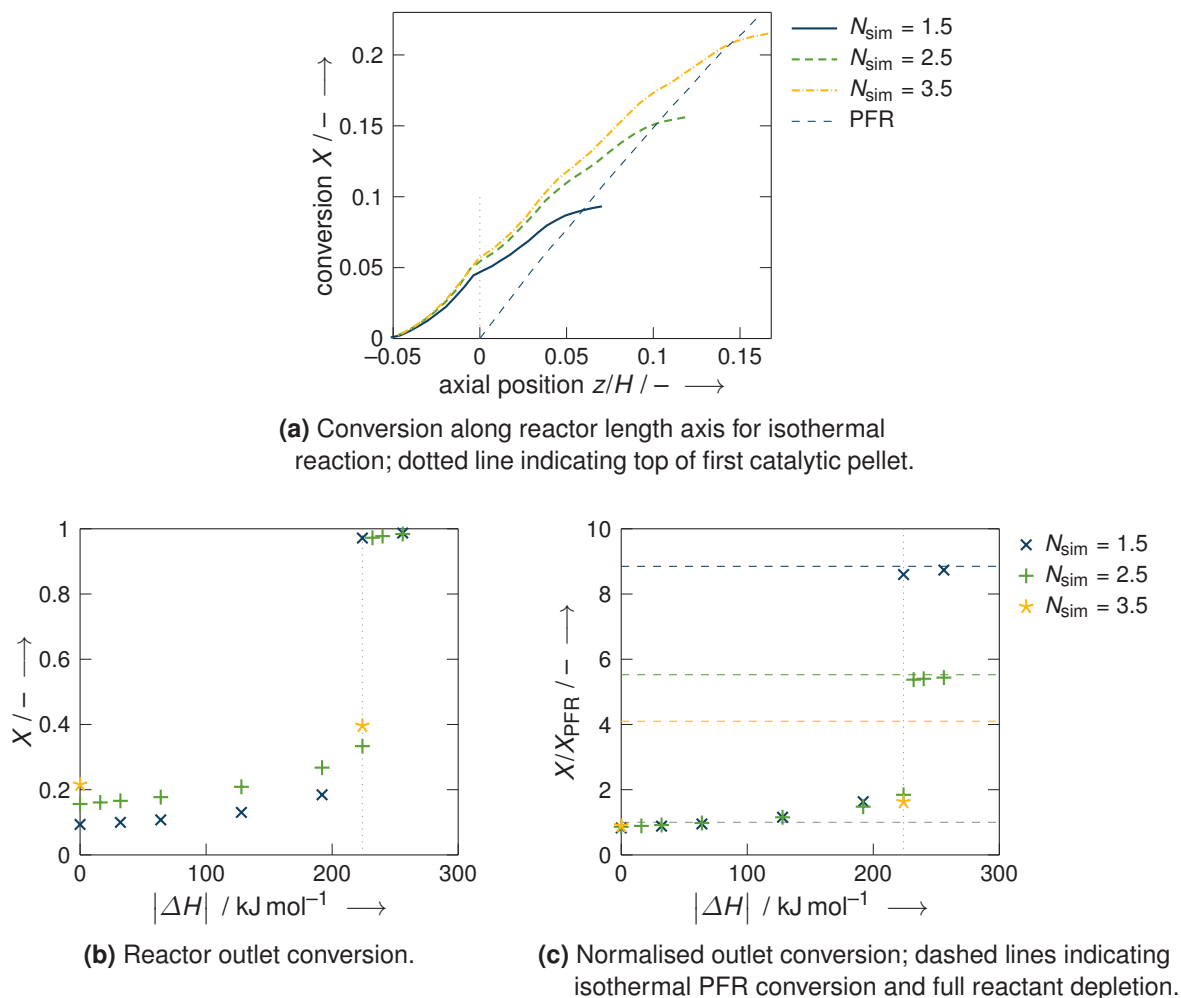


**Figure 9.13:** Influence of number of catalytic pellets considered for simulation domain on SPSR conversion.

Comparison of the conversion along the reactor length axis for an isothermal surface reaction with ideal plug flow is displayed in Figure 9.13a for all three considered simulation domains, with 1.5, 2.5 and 3.5 catalytic pellets. It is apparent from the curves that covering more catalytic pellets within the simulation domain leads to a longer reactor, which is reflected by the presence of conversion values for higher axial positions when considering more catalytic pellets. Also, the conversion at the reactor outlet is higher with increasing number of simulated pellets as the outlet is shifted further down the string of catalytic pellets. Comparing the conversion in the vicinity of the first catalytic pellet for simulation domains spanning over 2.5 and 3.5 catalytic pellets reveals similar behaviour, though the curve is slightly lower for the case with 2.5 pellets. Reducing the simulation domain to 1.5 catalytic pellets leads to a significant reduction in conversion, but still maintaining the general shape of the conversion curve.

However, we are more interested in the nonisothermal reactor behaviour. The parameter study on the influence of the heat of reaction as presented in Section 9.5.1.2 is repeated for a number of cases with 1.5 pellets. Of course, the conversion at the reactor outlet is reduced



when considering fewer catalytic pellets, visible in a vertical shift to lower conversion values in Figure 9.13b, though the general trend is preserved with a gradual increase of conversion with exothermicity and a jump once a hot spot is formed. The thermal runaway happens at lower heats of reaction when considering fewer pellets. Two cases with 3.5 simulated catalytic pellets are performed, the isothermal case and an exothermic case with a heat of reaction of  $\Delta H = -224 \text{ kJ mol}^{-1}$ , where there appears to be a difference in the results for fewer simulated pellets. As expected and already seen from Figure 9.13a, conversion in the isothermal case is higher than for the two corresponding cases with fewer simulated pellets. The conversion in the exothermic case, at a heat of reaction where runaway already occurred for the set-up with 1.5 but not with 2.5 catalytic pellets, indicates stable reactor operation.

Recapitulating previous findings on hot spot formation and reactor runaway, it should be emphasised that only the first catalytic pellet in the string is crucial, where the reactant is already consumed near to completion. Any additionally simulated pellet does not contribute significantly to reactor conversion, but increases the confining wall section available for reactor cooling. Therefore, runaway is shifted to higher heats of reaction when considering more catalytic pellets in the simulation domain.

Figure 9.13c shows the conversion at the outlet normalised with the conversion in a corresponding isothermal plug flow reactor. The dashed lines indicating full reactant depletion are adjusted according to the number of simulated catalytic pellets and the corresponding ideal plug flow conversion values (cf. Figure 9.13a).

Although the influence of the outlet boundary condition on the first catalytic pellet in the single pellet string arrangement vanishes for 2.5 and more simulated pellets, it appears to be sufficient to use 1.5 pellets only for a general investigation of heat effects in SPSRs. This represents a reasonable worst case scenario with least wall surface available for reactor cooling.

#### 9.5.1.5 Activation energy

The influence of activation energy on the conversion behaviour of single pellet string reactors with varying heat of reaction is investigated with set-ups covering 1.5 catalytic pellets only, as discussed previously. The results presented in Figure 9.14 reveal that thermal runaway is shifted to lower heats of reaction with increasing activation energy. Remarkably, the data points can be shifted to a common curve by scaling the heat of reaction values plotted on the abscissa with the activation energy as presented in Figure 9.14b.

This compares well with literature contributions on the influence of the activation energy on reactor sensitivity. Based on calculations on empty tubular reactors, already Bilous and Amundson [183] concluded that the reactor sensitivity was more pronounced when doubling the activation energy. Also, simulations by Balakotaiah et al. [198] showed an increased

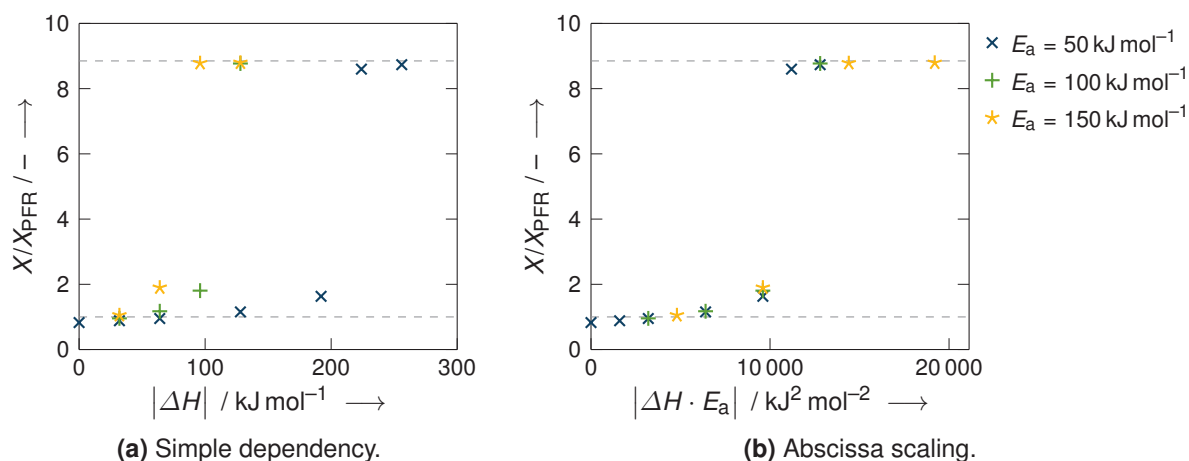


**Figure 9.14:** Influence of activation energy and heat of reaction on conversion behaviour in SPSRs; dashed lines indicating isothermal PFR conversion and full reactant depletion.

tendency of a catalytic reactor to runaway at higher activation energy. An increased sensitivity to temperature variations was observed by Quina and Ferreira [199] for a side reaction to the methanol oxidation to formaldehyde, namely the subsequent product oxidation, which they attributed to the higher activation energy of this reaction.

### 9.5.1.6 Reactor scale

Figure 9.15 provides simulation results for SPSR scenarios with varying reactor scale obtained by increasing the reactor geometry by factors of 1.5 and 2.0 and adjusting inlet velocity and reaction rate coefficient accordingly. It can be seen that thermal runaway occurs at lower heats of reaction with increasing reactor scale. A correlation between normalised reactor outlet conversion and heat of reaction times pellet diameter squared as displayed in Figure 9.15 appears to bring the simulations on to a common line.

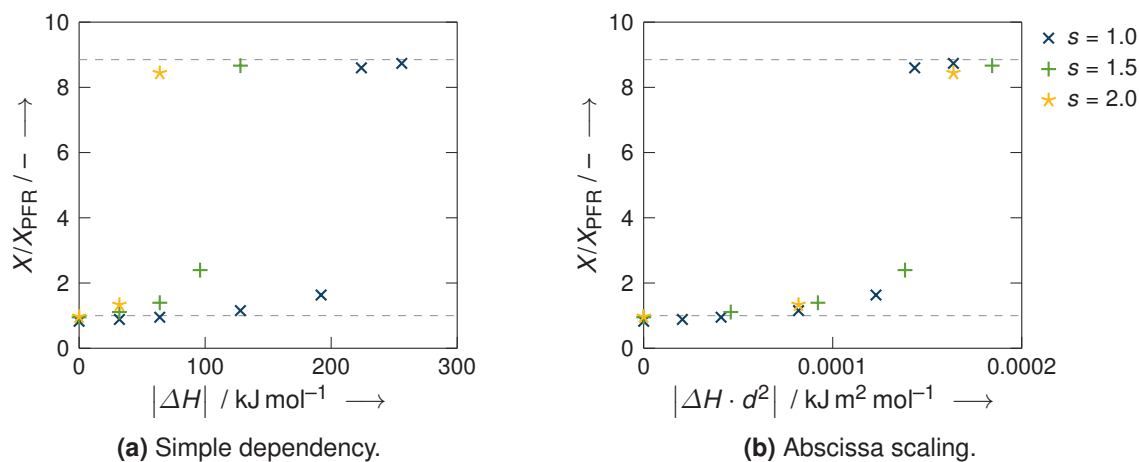


**Figure 9.15:** Influence of reactor scale and heat of reaction on conversion behaviour in SPSRs; dashed lines indicating isothermal PFR conversion and full reactant depletion.

### 9.5.1.7 Number of catalytic pellets

The number of catalytic pellets in the SPSR has direct influence on the inlet velocity and the reaction rate constant. It should be noted that only the uppermost 1.5 catalytic pellets in the single pellet string arrangement are covered by the simulation domain. The results illustrated in Figure 9.16 for isothermal reactor operation are consistent with the outcomes of Chapter 7, with conversion values approaching ideal plug flow behaviour with increasing number of pellets. Investigations with an exothermic surface reaction with a heat of reaction of  $\Delta H = -64 \text{ kJ mol}^{-1}$  reveal enhanced conversion values as compared to the isothermal case, maintaining the general trend of approaching an asymptotic conversion value for set-ups with numerous catalytic pellets.

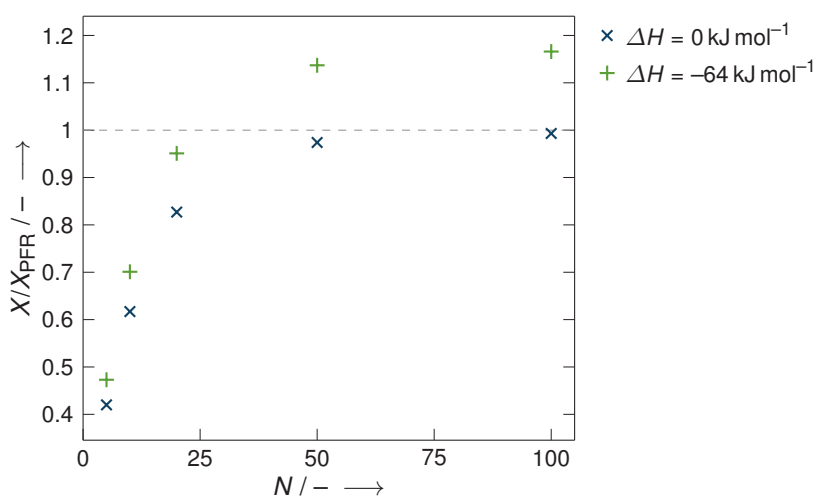


**Figure 9.16:** Influence of number of catalytic pellets in SPSR arrangement on conversion behaviour in SPSRs; dashed line indicating isothermal PFR conversion.

### 9.5.1.8 Notional gas pressure

Doubling the notional gas pressure within the SPSR set-up causes roughly a density doubling, increasing the amount of reactant available in the system. As a consequence, more reactant can be consumed, thus increasing the heat generated by the exothermic reaction. This is in line with the simulation results shown in Figure 9.17a for varying heat of reaction at two outlet pressures where the runaway is shifted to lower heats of reaction at higher pressure. This is in line with the observation by Maria and Stefan [193] of a sharply rising hot spot at increased reactor inlet pressure based on numerical simulations for determining the operational safety limits for nitrobenzene hydrogenation in fixed-bed reactors.

Another common line can be obtained when plotting conversion against the product of heat of reaction and outlet pressure as can be seen from Figure 9.17b.

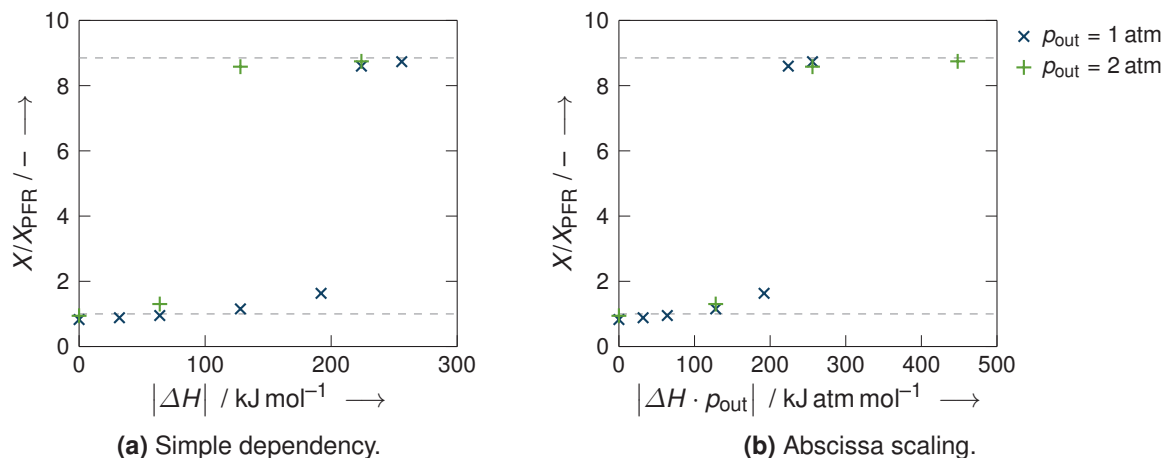


**Figure 9.17:** Influence of notional gas pressure on conversion behaviour in SPSRs; dashed lines indicating isothermal PFR conversion and full reactant depletion.

### 9.5.1.9 Reactor conversion

The variation in reactor conversion refers to the conversion used to specify the isothermal reaction rate coefficient  $k(T_0)$  based on ideal plug flow behaviour. Therefore, changes to the reactor conversion are directly related to the reaction rate. For isothermal set-ups, this may eventually lead to local reactant depletion close to the catalytic surface, the result of which is a reduced overall conversion. A gradual increase of this mass transfer effect with increasing reaction rate coefficient can be seen in Figure 9.18 based on the overall conversion as observed after the first 1.5 catalytic pellets. The conversion behaviour in the isothermal case is therefore closer to ideal plug flow at lower values of the reaction rate coefficient. On the contrary, higher reaction rates cause an enhanced heat release in case of exothermic reactions which accelerates the reaction and therefore increases the overall conversion. The conversion reduction due to mass transfer effects is overruled by

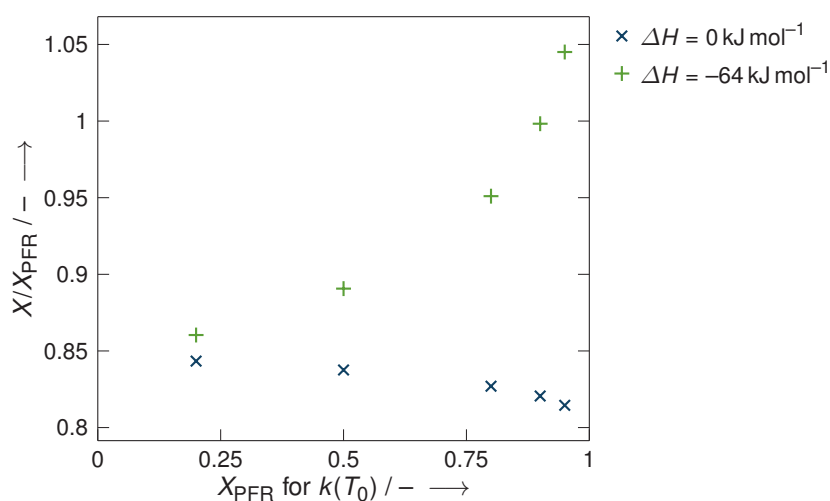


**Figure 9.18:** Influence of conversion used for determination of reaction rate coefficient on conversion behaviour in SPSRs.

the reaction enhancement as a result of temperature increase originating from the heat of reaction.

#### 9.5.1.10 Heat capacity

Heat removal in the considered SPSR set-up is achieved by heat exchange with the reactor wall which has a constant temperature and by convection with the reaction medium. The latter is affected by the heat capacity of the fluid. Simulations with varying fluid heat capacity, which is assumed independent of temperature, show the expected increase in conversion with decreasing heat capacity as can be seen from Figure 9.19 for set-ups considering an exothermic reaction with  $\Delta H = -64 \text{ kJ mol}^{-1}$ . At very low heat capacities, thermal runaway can be observed as a result of insufficient heat removal.

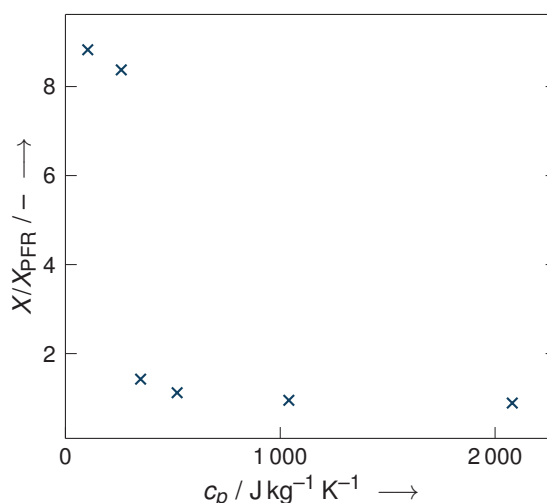


**Figure 9.19:** Influence of fluid heat capacity on conversion behaviour in SPSRs;  $\Delta H = -64 \text{ kJ mol}^{-1}$ .

#### 9.5.1.11 Thermal conductivity

The temperature profiles in Figure 9.8 indicated only limited temperature variation in the catalytic pellets for SPSRs in stable operation and steep temperature gradients when hot spot formation occurred. According to Figure 9.20 variations to the thermal conductivity of the catalytic pellets for an exothermic reaction with  $\Delta H = -64 \text{ kJ mol}^{-1}$  show an increase in conversion with decreasing thermal conductivity. This is in line with Balakotaiah et al. [198] who concluded that a higher interparticle heat transfer resistance, i.e. a lower thermal conductivity, increases the tendency of a catalytic reactor to runaway.

A thermal runaway situation could not be obtained with the chosen heat of reaction, but is likely to happen at higher heats of reaction and possibly also at lower thermal conductivities. However, simulations with lower values of the thermal conductivity were not feasible with the used simulation settings and may require further mesh refinement to capture steeper temperature gradients within the pellets.

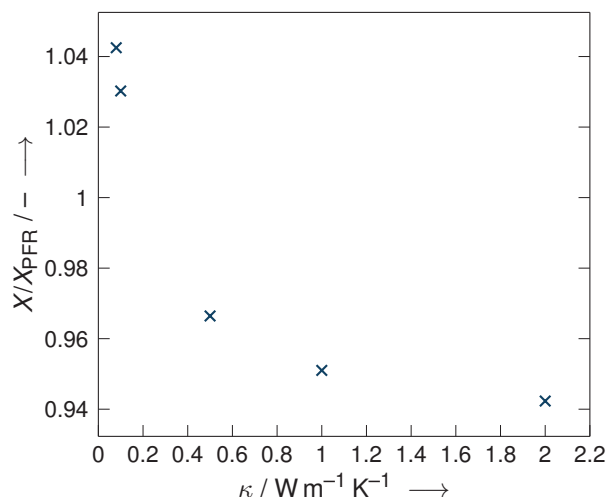


**Figure 9.20:** Influence of thermal conductivity within catalytic pellets on conversion behaviour in SPSRs;  $\Delta H = -64 \text{ kJ mol}^{-1}$ .

A closer look on the temperature profiles inside the reactor as detailed in Figure 9.21 reveals a more heterogeneous nature of the temperature field for low thermal conductivity of the catalytic pellets. On one hand, lower temperatures can be observed in the catalytic pellets at the wall touching side and on the other hand higher temperature increased maximum temperatures at the top of the first catalytic pellet and around the touching point of first and second catalytic pellet. The temperature maximum at the top may be attributed to a high reaction rate with maximum reactant concentration whereas at the touching point heat removal by convection with the fluid may be limiting for heat removal. Contrary, an increase in thermal conductivity of the catalytic pellet flattens the temperature gradient inside the pellet, spreading the heat generated by the exothermic reaction by thermal conductivity. This lowers the maximum temperature at the pellet surface which results in a reduced overall conversion.

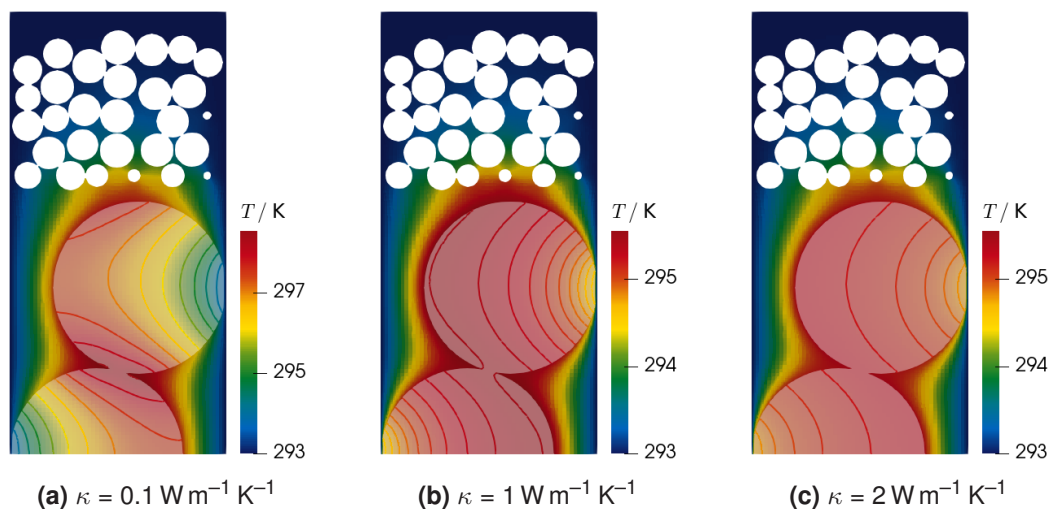


**Figure 9.21:** Temperature profiles in plane through centre points of catalytic pellet for varying thermal conductivity of the catalytic pellets;  $\Delta H = -64 \text{ kJ mol}^{-1}$ .

In light of these results, neglecting the thermal conductivity within the pellets of the inert pre-bed by only considering those as holes in the fluid domain poses a worst case scenario. Including the inert particles as own solid domain in the simulation should result in a spread of the heat generated by the exothermic reaction further into the pre-bed. This would increase the driving force for heat removal through the wall section surrounding the inert bed due to higher temperature gradients which in turn should lower the average temperature in the simulation domain and thereby reduce the overall conversion.

### 9.5.1.12 Diffusion coefficient

So far, the molecular diffusion coefficient within the fluid was treated as temperature independent. This assumption is dropped in this scenario, considering a temperature dependency of the diffusion coefficient following a power law as specified in Eq. (9.14). The data in Figure 9.22 justifies this assumption for SPSRs in stable operation, that is with no thermal runaway. In these cases, temperature variations within the reactor are small and the influence on the diffusion coefficient marginal. When it comes to thermal runaway, temperature ranges are significantly larger and the influence of the diffusion coefficient's temperature dependency on conversion clearly visible. The jump in conversion takes off at a similar heat of reaction but with a smoother gradient.

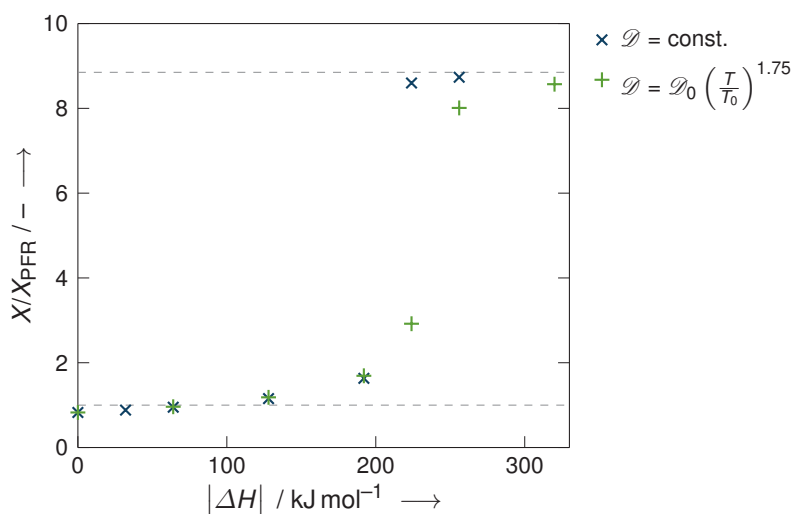


**Figure 9.22:** Influence of temperature dependency of the molecular diffusion coefficient on conversion behaviour in SPSRs for varying heats of reaction; dashed lines indicating isothermal PFR conversion and full reactant depletion.

### 9.5.1.13 Dynamic viscosity

The simplification of specifying a temperature independent dynamic viscosity in the remainder of the presented parameter study is dropped in this scenario, where the dynamic viscosity is expressed by Sutherland's formula (cf. Eq. (9.12)). It should be noted that the results presented in Figure 9.23 are obtained by simulations with 2.5 simulated pellets.

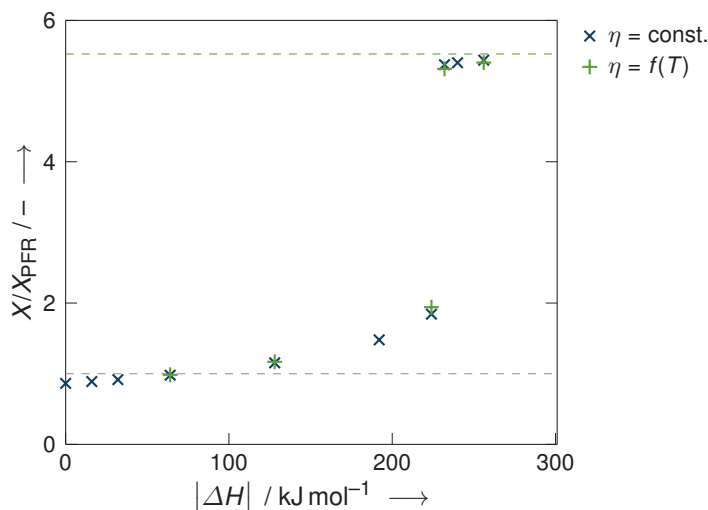


**Figure 9.23:** Influence of temperature dependency of the dynamic viscosity on conversion behaviour in SPSRs for varying heats of reaction; dashed lines indicating isothermal PFR conversion and full reactant depletion.

As can be concluded from Figure 9.23, considering a temperature dependent fluid viscosity has no significant influence on the conversion behaviour for a hypothetical first-order heterogeneously catalysed gas phase reaction. The conversion values in the stable operating reaction are of similar value compared to simulations with a constant dynamic viscosity. Also, the sudden jump in conversion values, related to reactor runaway, appears at comparable heat of reaction values. At higher exothermicity, the conversion values are again similar to the results with constant dynamic viscosity. Therefore, the initial assumption of considering a temperature independent dynamic viscosity for the fluid flowing through the single pellet string reactor is validated.



### 9.5.2 Adaptation of Benneker criterion

Thermal effects in real reacting systems are known to give rise to buoyancy effects, which may have significant influence on the flow behaviour through macroscopic fixed bed reactors. Benneker, Kronberg and Westerterp [206] investigated the influence of buoyancy effects induced by density gradients on axial mixing in gas flows through packed beds by means of displacement experiments. They observed an enhancement of axial dispersion due to secondary flows originating from free convection, which was more severe with increasing pellet and bed diameter. It should be noted that the experiments were carried out with a non-reactive system at elevated pressure in beds with diameter aspect ratios of  $3.68 \leq D/d \leq 22.7$  and Reynolds numbers  $5 \leq Re \leq 300$ , where density gradients were induced by step changes to the feed gas composition.

Based on their experimental data, Benneker et al. [206, 213] established a correlation between enhanced mixing in axial direction, expressed as ratio of Bodenstein numbers, and a dimensionless expression describing the stability of the flow of the following form:

$$\frac{Bo_0}{Bo} = f \left( \frac{Gr}{\frac{600}{Sc} + Re^2} \right). \quad (9.31)$$

The dimensionless numbers Bodenstein  $Bo$ , Grashof  $Gr$ , Schmidt  $Sc$  and Reynolds  $Re$  are defined as

$$Bo = \frac{u_0 d}{\bar{\varepsilon} D_{ax}} \quad Gr = \frac{\Delta\rho g d^2 D^2}{\rho_0 H \nu^2} \quad Sc = \frac{\nu}{\mathcal{D}} \quad Re = \frac{u_0 d}{\nu}, \quad (9.32)$$

where  $u_0$  is the superficial fluid velocity,  $d$  the pellet diameter,  $\bar{\varepsilon}$  the mean bed voidage,  $D_{ax}$  the axial dispersion coefficient,  $\Delta\rho$  the density gradient,  $\rho$  a reference density,  $g$  the gravitational constant,  $D$  the bed diameter,  $H$  the height of the packing,  $\nu$  the kinematic viscosity and  $\mathcal{D}$  the molecular diffusion coefficient.

Figure 9.24 is taken from the publication by Benneker et al. [206] to visualise their correlation. The empirical constant of 600 in Equation (9.31) acts as a weighting factor of the two stabilising effects opposing free convection at different flow conditions. In the laminar flow regime, the secondary flows resulting from free convection due to density gradients in the fluid are opposed by mixing on the basis of molecular diffusion and the above correlation reduces to

$$\frac{Bo_0}{Bo} = f(Gr Sc) = f \left( \frac{\Delta\rho g d^2 D^2}{\rho H \nu \mathcal{D}} \right). \quad (9.33)$$

It can be seen from the equation above that there is little one can do to suppress density induced free convection. Also, the enhancement of the effect at larger scale becomes easily accessible.

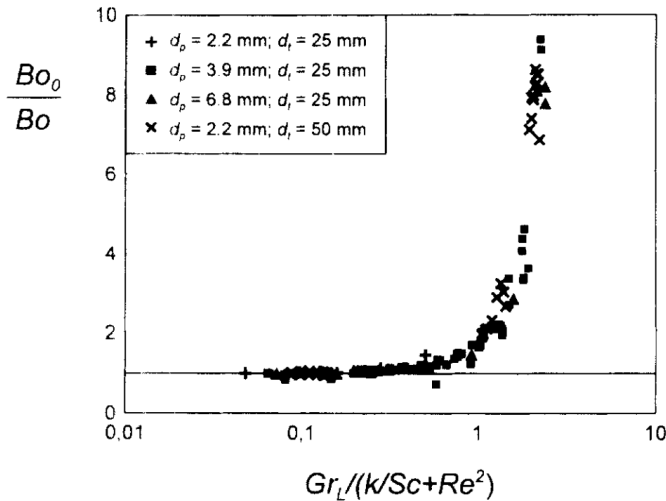


**Figure 9.24:** Enhancement of axial mixing as a result of buoyancy effects; plot taken from Benneker et al. [206],  $k = 600$ .

At larger flow velocities, the free convection is opposed by the forced convection of the flow through the bed and the correlation reduces to

$$\frac{Bo_0}{Bo} = f\left(\frac{Gr}{Re^2}\right) = f\left(\frac{\Delta\rho g D^2}{\rho H u_0^2}\right). \quad (9.34)$$

The pellet diameter has no longer an influence and increasing the flow velocity helps stabilising the system, thus reducing axial dispersion due to secondary flows.

The simulation results obtained for the various SPSR scenarios considered in this study do not reveal secondary flows as a result of density induced free convection within the reactor. However, an influence of increasing temperature on reaction stability could be observed, ultimately leading to thermal runaway. Still, parallels can be drawn between the Benneker criterion on the enhancement of axial dispersion and the observed conversion behaviour of exothermic reactions in SPSRs. Basically, both effects are mainly driven by temperature. Therefore, the question is how to get the heat away. At high Reynolds number flow, which tends to dominate at industrial scale, heat removal is enhanced with increasing flow rate. On the other hand, there is little one can do except external cooling at low gas flow rates.

In a first attempt to correlate the obtained data, the conversion results are plotted against the dimensionless expression proposed by Benneker et al. [206] as displayed in Figure 9.25a. Unlike in the original plot, conversion values are plotted on the ordinate rather than a ratio of Bodenstein numbers representing the enhancement of axial dispersion and resulting values on the abscissa are several orders of magnitude lower. Despite this, a similar trend is observed for the data points with a near constant value gradually increasing up to a point where the curve shows a steep slope. This is more pronounced when normalising the ordinate axis with the corresponding ideal plug flow conversion as depicted in Figure 9.25b. Both plots clearly reveal a region where stable reactor operation is possible before runaway

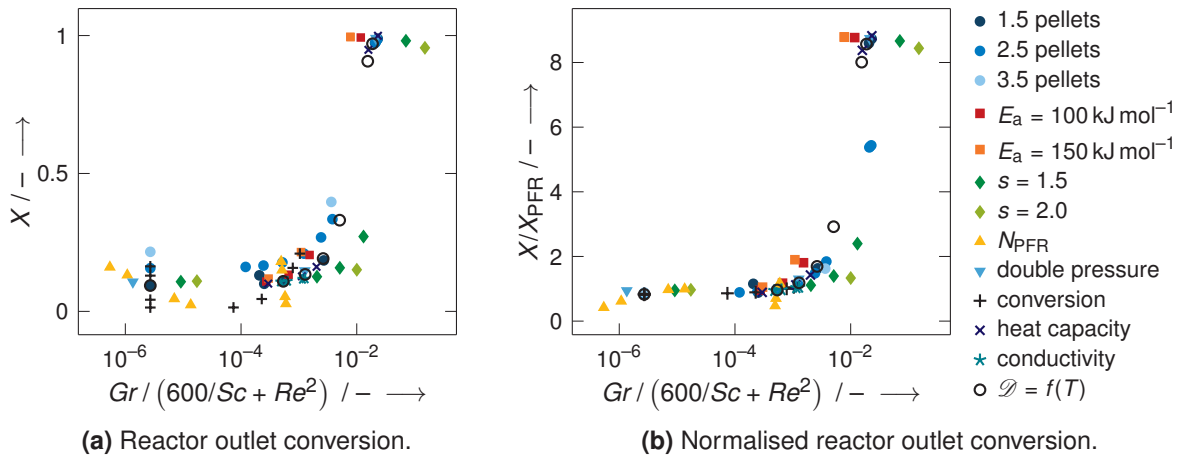


**Figure 9.25:** Adaptation of Benneker criterion to conversion of exothermic reactions in SPSRs.

occurs. However, this plot is of limited practical use because the values required for the dimensionless expression are not all known a priori.

### 9.5.3 Criterion on thermal runaway

In a second attempt, the data are correlated only with previously known parameters. The effect of the various parameters included in this study on conversion and ultimately on thermal runaway were presented in detail earlier in this chapter. To summarise, whether a SPSR with exothermic reaction will remain stable is entirely related to heat of reaction and its removal. Most influential parameters which accelerate thermal runaway are first of all the heat of reaction, activation energy and geometry scale. Also, conversion increases with the reaction rate coefficient, determined here by a set conversion of a corresponding ideal plug flow reactor. An increase in the heat capacity of the fluid and, though less pronounced, in thermal conductivity of the catalytic pellet enhance heat removal and thus counteract the heat released by the exothermic surface reaction.

Figure 9.26 presents the conversion, which is essentially a surrogate of the Bodenstein number used by Benneker, against an abscissa which has been constructed from the results of the parameter study presented in Section 9.5.1 and draws all of the simulations into a single curve. It shows that for values of the abscissa below five, the conversion after the first few simulated catalytic pellets is relatively low and therefore not affected by thermal runaway; for values above five, thermal runaway rapidly becomes dominant. Thus the value of this abscissa can be used as a criterion to estimate the onset of thermal runaway based on a priori known parameters, assuming negligible changes in fluid heat capacity and solid thermal conductivity with temperature, and hence be used as a design and operation constraint where stable operation is attributed to a threshold value of

$$\Delta H \cdot E_a \cdot d^2 \cdot X_{PFR,k} \cdot c_p^{-1} \cdot \kappa^{-0.4} < 5 \text{ m}^{3.6} \text{ kg}^{1.6} \text{ s}^{-0.8} \text{ K}^{1.4} \text{ mol}^{-2}. \quad (9.35)$$

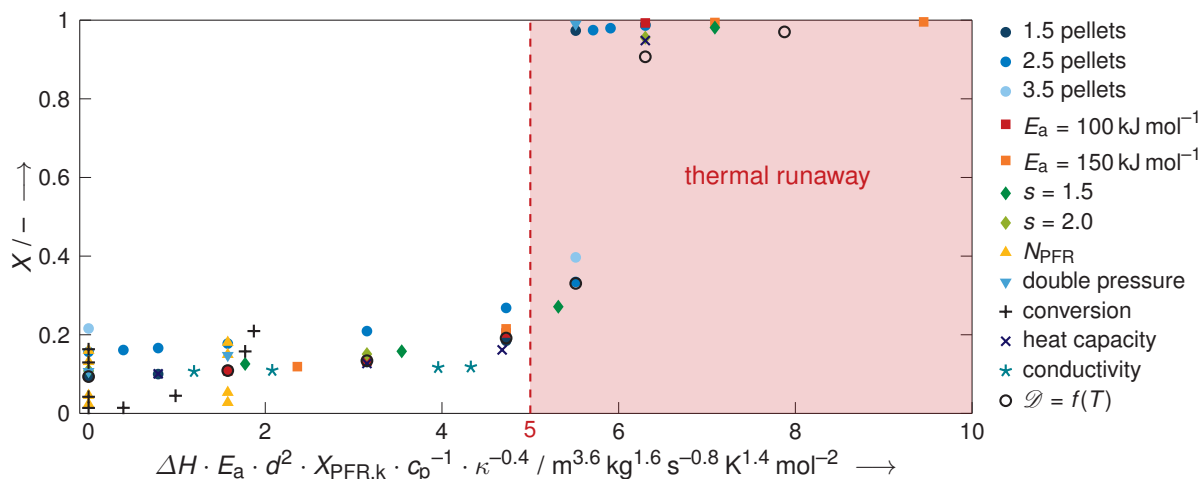


**Figure 9.26:** Distinction between stable reactor operation and thermal runaway for exothermic reactions in SPSRs based on reaction parameters, pellet diameter and material properties.

The absolute conversion values in Figure 9.26 are of limited significance. They solely refer to the conversion at the reactor outlet which ranges between 1.5 and 3.5 pellets into the catalytic bed within the presented data set. Nonetheless, in the considered SPSR set-up with cooling at a fixed wall temperature everything depends on the conversion on the first catalytic pellet in the bed. Here, maximum reactant is available and temperature does not increase down the bed. If conversion at this stage of the bed is moderate, the whole reactor region downstream will not be subject to thermal runaway either.

Diluting the feed with an inert is not considered within this study but is expected to shift the threshold towards higher values.

## 9.6 Summary and conclusion

In this chapter on single pellet string reactors the numerical investigation of specially arranged spherical pellets in cylindrical confining walls was extended to nonisothermal scenarios including the impact of thermal effects. An exothermic surface reaction was chosen to act as heat source whereas the surrounding cylindrical wall was set to a constant cooling temperature. Our expectation to encounter deviations to plug flow behaviour induced by buoyancy effects, such as those reported by Benneker et al. [206] in packed beds with larger diameter aspect ratio and at elevated pressure, was not met. Rather, the results revealed that plug flow like behaviour was seriously undermined only when thermal runaway occurred. This happened to be the case when the exothermicity of the considered surface reaction was of such magnitude as to create a local hot spot at the first catalytic pellet in the single pellet string arrangement, accelerating the reaction and causing the reactant to be consumed near to completion. Hot spot formation further down the reactor could not be observed, which is in line with setting a fixed cooling temperature at the reactor wall.

By this means no heat accumulation leading to reaction enhancement is accessible in the remaining bed.

Therefore, the first pellet in the catalytic single pellet string is the key determinant of the reactor's behaviour. If the conditions on the first pellet do not lead to a local hot spot and thermal runaway of the reaction, the remaining pellets downstream along the string will be fine. Besides variations to the heat of reaction, a parameter study aiming at characterising the conversion behaviour of exothermal reactions in single pellet string reactors was conducted. This revealed a region where stable reactor operation was possible based on heat of reaction, activation energy, reactor scale, corresponding plug flow conversion, fluid heat capacity and thermal conductivity of the catalyst material – all a priori known values if one assumes temperature independence of the latter two properties. Variations of the height of the inert bed and of the number of simulated pellets as well as considering the temperature dependence of the diffusion coefficient showed only minor influence.

Analysing the results disclosed a sharp threshold between near plug flow behaviour, albeit with some axial dispersion<sup>1</sup>, and thermal runaway occurring in the vicinity of the first catalytic pellet in the string. This was seen both in a Benneker-like criterion and a newly proposed criterion, which allows prediction of when thermal runaway will occur based only on a priori known values.

Including thermal effects not only in the fluid domain but also within the catalytic pellets required special attention to handling the contact points between pellets and the surrounding wall. While relying on the common approach of assuming bridges at contact points between catalytic pellets, this led to suspiciously steep temperature gradients when applied to pellet-to-wall contacts with unrealistically high temperature ranges across the pellet. Therefore, gaps were introduced at catalytic pellet-to-wall contacts which poses a worst case considering the reduced tolerance of the reactor set-up towards the amount of heat generated by the reaction before thermal runaway.

Future work may focus on a possibility to further push the stability limit, possibly by considering the first pellet in the single pellet string to be inert and only from the second onwards catalytic. Also, the influence of pellet shape on deviation to ideal plug flow is of interest as well as trickle-bed operation.

---

<sup>1</sup> Please refer to Chapter 7 for further details on dispersion in SPSRs.

## 9.S Supporting information

### 9.S.1 Grid-independence study

The uncertainty due to the spacial discretisation of the computational domain was estimated following the procedure proposed by the Fluids Engineering Division of ASME [49].

Two scenarios were considered for analysing the influence of the mesh refinement, the isothermal base case and the case with  $\Delta H = -64 \text{ kJ mol}^{-1}$  from the scenario of varying heat of reaction. Given the isothermal particle assumption in the first case, only the mesh grading of the fluid domain was refined respectively coarsened whereas the mesh grading was varied for both fluid and solid domain in the second case. The corresponding mesh details as well as the calculations of the error estimates according to Celik et al. [49] are summarised in Table 9.2.

**Table 9.2:** Mesh details and discretisation error calculations.

	isothermal base case	$\Delta H = -64 \text{ kJ mol}^{-1}$
$N_1$	11 194 295 *	18 015 424 **
$N_2$	4 836 237 *	7 336 303 **
$N_3$	2 037 680 *	3 086 718 **
$r_{21}$	1.32	1.35
$r_{32}$	1.33	1.33
$\phi_1$	0.177 23	0.177 30
$\phi_2$	0.177 56	0.177 56
$\phi_3$	0.178 02	0.178 04
$\rho$	1.03	2.16
$\phi_{\text{ext}}^{32}$	0.176	0.177
$e_{\text{a}}^{32}$	0.26 %	0.27 %
$e_{\text{ext}}^{32}$	0.76 %	0.31 %
$GC_{\text{medium}}^{32}$	0.94 %	0.39 %

\* Fluid domain only.

\*\* Fluid and solid domain.

Throughout this chapter, the settings underlying the medium grid ( $N_2$ ) have been used for the presented CFD simulation results. According to Table 9.2, the numerical uncertainty of this medium grid solution, expressed by the grid convergence index  $GC_{\text{medium}}^{32}$ , is below 1 % in both cases.

### 9.S.2 Influence of contact point handling

From a geometrical point of view, the contact between two adjacent spheres as well as between spheres and the surrounding wall are touching points. However, *point* contacts

cannot be represented with the discrete mesh of the computational domain. In Chapter 7 only the fluid domain was considered and contact point handling was not of an issue. The contact points were refined to a certain extent based on the mesh settings, resulting in contact areas rather than points. When the contact areas are small enough, the influence on the simulation results diminishes (cf. Section 7.S.2). However, when including thermal effects, more care should be taken due to the significant influence of conduction on the heat transfer. A strategy to avoid point contacts and thus the issue of discretisation thereof is the volume reduction or enlargement of particles. However, this is expected to have a larger influence on fluid hydrodynamics by increasing, respectively reducing, the void space between particles as well as on the conversion of a heterogeneously catalysed reaction due to changes to the catalytic surface area. This is in line with the findings reported by Dixon et al. [212] that the two global methods, particle volume reduction and enlargement, result in high errors considering drag coefficients and particle-particle heat transfer. Here, only the options of introducing either narrow bridge contacts or cutting thin gaps between adjacent solid geometry features are considered (cf. options bridge and cap in Figure 9.2). The contact between two catalytic pellets, that is solids of the same material, is assumed to be a touching contact, thus enabling direct heat transport by conduction between adjacent pellets. Also, there are no steep temperature gradients expected around these touching points. On the other hand, the contact between catalytic pellets and the surrounding wall, which are most likely not of the same material, may experience a much larger temperature difference, especially given the constant cooling temperature of the wall. Based on preliminary simulations with bridge contacts, which resulted in unrealistically high temperature ranges across the catalytic pellets, it was decided to use gaps around this type of contact points instead. This diminishes the heat removal through the reactor wall, thus posing a worst case scenario in regard of the reactor's tolerance to the heat of reaction before thermal runaway.

To confirm the early assumption and demonstrate the influence of the contact point handling between catalytic pellets and the surrounding reactor wall, four set-ups from the single pellet string reactor scenario with varying heat of reaction were re-evaluated using bridge contacts instead of gaps, i.e., caps in Figure 9.2. The resulting temperature profiles in the plane through the centre points of the catalytic pellets are shown in Figure 9.27. The case with a moderate heat of reaction of  $\Delta H = -64 \text{ kJ mol}^{-1}$ , depicted in Figure 9.27a, reveals a relatively narrow band of pellet wall temperatures distributed along the catalytic pellets but close to the touching points with the wall, where cold-spots are clearly visible. These are directly related to the improved heat removal by conduction to the reactor wall at constant coolant temperature when considering bridges around the contact points. However, these cold-spots give rise to unrealistically high temperature gradients across the individual catalytic pellets, especially when looking at the following figures related to reactions with increasing exothermicity as can be seen in Figures 9.27b to 9.27d. With increasing exothermicity the rise in maximum reaction rate, related to the temperature by



the Arrhenius equation, and its shift further to the uppermost catalytic pellet lead to reactant depletion further down the reactor. Ultimately, this leads to a locally restricted hot spot at the front of the first catalytic pellet where the conversion results in reactant depletion.

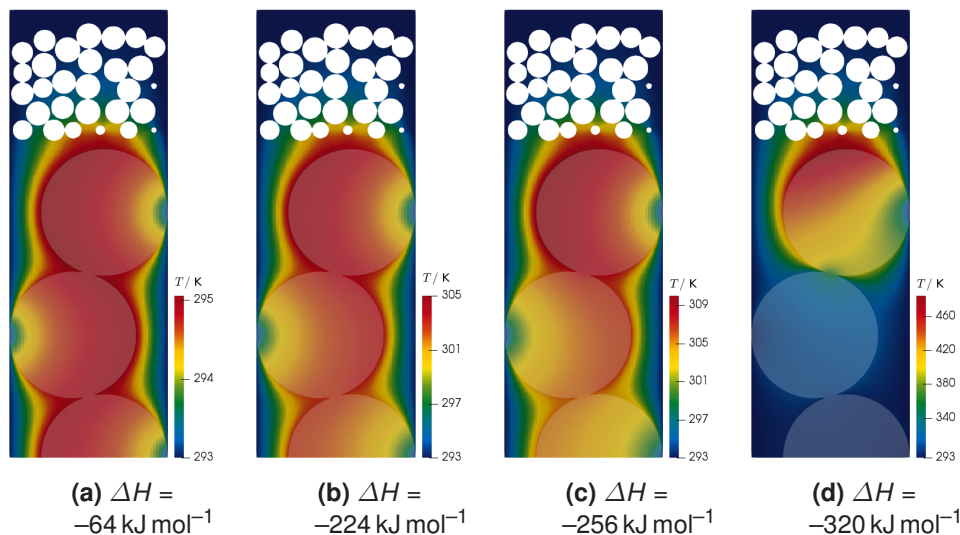
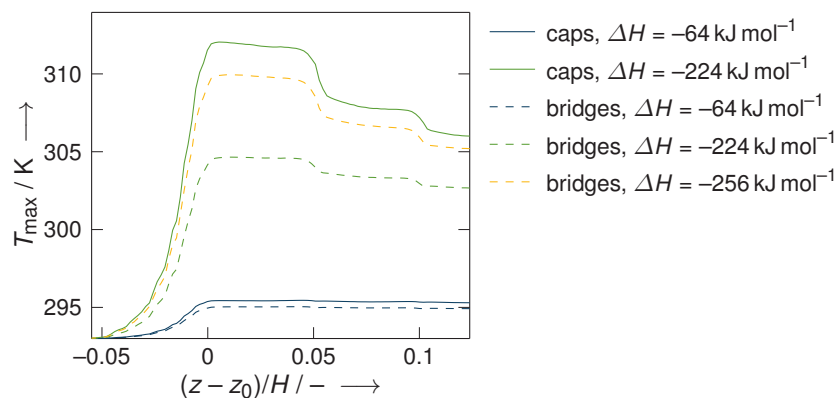


**Figure 9.27:** Temperature profiles in plane through centre points of catalytic pellets for varying heat of reaction with bridges at contact points between pellets and wall.

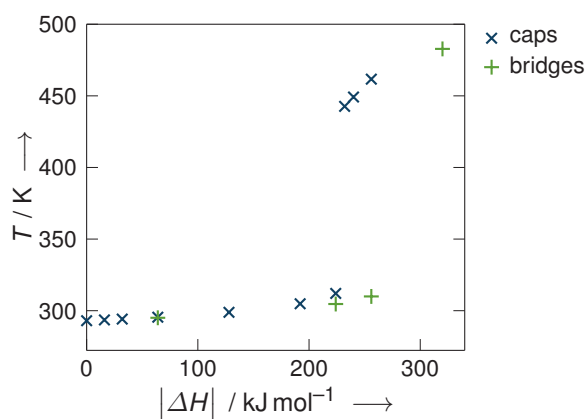
The uniform band of maximum temperatures along the reactor length axis for the case with lowest heat of reaction is also evident from Figure 9.28a, for both considered options of handling the contact points between catalytic pellets and the surrounding reactor wall, namely caps and bridges. However, already at a heat of reaction of  $\Delta H = -64 \text{ kJ mol}^{-1}$  the enhanced heat removal by conduction from pellet to reactor wall is evident. The maximum temperatures are lower throughout the reactor when considering bridges instead of caps. With increasing exothermicity, the maximum temperatures are less homogeneously distributed along the upper section of the catalytic bed. Rather, the maximum is clearly located at the front of the first catalytic pellet and the maximum temperature decreases with each pellet. Also, the effect of the enhanced heat removal by conduction between pellets and wall is more significant. In case of bridges instead of caps at the pellet-wall contact, the single pellet string reactor with a heat of reaction of  $\Delta H = -256 \text{ kJ mol}^{-1}$  exhibits stable operation rather than its counterpart which was subject to runaway at corresponding conditions but with gaps between catalytic pellet and surrounding wall (cf. Figures 9.7, 9.8 and 9.10). As can be seen from Figures 9.28b and 9.28c, the maximum hot spot temperature as well as the conversion at the outlet of the considered simulation domain (2.5 catalytic pellets in the shown cases) reveal a shift of the tolerable heat of reaction before runaway to higher values. This is in line with the preliminary assumption. The conducted parameter study presented in this chapter thus represents a conservative approach. It is expected that experimental results would be in between the simulation results considering caps and bridges.

An alternative approach to modelling the contact points would be to introduce bridges with an effective heat transfer coefficient depending on the properties of the solid and the

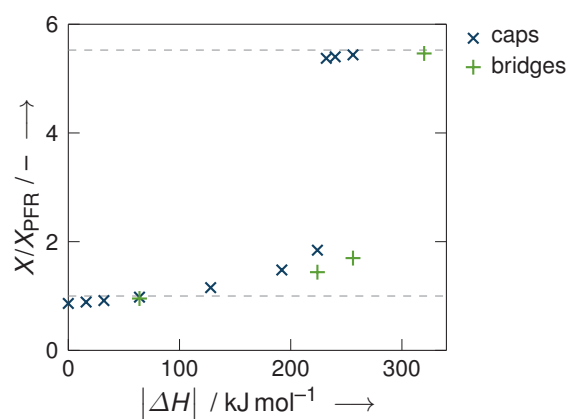




(a) Maximum temperature along the reactor.



(b) Hot spot temperature.



(c) Outlet conversion.

**Figure 9.28:** Influence of handling the contact points between catalytic pellets and reactor wall; dashed lines in subfigure (c) indicating isothermal PFR conversion and full reactant depletion.

surrounding fluid, as proposed by Dixon et al. [212]. However, this is out of the scope of this project and would require extensive experimental data for validation.



## 10 Summary and outlook

Fixed-bed reactor modelling, which is the underlying theme of this thesis, is a very broad topic. Three key aspects were investigated in depth, namely numerical packing generation, simulation of pellet shrinkage within packed beds and the behaviour of single pellet string reactors as a special type of fixed-bed reactor.

Numerous CFD simulations were performed during the course of this dissertation, which made it especially useful to choose an automated approach, realized through Bash and Python scripting as presented in Chapter 4. By this means, multiple entire simulation runs covering preprocessing with parameter variation, geometry set-up and mesh generation, cold-flow and reaction simulation as well as post-processing could be handled easily. Throughout this work, all simulations were performed with open-source software. The applied automation routine exceeded the comfortable handling as known from commercial software packages by including an extensive parameter variation functionality across numerous individual simulation runs. This provided a convenient framework allowing for time savings and productivity gain in executing the conducted open-source random packing generation and CFD studies.

In this work, the software packages LIGGGHTS<sup>®</sup> and Blender<sup>™</sup> were utilised for numerical packing generation, as detailed in Chapter 5. The influence of packing characteristics, i.e. pellet insertion height, bed length and height effects as well as the influence of material properties on the resulting local voidage profiles and mean bed voidage of beds of spheres in cylindrical containers with moderate diameter aspect ratio were investigated. The results covered the full range of packing modes from very loose to highly dense. For an unbiased comparison of mean bed voidages it was found to be of genuine importance to exclude the top and bottom most sections of the bed which are less dense than the rest of the bed. Due to its effects on the packing arrangement, the insertion height was fixed at two different heights for the subsequent investigation of the effect of material properties on the obtained bed. While the influence of the coefficients of friction and restitution, the latter limited to rough pellets, on mean bed voidage was found to be statistically significant, this was not the case for the material properties density, Young's modulus and Poisson's ratio. A closer look on the radial voidage profiles revealed a deeper insight into the local structure of the obtained random packings, yielding a novel expression for the position of the first radial voidage minimum next to the confining wall. All in all, there is not the one set of parameters that leads to *the* representative packing. Rather, any combination of a chosen packing mode together with a set of material properties results in a specific packing. The relevant

parameters should thus be carefully chosen to numerically obtain a good representative of the corresponding *real* packing.

Pellet shrinkage, as may be encountered during reductive activation within fixed-bed reactors, was incorporated to the packing generation routine with Blender™ in Chapter 6, covering random packing generation, pellet shrinkage within the bed and the related settling of the pellets. This allows to predict the effects of pellet shrinkage within random packings on pellet arrangement and subsequently on flow hydrodynamics. Investigation of two scenarios of narrow beds made of tablets indicated a higher mean voidage of the bed after pellet shrinkage that was, at first counterintuitively, accompanied by a pressure drop per unit length of bed below expectation. A closer look revealed a higher local order within the tablet arrangement near the wall for the shrunk bed with a region of low voidage between the first and second ring of pellets from the tube wall as compared to the initial bed before pellet shrinkage. The presented scenarios demonstrated the feasibility and indicated the potential of simulating pellet shrinkage within random packings.

The concept of single pellet string reactors, where pellets are packed in tubes of only slightly larger diameter, has lately experienced a renewed interest. In Chapter 7, a comprehensive characterisation of the reactor performance was presented for spherical, non-porous pellets in cylindrical confining walls based on CFD simulations where it was assumed that flow and reaction are independent of each other. A parameter study on conversion and residence time behaviour under variation of reactor geometry and fluid properties considering laminar flow and an isothermal, isomolar, hypothetical first order irreversible gas-phase reaction  $A \longrightarrow B$  with no change in gas density that is taking place at the catalytic pellet surface was conducted. The results revealed that a close approximation to plug flow with conversion deviating less than 5% can be achieved readily and conversion was found to be enhanced in reactors at larger scale, with smaller diameter aspect ratio and with more catalytic pellets. An investigation of the laminar flow behaviour within the considered single pellet string reactors using a non-diffusive numerical tracer resulted in similar trends for the residence time distributions, but for two expectations: increasing the reactor scale improved conversion whilst apparently yielding a less plug flow like residence time distribution and adding inert fines to the free space surrounding the catalyst pellets reduces the overall bed conversion despite yielding a more plug flow like residence time behaviour. As the deviation to plug flow was found to be consistent and predictable, a novel design criterion for single pellet string reactors based only on the reactor geometry, fluid properties and flow velocity was developed in order to enable a priori predictions of the expected deviation to plug flow conversion. Applicability tests of existing design criteria intended for conventional fixed-bed reactors showed that the considered single pellet string reactor scenarios are within the range of the axial dispersion criterion by Gierman [7], the Carberry criterion [33, 163] on external mass transfer limitations was far from significant as expected for heterogeneous gas phase reactions. Also, the conversion reduction by bed dilution with inert fines was

---

within a corresponding criterion by Berger et al. [70, 71] while the criterion on negligible radial dispersion by Chu and Ng [8] cannot be met by the defined reactor geometry. All in all, single pellet string reactors were found to be a reliable, risk-reducing and cost-effective option for catalyst testing and kinetic measurement at small scale.

The pressure drop behaviour across the previously considered single pellet string reactors is investigated in Chapter 8 by means of CFD simulations. Variations in fluid viscosity, flow velocity, diameter aspect ratio and reactor scale led to the expected trends such that the general trend of the Blake-Kozeny equation was met. However, deviations to the correlation were present which underlines the importance of the influence of the confining wall that cannot be neglected for this very narrow type of fixed-bed reactor. By introducing a geometry-based weighting factor that scales the influence of the wall effect by the diameter aspect ratio as part of an equivalent diameter expression, the agreement between the simulated pressure drop and the predictions by the correlation could be improved significantly. Even higher agreement could be obtained when introducing five fitting parameters to the weighting factor expression. Using a weighing factor improved the pressure drop predictions also compared to other correlations available from literature.

Finally, the investigation of the single pellet string reactor was extended to cover the impact of thermal effects in Chapter 9. By means of CFD simulations, the nonisothermal behaviour of a heterogeneously catalysed, exothermic gas-phase reaction within wall cooled single pellet string reactors was characterised where the pellets were assumed to be non-porous. To include the thermal conductivity within the pellets, these had to be included in the simulation domain. When varying the heat of reaction, thermal runaway could be observed. The related steep gradients in temperature and concentrations required a finer computational mesh than used before. Also, the chosen set-up with an exothermic surface reaction and wall cooling, only allowed thermal runaway to take place at the first catalytic pellet within the string. As a results, only the first 2.5 pellets within the single pellet string were considered for simulation in an extended parameter study, revealing a region where stable reactor operation is possible considering the influence of the heat of reaction, activation energy, reactor scale, the corresponding ideal plug flow conversion, fluid heat capacity and the thermal conductivity of the catalyst material. Other influencing factors such as the height of an inert pre-bed, the number of simulated pellets and including the temperature-dependency of the diffusion coefficient showed only little influence. In fact, close analysis of the simulation results showed a sharp threshold between near plug flow behaviour and thermal runaway within the vicinity of the first catalytic pellet in the string. It should be noted that the plug flow like behaviour observed in the isothermal studies in Chapter 7 was not undermined by buoyancy effects but only when thermal runaway occurred. This led to a novel criterion for thermal runaway in single pellet string reactors based solely on a priori known values, if assuming temperature independency of the material properties.

Another aspect arising from the inclusion of thermal effects within both fluid and catalytic

solid was the required special treatment of contact points, both between subsequent pellets and pellet-wall contacts. While following the common approach of assuming solid bridges between pellets, a small gap was introduced between the catalytic pellets and the confining wall. This poses the worst case regarding reactor cooling and thus the reactor's tolerance towards the amount of heat generated by the thermal reaction before runaway.

The work presented in this thesis contributes towards a deeper understanding of numerical packing generation including potential pellet shrinkage during chemical activation of the catalytic pellets as well as the behaviour of single pellet string reactors as a very special type of fixed-bed reactor by means of numerical simulation. The systematic investigation of the influence of material properties on pellet arrangement within numerically generated random packed beds is meant to highlight the importance of choosing appropriate parameter settings to best resemble a real packing and thus emphasises the importance of the packing generation itself, an unfortunately too often underrated step. The excursus on pellet shrinkage within random packings demonstrates the possibilities that simulation can offer, especially regarding local packing structures that may determine the behaviour of a reactor rather than when only considering average bed properties. The performed reactor simulations focus on the single pellet string reactor, offering a systematic characterisation of this type of reactor including variations in geometry, details on the pressure drop and nonisothermal conditions and resulting in a design criterion to ensure near plug flow behaviour as well as a criterion to determine thermal runaway. Both proposed criteria are solely based on a priori known values making them a powerful tool to design single pellet string reactor systems as for example for catalyst testing or kinetic experiments.

Though the presented investigation on numerical packing generation as well as the work on the single pellet string reactor concept are limited to spherical pellets in cylindrical confining walls, it is anticipated that the observed trends hold for other pellet and wall geometries. When simulating the shrinkage of tablets within a random packed bed, a homogeneous shrinkage rate across the entire bed was assumed. Possible future studies should embed the proposed shrinkage routine in a more complex simulation framework, that may enable to consider individual pellet shrinkages based on local temperature or conversion by a closer coupling of the packing generation with the CFD simulation. Looking at the single pellet string reactor characterisations, a clear limitation is the assumption of a monomolecular reaction where both reactants and products have the same fluid properties as well as the restriction to laminar flow. Further simulations should extend the range of validity of the proposed criteria as well as cover further aspects of the single pellet string reactor behaviour. This should include but is not limited to looking into turbulent flow scenarios, the influence of the shape of catalyst particles as well as liquid reactants and trickle-bed operation.

Going back to the generalised life cycle of a catalytic fixed-bed reactor as shown in Chapter 1, bed densification during reactor operation is another interesting topic which may

---

be incorporated into the proposed packing generation routine. Instead of pellet shrinkage, the entire bed may be subject to vibration and the response of the bed investigated. Further, catalyst poisoning would be an interesting research question with regard to thermal runaway in single pellet string reactors.





# Bibliography

- [1] G. Eigenberger and W. Ruppel, Catalytic Fixed-Bed Reactors in *Ullmann's Encyclopedia of Industrial Chemistry*, American Cancer Society, **2012**, DOI 10.1002/14356007.b04\_199.pub2.
- [2] G. F. Froment, Fixed Bed Catalytic Reactors. Technological and Fundamental Design Aspects, *Chem. Ing. Tech.* **1974**, *46*, 374–386, DOI 10.1002/cite.330460903.
- [3] G. F. Froment, K. B. Bischoff and J. De Wilde, *Chemical Reactor Analysis and Design*, 3rd, John Wiley & Sons, **2010**, 912 pp.
- [4] D. S. Scott, W. Lee and J. Papa, The measurement of transport coefficients in gas-solid heterogeneous reactions, *Chem. Eng. Sci.* **1974**, *29*, 2155–2167, DOI 10.1016/0009-2509(74)80023-0.
- [5] R. Moonen, J. Alles, E.-J. Ras, C. Harvey and J. A. Moulijn, Performance testing of hydrodesulfurization catalysts using a single-pellet-string reactor, *Chem. Eng. Technol.* **2017**, *40*, 2025–2034, DOI 10.1002/ceat.201700098.
- [6] D. E. Mears, The role of axial dispersion in trickle-flow laboratory reactors, *Chem. Eng. Sci.* **1971**, *26*, 1361–1366, DOI 10.1016/0009-2509(71)80056-8.
- [7] H. Gierman, Design of laboratory hydrotreating reactors, *Appl. Catal.* **1988**, *43*, 277–286, DOI 10.1016/s0166-9834(00)82732-3.
- [8] C. F. Chu and K. M. Ng, Flow in packed tubes with a small tube to particle diameter ratio, *AIChE J.* **1989**, *35*, 148–158, DOI 10.1002/aic.690350116.
- [9] O. Šolvová and P. Schneider, Axial dispersion in single-pellet-string columns packed with cylindrical particles, *Chem. Eng. Sci.* **1994**, *49*, 401–408, DOI 10.1016/0009-2509(94)87011-x.
- [10] Y. Guangsuo, Y. Jianguo and Y. Zunhong, The measurement of effective diffusivity for sulfur-tolerant methanation catalyst, *Chemical Engineering Journal* **2000**, *78*, 141–146, DOI 10.1016/s1385-8947(00)00129-7.
- [11] A. I. Hipolito, M. Rolland, C. Boyer and C. de Bellefon, Single Pellet String Reactor for Intensification of Catalyst Testing in Gas/Liquid/Solid Configuration, *Oil Gas Sci. Technol.* **2010**, *65*, 689–701, DOI 10.2516/ogst/2009079.
- [12] A. Müller, J. Petschick and R. Lange, Model-Based Investigation of a Pellet String Reactor, *Procedia Eng.* **2012**, *42*, 1189–1201, DOI 10.1016/j.proeng.2012.07.511.

- [13] M. Behnam, A. G. Dixon, P. M. Wright, M. Nijemeisland and E. H. Stitt, Comparison of CFD simulations to experiment under methane steam reforming reacting conditions, *Chem. Eng. J.* **2012**, *207-208*, 690–700, DOI 10.1016/j.cej.2012.07.038.
- [14] A. Klyushina, K. Pacultová and L. Obalová, Advantage of the single pellet string reactor for testing real-size industrial pellets of potassium-doped CoMnAl catalyst for the decomposition of N<sub>2</sub>O, *React. Kinet. Mech. Catal.* **2015**, *115*, 651–662, DOI 10.1007/s11144-015-0871-y.
- [15] A. Müller, J. Kanz, S. Haase, K. Becker and H.-M. Vorbrodtt, Novel continuous catalytic hydrogenation process for the synthesis of diacetone-D-allose, *Chem. Eng. Process. Process Intensif.* **2017**, *113*, 2–13, DOI 10.1016/j.cep.2016.10.013.
- [16] V. Petrazzuoli, M. Rolland, A. Mekki-Berrada, O. Said-Aizpuru and Y. Schuurman, Choosing the right packing in millipacked bed reactors under single phase gas flow, *Chemical Engineering Science* **2021**, *231*, 116314, DOI 10.1016/j.ces.2020.116314.
- [17] J. A. Moulijn, A. Tarfaoui and F. Kapteijn, General aspects of catalyst testing, *Catal. Today* **1991**, *11*, 1–12, DOI 10.1016/0920-5861(91)87002-5.
- [18] A. G. Dixon, M. Nijemeisland and E. H. Stitt, Packed Tubular Reactor Modeling and Catalyst Design using Computational Fluid Dynamics in *Computational Fluid Dynamics*, Elsevier, **2006**, pp. 307–389, DOI 10.1016/s0065-2377(06)31005-8.
- [19] N. Jurtz, M. Kraume and G. D. Wehinger, Advances in fixed-bed reactor modeling using particle-resolved computational fluid dynamics (CFD), *Rev. Chem. Eng.* **2019**, *35*, 139–190, DOI 10.1515/revce-2017-0059.
- [20] Free Software Foundation, GNU Bash.
- [21] G. van Rossum and F. L. Drake, Jr., *Python tutorial*, Centrum voor Wiskunde en Informatica Amsterdam, **1995**.
- [22] C. Kloss, C. Goniva, A. Hager, S. Amberger and S. Pirker, Models, algorithms and validation for opensource DEM and CFD-DEM, *Prog. Comput. Fluid Dyn.* **2012**, *12*, 140–152, DOI 10.1504/pcf.d.2012.047457.
- [23] Blender Foundation, Blender 2.76b, software package, **2015**.
- [24] H. G. Weller, G. Tabor, H. Jasak and C. Fureby, A tensorial approach to computational continuum mechanics using object-oriented techniques, *Comput. Phys.* **1998**, *12*, 620–631, DOI 10.1063/1.168744.
- [25] O. Levenspiel, *Chemical Reaction Engineering*, 3rd ed., John Wiley & Sons, Inc., **1998**, 704 pp.
- [26] C. Perego and S. Peratello, Experimental methods in catalytic kinetics, *Catal. Today* **1999**, *52*, 133–145, DOI 10.1016/s0920-5861(99)00071-1.

- [27] H. S. Fogler, *Elements of Chemical Reaction Engineering*, 4th ed., Pearson Education International, **2006**.
- [28] O. Levenspiel, *Tracer Technology*, Springer-Verlag GmbH, **2011**.
- [29] H. Heinemann, Chapter 4. Catalyst performance testing, *Catal. Today* **1994**, *22*, 281–293, DOI 10.1016/0920-5861(94)80105-3.
- [30] Y. Schuurman, Aspects of kinetic modeling of fixed bed reactors, *Catal. Today* **2008**, *138*, 15–20, DOI 10.1016/j.cattod.2008.04.041.
- [31] D. E. Mears, Tests for Transport Limitations in Experimental Catalytic Reactors, *Ind. Eng. Chem. Process Des. Dev.* **1971**, *10*, 541–547, DOI 10.1021/i260040a020.
- [32] D. E. Mears, Diagnostic criteria for heat transport limitations in fixed bed reactors, *J. Catal.* **1971**, *20*, 127–131, DOI 10.1016/0021-9517(71)90073-x.
- [33] J. J. Carberry, *Catalysis in*, Springer-Verlag Berlin Heidelberg, **1987**, Chapter Physico-Chemical Aspects of Mass and Heat Transfer in Heterogeneous Catalysis, pp. 131–171.
- [34] S. T. Sie, Advantages, Possibilities, and Limitations of Small-Scale Testing of Catalysts for Fixed-Bed Processes in *ACS Symposium Series*, American Chemical Society, **1996**, pp. 6–41, DOI 10.1021/bk-1996-0634.ch002.
- [35] D. A. Hickman, J. C. Degenstein and F. H. Ribeiro, Fundamental principles of laboratory fixed bed reactor design, *Curr. Opin. Chem. Eng.* **2016**, *13*, 1–9, DOI 10.1016/j.coche.2016.07.002.
- [36] S. T. Sie, Miniaturization of hydroprocessing catalyst testing systems: Theory and practice, *AIChE J.* **1996**, *42*, 3498–3507, DOI 10.1002/aic.690421219.
- [37] P. A. Cundall and O. D. L. Strack, A discrete numerical model for granular assemblies, *Géotechnique* **1979**, *29*, 47–65, DOI 10.1680/geot.1979.29.1.47.
- [38] M. Jean, The non-smooth contact dynamics method, *Comput. Methods Appl. Mech. Eng.* **1999**, *177*, 235–257, DOI 10.1016/s0045-7825(98)00383-1.
- [39] J. J. Moreau, Numerical aspects of the sweeping process, *Comput. Methods Appl. Mech. Eng.* **1999**, *177*, 329–349, DOI 10.1016/s0045-7825(98)00387-9.
- [40] F. White, *Fluid Mechanics*, McGraw-Hill Science/Engineering/Math, **2010**.
- [41] H. K. Versteeg and W. Malalasekera, *An Introduction to Computational Fluid Dynamics – The Finite Volume Method*, 2nd ed., Pearson Education Limited, **2007**.
- [42] R. B. Bird, W. E. Stewart and E. N. Lightfoot, *Transport Phenomena*, John Wiley and Sons Ltd, **2006**, 928 pp.
- [43] B. Andersson, R. Andersson, L. Hakansson, M. Mortensen, R. Sudiyo and B. van Wachem, *Computational Fluid Dynamics for Engineers*, Cambridge University Press, **2011**, DOI 10.1017/CB09781139093590.

- [44] C. J. Greenshields, OpenFOAM User Guide, Version 2.4.0, CFD Direct Ltd., **2015**.
- [45] C. J. Greenshields, OpenFOAM Programmer's Guide, Version 2.4.0, CFD Direct Ltd., **2015**.
- [46] C. J. Greenshields, OpenFOAM User Guide, Version 4.0, CFD Direct Ltd., **2016**.
- [47] T. Marić, J. Höpken and K. Mooney, *The OpenFOAM<sup>®</sup> Technology Primer*, Sourceflux, **2014**.
- [48] J. H. Ferziger and M. Peric, *Computational Methods for Fluid Dynamics*, Springer, **2001**.
- [49] I. B. Celik, U. Ghia, P. J. Roache, C. J. Freitas, H. Coleman and R. E. Raad, Procedure for Estimation and Reporting of Uncertainty Due to Discretization in CFD Applications, *J. Fluids Eng.* **2008**, *130*, 078001, DOI 10.1115/1.2960953.
- [50] J. J. Carberry, First order rate processes and axial dispersion in packed bed reactors, *Can. J. Chem. Eng.* **1958**, *36*, 207–209, DOI 10.1002/cjce.5450360503.
- [51] S. Ergun, Fluid flow through packed columns, *Chem. Eng. Prog.* **1952**, *48*, 89–94.
- [52] M. F. Edwards and J. F. Richardson, Gas dispersion in packed beds, *Chem. Eng. Sci.* **1968**, *23*, 109–123, DOI 10.1016/0009-2509(68)87056-3.
- [53] T. C.-S. Hsiang and H. W. Haynes, Axial dispersion in small diameter beds of large, spherical particles, *Chem. Eng. Sci.* **1977**, *32*, 678–681, DOI 10.1016/0009-2509(77)80236-4.
- [54] T.-S. Chou and L. L. Hegedus, Transient diffusivity measurements in catalyst pellets with two zones of differing diffusivities, *AIChE J.* **1978**, *24*, 255–260, DOI 10.1002/aic.690240214.
- [55] M.-D. Lee, S.-H. Shen, T.-K. Chung and C.-K. Kuei, Flow and dispersive behaviours of cylindrical pellet string reactor, *AIChE J.* **1984**, *30*, 639–641, DOI 10.1002/aic.690300416.
- [56] E. Tsotsas and E. U. Schlünder, Measurements of mass transfer between particles and gas in packed tubes at very low tube to particle diameter ratios, *Wärme - und Stoffübertragung* **1990**, *25*, 245–256, DOI 10.1007/BF01785411.
- [57] R. K. Sharma, D. L. Cresswell and E. J. Newson, Effective diffusion coefficients and tortuosity factors for commercial catalysts, *Ind. Eng. Chem. Res.* **1991**, *30*, 1428–1433, DOI 10.1021/ie00055a004.
- [58] V. M. H. Govindarao, K. V. S. Ramrao and A. V. S. Rao, Structural characteristics of packed beds of low aspect ratio, *Chem. Eng. Sci.* **1992**, *47*, 2105–2109, DOI 10.1016/0009-2509(92)80330-f.
- [59] R. M. Fand, M. Sundaram and M. Varahasamy, Incompressible Fluid Flow Through Pipes Packed With Spheres at Low Dimension Ratios, *J. Fluids Eng.* **1993**, *115*, 169, DOI 10.1115/1.2910102.

- [60] A. G. Dixon, Heat Transfer in Fixed Beds at Very Low ( $<4$ ) Tube-to-Particle Diameter Ratio, *Ind. Eng. Chem. Res.* **1997**, *36*, 3053–3064, DOI 10.1021/ie9605950.
- [61] W. Reichelt, Zur Berechnung des Druckverlustes einphasig durchströmter Kugel- und Zylinderschüttungen, *Chem. Ing. Tech.* **1972**, *44*, 1068–1071, DOI 10.1002/cite.330441806.
- [62] N.-S. Cheng, Wall effect on pressure drop in packed beds, *Powder Technol.* **2011**, *210*, 261–266, DOI 10.1016/j.powtec.2011.03.026.
- [63] Z. Guo, Z. Sun, N. Zhang, M. Ding and J. Wen, Experimental characterization of pressure drop in slender packed bed ( $1 < D/d < 3$ ), *Chem. Eng. Sci.* **2017**, *173*, 578–587, DOI 10.1016/j.ces.2017.08.022.
- [64] H. P. A. Calis, J. Nijenhuis, B. C. Paikert, F. M. Dautzenberg and C. M. van den Bleek, CFD modelling and experimental validation of pressure drop and flow profile in a novel structured catalytic reactor packing, *Chem. Eng. Sci.* **2001**, *56*, 1713–1720, DOI 10.1016/S0009-2509(00)00400-0.
- [65] S. J. P. Romkes, F. M. Dautzenberg, C. M. van den Bleek and H. P. A. Calis, CFD modelling and experimental validation of particle-to-fluid mass and heat transfer in a packed bed at very low channel to particle diameter ratio, *Chem. Eng. J.* **2003**, *96*, 3–13, DOI 10.1016/j.cej.2003.08.026.
- [66] R. Langsch, S. Haase and R. Lange, Hydrodynamik und Stofftransport in einem Perlschnurreaktor für Gas/Flüssig/Fest-Reaktionen, *Chem. Ing. Tech.* **2013**, *85*, 642–655, DOI 10.1002/cite.201200189.
- [67] A. Müller, M. Ludwig, M. Arlit and R. Lange, Evaluation of reactor concepts for the continuous production of fine chemicals using the selective hydrogenation of cinnamaldehyde over palladium catalysts, *Catal. Today* **2015**, *241*, 214–220, DOI 10.1016/j.cattod.2013.12.051.
- [68] L. E. Kallinikos and N. G. Papayannakos, Operation of a Miniscale String Bed Reactor in Spiral Form at Hydrotreatment Conditions, *Ind. Eng. Chem. Res.* **2007**, *46*, 5531–5535, DOI 10.1021/ie070309s.
- [69] C. M. van den Bleek, K. van der Wiele and P. J. van den Berg, The effect of dilution on the degree of conversion in fixed bed catalytic reactors, *Chem. Eng. Sci.* **1969**, *24*, 681–694, DOI 10.1016/0009-2509(69)80061-8.
- [70] R. J. Berger, J. Pérez-Ramírez, F. Kapteijn and J. A. Moulijn, Catalyst performance testing: bed dilution revisited, *Chem. Eng. Sci.* **2002**, *57*, 4921–4932, DOI 10.1016/S0009-2509(02)00273-7.
- [71] R. J. Berger, J. Pérez-Ramírez, F. Kapteijn and J. A. Moulijn, Catalyst performance testing: the influence of catalyst bed dilution on the conversion observed, *Chem. Eng. J.* **2002**, *90*, 173–183, DOI 10.1016/S1385-8947(02)00078-5.

- [72] A. G. Dixon and M. Nijemeisland, CFD as a Design Tool for Fixed-Bed Reactors, *Ind. Eng. Chem. Res.* **2001**, *40*, 5246–5254, DOI 10.1021/ie001035a.
- [73] J. Fernengel, F. Habla and O. Hinrichsen, Scripting as an approach to automated CFD simulation for packed bed catalytic reactor modeling, *Chem. Ing. Tech.* **2018**, *90*, 685–689, DOI 10.1002/cite.201700153.
- [74] T. Atmakidis and E. Y. Kenig, CFD-based analysis of the wall effect on the pressure drop in packed beds with moderate tube/particle diameter ratios in the laminar flow regime, *Chem. Eng. J.* **2009**, *155*, 404–410, DOI 10.1016/j.cej.2009.07.057.
- [75] T. Eppinger, K. Seidler and M. Kraume, DEM-CFD simulations of fixed bed reactors with small tube to particle diameter ratios, *Chem. Eng. J.* **2011**, *166*, 324–331, DOI 10.1016/j.cej.2010.10.053.
- [76] G. D. Wehinger and M. Kraume, CFD als Designtool für Festbettreaktoren mit kleinem Rohr-zu-Pelletdurchmesser-Verhältnis: Heute oder in Zukunft?, *Chem. Ing. Tech.* **2017**, *89*, 447–453, DOI 10.1002/cite.201600155.
- [77] G. D. Wehinger, M. Kraume, V. Berg, O. Korup, K. Mette, R. Schlögl, M. Behrens and R. Horn, Investigating dry reforming of methane with spatial reactor profiles and particle-resolved CFD simulations, *AIChE J.* **2016**, *62*, 4436–4452, DOI 10.1002/aic.15520.
- [78] A. G. Dixon, G. Walls, H. Stanness, M. Nijemeisland and E. H. Stitt, Experimental validation of high Reynolds number CFD simulations of heat transfer in a pilot-scale fixed bed tube, *Chem. Eng. J.* **2012**, *200-202*, 344–356, DOI 10.1016/j.cej.2012.06.065.
- [79] B. Haddadi, C. Jordan, H. R. Norouzi and M. Harasek, Investigation of the pressure drop of random packed bed adsorbers, *Chemical Engineering Transactions* **2016**, *52*, 439–444, DOI 10.3303/CET1652074.
- [80] G. Boccardo, F. Augier, Y. Haroun, D. Ferré and D. L. Marchisio, Validation of a novel open-source work-flow for the simulation of packed-bed reactors, *Chem. Eng. J.* **2015**, *279*, 809–820, DOI 10.1016/j.cej.2015.05.032.
- [81] H. Bai, J. Theuerkauf, P. A. Gillis and P. M. Witt, A Coupled DEM and CFD Simulation of Flow Field and Pressure Drop in Fixed Bed Reactor with Randomly Packed Catalyst Particles, *Ind. Eng. Chem. Res.* **2009**, *48*, 4060–4074, DOI 10.1021/ie801548h.
- [82] U. Ayachit, *The ParaView Guide: A Parallel Visualization Application*, Kitware, **2015**.
- [83] E. Coumans, Bullet 2.83 Physics SDK Manual, **2015**.
- [84] M. Maestri and A. Cuoci, Coupling CFD with detailed microkinetic modeling in heterogeneous catalysis, *Chem. Eng. Sci.* **2013**, *96*, 106–117, DOI 10.1016/j.ces.2013.03.048.



- [85] M. Rhodes, *Introduction to Particle Technology*, John Wiley & Sons, Ltd, **2008**, DOI 10.1002/9780470727102.
- [86] J. S. Goodling, R. I. Vachon, W. S. Stelplflug, S. J. Ying and M. S. Khader, Radial porosity distribution in cylindrical beds packed with spheres, *Powder Technol.* **1983**, *35*, 23–29, DOI 10.1016/0032-5910(83)85022-0.
- [87] J. Fernengel and O. Hinrichsen, Influence of material properties on voidage of numerically generated random packed beds, *Chem. Eng. Sci.* **2021**, *233*, 116406, DOI 10.1016/j.ces.2020.116406.
- [88] B. Partopour and A. G. Dixon, 110<sup>th</sup> Anniversary: Commentary: CFD as a Modeling Tool for Fixed Bed Reactors, *Ind. Eng. Chem. Res.* **2019**, *58*, 5733–5736, DOI 10.1021/acs.iecr.8b06380.
- [89] A. Jafari, P. Zamankhan, S. M. Mousavi and K. Pietarinen, Modeling and CFD simulation of flow behavior and dispersivity through randomly packed bed reactors, *Chem. Eng. J.* **2008**, *144*, 476–482, DOI 10.1016/j.cej.2008.07.033.
- [90] S. Ahmadi and F. Sefidvash, Study of pressure drop in fixed bed reactor using a computational fluid dynamics (CFD) code, *ChemEngineering* **2018**, *2*, 14, DOI 10.3390/chemengineering2020014.
- [91] A. Pavlišič, R. Ceglar, A. Pohar and B. Likozar, Comparison of computational fluid dynamics (CFD) and pressure drop correlations in laminar flow regime for packed bed reactors and columns, *Powder Technol.* **2018**, *328*, 130–139, DOI 10.1016/j.powtec.2018.01.029.
- [92] E. M. Moghaddam, E. A. Foumeny, A. I. Stankiewicz and J. T. Padding, Hydrodynamics of narrow-tube fixed bed reactors filled with Raschig rings, *Chemical Engineering Science: X* **2020**, *5*, 100057, DOI 10.1016/j.cesx.2020.100057.
- [93] M. Nijemeisland and A. G. Dixon, Comparison of CFD simulations to experiment for convective heat transfer in a gas–solid fixed bed, *Chem. Eng. J.* **2001**, *82*, 231–246, DOI 10.1016/s1385-8947(00)00360-0.
- [94] M. Nijemeisland and A. G. Dixon, CFD study of fluid flow and wall heat transfer in a fixed bed of spheres, *AIChE J.* **2004**, *50*, 906–921, DOI 10.1002/aic.10089.
- [95] Y. Dong, B. Sosna, O. Korup, F. Rosowski and R. Horn, Investigation of radial heat transfer in a fixed-bed reactor: CFD simulations and profile measurements, *Chem. Eng. J.* **2017**, *317*, 204–214, DOI 10.1016/j.cej.2017.02.063.
- [96] Y. Li, C. Lu, X. Cao, Z. Geng and M. Zhang, CFD study on partial oxidation of methane in fixed-bed reactor, *Can. J. Chem. Eng.* **2019**, DOI 10.1002/cjce.23644.

- [97] K. G. Manoharan and V. V. Buwa, Structure-resolved CFD simulations of different catalytic structures in a packed bed, *Ind. Eng. Chem. Res.* **2019**, *58*, 22363–22375, DOI 10.1021/acs.iecr.9b03537.
- [98] Z. Minhua, D. He and G. Zhongfeng, A particle-resolved CFD model coupling reaction-diffusion inside fixed-bed reactor, *Adv. Powder Technol.* **2019**, *30*, 1226–1238, DOI 10.1016/j.apt.2019.03.019.
- [99] G. D. Wehinger and S. Fleischlen, Computational Fluid Dynamics Modeling of Radiation in a Steam Methane Reforming Fixed-Bed Reactor, *Ind. Eng. Chem. Res.* **2019**, *58*, 14410–14423, DOI 10.1021/acs.iecr.9b01265.
- [100] H. Wu, N. Gui, X. Yang, J. Tu and S. Jiang, Numerical simulation of heat transfer in packed pebble beds: CFD-DEM coupled with particle thermal radiation, *Int. J. Heat Mass Transfer* **2017**, *110*, 393–405, DOI 10.1016/j.ijheatmasstransfer.2017.03.035.
- [101] G. Boccardo, E. Crevacore, R. Sethi and M. Icardi, A robust upscaling of the effective particle deposition rate in porous media, *J. Contam. Hydrol.* **2018**, *212*, 3–13, DOI 10.1016/j.jconhyd.2017.09.002.
- [102] G. Boccardo, I. M. Sokolov and A. Paster, An improved scheme for a Robin boundary condition in discrete-time random walk algorithms, *J. Comput. Phys.* **2018**, *374*, 1152–1165, DOI 10.1016/j.jcp.2018.08.009.
- [103] G. Boccardo, E. Crevacore, A. Passalacqua and M. Icardi, Computational analysis of transport in three-dimensional heterogeneous materials, *Computing and Visualization in Science* **2020**, *23*, DOI 10.1007/s00791-020-00321-6.
- [104] M. Leva, Fluid flow through packed beds, *Chemical Engineering* **1949**, *56*, 115–117.
- [105] L. H. S. Roblee, R. M. Baird and J. W. Tierney, Radial porosity variations in packed beds, *AIChE J.* **1958**, *4*, 460–464, DOI 10.1002/aic.690040415.
- [106] G. D. Scott, Packing of spheres: Packing of equal spheres, *Nature* **1960**, *188*, 908–909, DOI 10.1038/188908a0.
- [107] J. C. Macrae and W. A. Gray, Significance of the properties of materials in the packing of real spherical particles, *Br. J. Appl. Phys.* **1961**, *12*, 164–172, DOI 10.1088/0508-3443/12/4/309.
- [108] R. Rutgers, Packing of spheres, *Nature* **1962**, *193*, 465–466, DOI 10.1038/193465a0.
- [109] R. F. Benenati and C. B. Brosilow, Void fraction distribution in beds of spheres, *AIChE J.* **1962**, *8*, 359–361, DOI 10.1002/aic.690080319.
- [110] K. Ridgway and K. J. Tarbuck, Radial voidage variation in randomly-packed beds of spheres of different sizes, *J. Pharm. Pharmacol.* **1966**, *18*, 168S–175S, DOI 10.1111/j.2042-7158.1966.tb07980.x.



- [111] S. Debbas and H. Rumpf, On the randomness of beds packed with spheres or irregular shaped particles, *Chem. Eng. Sci.* **1966**, *21*, 583–608, DOI 10.1016/0009-2509(66)85072-8.
- [112] G. D. Scott and D. M. Kilgour, The density of random close packing of spheres, *J. Phys. D: Appl. Phys.* **1969**, *2*, 863–866, DOI 10.1088/0022-3727/2/6/311.
- [113] D. P. Haughey and G. S. G. Beveridge, Structural properties of packed beds - A review, *Can. J. Chem. Eng.* **1969**, *47*, 130–140, DOI 10.1002/cjce.5450470206.
- [114] A. G. Dixon, Correlations for wall and particle shape effects on fixed bed bulk voidage, *Can. J. Chem. Eng.* **1988**, *66*, 705–708, DOI 10.1002/cjce.5450660501.
- [115] K. G. Allen, T. W. von Backström and D. G. Kröger, Packed bed pressure drop dependence on particle shape, size distribution, packing arrangement and roughness, *Powder Technol.* **2013**, *246*, 590–600, DOI 10.1016/j.powtec.2013.06.022.
- [116] A. B. Yu and R. P. Zou, Prediction of the porosity of particle mixtures, *Kona Powder Part. J.* **1998**, *16*, 68–81, DOI 10.14356/kona.1998010.
- [117] S. Afandizadeh and E. A. Foumeny, Design of packed bed reactors: guides to catalyst shape, size and loading selection, *Appl. Therm. Eng.* **2001**, *21*, 669–682, DOI 10.1016/s1359-4311(00)00072-7.
- [118] Z. P. Zhang, L. F. Liu, Y. D. Yuan and A. B. Yu, A simulation study of the effects of dynamic variables on the packing of spheres, *Powder Technol.* **2001**, *116*, 23–32, DOI 10.1016/s0032-5910(00)00356-9.
- [119] R. P. Zou and A. B. Yu, The packing of spheres in a cylindrical container: the thickness effect, *Chem. Eng. Sci.* **1995**, *50*, 1504–1507, DOI 10.1016/0009-2509(94)00483-8.
- [120] A. de Klerk, Voidage variation in packed beds at small column to particle diameter ratio, *AIChE J.* **2003**, *49*, 2022–2029, DOI 10.1002/aic.690490812.
- [121] F. Benyahia and K. E. O'Neill, Enhanced Voidage Correlations for Packed Beds of Various Particle Shapes and Sizes, *Part. Sci. Technol.* **2005**, *23*, 169–177, DOI 10.1080/02726350590922242.
- [122] A. M. Ribeiro, P. Neto and C. Pinho, Mean Porosity and Pressure Drop Measurements in Packed Beds of Monosized Spheres: Side Wall Effects, *IRECHE* **2010**, *2*, 40–46.
- [123] M. Leva and M. Grummer, Pressure drop through packed tubes, Part III: Prediction of voids in packed tubes, *Chem. Eng. Prog.* **1947**, *43*, 713.
- [124] K. Ridgway and K. J. Tarbuck, Voidage fluctuations in randomly-packed beds of spheres adjacent to a containing wall, *Chem. Eng. Sci.* **1968**, *23*, 1147–1155, DOI 10.1016/0009-2509(68)87099-x.

- [125] G. E. Mueller, Radial void fraction distributions in randomly packed fixed beds of uniformly sized spheres in cylindrical containers, *Powder Technol.* **1992**, *72*, 269–275, DOI 10.1016/0032-5910(92)80045-x.
- [126] M. Suzuki, T. Shinmura, K. Iimura and M. Hirota, Study of the Wall Effect on Particle Packing Structure Using X-ray Micro Computed Tomography, *Adv. Powder Technol.* **2008**, *19*, 183–195, DOI 10.1163/156855208x293817.
- [127] A. Sederman, P. Alexander and L. Gladden, Structure of packed beds probed by Magnetic Resonance Imaging, *Powder Technol.* **2001**, *117*, 255–269, DOI 10.1016/s0032-5910(00)00374-0.
- [128] G. E. Mueller, Radial porosity in packed beds of spheres, *Powder Technol.* **2010**, *203*, 626–633, DOI 10.1016/j.powtec.2010.07.007.
- [129] S. C. Reyes and E. Iglesia, Monte Carlo simulations of structural properties of packed beds, *Chem. Eng. Sci.* **1991**, *46*, 1089–1099, DOI 10.1016/0009-2509(91)85102-4.
- [130] T. Zeiser, P. Lammers, E. Klemm, Y. W. Li, J. Bernsdorf and G. Brenner, CFD-calculation of flow, dispersion and reaction in a catalyst filled tube by the lattice Boltzmann method, *Chem. Eng. Sci.* **2001**, *56*, 1697–1704, DOI 10.1016/s0009-2509(00)00398-5.
- [131] H. Freund, T. Zeiser, F. Huber, E. Klemm, G. Brenner, F. Durst and G. Emig, Numerical simulations of single phase reacting flows in randomly packed fixed-bed reactors and experimental validation, *Chem. Eng. Sci.* **2003**, *58*, 903–910, DOI 10.1016/s0009-2509(02)00622-x.
- [132] H. Freund, J. Bauer, T. Zeiser and G. Emig, Detailed simulation of transport processes in fixed-beds, *Ind. Eng. Chem. Res.* **2005**, *44*, 6423–6434, DOI 10.1021/i0489453.
- [133] G. E. Mueller, Numerically packing spheres in cylinders, *Powder Technol.* **2005**, *159*, 105–110, DOI 10.1016/j.powtec.2005.06.002.
- [134] J. Theuerkauf, P. Witt and D. Schwesig, Analysis of particle porosity distribution in fixed beds using the discrete element method, *Powder Technol.* **2006**, *165*, 92–99, DOI 10.1016/j.powtec.2006.03.022.
- [135] S. Rebughini, A. Cuoci and M. Maestri, Handling contact points in reactive CFD simulations of heterogeneous catalytic fixed bed reactors, *Chem. Eng. Sci.* **2016**, *141*, 240–249, DOI 10.1016/j.ces.2015.11.013.
- [136] S. Das, N. G. Deen and J. A. M. Kuipers, A DNS study of flow and heat transfer through slender fixed-bed reactors randomly packed with spherical particles, *Chem. Eng. Sci.* **2017**, *160*, 1–19, DOI 10.1016/j.ces.2016.11.008.

- [137] P. Lovreglio, S. Das, K. A. Buist, E. A. J. F. Peters, L. Pel and J. A. M. Kuipers, Experimental and numerical investigation of structure and hydrodynamics in packed beds of spherical particles, *AIChE J.* **2018**, *64*, 1896–1907, DOI 10.1002/aic.16127.
- [138] B. Partopour and A. G. Dixon, An integrated workflow for resolved-particle packed bed models with complex particle shapes, *Powder Technol.* **2017**, *322*, 258–272, DOI 10.1016/j.powtec.2017.09.009.
- [139] E. M. Moghaddam, E. A. Foumeny, A. I. Stankiewicz and J. T. Padding, Rigid Body Dynamics Algorithm for Modeling Random Packing Structures of Nonspherical and Nonconvex Pellets, *Ind. Eng. Chem. Res.* **2018**, *57*, 14988–15007, DOI 10.1021/acs.iecr.8b03915.
- [140] S. Flaischlen and G. D. Wehinger, Synthetic Packed-Bed Generation for CFD Simulations: Blender vs. STAR-CCM+, *ChemEngineering* **2019**, *3*, 52, DOI 10.3390/chemengineering3020052.
- [141] C. Kloss, LIGGGHTS<sup>®</sup>-PUBLIC Documentation, Version 3.X, DCS Computing GmbH, Linz, Austria, **2016**.
- [142] Y. Li, Y. Xu and C. Thornton, A comparison of discrete element simulations and experiments for ‘sandpiles’ composed of spherical particles, *Powder Technol.* **2005**, *160*, 219–228, DOI 10.1016/j.powtec.2005.09.002.
- [143] M. Jahani, A. Farzanegan and M. Noaparast, Investigation of screening performance of banana screens using LIGGGHTS DEM solver, *Powder Technol.* **2015**, *283*, 32–47, DOI 10.1016/j.powtec.2015.05.016.
- [144] B. Gong, Y. Feng, H. Liao, Y. Liu, X. Wang and K. Feng, Discrete element modeling of pebble bed packing structures for HCCB TBM, *Fusion Eng. Des.* **2017**, *121*, 256–264, DOI 10.1016/j.fusengdes.2017.08.002.
- [145] A. Džiugys and B. Peters, An approach to simulate the motion of spherical and non-spherical fuel particles in combustion chambers, *Granular Matter* **2001**, *3*, 231–266, DOI 10.1007/p100010918.
- [146] A. D. Renzo and F. P. D. Maio, Comparison of contact-force models for the simulation of collisions in DEM-based granular flow codes, *Chem. Eng. Sci.* **2004**, *59*, 525–541, DOI 10.1016/j.ces.2003.09.037.
- [147] E. Izadi and A. Bezuijen, Simulating direct shear tests with the Bullet physics library: A validation study, *PLOS ONE* **2018**, *13*, (Ed.: F. Portioli), e0195073, DOI 10.1371/journal.pone.0195073.
- [148] J. Bender, K. Erleben and J. Trinkle, Interactive simulation of rigid body dynamics in computer graphics, *Comput. Graphics Forum* **2014**, *33*, 246–270, DOI 10.1111/cgf.122272.

- [149] F. Radjai and V. Richefeu, Contact dynamics as a nonsmooth discrete element method, *Mech. Mater.* **2009**, *41*, 715–728, DOI 10.1016/j.mechmat.2009.01.028.
- [150] K. Erleben, J. Sparring, K. Henriksen and H. Dohlmann, *Physics-Based Animation*, 1st ed., Charles River Media, Inc., **2005**.
- [151] K.-W. Lim, K. Krabbenhoft and J. E. Andrade, A contact dynamics approach to the Granular Element Method, *Comput. Methods Appl. Mech. Eng.* **2014**, *268*, 557–573, DOI 10.1016/j.cma.2013.10.004.
- [152] T. Beck, *Blender 2.7*, Rheinwerk Verlag GmbH, **2017**, 908 pp.
- [153] G. E. Mueller, A simple method for determining sphere packed bed radial porosity, *Powder Technol.* **2012**, *229*, 90–96, DOI 10.1016/j.powtec.2012.06.013.
- [154] P. H. Mott and C. M. Roland, Limits to Poisson's ratio in isotropic materials, *Phys. Rev. B* **2009**, *80*, DOI 10.1103/physrevb.80.132104.
- [155] R. H. Perry and D. W. Green, *Perry's Chemical Engineers' Handbook*, McGraw-Hill Professional, **1997**.
- [156] R. Bedre, renesbedre/bioinfokit: Bioinformatics data analysis and visualization toolkit, **2020**, DOI 10.5281/zenodo.3965241.
- [157] E. Ostertagová and O. Ostertag, Methodology and application of one-way ANOVA, *American Journal of Mechanical Engineering* **2013**, *1*, 256–261, DOI 10.12691/ajme-1-7-21.
- [158] A. Boeing and T. Bräunl in Proceedings of the 5th International Conference on Computer Graphics and Interactive Techniques in Australia and Southeast Asia - GRAPHITE '07, ACM Press, **2007**, pp. 281–288, DOI 10.1145/1321261.1321312.
- [159] N. Jurtz, P. Waldherr and M. Kraume, Numerical analysis of the impact of particle friction on bed voidage in fixed-beds, *Chem. Ing. Tech.* **2019**, *91*, 1260–1266, DOI 10.1002/cite.201800190.
- [160] J. von Seckendorff, N. Szesni, R. Fischer and O. Hinrichsen, Experimental characterization of random packed spheres, cylinders and rings, and their influence on pressure drop, *Chem. Eng. Sci.* **2020**, *222*, 115644, DOI 10.1016/j.ces.2020.115644.
- [161] J. Fernengel, R. Weber, N. Szesni, R. W. Fischer and O. Hinrichsen, Numerical Simulation of Pellet Shrinkage within Random Packed Beds, *Ind. Eng. Chem. Res.* **2021**, *60*, 6863–6867, DOI 10.1021/acs.iecr.0c05307.
- [162] *Ullmann's encyclopedia of industrial chemistry*, Wiley-VCH Verlag GmbH & Co. KGaA, **2000**, DOI 10.1002/14356007.
- [163] *Handbook of Heterogeneous Catalysis*, (Eds.: G. Ertl, H. Knözinger, F. Schüth and J. Weitkamp), Wiley-VCH Verlag GmbH & Co. KGaA, Weinheim, **2008**, DOI 10.1002/9783527610044.

- [164] C. H. Bartholomew and R. J. Farrauto, *Fundamentals of Industrial Catalytic Processes*, John Wiley & Sons, Inc., **2005**, DOI 10.1002/9780471730071.
- [165] L. Lloyd, *Handbook of Industrial Catalysts*, Springer US, **2011**, 512 pp.
- [166] M. E. Kinaci, T. Lichtenegger and S. Schneiderbauer in Proceedings of the V International Conference on Particle-Based Methods - Fundamentals and Applications. PARTICLES 2017. Hannover, Germany, 26-28 October 2017. (Eds.: P. Wriggers, M. Bischoff, E. Onate, D. R. J. Owen and T. Zohdi), CIMNE, Barcelona, Spain, **2017**, Chapter Modelling of chemical reactions in metallurgical processes. Pp. 813–824.
- [167] J. Azmir, Q. Hou and A. Yu, CFD-DEM simulation of drying of food grains with particle shrinkage, *Powder Technol.* **2019**, *343*, 792–802, DOI 10.1016/j.powtec.2018.11.097.
- [168] C. Bruch, B. Peters and T. Nussbaumer, Modelling wood combustion under fixed bed conditions, *Fuel* **2003**, *82*, 729–738, DOI 10.1016/s0016-2361(02)00296-x.
- [169] A. Anca-Couce, N. Zobel and H. A. Jakobsen, Multi-scale modeling of fixed-bed thermo-chemical processes of biomass with the representative particle model: Application to pyrolysis, *Fuel* **2013**, *103*, 773–782, DOI 10.1016/j.fuel.2012.05.063.
- [170] G. Guiochon, T. Farkas, H. Guan-Sajonz, J.-H. Koh, M. Sarker, B. J. Stanley and T. Yun, Consolidation of particle beds and packing of chromatographic columns, *J. Chromatogr. A* **1997**, *762*, 83–88, DOI 10.1016/s0021-9673(96)00642-5.
- [171] A. Farsi, J. Xiang, J. Latham, M. Carlsson, E. Stitt and M. Marigo, Strength and fragmentation behaviour of complex-shaped catalyst pellets: A numerical and experimental study, *Chem. Eng. Sci.* **2020**, *213*, 115409, DOI 10.1016/j.ces.2019.115409.
- [172] B. Eisfeld and K. Schnitzlein, The influence of confining walls on the pressure drop in packed beds, *Chem. Eng. Sci.* **2001**, *56*, 4321–4329, DOI 10.1016/s0009-2509(00)00533-9.
- [173] J. Fernengel, L. Bolton and O. Hinrichsen, Characterisation and design of single pellet string reactors using numerical simulation, *Chem. Eng. J.* **2019**, *373*, 1397–1408, DOI 10.1016/j.cej.2019.03.114.
- [174] E. R. S. Winter, Diffusion properties of gases. Part IV. – The self-diffusion coefficients of nitrogen, oxygen and carbon dioxide, *Trans. Faraday Soc.* **1951**, *47*, 342–347, DOI 10.1039/TF9514700342.
- [175] K. Elgeti, A new equation for correlating a pipe flow reactor with a cascade of mixed reactors, *Chem. Eng. Sci.* **1996**, *51*, 5077–5080, DOI 10.1016/s0009-2509(96)00342-9.

- [176] N. Wakao and T. Funazkri, Effect of fluid dispersion coefficients on particle-to-fluid mass transfer coefficients in packed beds, *Chem. Eng. Sci.* **1978**, *33*, 1375–1384, DOI 10.1016/0009-2509(78)85120-3.
- [177] J. Fernengel, L. Bolton and O. Hinrichsen, Numerical investigation of pressure drop in single pellet string reactors, *Chem. Eng. Technol.* **2020**, *43*, 172–178, DOI 10.1002/ceat.201900372.
- [178] E. Erdim, Ö. Akgiray and İ. Demir, A revisit of pressure drop-flow rate correlations for packed beds of spheres, *Powder Technol.* **2015**, *283*, 488–504, DOI 10.1016/j.powtec.2015.06.017.
- [179] F. C. Blake, The resistance of packing to fluid flow, *Trans. Am. Inst. Chem. Eng.* **1922**, *14*, 415–421.
- [180] J. Kozeny, Über kapillare Leitung des Wassers im Boden, *Sitzungsber. Akad. Wiss. Wien* **1927**, *136*, 271–306.
- [181] D. Mehta and M. C. Hawley, Wall Effect in Packed Columns, *Ind. Eng. Chem. Process Des. Dev.* **1969**, *8*, 280–282, DOI 10.1021/i260030a021.
- [182] J. Fernengel, L. Bolton and O. Hinrichsen, Pellet-string reactor gas-solid systems – Phase II, project report B20b, Eurokin, **2019**.
- [183] O. Bilous and N. R. Amundson, Chemical reactor stability and sensitivity: II. Effect of parameters on sensitivity of empty tubular reactors, *AIChE J.* **1956**, *2*, 117–126, DOI 10.1002/aic.690020124.
- [184] K. V. Raghaven, Temperature runaway in fixed bed reactors: online and offline checks for intrinsic safety, *J. Loss Prev. Process Ind.* **1992**, *5*, 153–159, DOI 10.1016/0950-4230(92)80018-4.
- [185] J. J. Carberry, The catalytic effectiveness factor under nonisothermal conditions, *AIChE J.* **1961**, *7*, 350–351, DOI 10.1002/aic.690070239.
- [186] V. Simanzhenkov, K. E. Serhal and S. Goodarznia, *US Pat.*, US20180272303A1 (Fribourg (CH)), **2018**.
- [187] G. Emig, H. Hofmann, U. Hoffmann and U. Fiand, Experimental studies on runaway of catalytic fixed-bed reactors (vinyl-acetate-synthesis), *Chem. Eng. Sci.* **1980**, *35*, 249–257, DOI 10.1016/0009-2509(80)80094-7.
- [188] E. G. Bauman and A. Varma, Parametric sensitivity and runaway in catalytic reactors: Experiments and theory using carbon monoxide oxidation as an example, *Chem. Eng. Sci.* **1990**, *45*, 2133–2139, DOI 10.1016/0009-2509(90)80087-u.
- [189] A. I. Anastasov, A study of the influence of the operating parameters on the temperature of the hot spot in a fixed bed reactor, *Chem. Eng. J.* **2002**, *86*, 287–297, DOI 10.1016/s1385-8947(01)00178-4.



- [190] R. J. van Welsenaere and G. F. Froment, Parametric sensitivity and runaway in fixed bed catalytic reactors, *Chem. Eng. Sci.* **1970**, *25*, 1503–1516, DOI 10.1016/0009-2509(70)85073-4.
- [191] A. Oroskar and S. A. Stern, Stability of chemical reactors, *AIChE J.* **1979**, *25*, 903–905, DOI 10.1002/aic.690250523.
- [192] V. Balakotaiah and D. Luss, Explicit runaway criterion for catalytic reactors with transport limitations, *AIChE J.* **1991**, *37*, 1780–1788, DOI 10.1002/aic.690371203.
- [193] G. Maria and D.-N. Stefan, Variability of operating safety limits with catalyst within a fixed-bed catalytic reactor for vapour-phase nitrobenzene hydrogenation, *J. Loss Prev. Process Ind.* **2010**, *23*, 112–126, DOI 10.1016/j.jlp.2009.06.007.
- [194] M. Morbidelli and A. Varma, A generalized criterion for parametric sensitivity: Application to thermal explosion theory, *Chem. Eng. Sci.* **1988**, *43*, 91–102, DOI 10.1016/0009-2509(88)87129-x.
- [195] M. Morbidelli and A. Varma, Parametric sensitivity and runaway in fixed-bed catalytic reactors, *Chem. Eng. Sci.* **1986**, *41*, 1063–1071, DOI 10.1016/0009-2509(86)87193-7.
- [196] J. J. Carberry and D. White, On the role of transport phenomena in catalytic reactor behavior, *Ind. Eng. Chem.* **1969**, *61*, 27–35, DOI 10.1021/ie50715a008.
- [197] M. Morbidelli and A. Varma, Parametric sensitivity in fixed-bed reactors: Inter- and intraparticle resistance, *AIChE J.* **1987**, *33*, 1949–1958, DOI 10.1002/aic.690331203.
- [198] V. Balakotaiah, D. Kodra and D. Nguyen, Runaway limits for homogeneous and catalytic reactors, *Chem. Eng. Sci.* **1995**, *50*, 1149–1171, DOI 10.1016/0009-2509(94)00463-2.
- [199] M. M. J. Quina and R. M. Q. Ferreira, Thermal Runaway Conditions of a Partially Diluted Catalytic Reactor, *Ind. Eng. Chem. Res.* **1999**, *38*, 4615–4623, DOI 10.1021/ie9807295.
- [200] M. Herskowitz and P. S. Hagan, A General Runaway Criterion For Fixed-bed Reactors, *Chem. Eng. Commun.* **1990**, *96*, 291–302, DOI 10.1080/00986449008911497.
- [201] P. S. Hagan, M. Herskowitz and C. Pirkle, A Simple Approach to Highly Sensitive Tubular Reactors, *SIAM J. Appl. Math.* **1988**, *48*, 1083–1101, DOI 10.1137/0148064.
- [202] T. Varga, F. Szeifert, J. Réti and J. Abonyi, Analysis of the runaway in an industrial heterocatalytic reactor in *Computer Aided Chemical Engineering*, Elsevier, **2007**, pp. 751–756, DOI 10.1016/s1570-7946(07)80148-9.

- [203] M. Gruber, C. Wieland, P. Habisreuther, D. Trimis, D. Schollenberger, S. Bajohr, O. vonMorstein and S. Schirrmeyer, Modeling and Design of a Catalytic Wall Reactor for the Methanation of Carbon Dioxide, *Chem. Ing. Tech.* **2018**, *90*, 615–624, DOI 10.1002/cite.201700160.
- [204] A. Kummer and T. Varga, Completion of thermal runaway criteria: Two new criteria to define runaway limits, *Chem. Eng. Sci.* **2019**, *196*, 277–290, DOI 10.1016/j.ces.2018.11.008.
- [205] C.-K. Cho, K. S. Chang and T. S. Cale, Thermal runaway prevention in catalytic packed bed reactor by solid temperature measurement and control, *Korean J. Chem. Eng.* **1993**, *10*, 195–202, DOI 10.1007/bf02705267.
- [206] A. H. Benneker, A. E. Kronberg and K. R. Westerterp, Influence of buoyancy forces on the flow of gases through packed beds at elevated pressures, *AIChE J.* **1998**, *44*, 263–270, DOI 10.1002/aic.690440205.
- [207] M. Kaushik, *Theoretical and Experimental Aerodynamics*, Springer-Verlag GmbH, **2019**.
- [208] S. Chapman and T. G. Cowling, *The Mathematical Theory of Non-uniform Gases: An Account of the Kinetic Theory of Viscosity, Thermal Conduction and Diffusion in Gases (Cambridge Mathematical Library)*, Cambridge University Press, **1970**.
- [209] B. E. Poling, J. M. Prausnitz and J. P. O'Connell, *The Properties of Gases and Liquids*, 5th ed., McGraw-Hill, New York, **2001**.
- [210] *American Institute of Physics Handbook*, 3rd, (Ed.: D. E. Gray), McGraw-Hill, New York, **1972**.
- [211] A. G. Dixon, Local transport and reaction rates in a fixed bed reactor tube: Endothermic steam methane reforming, *Chem. Eng. Sci.* **2017**, *168*, 156–177, DOI 10.1016/j.ces.2017.04.039.
- [212] A. G. Dixon, M. Nijemeisland and E. H. Stitt, Systematic mesh development for 3D CFD simulation of fixed beds: Contact points study, *Comp. Chem. Eng.* **2013**, *48*, 135–153, DOI 10.1016/j.compchemeng.2012.08.011.
- [213] A. H. Benneker, A. E. Kronberg, J. W. Post, A. G. J. Van Der Ham and K. R. Westerterp, Axial dispersion in gases flowing through a packed bed at elevated pressures, *Chemical engineering science* **1996**, *51*, 2099–2108, DOI 10.1016/0009-2509(96)00067-x.
- [214] J. Fernengel, J. von Seckendorff and O. Hinrichsen, Influence of cylinder-to-particle diameter ratio and filling speed on bed porosity of random packed beds of spheres in *Computer Aided Chemical Engineering*, Elsevier, **2018**, pp. 97–102, DOI 10.1016/b978-0-444-64235-6.50019-x.



- [215] J. Kleiner, B. Münch, F. Rößler, J. Fernengel, F. Habla and O. Hinrichsen, CFD simulation of single-phase heat transfer in a rotor-stator spinning disc reactor, *Chem. Eng. Process. Process Intensif.* **2018**, *131*, 150–160, DOI 10.1016/j.cep.2018.07.010.



# Nomenclature

## Latin Symbols

$a$	specific catalyst pellet surface area per unit reactor volume	$\text{m}^{-1}$
$a_v$	area per unit volume of catalyst	$\text{m}^{-1}$
$A$	area	$\text{m}^2$
$A_t$	cross sectional area of empty reactor tube	$\text{m}^2$
$c$	concentration	$\text{mol m}^{-3}$
$c_p$	specific heat capacity at constant pressure	$\text{J kg}^{-1} \text{K}^{-1}$
$c_v$	constant volume heat capacity at constant volume	$\text{J kg}^{-1} \text{K}^{-1}$
$d$	diameter, pellet diameter if not specified otherwise	$\text{m}$
$d_{32}$	Sauter mean diameter	$\text{m}$
$D$	tube diameter	$\text{m}$
$D_{\text{ax}}$	axial dispersion coefficient	$\text{m}^2 \text{s}^{-1}$
$\mathcal{D}$	molecular diffusion coefficient, here: self-diffusion coefficient	$\text{m}^2 \text{s}^{-1}$
$e$	coefficient of restitution	-
$e_a^{21}$	approximate relative error in mesh independency study	-
$e_{\text{ext}}^{21}$	extrapolated relative error in mesh independency study	-
$E$	residence time distribution	$\text{s}^{-1}$
$E$	Young's modulus	-
$E_a$	activation energy	$\text{kJ mol}^{-1}$
$f$	weighting factor	-
$g$	gravitational acceleration	$\text{m s}^{-2}$
$g$	gravitational constant	$\text{m s}^{-2}$
$GCI_{\text{fine}}^{21}$	fine-grid convergence index in mesh independency study	-
$h$	specific enthalpy	$\text{J kg}^{-1}$
$h$	tablet height	$\text{m}$
$H$	height of (catalytic) bed	$\text{m}$
$\Delta h$	pellet height shrinkage	%
$\Delta H$	heat of reaction	$\text{kJ mol}^{-1}$
$i$	index variable	-
$\mathbf{I}$	unit tensor	-
$k$	reaction rate constant	$\text{m s}^{-1}$
$k$	constant in Benneker criterion	-
$k_f$	interface mass transfer coefficient (fluid-to-solid)	$\text{m s}^{-1}$
$L$	reactor length including inlet and outlet section	$\text{m}$

$M$	molecular weight	$\text{g mol}^{-1}$
$n$	number of slices	-
$n$	reaction order	-
$N$	number of (catalytic) pellets	-
$N_{\text{TIS}}$	number of equivalent tanks-in-series	-
$N_1, N_2, N_3$	number of cells for mesh independency study	-
$p$	apparent order of the method in mesh independency study	-
$p$	pressure	Pa
$\Delta p$	pressure drop	mbar
$q$	heat flux	$\text{W m}^{-2}$
$r$	pellet radius	m
$r$	radial coordinate	m
$r_{12}, r_{23}$	refinement factors for mesh independency study	m
$\Delta r$	pellet radial shrinkage	%
$R$	tube radius	m
$R$	universal gas constant	$\text{J mol}^{-1} \text{K}^{-1}$
$R^{\text{obs}}$	observed global rate of reaction	$\text{mol s}^{-1} \text{m}^{-3}$
$s$	reactor scale	-
$\Delta s$	threshold on pellet movement	m
$S$	surface area	$\text{m}^2$
$t$	time	s
$T$	temperature	K
$u$	velocity vector	$\text{m s}^{-1}$
$\bar{u}$	mean velocity	$\text{m s}^{-1}$
$u_0$	superficial velocity	$\text{m s}^{-1}$
$V$	volume	$\text{m}^3$
$\dot{V}$	volumetric flow rate	$\text{m}^3 \text{s}^{-1}$
$X$	conversion	-
$Y$	mass fraction	-
$x, y, z$	Cartesian coordinates	m
$z$	axial coordinate	m

### Greek Symbols

$\alpha$	thermal diffusivity	$\text{m}^2 \text{s}^{-1}$
$\delta$	distance between confining wall and first minimum in radial voidage profiles	m
$\varepsilon$	local bed voidage	-
$\bar{\varepsilon}$	mean bed voidage	-
$\eta$	dynamic viscosity	$\text{kg m}^{-1} \text{s}^{-1}$
$\kappa$	thermal conductivity	$\text{W m}^{-1} \text{K}^{-1}$

$\mu$	coefficient of friction	-
$\nu$	kinematic viscosity	$\text{m}^2 \text{s}^{-1}$
$\nu$	Poisson's ratio	-
$\rho$	density	$\text{kg m}^{-3}$
$\tau$	viscous stress tensor	$\text{N m}^{-2}$
$\tau$	space time across the catalytic bed	s
$\phi$	critical variable as used in mesh independency study	var.
$\phi_{\text{ext}}^{21}$	extrapolated value in mesh independency study	var.

### Subscripts

A	base case
atm	atmospheric
ax	axial, longitudinal direction
BON	according to Benyahia and O'Neill [121]
cat	at the catalytic surface
cmp	comparative packing
cor	correlation
dil	catalytic bed diluted with inert fines
f	fluid
i	pellet index
in	inlet
inert	inert surface
ini	initial packing
ins	insertion
m	modified equivalent
max	maximum
min	minimum
out	outlet
p	pellet
rad	radial
s	solid
s	surface
shr	shrunk packing
sim	simulation
solid	occupied by solid
surf	surface, both inert and catalytic
t	cross-sectional
t	tube, outer confining wall
total	total amount
void	empty, void

w	reactor wall
z	axial direction
$\Sigma$	total
0	reference conditions
0	catalytic bed entrance
1	first catalytic particle

### Dimensionless Numbers

$Bo$	Bodenstein number, here: $Bo = \frac{u_0 d}{\bar{\varepsilon} D_{ax}}$
$Ca$	Carberry number $Ca = \frac{R^{obs}}{k_f a_v C_0}$
$Gr$	Grashof number $Gr = \frac{\Delta\rho g d^2 D^2}{\rho_0 H \nu^2}$
$Pe$	Péclet number $Pe = \frac{u_0 d}{\mathcal{D}}$
$Pr$	Prandtl number $Pr = \frac{\nu}{\alpha} = \frac{\eta c_p}{k_f}$
$Re$	Reynolds number $Re = \frac{u_0 d}{\nu}$
$Re_{bed}$	bed Reynolds number $Re_{bed} = \frac{u_0 d}{\nu(1-\bar{\varepsilon})}$
$Re_p$	particle Reynolds number $Re_p = \frac{u_0 d}{\nu}$
$Sc$	Schmidt number $Sc = \frac{\nu}{\mathcal{D}}$
$Sh$	Sherwood number $Sh = \frac{k_f d}{\mathcal{D}}$

Note: Care should be taken regarding the ambiguous usage of  $Bo$  and  $Pe$  in literature. Here,  $Bo$  is used for axial dispersion while  $Pe$  is related to molecular diffusion. Variations in literature also cover the characteristic length, where here the pellet diameter is used.

### Abbreviations

CD	contact dynamics
CFD	computational fluid dynamics
DEM	distinct element method
GCI	grid convergence index
NTP	normal temperature and pressure
PFR	plug flow reactor
RTD	residence time distribution
SPSR	single pellet string reactor
TIS	tanks-in-series model

# Figures

1.1	Generalised life cycle of a catalytic fixed-bed reactor. . . . .	2
4.1	Flow chart of automated simulation routine. . . . .	23
4.2	Principle of mesh generation from hexahedral background mesh and surface with snappyHexMesh, shown for packed bed of spheres in cylindrical confined walls. . . . .	24
4.3	Excerpt of Python script for local voidage evaluation using ParaView <sup>®</sup> functionality. . . . .	25
4.4	Packing geometry and flow hydrodynamics for packed bed with $D/d = 2$ . . .	27
4.5	Radial voidage profiles for packed beds with $D/d = 2, 7.35$ and $8.41$ . . . . .	27
4.6	Area averaged pressure and conversion profiles along the reactor length axis. . . . .	28
5.1	2D view of packing obtained by simulation with LIGGGHTS <sup>®</sup> for bed with $D/d = 8.41$ , $N = 1000$ and $H_{ins} = 18d$ (a), together with corresponding position of pellet centre points in plane spanning bed height and radius (b) as well as longitudinal voidage profile (c). . . . .	41
5.2	Influence of pellet number, insertion height and voidage evaluation on mean bed voidage for beds with $D/d = 8.41$ . . . . .	43
5.3	Variation of mean bed voidage in sections along the bed height for beds with $D/d = 8.41$ and a fixed insertion height of $165d$ ; section positions measured from packing bottom. . . . .	43
5.4	Influence of material properties on mean bed voidage for packings with $H/d \approx 30$ based on parameter default values as detailed in Table 5.2 unless specified otherwise; reduced by $5d$ from bottom and $4d$ from top of packing for voidage evaluation. . . . .	46
5.5	Influence of Poisson's ratio and Young's modulus on mean bed voidage for packings with $H/d \approx 30$ based on parameter default values as detailed in Table 5.2 unless specified otherwise and simulated with LIGGGHTS <sup>®</sup> ; reduced by $5d$ from bottom and $4d$ from top of packing for voidage evaluation. . . . .	47
5.6	Range of obtained mean bed voidage as a function of diameter aspect ratio in comparison to literature correlations. . . . .	48
5.7	Radial voidage profiles for beds simulated with LIGGGHTS <sup>®</sup> , excluding $5d$ and $4d$ from bottom and top of packing, respectively. . . . .	50

5.8	Trigonometrical considerations leading to analytical position of local minimum in radial voidage profile next to the confining wall. . . . .	51
5.9	Development of mean and standard deviation with increasing number of simulations per data point. . . . .	55
5.10	Boxplot of group data considered for ANOVA of packed beds with $D/d = 5.6$ and an insertion height of $40d$ as generated with LIGGGHTS <sup>®</sup> . Whiskers restricted to 1.5 times the interquartile range, data outside this range shown as outlier. . . . .	56
5.11	Boxplot of group data considered for ANOVA of packed beds with $D/d = 5.6$ and an insertion height of $200d$ as generated with LIGGGHTS <sup>®</sup> . Whiskers restricted to 1.5 times the interquartile range, data outside this range shown as outlier. . . . .	57
5.12	Boxplot of group data considered for ANOVA of packed beds with $D/d = 5.6$ and an insertion height of $40d$ as generated with Blender <sup>™</sup> . Whiskers restricted to 1.5 times the interquartile range, data outside this range shown as outlier. . . . .	58
5.13	Boxplot of group data considered for ANOVA of packed beds with $D/d = 5.6$ and an insertion height of $200d$ as generated with Blender <sup>™</sup> . Whiskers restricted to 1.5 times the interquartile range, data outside this range shown as outlier. . . . .	58
6.1	Simplified flowchart of random packing generation including routine for pellet shrinkage and settling of the bed. . . . .	62
6.2	Packings as obtained by simulation. Planes enclosing bulk packing, cylindrical tubes indicating considered flow domain. . . . .	64
6.3	Local voidage profiles for <i>Case 2</i> . . . . .	65
6.4	Tablet midpoints for <i>Case 2</i> , excluding $2d$ at bed ends. . . . .	66
6.5	Effect of shrinkage on pellet arrangement for <i>Case 2</i> . . . . .	67
6.6	Area-averaged pressure losses for <i>Case 2</i> . Lines indicate positions used for evaluating pressure drop per unit length. . . . .	68
6.7	Comparison of simulated pressure drops for <i>Case 2</i> with Einfeld-Schnitzlein [172] correlation. . . . .	69
7.1	General structure of background mesh; top view, front view and cross-section as indicated in front view (from left to right). . . . .	81
7.2	Lateral cuts through geometry (a) and final mesh of flow domain (b and c) for base case SPSR ( <i>scenario a</i> ). . . . .	86
7.3	Flow field inside base case SPSR ( <i>scenario a</i> ) shown in lateral cut through the reactor (a) and as streamline plot (b). Scale adjusted to catalytic section, geometry of bottom six spheres shown for visualisation. . . . .	87
7.4	Residence time distribution for base case SPSR ( <i>scenario a</i> ). . . . .	87



7.5	Conversion in base case SPSR ( <i>scenario a</i> ). Particle based conversion values shown at centre point position of corresponding particles. . . . .	88
7.6	Residence time distributions for SPSR scenarios. . . . .	90
7.7	Conversion along the reactor for SPSR scenarios. PFR conversion shown for comparison. . . . .	92
7.8	Influence of cylinder-to-particle diameter ratio and particle number on overall reactor conversion. . . . .	93
7.9	Overview of overall bed conversion results for simulated SPSR scenarios; dashed line indicating 5% deviation in conversion as compared to ideal plug flow behaviour. . . . .	94
7.10	Evaluation of axial dispersion criterion in the form proposed by Gierman [7] for simulated SPSRs; dashed line indicating threshold value. . . . .	95
7.11	Evaluation of Carberry criterion on external mass transfer limitations [163] for simulated SPSRs; dashed line indicating threshold value. . . . .	96
7.12	Trend analysis showing deviation to plug flow conversion as function of particle number, cylinder-to-particle diameter ratio and Péclet number. . . . .	97
7.13	Slice along longitudinal axis of inlet and outlet geometry set-ups with empty tube sections of $2d$ length, inert beds of $1d$ length and virtually no inlet and outlet sections (top to bottom). . . . .	100
7.14	Conversion results for SPSR <i>scenario a</i> with varying in-/oulet geometry and velocity inlet boundary condition. . . . .	101
7.15	Effect of reduced diffusion coefficient on bed conversion for SPSR of <i>scenario a</i> with $2d$ empty inlet and outlet length and parabolic inlet velocity. . . . .	101
7.16	Conversion across the reactor for SPSR of <i>scenario a</i> with reduced particle number of $N = 5$ using meshes with different refinement according to Table 7.3. . . . .	103
7.17	Comparison of conversion in SPSRs where the void space is filled with fines of different size with shortened base case, considering only the first five pellets, and corresponding PFR conversion. . . . .	104
7.18	Residence time distributions for SPSR with variation in fluid viscosity. . . . .	104
7.19	Conversion along the reactor for SPSR scenario with variation in gas viscosity. PFR conversion shown for comparison. . . . .	105
7.20	Conversion along the reactor for SPSR scenarios with variation in reactant concentration, $c_a$ corresponding to pure feed. PFR conversion shown for comparison. . . . .	105
7.21	Comparison of residence time behaviour of base case SPSR ( <i>scenario a</i> ) with diffusive and non-diffusive tracer. . . . .	106
7.22	Comparison of residence time distributions for SPSRs with varying diameter aspect ratio using a non-diffusive and a diffusive tracer. . . . .	107
7.23	Trend analysis showing deviation to plug flow conversion as function of conversion on first pellet normalised with overall bed conversion. . . . .	109

8.1	Bottom section of a SPSR showing trigonometric expressions used for analytical pellet positions. . . . .	115
8.2	Normalised average cross-sectional pressure for the base case SPSR as function of axial position. . . . .	117
8.3	Influence of fluid viscosity, flow velocity, diameter aspect ratio and geometry scaling factor on pressure drop. . . . .	118
8.4	Comparison of pressure drop across SPSR variations with Ergun [51] and Blake-Kozeny [179, 180] equation using a modified equivalent diameter [4]. . . . .	119
8.5	Comparison of simulation results for pressure drop per unit length in SPSRs with literature and own correlations. Variations in diameter aspect ratio marked to ease allocation. . . . .	120
8.6	Wall surface weighting factor as function of diameter aspect ratio. . . . .	122
9.1	Schematic view of bottom three pellets in SPSR with trigonometric relations required for analytical pellet positions. . . . .	133
9.2	Common strategies of contact point handling, after Dixon et al. [212]; methods used in this study indicated by bold font. . . . .	138
9.3	Geometry set-up showing top section of a SPSR including an inert pre-bed with labelling of boundaries. Inserts show contact point treatment between catalytic pellets and confining wall (top) and between adjacent catalytic pellets (bottom). . . . .	138
9.4	Space mesh for fluid and catalytic solid domain. Inserts show mesh details at solid-fluid interphase (top), between catalytic pellets and confining wall (centre) and close to contact point between adjacent catalytic pellets (bottom). . . . .	147
9.5	Visualisation of simulation results for base case isothermal SPSR. . . . .	147
9.6	Conversion along the reactor length axis in base case isothermal SPSR. . . . .	148
9.7	Reactant weight fraction in SPSR scenarios with varying heat of reaction, contours from $Y = 0.99$ downwards in steps of $\Delta Y = 0.02$ . . . . .	149
9.8	Temperature profiles in plane through centre points of catalytic pellets for varying heat of reaction. . . . .	149
9.9	Parametric sensitivity of the maximum temperature in a SPSR along the reactor length axis with respect to the heat of reaction for a hypothetical first order, irreversible, heterogeneously catalysed gas phase reaction. . . . .	150
9.10	Influence of increasing heat of reaction for exothermic reactions on SPSR conversion and reactor temperatures. . . . .	152
9.11	Convergence monitoring for SPSR of the scenario <i>heat of reaction</i> with $\Delta H = -224 \text{ kJ mol}^{-1}$ . . . . .	154
9.12	Influence of inert pre-bed height on SPSR conversion; dashed lines indicating isothermal PFR conversion and full reactant depletion. . . . .	155
9.13	Influence of number of catalytic pellets considered for simulation domain on SPSR conversion. . . . .	156

9.14 Influence of activation energy and heat of reaction on conversion behaviour in SPSRs; dashed lines indicating isothermal PFR conversion and full reactant depletion. . . . .	158
9.15 Influence of reactor scale and heat of reaction on conversion behaviour in SPSRs; dashed lines indicating isothermal PFR conversion and full reactant depletion. . . . .	158
9.16 Influence of number of catalytic pellets in SPSR arrangement on conversion behaviour in SPSRs; dashed line indicating isothermal PFR conversion. . . . .	159
9.17 Influence of notional gas pressure on conversion behaviour in SPSRs; dashed lines indicating isothermal PFR conversion and full reactant depletion. . . . .	160
9.18 Influence of conversion used for determination of reaction rate coefficient on conversion behaviour in SPSRs. . . . .	160
9.19 Influence of fluid heat capacity on conversion behaviour in SPSRs; $\Delta H = -64 \text{ kJ mol}^{-1}$ . . . . .	161
9.20 Influence of thermal conductivity within catalytic pellets on conversion behaviour in SPSRs; $\Delta H = -64 \text{ kJ mol}^{-1}$ . . . . .	162
9.21 Temperature profiles in plane through centre points of catalytic pellet for varying thermal conductivity of the catalytic pellets; $\Delta H = -64 \text{ kJ mol}^{-1}$ . . . . .	162
9.22 Influence of temperature dependency of the molecular diffusion coefficient on conversion behaviour in SPSRs for varying heats of reaction; dashed lines indicating isothermal PFR conversion and full reactant depletion. . . . .	163
9.23 Influence of temperature dependency of the dynamic viscosity on conversion behaviour in SPSRs for varying heats of reaction; dashed lines indicating isothermal PFR conversion and full reactant depletion. . . . .	164
9.24 Enhancement of axial mixing as a result of buoyancy effects; plot taken from Benneker et al. [206], $k = 600$ . . . . .	166
9.25 Adaptation of Benneker criterion to conversion of exothermic reactions in SPSRs. . . . .	167
9.26 Distinction between stable reactor operation and thermal runaway for exothermic reactions in SPSRs based on reaction parameters, pellet diameter and material properties. . . . .	168
9.27 Temperature profiles in plane through centre points of catalytic pellets for varying heat of reaction with bridges at contact points between pellets and wall. . . . .	172
9.28 Influence of handling the contact points between catalytic pellets and reactor wall; dashed lines in subfigure (c) indicating isothermal PFR conversion and full reactant depletion. . . . .	173



# Tables

4.1	Results of fixed bed reactor simulations. . . . .	26
5.1	Parameter settings for evaluation of packing characteristics; simulations with LIGGGHTS <sup>®</sup> only. . . . .	39
5.2	Parameter settings for variation of material properties, default values highlighted in bold. . . . .	40
6.1	Parameters for bed generation and flow simulation. . . . .	63
6.2	Properties of simulated beds. Voidage and pressure values based on reduced bed excl. sections of $2d$ from both ends. . . . .	65
6.3	Mesh details and discretisation error calculations. . . . .	73
7.1	Geometry settings of single pellet string reactor scenarios. . . . .	85
7.2	Threshold values of proposed design criterion based on particle number, cylinder-to-particle diameter ratio and Péclet number for deviations to plug flow conversion of less than 1 %, 5 % and 10 %. . . . .	98
7.3	Key parameters of meshes considered in grid-independence study. . . . .	102
7.4	Comparison of dimensionless group $u_0 H/D_{ax}$ obtained from RTDs with non-diffusive and diffusive numerical tracers. . . . .	108
7.5	Threshold values of conversion on first particle normalised with overall bed conversion for deviations to plug flow conversion of less than 1 %, 5 % and 10 % for SPSR with 20 and 50 catalytic particles. . . . .	109
8.1	Geometry and fluid properties of considered single pellet string reactors. . . . .	116
9.1	Geometry and thermophysical properties of considered single pellet string reactor variations. . . . .	145
9.2	Mesh details and discretisation error calculations. . . . .	170



# Publications

## Journal Publications

- J. Fernengel, F. Habla and O. Hinrichsen, Scripting as an approach to automated CFD simulation for packed bed catalytic reactor modeling, *Chem. Ing. Tech.* **2018**, *90*, 685–689, DOI 10.1002/cite.201700153.
- J. Fernengel, J. von Seckendorff and O. Hinrichsen, Influence of cylinder-to-particle diameter ratio and filling speed on bed porosity of random packed beds of spheres in *Computer Aided Chemical Engineering*, Elsevier, **2018**, pp. 97–102, DOI 10.1016/b978-0-444-64235-6.50019-x.  
J. Fernengel and J. von Seckendorff contributed equally to this work.
- J. Kleiner, B. Münch, F. Rößler, J. Fernengel, F. Habla and O. Hinrichsen, CFD simulation of single-phase heat transfer in a rotor-stator spinning disc reactor, *Chem. Eng. Process. Process Intensif.* **2018**, *131*, 150–160, DOI 10.1016/j.cep.2018.07.010.
- J. Fernengel, L. Bolton and O. Hinrichsen, Characterisation and design of single pellet string reactors using numerical simulation, *Chem. Eng. J.* **2019**, *373*, 1397–1408, DOI 10.1016/j.cej.2019.03.114.
- J. Fernengel, L. Bolton and O. Hinrichsen, Numerical investigation of pressure drop in single pellet string reactors, *Chem. Eng. Technol.* **2020**, *43*, 172–178, DOI 10.1002/ceat.201900372.
- J. Fernengel and O. Hinrichsen, Influence of material properties on voidage of numerically generated random packed beds, *Chem. Eng. Sci.* **2021**, *233*, 116406, DOI 10.1016/j.ces.2020.116406.
- J. Fernengel, R. Weber, N. Szesni, R. W. Fischer and O. Hinrichsen, Numerical Simulation of Pellet Shrinkage within Random Packed Beds, *Ind. Eng. Chem. Res.* **2021**, *60*, 6863–6867, DOI 10.1021/acs.iecr.0c05307.

## Oral Presentations

- J. Fernengel, F. Habla, O. Hinrichsen, Scripting as an approach to automated CFD simulation for packed bed catalytic reactor modelling, *11<sup>th</sup> OpenFOAM<sup>®</sup> Workshop 2016*, Guimarães, Portugal.
- J. Fernengel, J. von Seckendorff, O. Hinrichsen, Influence of Cylinder-to-Particle Diameter Ratio and Filling Speed on Bed Porosity of Random Packed Beds of Spheres, *28<sup>th</sup> European Symposium on Computer Aided Process Engineering 2018*, Graz, Austria.
- J. Fernengel, L. Bolton, O. Hinrichsen, Characterisation and Design of Single Pellet String Reactors using Numerical Simulation, *XXIII International Conference on Chemical Reactors 2018*, Ghent, Belgium.
- J. Fernengel, L. Bolton, O. Hinrichsen, Numerical Parameter Study on Single Pellet String Reactors - a Reactor Concept for Heterogeneous Catalysis, *Jahrestreffen Reaktionstechnik 2019*, Würzburg, Germany.

## Poster Presentations

- J. Fernengel, F. Habla, O. Hinrichsen, Scripting as an approach to automated CFD simulation for packed bed catalytic reactor modelling, *Jahrestreffen Reaktionstechnik 2017*, Würzburg, Germany.
- J. Fernengel, O. Hinrichsen, Numerical Parameter Study on Bed Porosity of Random Packed Beds of Spheres, *Jahrestreffen Reaktionstechnik 2018*, Würzburg, Germany.
- J. Fernengel, O. Hinrichsen, Numerical Parameter Study on Bed Porosity of Random Packed Beds of Spheres – Software Comparison, *25<sup>th</sup> International Symposium on Chemical Reaction Engineering 2018*, Florence, Italy.
- J. Fernengel, N. Szesni, R. Fischer, O. Hinrichsen, Numerical Simulation of Pellet Shrinkage in Random Packed Beds – Feasibility Study –, *Jahrestreffen Reaktionstechnik 2020*, Würzburg, Germany. (online event)
- J. Fernengel, C. Bauer, O. Hinrichsen, Influence of Material Properties on Porosity of Numerically Generated Random Packed Beds of Spheres, *26<sup>th</sup> International Symposium on Chemical Reaction Engineering 2021*, New Delhi, India. (online event)
- J. Fernengel, R. Weber, N. Szesni, R. Fischer, O. Hinrichsen, Numerical Simulation of Pellet Shrinkage in Random Packed Beds – Feasibility Study –, *26<sup>th</sup> International Symposium on Chemical Reaction Engineering 2021*, New Delhi, India. (online event)